System Biology of Aging

-- Exploring the System Nature of Aging employing Reliability Theory

Dr. rer. nat. Lei Mao, M.Comp.Sc.(Bioinformatics)

Habilitationsschrift an der Fakultät III
Prozesswissenschaften
Der Technischen Universität Berlin

Lehrgebiet:
Mikrobiologie und Genetik

Eröffnung des Verfahrens: 9. September 2009
Verleihung der Lehrbefähigung: 15. Dezember 2010
Ausstellung der Urkunde: 23. Januar 2011
Aushändigung der Urkunde: 10. Februar 2011

Gutachter:

Professor Dr. Jens Kurreck
Professor Dr. Karl Sperling
Professor Jiri Ferejt
Professor Dr. Peter Hammerstein

Berlin, 2010
D83

Diese kumulative Schrift gründet sich auf die folgenden Originalarbeiten:

Kasper, G., **Mao, L.**, Geissler, S., Trippens, J., Kuehnisch, J., Tschirschmann, M., Kaspar, K., Perka, C., Duda, G. N., and Klose, J. (2009). Insights into mesenchymal stem cell ageing: Involvement of antioxidant defence and actin cytoskeleton. ***Stem Cells***. Feb;26;27(6):1288-1297.

Nebrich, G., Herrmann, M., Hartl, D., Diedrich, M., Kreitler, T., Wierling, C., Klose, J., Giavalisco, P., Zabel, C., and **Mao, L.** (2009). PROTEOMER: A workflow-optimized laboratory information management system for 2-D electrophoresis-centered proteomics. ***Proteomics*** Apr;9(7):1795-808.

Mao, L., Hartl, D., Nolden, T., Koppelstatter, A., Klose, J., Himmelbauer, H., and Zabel, C. (2008). Pronounced alterations of cellular metabolism and structure due to hyper- or hypo-osmosis. ***J Proteome Res*** 2008 Sep;7(9):3968-83 Epub 2008 Jul 23.

Zabel, C., **Mao, L.**, Woodman, B., Rohe, M., Wacker, M. A., Klaere, Y., Koppelstaetter, A., Nebrich, G., Klein, O., Grams, S., et al. (2009). A large number of protein expression changes occur early in life and precede phenotype onset in a mouse model for Huntington's disease. ***Mol Cell Proteomics*** Apr;8(4):720-34.

Diedrich, M., **Mao, L.**, Bernreuther, C., Zabel, C., Nebrich, G., Kleene, R., and Klose, J. (2008). Proteome analysis of ventral midbrain in MPTP-treated normal and L1cam transgenic mice. ***Proteomics*** Mar;8(6):1266-75.

Hartl, D., Irmler, M., Romer, I., Mader, M. T., **Mao, L.**, Zabel, C., de Angelis, M. H., Beckers, J., and Klose, J. (2008a). Transcriptome and proteome analysis of early embryonic mouse brain development. ***Proteomics*** Mar;8(6):1257-65.

Hartl, D., Rohe, M., **Mao, L.**, Staufenbiel, M., Zabel, C., and Klose, J. (2008b). Impairment of adolescent hippocampal plasticity in a mouse model for Alzheimer's disease precedes disease phenotype. ***PLoS ONE*** Jul 23;3(7):e2759.

Mao, L., Zabel, C., Herrmann, M., Nolden, T., Mertes, F., Magnol, L., Chabert, C., Hartl, D., Herault, Y., Delabar, J. M., et al. (2007). Proteomic shifts in embryonic stem cells with gene dose modifications suggest the presence of balancer proteins in protein regulatory networks. ***PLoS ONE*** Nov 28;2(11):e1218.

Mao, L., Zabel, C., Wacker, M. A., Nebrich, G., Sagi, D., Schrade, P., Bachmann, S., Kowald, A., and Klose, J. (2006). Estimation of the mtDNA mutation rate in aging mice by proteome analysis and mathematical modeling. ***Exp Gerontol*** Jan;41(1):11-24. Epub 2005 Nov 2022.

Zabel, C., Sagi, D., Kaindl, A. M., Steireif, N., Klare, Y., **Mao, L.**, Peters, H., Wacker, M. A., Kleene, R., and Klose, J. (2006). Comparative proteomics in neurodegenerative and non-neurodegenerative diseases suggest nodal point proteins in regulatory networking. ***J Proteome Res*** Aug;5(8):1948-58.

Erklärungen

a) Ich versichere hiermit an Eidesstatt, dass die vorliegende Habilitationsschrift ohne fremde Hilfe verfasst, die beschriebene Ergebnisse selbst gewonnen, die Angaben über die Zusammenarbeit mit anderen Wissenschaftern und die zugrunde liegende Literatur vollständig sind.

b) Ich erkläre hiermit, dass ich **nicht** bereits in einem Habilitationsverfahren, für das Fachgebiet, für das die Lehrbefähigung festgestellt werden soll, oder für ein verwandtes Fachgebiet gescheitert bin.

c) Ein akademischer Grad wurde mir **nicht** entzogen und es liegen keine Tatsachen vor, die die Entziehung eines akademischen Grades rechtfertigen.

d) An einer anderen Hochschule wurde von mir **kein** Habilitationsgesuch eingereicht.

e) Ich erkläre hiermit, dass ein Strafverfahren beim Gericht nicht anhängig ist.

f) Ich erkläre hiermit, dass mir die Habilitationsordnung vom 13.6.1993 bekannt ist.

g) Ich erkläre hiermit, dass die Lehrveranstaltungen selbständig vorbereitet und abgehalten wurden.

……

(Unterschrift)

Abkürzungsverzeichnis:

AD:	Alzheimer disease
HD:	Huntington disease
MPTP:	1-methyl-4-phenyl-1,2,3,6-tetrahydropyridene hydrochloride
MSC:	mesenchymal stem cells
ND:	neurodegenerative disease
PD:	Parkinson diseases
ROS:	reactive oxygen species

System Biology of Aging

Exploring the System Nature of Aging employing Reliability Theory

Table of contents

1 Introduction

1.1 Mankind is growing older worldwide

Human life expectancy has been constantly and almost linearly rising during the last 160 years (Oeppen and Vaupel, 2002) (Fig.1). According to a recent report from the United Nations, the number of old people (age 60 and over) will exceed the number of children worldwide for the first time in human history by year 2047 (Nature collections September 2007). Indeed, the fastest growing population among the elderly is the oldest – those aged 80 years and beyond.

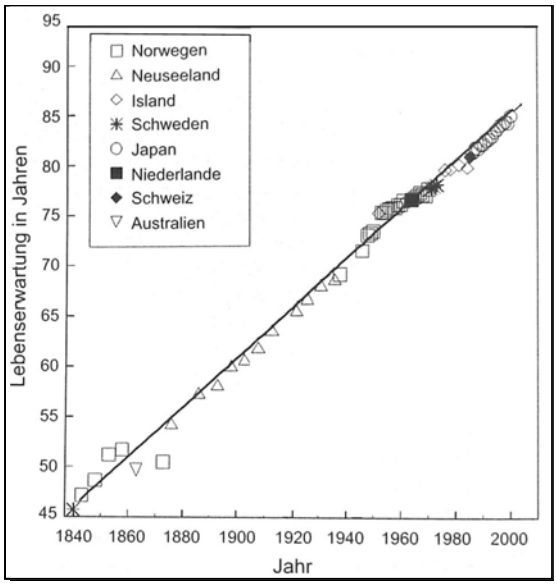

Fig. 1: Record female life expectancy from 1840 to 2002. The linear regression trend is depicted by a bold black line and the extrapolated trends by dashed lines (Oeppen and Vaupel, 2002).

The implications of this shift in demographics are huge and touch all facets of human life – social, political and economic. This change of global demographic structure, and simultaneously the lack of a proper understanding of the aging process, makes the investigation of the underlying principles of the aging process not only a scientifically fascination, but also a social and economical necessity. It is vital that we learn more about the process of aging by probing the molecular mechanisms, and unravel the intricate connections that exist between growing old and disease.

1.2 What is aging?

As aging is such a fundamental and fascinating process, even young children can instinctively tell young from old. However, things become more complicated when it comes to a formal definition of aging. Harman stated that “Aging is the progressive accumulation of changes with time that are associated with, or responsible for, the ever-increasing susceptibility to disease and death which accompanies advancing age” (Harman, 1981). However, the

deficiency of such elaborate definitions is the mix-up of the phenotypes of aging (for example winkle skin, or gray hair) with aging process itself.

Down to the ground, aging can be defined as the increasing risk of death with the passage of time. Systems with constant risk of death are considered as a "non-aging system" (Gavrilov and Gavrilova, 2002). For instance, although radioactive elements decay with time, they are regarded as non-aging systems, since their decay rate is constant along with time. Otherwise, if the failure rate increases with time, we have an aging system (Fig.2).

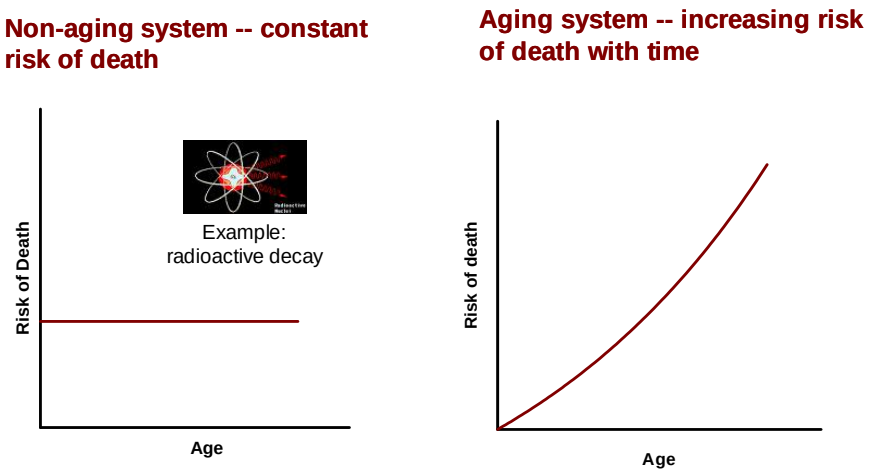

Fig. 2: Definition of aging. Systems with constant risk of decay, such as radioactive elements, are regarded as non-aging systems (left). Systems with increasing decay rate over time are aging systems (right).

Different biological species have widely differing maximum lifespan. Among the shortest lived animals are insects and small *crustacea*, some with a lifespan of less than a week. Human beings have very high life expectancy under mammals. However, there are quite a few species, especially plants that live much longer (Leaman and Beamish, 1984; Thompson and Jones, 1980). Certain plants, like the creosote bush, can reach a lifespan of more than 11,000 years (Vasek, 1980). The enormous variation in lifespan among species hints that lifespan is an adaptation to environmental and ecological constraints.

1.3 Descriptive laws on aging phenomenon

More than 170 years ago, Benjamin Gompertz described that the mortality growth of human and many other species can be approximated by an exponential function (Gompertz, 1825). The extended form of the Gompertz equation, the Gompertz-Makeham equation (Makeham, 1860) reads:

$$m(t) = I \cdot e^{Gt} + E(t) \qquad \textit{(Eq.1)}$$

Here, the parameters “I” represents intrinsic vulnerability of a given population, which can be considered as a measure of basic protection of an organism against failure and damage (error-prone/fault-resistant design). “G” represents the aging rate. It shows how fast this protection deteriorates. “E”, also denoted as “Makeham factor”, represents the external mortality. It is controlled by hazard factors specific to the inhabited ecological niche. Together, the Gompertz-Makeham equation states that the lifespan of a population is related to its genus and the environmental parameters.

When the Gompertz-Makeham function is plotted on a logarithmic scale, the graph becomes linear with the slope being equal to the aging rate “G”. Thus, “G” can be regarded as a measure (the actual biomarker) for the aging rate of a given population (Fig.3). For instance, the time it takes for the intrinsic mortality to double for human is a constant value between 8-9 years. This value has remained unchanged during the past 160 years despite the drastic gains in human lifespan.

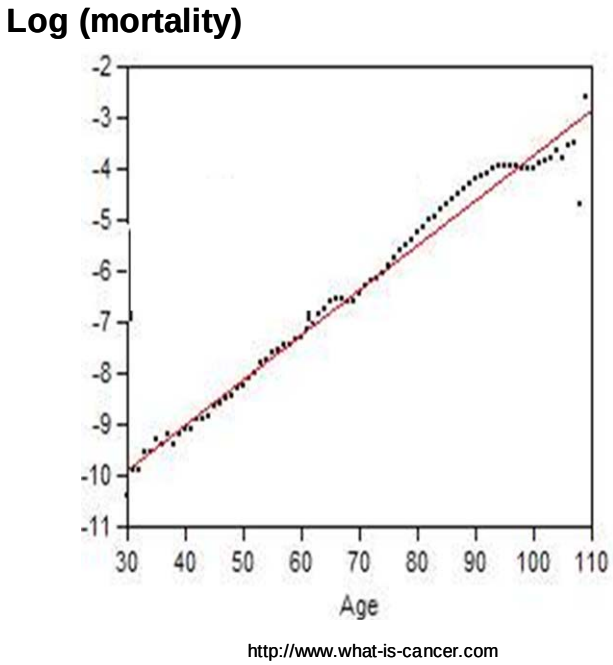

Fig. 3: The time-dependent mortality increase of human can be approximated by the exponential function described by Gompertz-Makeham curves. It shows that human has constant mortality doubling time of 8-9 year.

In contrast to aging rate, intrinsic vulnerability and external mortality stem from environmental risks, e.g. control and elimination of predators, or infectious diseases can alter “I” and/or “E”, and thus alter death toll with advancing age. The Gompertz-Makeham equation splits the mortality rate of biological organisms into two different aspects: intrinsic and extrinsic mortality. In this way, it explains on the one hand the frequently observed species-specific exponentially increasing death rate, and on the other hand the mortality force due to environmental hazard. This equation has since then been widely used in gerontology.

Surprisingly, in the 90s, Carey (Carey et al., 1992) reported that the mortality rate for medflies Ceratitis capitata declined at very old stage, before they finally increase again for extremely old ages (Fig.4). This apparent deviation from the Gompertz-Makeham law was termed “late-life mortality decline”. Similar observations have also been accumulated for human populations, when death rate stops to increase exponentially at around 90 years of ages and levels-off to the late-life mortality plateau around 100 years of age. Importantly, the growing size of elderly populations during the recent years supports that this observation is no false extrapolation due to bad data quality.

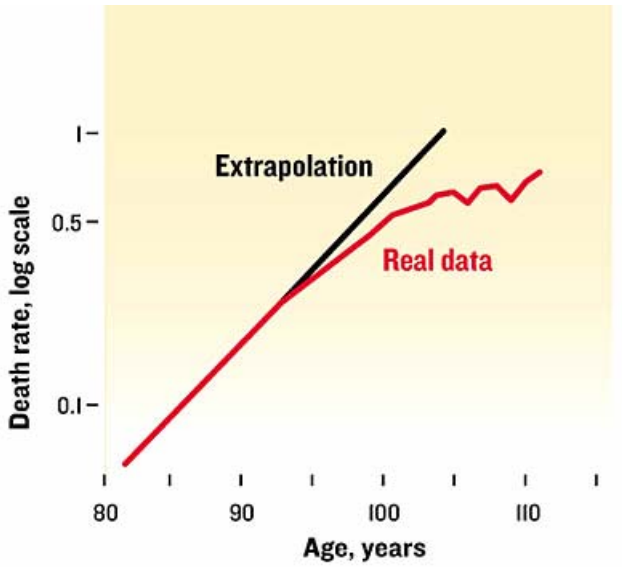

Fig. 4: Human beings and many other species demonstrate late-life mortality decline phenomenon, which deviate from the description of Gompertz-Makeham law.

Such late-life mortality decline transforms the straight line predicted by the Gompertz-Makeham law into a Weibull curve (introduced by Waloddi Weibull, a Swedish physicist in 1939). This strongly limits the descriptive power of the Gompertz-Makeham law.

1.4 Current view of aging mechanism

There are well over 300 theories on aging mechanism (Medvedev, 1990). Most of them are dying due to their old age. In the following, we shall briefly review a selected subset of the remaining ones, among which the rate of living theory could be the oldest.

Rate of living theory

Back to year 1908, the German physiologist Max Rubner (1854-1932) proposed a relation between metabolic rate, body mass and longevity. His idea was that aging rate could be positively correlated to the specific metabolic rate of an organism, defined as metabolic rate per bodyweight. This could explain why lumpy and slow-moving animals (such as turtles or elephant) have longer lifespan than those small and active ones (such as mouse or rabbit). Although intuitive, this rate of living theory is not widely applicable. A typical counter example is the comparison of mice and bats: both of them are small mammals. The brown

bats are almost half the size of house mice, while being more active. The rate of living theory would predict that the bats have shorter lifespan compared to mice. However, the brown bats living in wildness easily surpass 30 years of age, while the house mice only live for 3.5 years.

Telomerase theory

Telomeres are the physical ends of linear eukaryotic chromosomes. They consist of special short repetitive sequences and prevent the chromosome ends from abnormal recombination and degradation (Zakian, 1995). Since DNA can only replicate in the 5'-3' direction (Olovnikov, 1973; Watson, 1972), this results in an incomplete replication of the 3'-end of the telomere during each rounds of mitosis. The germ line, cancer cells and unicellular organisms prevent the erosion of their telomeres by expressing the enzyme telomerase that extends telomeres by synthesizing telomeric DNA *de novo*. However, this enzyme is not universally expressed in most somatic tissues. In 1990, Harley showed that human fibroblast do loose telomeric DNA upon each cell division (Harley et al., 1990). Consequently, telomere shortening was proposed to be responsible for aging (Harley et al., 1990; Harley et al., 1992; Wright and Shay, 1992). It was supposed that extensively shortened telomeres activate certain mechanisms that prevent further cell division, and thus generate senescent phenotype (Hayflick and Moorhead, 1961).

However, subsequent experiments showed that transgenic mice overexpressing telomerase in most tissues showed no increase in their lifespan (Artandi et al., 2002). On the other hand, post mitotic cells like nerve or muscle cells do get old without loosing telomere extensively. During the recent years, it has been established that telomere shortening is likely the cause of cellular senescence (for instance the Hayflick limit of cell division), but its relevance for organism aging remains unclear.

Free radical theory

One of the most popular mechanistic aging theories is the free radical theory. Accordingly, unstable and highly reactive radical species create damage to various cellular macromolecules that gives rise to symptoms which we recognize as aging (Harman, 1956; Harman, 1981).

While most eukaryotes depend on oxygen for their energy production via oxidative phosphorylation in the mitochondria, long term exposure to oxygen is lethal (Joenje, 1989). The sophisticated cellular defense systems like superoxide dismutase, catalase or glutathione peroxidise indicate the size of the threat posed by free radicals.

In fact, the damaging molecular species is not oxygen itself, but reactive oxygen species (ROS) like the superoxide radical (O2.-), hydrogen peroxide (H2O2), or the hydroxyl radical (OH.). Radical possess unpaired electrons. Most of them are very reactive because of the tendency of electrons to pair. The reaction of a free radical with a stable molecule generates another radical. Such events often result in chain reaction in which a single free radical swiftly consumes many stable molecules. It has been observed that the cellular ROS level increases with age in different species including human (Farmer and Sohal, 1989; Jozwiak and Jasnowska, 1985; Sawada and Carlson, 1987; Sohal and Sohal, 1991).

The oxidation of polyunsaturated fatty acid, readily occurs by such a free radical chain reaction (Pryor, 1973). The reaction products, lipid peroxides, change the chemical and mechanical properties of the biological membrane. More than 20 different oxidative DNA damage products are known, among which the levels of 8-hydroxy-2'-deoxyguanosine (OH8dG) (Fraga et al., 1990), thymine glycol or thymidine glycol have been shown to increase during aging (Adelman et al., 1988). Furthermore, hydroxyl radicals cause protein fragmentation (Davies et al., 1987) and amino acid modifications (Garner et al., 2000), which in turn leads to frequent protein aggregation due to altered electronic charge pattern of many cellular proteins.

Since most of the cellular ROS are produced inside of mitochondria, the free radical theory of aging has been extended to the mitochondrial theory of aging. Although still developing, this mitochondrial aging theory appears to be a very promising mechanistic aging theory.

Mitochondrial theory of aging

Free radicals are inevitable by-products of cell metabolism. Most of the cellular radical production originates from the respiration chain of mitochondria, the energy producing organelles of eukaryotes (Halliwell, 1989). Under physiological conditions, 1-2% of the consumed oxygen is converted into free oxygen radicals (O2.-) and subsequently to H2O2 (Joenje, 1989), hydroxyl radial (OH.) and perhydroxyl radical (HO2.).

Mitochondria contain their own genetic material in form of small circular DNA (mtDNA) which codes for a minority of the mitochondrial proteins (Anderson et al., 1981). All the proteins encoded by mammalian mtDNA are exclusively involved in the energy generation pathways. This means that damage to the mtDNA will directly impair ATP production. Therefore it was proposed that the accumulation of impaired mitochondria caused by ROS-induced mtDNA mutations is one of the driving forces of aging (Kowald and Kirkwood, 1999; Linnane et al., 1989; Richter, 1988).

An increasing body of literature suggests a pivotal role of mitochondria in aging and age-related diseases (Harman, 1972; Wallace, 1997). There are evidences showing that the level of mutated mtDNA do increase over time (Boffoli et al., 1994; Brierley et al., 1998; Kopsidas et al., 1998). The study of Khrapko (Khrapko et al., 1999) confirms that a small number of old cells (13%) harbor a high fraction of deleted mtDNA (2-60%). Aiken's group showed that muscle fibers with sections of abnormally low activity of the mitochondrial enzymes cytochrome c oxidase and a high level of succinate dehydrogenase increased with age (Cao et al., 2001; Lopez et al., 2000; Pak et al., 2003).

Therefore, the question was not if mtDNA mutations accumulate with age, but if this accumulation is relevant for the organism aging. The answer to this question is directly correlated with the mtDNA mutation rate.

If the mutation rate is too slow, the efficacy of mitochondrial mutations on aging will be negligible for the organism, since there is not enough time in the lifespan of an individual to acquire mitochondrial mutants to a significant degree. On the other hand, too fast a mutation

rate will obviously lead to certain disease phenotypes, rather than aging. Thus, the value range of mtDNA mutation is the key factor influencing the velocity of functional mitochondrial lost in a living cell. Unfortunately, it is currently difficult to assess the level of mutant mtDNA within living cells. This is due to two reasons: Mitochondria replicate independently from the nucleus. A typical eukaryotic cell contains hundreds to thousands of mitochondria that form a population of independently growing entities. Furthermore, each organelle contains 5-10 copies of mtDNA (Satoh and Kuroiwa, 1991). This leaves room for competition and selection among mitochondria as well as among their host cells.

In an own study (Mao et al., 2006), we made an alternative approach to access indirectly the mtDNA mutation rate by combining a proteomic study and a kinetic model on mitochondrial population. Our mathematical model predicts an increase of the fraction of damage mitochondria with time, leading to a constant increase of oxidative stress with age (see chapter 4.2.2). Combining experimental data, we estimated the mtDNA mutation rate in mice to be in the magnitude of 10E-9 to 10E-8 per mtDNA molecule per day. This value range leaves space for intact organism reproduction, while at the same time supports that mtDNA mutation is an important factor contributing to aging process.

1.5 Shortcoming of existing aging theories

The theories described in the above section represent only a tiny fraction of the existing mechanistic aging theories. Although no consensus exists in the wide pellet of aging theories, one common denominator is that aging is in essence always explained through the aging of organisms' components: Aging of an organism is due to aging of organs, aging of organ is due to aging of cells, and so on. When moving in succession from the aging of organism to the aging or organs, tissue, cells, proteins, we eventually come to atoms, which are known not to age (atoms have constant decay rate independent with time) (see chapter 1.2).

Indeed, recent studies found that many sub-components of biological elements have constant failure rates independent with age. For example, the risk of neuronal cell death is independent of age, but dies at a constant rate in a broad spectrum of age-related neurodegenerative conditions (Burns et al., 2002). These include cerebellum granule cells in mouse model of Parkinson's diseases and Huntington's disease (Clarke et al., 2000). An apparent lack of cellular aging is also observed in the cases of human amyotrophic lateral sclerosis (Clarke et al., 2001), retinitis pigmentosa (Burns et al., 2002; Clarke et al., 2000; Massof, 2002) and idiopathic Parkinsonism (Calne, 1994; Schulzer et al., 1994). This poses us the challenge of how to explain the aging of a system built of non-aging elements?

1.6 Evolutionary theories explore aging at the system level

This question invites us to think about the possible system nature of aging and whether aging may be a property of the system as a whole. One such step ahead is the evolvement of evolution theories of aging, which try to make a bigger picture of the aging phenomenon by integrating natural selection pressure. From the point of evolution, explanations of aging and the limited longevity of biological species are based on two major theories: the mutation

accumulation theory (Medawar, 1952) and the antagonistic pleiotropy theory (Williams, 1957).

1.6.1 Mutation accumulation theory

Medawar was the first to present a theory for the evolution of the aging process based on the idea of mutation accumulation (Medawar, 1952). Accordingly, aging might be caused by an accumulation of deleterious genes that are only expressed late in life. A mutant gene that kills young children will be strongly selected against, whereas a lethal mutation that affects only people over the reproduction period will experience virtually no selection pressure. These late-acting deleterious mutations will eventually accumulate, leading to an increase in mortality rate late in life.

One example of such late-onset deleterious genes could be those responsible for human familial non-polyposis colorectal cancer, which is caused by mutations in genes for DNA mismatch repair (Eshleman and Markowitz, 1996). The median age of onset of this disease is 48 years (Petrelli et al., 1996). Thus, most people that carry this type of mutation do not develop the cancer until they have advanced into their reproductive age.

1.6.2 Antagonistic pleiotropy theory

Pleiotropy describes the effect of a single gene on multiple phenotypic traits. Genes that affect two or more traits are called pleiotropic genes. Effects that increase fitness through one trait at the expense of a reduced fitness of another trait are antagonistic. The antagonistic pleiotropy theories state that late-acting deleterious genes might even be favored by positive selection and be actively accumulated in populations in case they have beneficial effects early in life(Williams, 1957) (traces such as high blood pressure, high cholesterol level. Thus, aging can occur as a side effect of the antagonistic pleiotrpy property of these genes.

One example of such antagonistic pleiotropic genes is the gene for the hormone testosterone in men. In youth, testosterone has positive effects including increasing reproductive fitness. However, later in life, negative effects of this gene come into action, such as increased susceptibility to prostate cancer. Another example is the tumor suppressor gene p53, which also suppresses stem cells regeneration which replenish worn-out tissues (Rodier et al., 2007).

1.7 Limitations of evolutionary theories

Although the evolutionary theories have largely increased our understanding of aging, they have their intrinsic limitations. Firstly, all evolutionary theories have in common that they rely on group selection, the selection of a trait that is beneficial for the group, but could be detrimental to the individual. However, group selection only works under very special circumstances like small patch size and low migration rates (Maynard Smith, 1987), whereas aging is a very general phenomenon that is also observed in many other complex systems (even technical devices) that do not reproduce and therefore are not subjected to evolution through natural selection.

Moreover, the late-life mortality deceleration phenomenon, which has become established in modern society can not be explained by the evolutionary theories. This calls for a more general explanation of this apparently paradoxical “no aging at extreme ages” phenomenon.

Presumably, the particular mechanisms of aging may be very different across systems, even across biological species, but a more general explanation of aging might exist in addition to the mutation accumulation and antagonistic pleiotropy theories.

2 Aim of the Study

The aim of this work was to gain insight into the general mechanism of aging through the system biology approach. This will be achieved by the application of system engineering theory on the experimental data from biological organisms.

3 Methods

The proceeding of the current work can be subdivided into three interconnected parts respecting the route approaching the aim of the study.

3.1 Exploration of relevant theory from system engineering

First, a comprehensive exploration of relevant theory from system engineering field was carried out to discover parsimonious relevant theories on general mechanism of aging.

3.2 Genetic and proteomics analyses at selected levels of detail

In the second part, genetic and proteomic analysis were conduced at selected levels of details, in order to verify the applicability of the theoretical frameworks. This encompasses:

- Analysis of mouse mitochondrial protein alterations during aging for the access of error accumulations in the cells **(Mao et al., 2006)**.

- System disturbance analysis on transgenic mouse embryonic cell lines in order to probe the fault-tolerant property of biological systems **(Mao et al., 2007)**.

- Investigations on mouse brain organogenesis on the establishment of system redundancy in biological organism **(Hartl et al., 2008a)**.

- Study on functional and population dynamics in young and old rat mesenchymal stem cells **(Kasper et al., 2009)**.

- Combined proteomic and transcriptomic analyses on different neurodegenerative disease models in order to elucidate the common aspects between aging and age-related diseases **(Diedrich et al., 2008; Hartl et al., 2008b; Zabel et al., 2008)**.

3.3 System analyses on experimental data

In parallel, system biological approaches were integrated with experimental data for the understanding of the system nature of aging, and to obtain valuable implementations on aging research. This includes:

- Kinetic modeling of the mitochondrial population dynamics to investigate the mitochondrial damage accumulation during aging **(Mao et al., 2006)**.

- Mathematical simulation of reliability model for the access of the influence of system redundancy on system reliability and aging (manuscript in preparation).

- System robustness analysis on protein interaction network to probe the robustness of biological systems **(Mao et al., 2007)**.

- System coherence analysis using Petri-net simulation for the investigation of the relation of cell volume regulation and protein metabolism **(Mao et al., 2008)**.

- Construction of a bioinformatics tool for large-scale data cross comparison and integration **(Nebrich et al., 2009; Zabel et al., 2006)**.

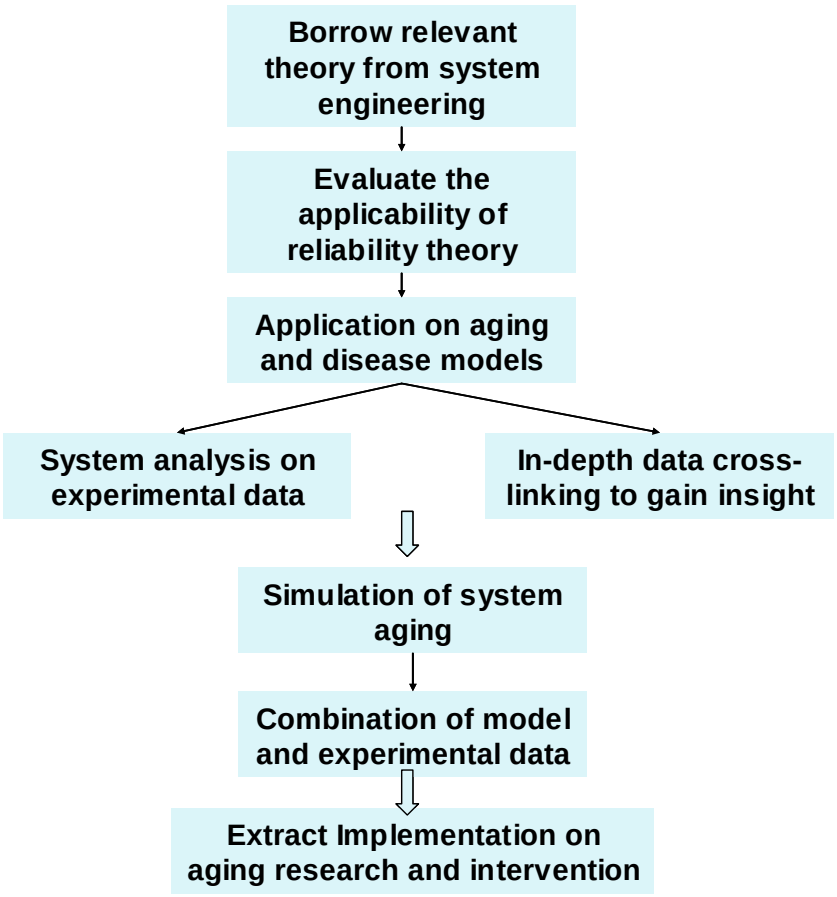

Fig. 5: Workflow of the current work.

4 Results and Discussion

4.1 Reliability theory treats aging as a system phenomenon

Upon exploring a more general aging mechanism, I came across the reliability theory of system engineering (Barlow and Proschan, 1996; Gnedenko et al., 1999). The reliability of a system refers to a system's ability to operate properly according to a predefined standard (Crowder et al., 1991). In turn, the rate of reliability decline is equivalent to the aging rate in demography and gerontology.

The reliability theory states that the fidelity of a complex system can be acquired through the fault-tolerant system design, which is the proper arrangement of system sub-components (Fig.6). If the sub-components are connected in series as a chain of single elements, failure of any one component will lead to the failure of the whole system. In contrast, if sub-components are multiplied and connected in parallel, the system only fails when all components of a given module fail (Fig.6). The most popular fault-tolerant design is a hybrid redundancy structure called series-parallel design (Fig.6b), where modules are connected in series, while subcomponents of each key module present redundantly and are connected in parallel.

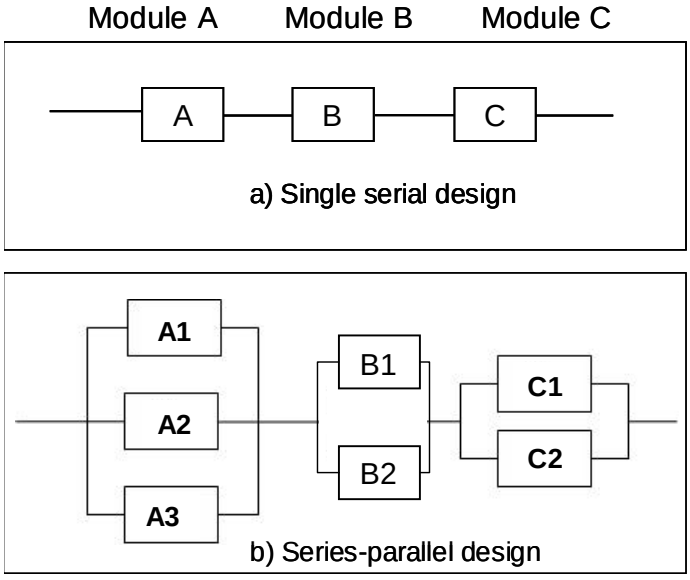

Fig. 6: Comparison of fault-tolerant to non fault-tolerant design. Both systems a and b are consisted of three serially connected modules A, B and C. System a represents a single serial design, where each module contains only one subcomponent. Failure of any subcomponent will lead to overall system outage. In contrast, in each module of system b, system subcomponents are redundant and connected in parallel. Such series-parallel design grants the system with high reliability.

For example, a reliability engineered web server mirrors all their operations by duplicating calculation units (Ghosh et al., 2007). Multiple DNS (domain name system) servers exist for a particular domain, multiple RCDS (resource cataloguing and distribution system) servers for any portion of URI (Uniform Resource Identifier)-space may be registered in each DNS.

Fault-tolerance is achieved by permitting clients attempt to reach multiple servers before declaring failure. By this mean, the failure of one component does not lead to system service outage.

While fault-tolerant design's advantages are obvious, its obligatory disadvantage is central for aging research. One intrinsic disadvantage of such fault-tolerant system is that they are not readily checkable, and thus difficult to maintain. This will cause gradual error accumulation within the system, which leads to decreasing operating quality proportional to the severity of error accumulation.

The reliability theory states that the redundancy reduction of functional *system components over time* is the intrinsic cause of aging. By this means, the reliability theory applies to systems built of non-aging sub-components. This fundamentally deviates from other existing aging theory by explaining aging as a system level phenotype. Thus, the reliability theory could be a refreshing alternative as a general aging theory. In this sense, it is of great interest to investigate whether the reliability theory can be applied on living organism.

4.2 Is reliability theory applicable on biological systems?

Developed on the basis of technical gadgets in engineering field, does the reliability theory also apply to biological systems? The answer to this question depends on three points. First, is redundancy the core design principle of biological organisms? Second, is there a redundancy reduction of system subcomponents with time? Thirdly, do biological systems exhibit extensive fault-tolerant property?

4.2.1 Biological organisms are redundant at different levels

Apparently, from genes to RNA to protein, and to functional module of protein interaction network, biological organisms show many levels of redundancies. Starting from the genetic material, many higher organisms have 2n genome, with each gene appearing twice on two homologous chromosomes. Moreover, as an outcome of gene duplication during the evolution, multiple copies of numerous genes with identical or similar functions exist. This can be verified by the fact that knockout of many proposed essential genes leads to little phenotypic alteration (Vacik et al., 2005).

At the intracellular level, redundancy of the biological system is demonstrated by multiple copies of cell organelles (for example mitochondria); multiple mRNA copy numbers, multiple protein copies from a single mRNA template, just to name a few. At the molecular function level, proof-reading during DNA replication is achieved by different enzymes in parallel, mRNA are translated into proteins by several ribosomes organized as polysomes. At the tissue level, large numbers of cells are usually connected in parallel (muscle cells, hepatocytes, neurons) to form a tissue**.** Many essential organs are connected in parallel inside of a given functional module (two kidneys, two ovaries, lungs, several liver lobes, etc).

Taken together, redundancy structure appears to be the fundamental design principle at diverse levels of the biological system. This provides the basis for applying the reliability theory on living organisms.

4.2.2 Biological systems show extensive error accumulation

Down to the ground of genetic materials, the accumulation of somatic DNA mutation is an established fact (Pichiorri et al., 2008; Suh and Vijg, 2006). However, genetic material also exists in the form of mtDNA in eukaryotes. This prompted us to ask whether there is a redundancy reduction of functional mitochondria over time. This issue was investigated in mouse as a model **(Mao et al., 2006)**.

In a study on mitochondrial protein profile during mouse aging, we observed that there is a lost of functional mitochondrial respiratory chain proteins with time. Proteins with decreasing cellular concentration were observed in mitochondrial respiratory complex I and IV. This clearly indicates an accumulation of mtDNA mutations (Bruno et al., 1999; Rahman et al., 1999).

However, an extensive redundancy has been introduced by nature to make the respiratory system highly fault tolerant. Most cells contain hundreds to thousands of mitochondria, while each mitochondrion contains 5-10 copies of mtDNA. Variant mtDNAs co-effect to cause gene actions, which in turn result in cell actions (oxidative phosphorylation). The accumulation of mutated mitochondria with time is a consequence of the interplay of different components of a complex system. This includes the damage of free radicals to mitochondria, the competition of intact and mutated mitochondrial subpopulations, as well as the degradation kinetics of different mitochondria. Thus, the real strength of functional mitochondrial lost cannot be accessed without quantitative discussion.

Based on previous knowledge (Kowald and Kirkwood, 2000) and the data structure of our proteomic investigation, we constructed a mathematical model of the mitochondrial population dynamics considering the following points (Fig.7):

- Mitochondria are the main producer and targets of free radicals.
- Damaged mitochondria generate more radicals and less ATP.
- Since all genes necessary for mitochondrial replication are located in the nucleus, damaged mitochondria have a replication advantage over wild type mitochondria.

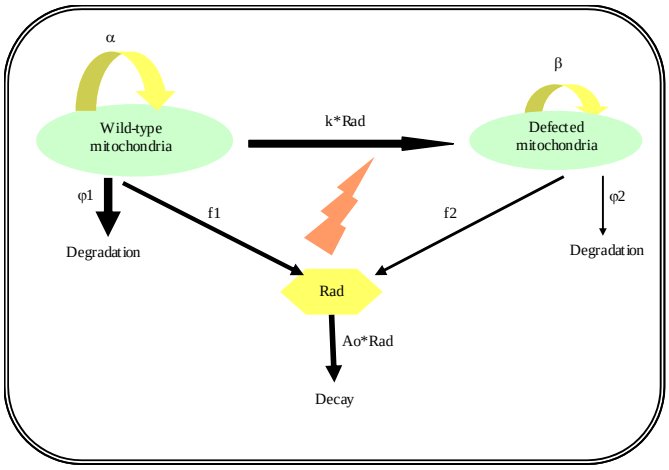

Fig. 7: Biochemical reactions described by the kinetic model. Two different classes of mitochondria were considered, those with intact genomes (Mw) and those with mutated genomes (Mm). The different classes produce different amounts of free radicals, which cause the transition of mitochondria from wild type to mutated type. Wild type and mutated mitochondria undergo reproduction and degradation at different rate constants.

This is a non-linear single compartment model with a set of three ordinary differential equations describing the dynamics of three species of the cell: wild type mitochondria (Mw), mutated mitochondria (Mm) and free radicals (Rad) (Fig.8).

$$\frac{dMw}{dt} = \alpha \cdot Mw \cdot (A - Mw - Mm) - k \cdot Rad \cdot Mw - \varphi_1 \cdot Mw$$

$$\frac{dMm}{dt} = \beta \cdot Mm \cdot (A - Mw - Mm) + k \cdot Rad \cdot Mw - \varphi_2 \cdot Mm$$

$$\frac{dRad}{dt} = f1 \cdot Mw + f2 Mm - \varphi_3 \cdot Rad$$

Fig. 8: A set of three ordinary differential equations describes the interaction of system components influencing the mitochondrial subpopulations. The first and third term in equation 1 and 2 represent the synthesis and degradation of the healthy and defective mitochondrial sub-populations, respectively. The second terms in Eq 1 and 2 describe the mutation reaction that transfers wild type mitochondria into mutated mitochondria.

This set of differential equations was solved numerically employing fourth order Runge-Kutta method. As shown in figure 9, our model faithfully predicted the proposed accumulation of defective mitochondria, and therefore a redundancy lost of functional mitochondria over time. According to the experimental data on mice, only around 30% of the functional mitochondria were still present in old stages (700 days).

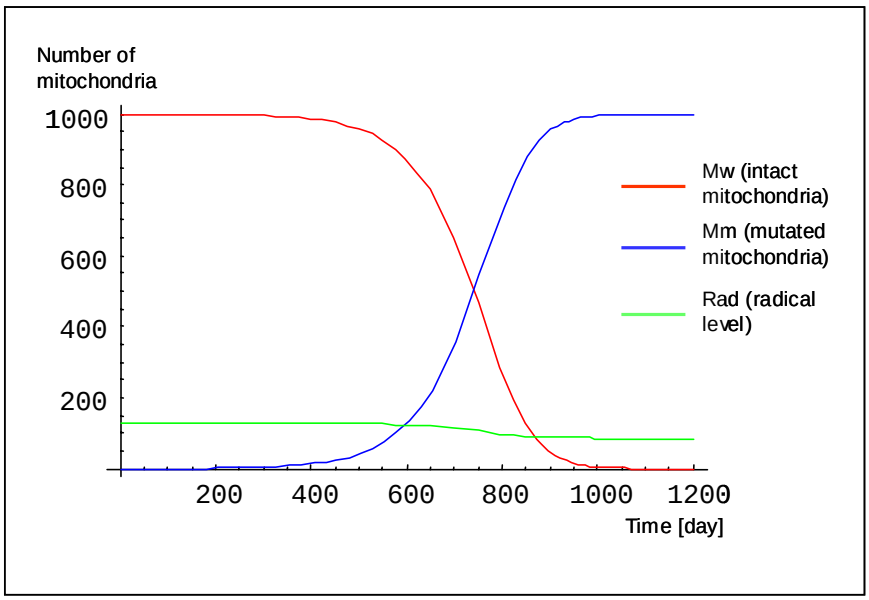

Fig. 9: Simulation results showing time courses of the components of the mathematical model on the mitochondrial subpopulation kinetics inside of a mouse cell. The population of wild type mitochondria decreased, while the number of mutated mitochondria in a cell increased with age.

Our observations support the hypothesis that the constant event of free radical induced mtDNA mutation causes a significant redundancy lost of functional mitochondria in the cellular system with age. Therefore, the mitochondrial influence on aging follows perfectly the redundancy lost principle proposed by the reliability theory.

4.2.3 Biological systems are tolerant against genetic perturbations

The best means to test whether living systems are genius fault-tolerant systems is to probe their fault-tolerant property. Fault-tolerance means that failure of individual component does not lead to system service breakdown. If this hypothesis holds, then small system perturbations should not lead to major system outcome. To test this, we investigated whether there exists such self-stabilization property in the biological system.

For this purpose, we carried out a system perturbation study (Mao et al., 2007) on a representative cellular system, the mouse embryonic stem cells. Specifically, we carried out investigations on six murine embryonic stem cell lines either overexpressed individual genes or displayed aneuploidy over a genomic region encompassing 14 genes. Proteins expressed in the cells were investigated by 2-D electrophoresis and altered protein expressions were recorded by comparison with the respective parental lines.

Our results showed that there is indeed an intrinsic balancing capacity of the cellular system upon genetic disturbances: At the phenotypic level, no difference was observed between transgenic and parental cell lines with respect to cellular morphology and growth behavior. All cell lines appeared healthy and were capable of effective germ-line transmission,

indicating the effective damping of the genetic perturbations. At the proteomic level, although a number of proteins showed significantly altered expression compared to their parental cell lines, no significant difference could be detected in the protein amount undergoing up and down-regulation (Fig.10). Most importantly, this was even true for the two cell lines with 14 genes altered, which showed a drastic imbalance in the number of proteins that underwent up or down-regulation. Accordingly, we assume that when the quantitative arrangement of the proteome is perturbed by gene dosage effects, it will be subjected to a rearrangement in order to achieve a new balance.

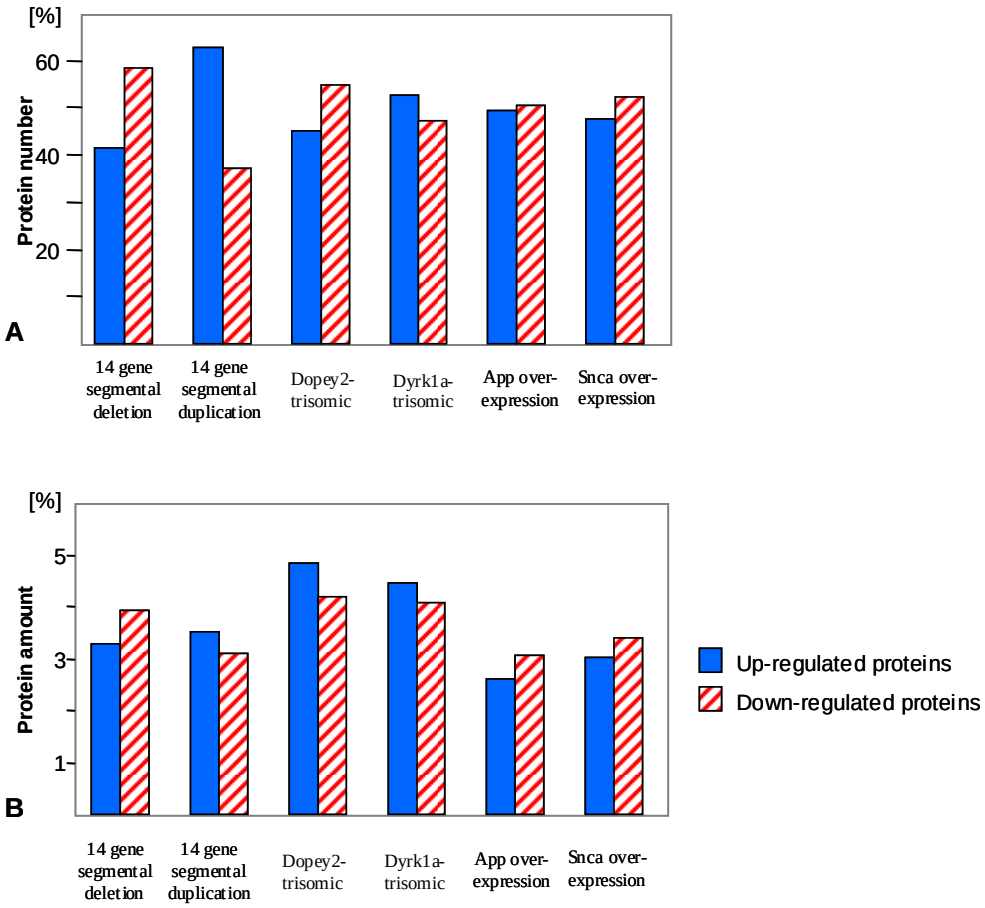

Fig. 10: Proteins that showed altered expression in transgenic ES cell lines. A: Number of altered proteins in each transgenic cell line, expressed as percentile of total number of altered proteins. B: Amount of proteins that underwent altered expression in each cell line, represented as percent of total spot volume that was up or down-regulated in transgenic cell lines. Dose alteration of 14 genes could no longer be balanced by an equivalent number of variant proteins. However, a balance remained at the level of protein concentrations.

When we investigated proteins that showed quantitative changes among the six cell lines with profound system analysis, we made the observation that the cellular proteome is kept quantitatively in balance by a particular class of proteins to which we refer as “balancer proteins”. Here, we proposed the balancer proteins as a class of proteins within the proteomic network that buffer or cushion a system, and thus oppose multiple system disturbances.

Applying the reliability theory, the balancer proteins could represent the highly redundant sub-components in the proteomic network (Fig.11). This view is further supported by the following points:

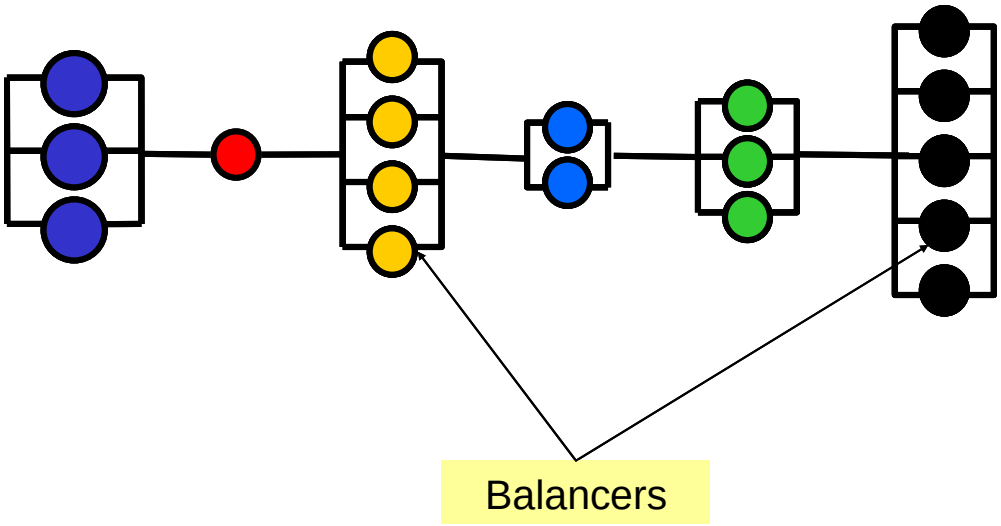

Fig. 11: Proposed position of "balancer" proteins in a fault-tolerant protein interaction network. Based on our observations, "balancer" proteins could be highly redundant system subcomponents inside the protein interaction network.

Firstly, balancer proteins were significantly more abundant in the cell (p=0.008). This suggests their high redundancy in the cellular proteome. Secondly, balancer proteins possess a low number of direct interaction partners. This indicates that they are predominantly internally connected in the respective network subgraph. Thirdly, balancer proteins had significantly more non-synonymous SNPs in their coding regions. Protein polymorphisms indicate proteins which became less constrained in the course of evolution (Khaitovich et al., 2005). As a consequence, proteins bearing a higher degree of polymorphisms may tend to be more flexible in their quantitative range. This again supports their redundant property. Regarding their functional aspects, the majority of the balancers are involved in protein chaperoning and catabolism processes. This highlights the importance of the proper maintenance and recycling inside of a highly evolved complex cellular system.

Next, we carried out an in-depth analysis of the robustness of the cellular protein interaction network. This is motivated by concepts from statistical mechanics and dynamical systems theory (Demetrius et al., 2004). The protein-protein interaction graph constructed from our data comprised 2677 nodes (distinct proteins, indicated by gene symbol). 96% of them could be linked to a giant network component with heterogeneous degree distribution. Figure 12a shows a subset of the protein-protein interaction network centered on the proteasome subunits. Noticeably, all balancer proteins belonged to the giant network component. This reinforces the central role of these balancer proteins in the preservation of proteomic network integrity.

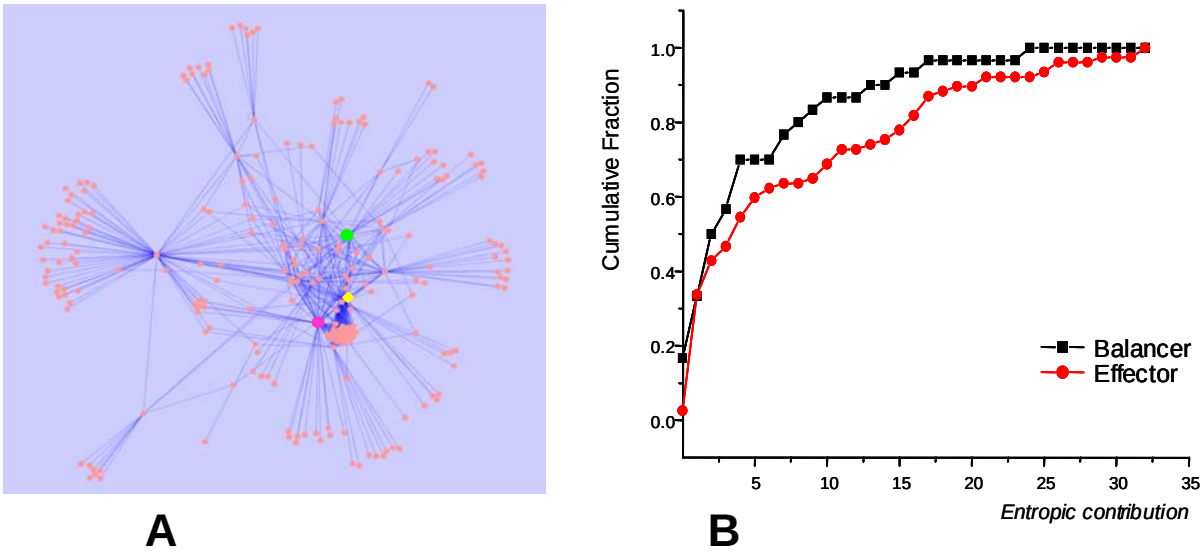

Fig. 12: System analyses on the protein interaction network suggest the contribution of redundant subcomponents proteins ("balancer") on the system reliability. A: Protein interaction subgraph showing the proteasome subunits, where notes denote proteins and the edges describe protein-protein interaction. B: Cumulative fraction plot of network entropy shows that "balancer" proteins contribute significantly higher in system robustness.

A resilience analysis showed that balancers possess significantly higher values of entropic contribution to the protein interaction network (Fig.12b). As network entropy is a measure of system robustness, this suggests that these proteins are of high importance in terms of system robustness. Together, the existence of such balancer proteins supports that the fault-tolerant protein interaction network is realized through the redundant system sub-components.

4.2.4 System redundancy is established during organogenesis

In the above sections, we see that the unit of the biological organism, the cell, can be considered as genius fault-tolerant system. Since multi-cellular biological organisms have come into being from a single fertilized egg, it is of interest to investigate how the fault-tolerant property is established during the early development of an organism. This process can be very nicely monitored at the proteomic level.

In a study on mouse embryonic brain development (Hartl et al., 2008a), we analyzed mouse brain samples at embryonic day 9.5 (E9.5), where mostly undifferentiated neuronal precursor cells are present, E11.5 when neuronal precursor cells start to differentiate into neurons, and E13.5, when neurogenesis is maximized. When the expansion phase (E9.5) was analyzed, we observed a significant increased expression of metabolism related proteins. This indicates that during this early organogenesis period, the major effort of the living system was the pure cell proliferation by symmetric mitosis. Such proliferation of neuronal precursor cells is the key process necessary to produce a sufficient number of cells for brain as a tissue, and at the same time for the brain to acquire the fault-tolerant property.

In contrast, the goal of the neurogenesis phase (E13.5) is the differentiation of neuron lineage and glial cell lineage via asymmetric mitosis. The shift from proliferation to neuronal differentiation is expressed as a significant decrease of metabolic and other house-keeping protein expressions, accompanied by a significant up-regulation of the neuro-specific proteins. Taken together, our investigation on mouse brain development shows that system redundancy in the mouse brain is established during the organogenesis through a two-step schedule: First the increase of system redundancy, then the increase of system complexity.

In summary, these studies provide strong evidences that the living system show extensive fault-tolerant property at both the cell physiological and the protein interaction network levels. We therefore conclude that the reliability theory can be applied on living systems.

4.3 Reliability model: simulation and implementations

In order to explore the influence of system redundancy design on system nature of aging, we set out to construct a mathematical model applying the reliability theory on living organism. Consider a reliability model of a simple parallel system with **n** initial elements. The redundancy degree of the system equals ***n***. We further assume that all elements are non-aging, but fail randomly and independently with a constant failure rate. The reliability of each single system component is denoted as ***p***.

System reliability ***R(t)*** is the probability of the system not failing during the period [0, t]. Since a simple parallel system looses its reliability only when all its redundant subcomponents fail, the system reliability ***R(t)=f(p, n)*** can be calculated as:

$$R=1-(1-p)^n. \qquad (Eq.2)$$

For $p=0.5$ and $n=3$, we have:

$$R=1-(1-0.5)^3=87.5\%. \qquad (Eq.3)$$

We see that although the reliability of a single component is very modest (p=0.5), the redundancy leads to a system overall reliability of over 85%. This value increases rapidly as the redundancy degree of the system increase. This exemplifies that high system reliability can be effectively achieved through system redundancy. In the following, we will see that this is at the cost of the increasing system failure rate (or aging rate):

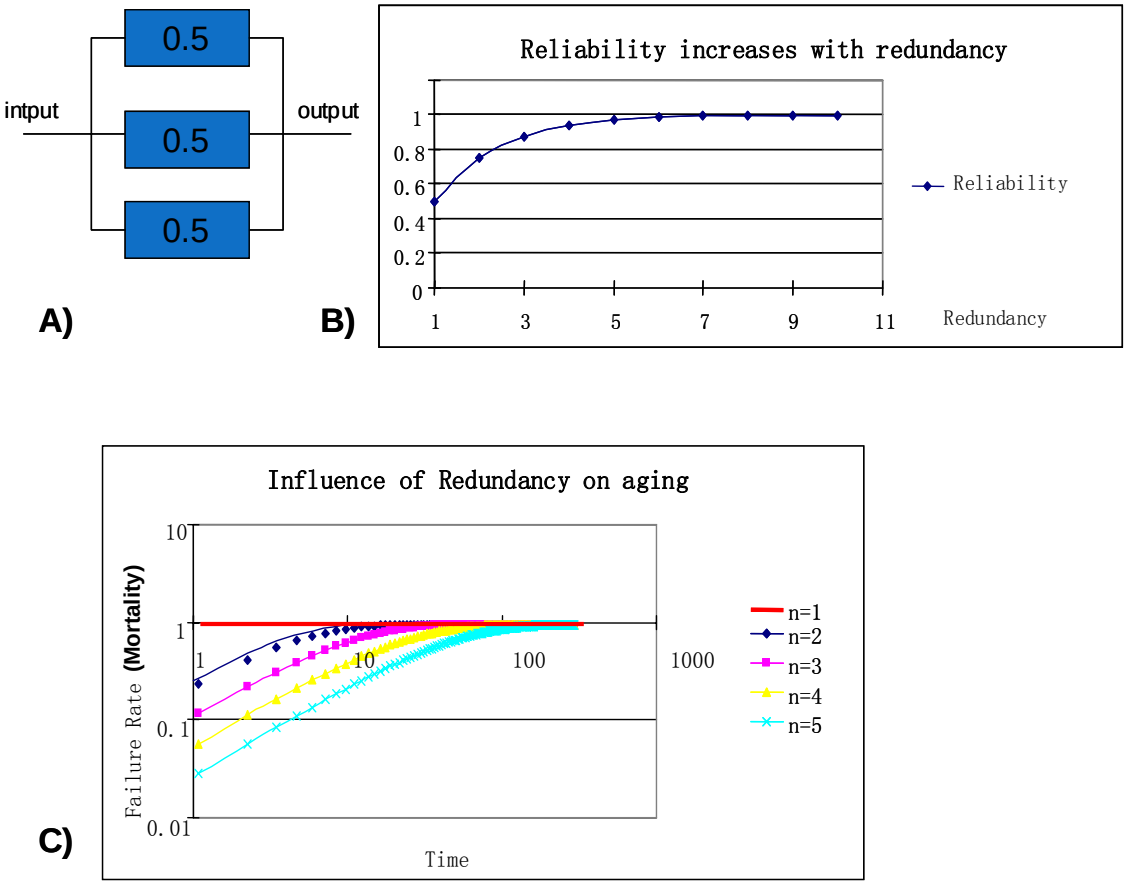

Fig. 13: An example calculation shows that system redundancy leads to high system reliability, but at the same time aging phenotype. A: Schematic illustration of a simple parallel system with 3-fold redundancy (the reliability of single component p=0.5). B: The system reliability increases rapidly with increasing redundancy. C illustrates that the failure rate (mortality rate) of the system increases drastically with the increasing redundancy degree.

As shown in Figure 13c, if no redundancy exists (n=1), the system has a constant mortality, thus exhibiting a non-aging property. As the redundancy increases (n≥2), a system constructed of non-aging elements starts to behave like an aging one, with its increasing mortality acceleration (aging rate) positively correlated with its redundancy degree. In fact, the mortality rate initially grows exponentially with time, following the Gompertz-Makeham law.

Applying to the biological system, when a single component system (*such as enzymes, viruses or microbial spore*) is exposed to hostile environment such as heat, their survival curve obeys virtually a non-aging mortality kinetics, showing linear semi-logarithmic form (Gouda et al., 2003; Kundi, 1999; Peleg et al., 2003). In contrast, the application of two-fold redundancy already leads to fault avoidance, but not extensive damage accumulation. High redundancy support genius fault-tolerancy, but also extensive damage accumulative, which leads to increasing failure rate with age, or otherwise called aging.

In an own study on the molecular aging phenotype of rat mesenchymal stem cells (MSC) (Kasper et al., 2009), we showed that on the one hand, there was a partial exhaustion of

progenitor cells probably due to apoptosis. The yield of MSCs in old donor was largely reduced. But importantly, it could be confirmed that the differentiation potential remained virtually untouched in young and old MSCs (Leskela et al., 2003). This provides evidence that MSCs are *per se* non-aging subcomponents. Their redundancy reduction is chief for the system level aging of adult stem cell populations.

At advanced age, the acceleration of the failure rate declines. The failure rate asymptotically approaches an upper limit equals to the failure rate of the single subcomponents, when no more redundancy exists. This transforms the time-dependent mortality rate from a straight line into a Weibull curve. This is the "no-aging at extreme old age" phenomenon observed in many species including human. Such "late-life mortality decline" becomes obvious only when the lifespan of a given biological species prolongs extensively due to the decreasing hazard factors in the ecological niche. This gives a logical explanation for the late-life mortality decline phenomenon that has been observed for human and some other species.

Thus, aging can be regarded as a direct consequence of the system's redundancy. Comparing to technical devices, the extraordinary degree of component miniaturization of biological systems (*the microscopic dimensions of cells, DNA and RNA*) permits the creation of a tremendous redundancy in the number of elements. This explains its extensive aging phenotype. Notice that the reliability model explains very elegantly both the observations made by Gompertz, and the "late-life mortality deceleration" phenomenon.

Importantly, implementation of this reliability model provides some insights for aging research: First, the obligatory error accumulation of the fault-tolerant system suggests that there could be some common origin among aging and late-onset diseases. Secondly, the reliability theory states that aging is primarily a phenotypic expression of different error accumulation. Therefore, research on aging should not be limited at the levels of qualitative changes (such as "aging genes" or "anti-aging genes"), because changes in quantity represent a more fundamental driving force of the aging process. Moreover, since damage accumulation is the true reason for aging, it can be alleviated through constant subcomponent renewal aiming at a delayed error accumulation. In the following, we discuss these points regarding their impact on aging research.

4.4 Possible common fatal origin for aging and age-related diseases

In the above section, we have shown that biological system can be considered as genius fault-tolerant system, whose high system subcomponent redundancy was established during organogenesis. Here, we asked what is the consequence should such embryonic established system redundancy be disturbed by gene mutations. For this purpose, we investigated different mouse models on age-related neurodegenerative diseases. Our aim was to see whether there is an intrinsic relation between aging and age-related diseases.

4.4.1 Impairment of neuronal plasticity proceeds Alzheimer pathology

Alzheimer disease (AD) is a typical late-onset neurodegenerative disease in human. Amyloid precursor protein (APP) is an important neuro-morphoregulatory protein, whose

overexpression and mutation can leads to idiopathic AD (Arendt, 2005). In a study of us on AD mouse model **(Hartl et al., 2008b)**, we compared the brain proteome of wild type and *App*-mutation mice at different age stages (from embryonic day 16 to 15-months). In this mouse model, the mutated APP transgenic expression started stably prior to embryonic day 16 and is sevenfold higher than endogenous APP expression. These mice show prominent amyloid plague phenotype starting from 6 month of age (Bornemann and Staufenbiel, 2000; Kuo et al., 2001).

We observed that brain maturation was severely impaired by APP mutation at age stages largely precedes AD pathology. This is inline with previous findings that Alzheimer disease is preceded by a long clinical silent period of several years to decades (Arendt, 2003; Lanz et al., 2003). Importantly, a significant number of protein alterations related to adolescent neuronal development in healthy young mice (2 month old) were largely absent in APP transgenic mice. The developmental period around two months of age represents adolescence in mice. At this age, mesocorticolimbic brain regions are exceedingly plastic in terms of synaptic reorganization and adult neurogenesis (Blakemore, 2008; Spear, 2000). APP is highly involved in neuronal plasticity associated dynamics (Gralle and Ferreira, 2007; Turner et al., 2003). APP mutation presumably alters dendritic spine number, morphology and dynamics of hippocampal neurons (Calabrese et al., 2007; Shrestha et al., 2006). This may cause a long-term impairment of the neuronal network, finally resulting in memory impairment in aged mice, when the redundancy reduction of functional neurons becomes predominant.

In conclusion, this study revealed that the APP mutation during brain organogenesis leads to early-stage redundancy lost of functional neurons, expressed as a decrease of neuronal plasticity. However, disease phenotype appears much later due to the intrinsic fault-tolerant property of the biological systems.

4.4.2 Initial decrease of system redundancy leads to Huntington pathology

Huntington's disease (HD) is an autosomal dominantly inherited monogenic disorder that usually appears in midlife in men (Wexler et al., 1991). The disease-triggering mutation consists of an unstable, elongated CAG trinucleotide repeat at the 5'-end of the Huntingtin gene. This cytosine-adenine-guanin repeat codes for a variable length of glutamines residues, which leads to illegitimate protein cross-linking and aggregation *in vivo* (Readercomment, 1993).

In a detailed time course study on a HD mouse model (Zabel et al., 2009), we investigated the disease kinetics of R6/2 mice for changes in the expression levels of brain proteome, starting prior to phenotype onset and continuing through the end stage of the disease. Similar as in the study on AD mouse model, we observed that extensive protein alterations already occurred at 2 weeks of age. In fact, the number and identity of protein alterations was equivalent to those found at the end stage of disease and showed a significant overlapping cellular pathways. We concluded that a perturbed expression of the transgenic fragment of Huntingtin significantly disturbed the delicate equilibrium of protein expression during normal development.

Taken together, such disease-triggering mutations disturb the development of the living system at very early phase (during the organogenesis). This leads to an initial redundancy reduction of functional subcomponents in that it increases the fraction of initial non-functional subcomponents. However, due to the fault-tolerance property of the system, these disturbed systems do not necessarily show pathological phenotypes immediately. It is the redundancy reduction along with time that leads to exhaustion of system reliability, and in turn the phenotypic prevalence. This correlates well with the late-onset properties of such mutation-led neurodegenerative diseases.

In the following, we shall see that this rational is even applicable when the genetic manipulation is not a disease-causing mutation, but an overexpression of a normally protective physiological molecule in mouse.

4.4.3 Transgenic mice are more vulnerable to Parkinson pathology

Parkinson's disease (PD) is one of the most common neurodegenerative disorders that affect approximately 3% of a population beyond the age of 65 years (Smeyne and Jackson-Lewis, 2005). One hallmark of PD is the degeneration of dopamine neurons in *substantia nigra*. Treatment of mice with the neurotoxin 1-methyl-4-phenyl-1,2,3,6-tetrahydropyridene hydrochloride (MPTP) is a well established animal model for induced Parkinsons disease (Mitsumoto et al., 1998; Schober, 2004). The metabolic product of MPTP (MPP^+) inhibits complex I of the mitochondrial electron transport chain and thus impairs oxidative phosphorylation. This results in severe leakage of ROS, and finally the death of dopaminergic neurons (Mitsumoto et al., 1998; Schober, 2004). Chronic MPTP toxicity causes prolonged inhibition of the mitochondrial respiratory chain and ubiquitin-proteasome activity, which constitutes prerequisites for the formation of Lewy bodies (Fornai et al., 2005; Tanaka et al., 2001).

The L1 cell adhesion molecule (*L1cam*) has been proposed to protect the dopaminergic neurons from degeneration during the development of Parkinson's disease. *L1cam* acts as a homophonic cell adhesion molecule. When triggered by a trans-interacting *L1cam* molecule from a neighboring cell or in the extracellular matrix, *L1cam* enhances neuronal survival and neurite outgrowth of dopaminergic neuronsin *in vitro* and *in vivo* (Hulley et al., 1998; Wolfer et al., 1998).

In an attempt to investigate the effect of *L1cam* on the MPTP response, we investigated protein expression patterns after MPTP-treatment in both wild type and transgenic mice overexpressing *L1cam* in the acute phase of MPTP toxicity (1 day after MPTP injection) and in the recovery phase (7 days after MPTP treatment) (Mitsumoto et al., 1998) **(Diedrich et al., 2008)**.

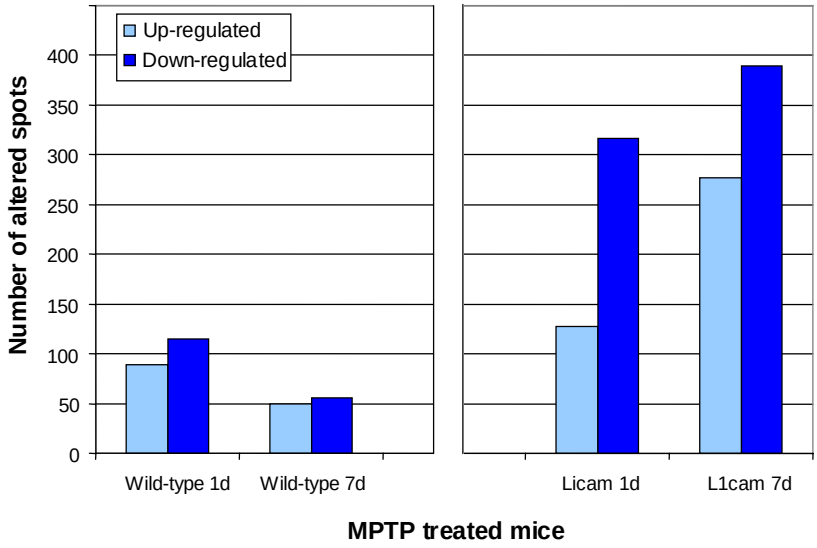

Fig. 14: Proteomic analysis on drug-induced PD mouse models. The bar chart shows the number of up- and down regulated proteins on day 1 and day 7 after MPTP-treatment in wild type and L1cam transgenic mice.

As shown in Figure 14, significantly more proteins were altered in *L1cam* transgenic than in wild type mice. The numbers of variant proteins in transgenic mice continue to increase from acute phase to recovery phase, indicating a further exaggeration of the PD pathology in *L1cam* mouse. This observation indicates a much stronger toxic effect of MPTP in transgenic than in wide type mice, thus clearly oppose previous description on the protective effect of *L1cam* on PD pathology (Wolfer et al., 1998).

Based on the reliability theory, we ration that although *L1cam* molecule acts protective for the neurons in the physiological condition, the overexpression of this protein primarily disturbs the embryonic development of the brain **(Hartl et al., 2008b; Zabel et al., 2008)**, assumedly in that it causes a predisposed reduced redundancy of functional subcomponents in the tissue. In turn, the drug treatment on transgenic mice requires additional compensatory effects of the affected tissue. This may explain an exaggerated response of *L1cam* transgenic mice to PD pathology.

Putting our observations on aging and age-related diseases into the theoretical framework of reliability theory, we propose that adult degenerative diseases and aging could be outcomes of the same fetal program. The stochastic events in early development generate personalized damage patterns, which in turn determine late-life aging and survival (Sapolsky and Finch, 2000). In this sense, there may be no specific elementary “aging process” *per se*. Any “therapy” against partial aspect of age-related changes will contribute to the delaying of aging. This opens a new field to be explored approaching personalized anti-aging medicine.

4.5 Anti-aging should target quantitative aspects

In order to approach anti-aging medicine, a first necessary step would be to elucidate the quantitative aspects during aging and age-related diseases. In this sense, a large-scale cross

comparison of models on aging and different age-related diseases would be essential. For this purpose, we developed a software tool that bears superior data cross-comparison capability **(Nebrich et al., 2009)**.

Through a sophisticated comparison of these large-scale studies, where aging is either alone or put in the contrast of different disease models, it was revealed that there is large overlap among different age-related diseases and aging **(Zabel et al., 2006)**. Specifically, the lost of redundancy is expressed quantitatively as three major aspects at the intracellular level: loss of functional mitochondria, loss of functional chaperons and the lost of functional proteasomes.

4.5.1 Proteasome Reduction represents a chief quantitative aspect in aging

Most prominently, in all these mouse models (Diedrich et al., 2008; Hartl et al., 2008b; Zabel et al., 2008), one of the consistent global findings was a down-regulation of protein involved in the ubiquitin-proteasome pathways. This encompasses of a total of 10 protein subunits in mouse proteasome.

In a mouse aging model, we investigated the whole process of mouse brain development, adulthood and aging (Manuscript in preparation). The severity of the redundancy lost of different protein categories with age were accessed with the help of a reliability model. Unlike other protein categories investigated, the aging rate of proteasome system is much higher than dictated by its system redundancy degree.

In contrast to non-living systems, cellular proteins are under constant recycle via either proteasome or lysosomal systems. The proteasome system therefore represents the constant renewal mechanism, which is most important for the maintenance of a fault-tolerant system. This raised the question what leads to a reduced function of the proteasomes in the aged?

4.5.2 Cellular dehydration could be responsible for proteasome function decline

In a parallel study, where we investigated cellular dehydration in both aging and age-related diseases, our attention was drawn on the relation between cell volume regulation, proteasome function and aging **(Mao et al., 2008)**. Here, we subjected the cells to altered osmotic environments (culturing in either hyper-osmotic or hypo-osmotic mediums) to probe the impact of cellular water content on cell physiology. Combining this basic experiment with system coherence analysis (Petri-net simulation), we see that cell biochemical functions are intrinsically connected to the cellular water content. The alteration of cell volume directly influences protein synthesis, protein maturing and proteasome-mediated protein degradation (Fig.15).

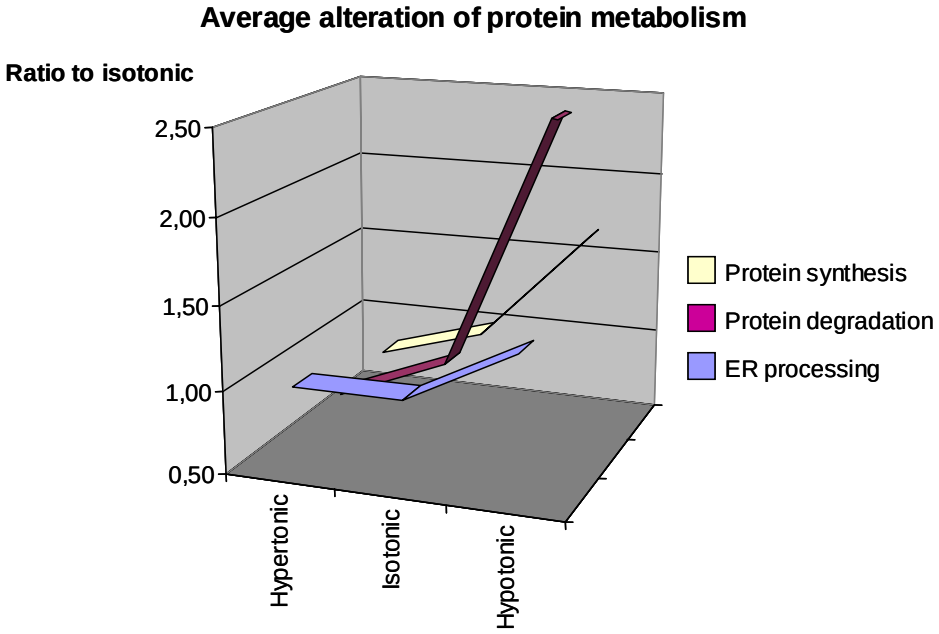

Fig. 15: Effect of cellular water content on protein metabolism in mouse embryonic stem cells. We observed up-regulated protein degradation in hypoosmotic culture condition, and a down-regulation of protein degradation in dehydrated cell.

Water-lost in cells along with time due to the altered charge pattern of the proteome will influences directly the proteasome function, and in turn impairs overall system repair mechanism (Lang et al., 1998). Protein aggregation in different age-related degenerative diseases is another indication for the cellular water loss. This suggests that the loss of cellular water might be a central aspect of system aging.

4.6 Possible Intervention on aging

The ultimate goal of aging research is to explore the scientific means aiming at elimination or reduction of many of the painful conditions that people experience as they grow older. The reliability theory implies that aging is a collective phenotypic expression of different levels of damage accumulation. Accordingly, strategies for anti-aging must tackle different quantitative aspects. In the following, we discuss a few points of possible aging interventions:

Early-life interventions

The redundancy of the biological system was largely established early in the organogenesis stage. Due to a lack of control at embryonic stage, living organisms could be confronted with a high initial load of damage, and therefore their lifespan and aging patterns may be sensitive to early-life conditions. Thus, means aiming at reduction of the early damages could contribute to aging retardation. This would include the prenatal prevention of mutations or the better protection of embryonic development. Specifically, the birth process in mammals could represent a high damage phase due to the sudden exposure of the fetus to a high oxygen environment (Gavrilov and Gavrilova, 2004). Strategies purposing the reduction of ROS insult on newborns could be helpful on delaying aging. Surely, such rationales need to be verified in the future.

Reinforce the system renewal mechanism

A more secure but complicated solution of aging intervention could be based on more rigorous repair to achieve delayed aging in the fault-tolerant system. This means that aging can be retarded through the constant detection and exchange of defective system subcomponents to prevent extensive damage accumulation. In the computing technology, Georgiadis proposed that, with the constant exchange of components, the system will remain well formed with respect to its failure rate (Georgiadis and J., 2002). Due to the high maintenance cost, however, this strategy is not commonly applied in engineering field. However, this strategy could represent a promising opportunity for promoting human health and longevity. For instance, it is imaginable to train the immune system to detect and eliminate non-functional cells and delete them along with time, the same way as they act against cancer cells. Together with regenerative medical approach, this will lead to a personalized anti-aging therapy.

In this scenarios, another anti-aging strategy could be to stimulate the system renewal mechanism though manual interference. It has been proposed in the aging research community (Kowald, personal communication) that constant attack on mitochondria using dedicated antibiotics could help to maintain the general quality of cellular mitochondria, and therefore contribute to aging retardation.

Recently, two independent research groups identified “forkhead box O3A” (*Foxo3A*) as a significant centenarians-related gene (Willcox et al., 2008). They found that a variant of this gene containing certain SNP pattern is strongly associated with longevity in humans. *Foxo3A* is involved in the insulin/IGF-1 signaling pathway. Deregulation of this transcription factor is involved in tumorgenesis such as acute leukemia (Myatt and Lam, 2007). Presumably, *Fox3A* triggers apoptosis of defective cells and thus could be actively involved in the selective detection and elimination of non-functional system subcomponents.

4.7 Ethical aspects of aging interventions

Not everyone agrees that it is desirable to pursue life extension scientifically. Two types of objections that are frequently brought forward are ethical aspects and that anti-aging could be against the natural law.

The most often raised ethical objection is that a possible life extension therapy will be very expensive and can therefore not be provided for everyone. This could create injustice between poor and rich societies. However, this point is only partially justified, as financial and social developments represent challenge parallel to scientific ones.

Respecting the latter point, the statement that anti-aging could be against nature law has long been loosing its ground completely. Most people agree that we shall search for a cure for cancer, AIDS or Alzheimer disease. Manipulating the aging process is just another activity that is “against the natural order”. Our current medical efforts are directed towards extending life at all costs. It is therefore difficult to see how we can accept curing the symptoms, but not accept curing the underlying causes of aging.

Finally, one must not confuse a non-aging state with immortality. Even if the aging process would be stopped completely, only the increase of mortality with time would be prevented, not the mortality itself. Even non-aging organisms have a finite average lifespan that is controlled by environmental risk and the intrinsic vulnerability (see chapter 1.3).

5 Conclusion and Outlook

As demonstrated by the success of evolutionary theories of aging, quite general theoretical considerations can be very useful when applied to aging research. The theoretical framework of reliability theory provides parsimonious explanations for diverse observations in aging.

The reliability theory states that redundancy is an important foundation for high reliability and robustness of the biological organism, and is a key notion for understanding the system nature of aging. Systems, which are redundant in numbers of irreplaceable (or not fully maintainable) elements, do deteriorate over time. Accordingly, aging is a direct consequence of investments into system reliability and durability.

Applying the reliability on the experimental data of biological systems, we concluded that lost of redundancy is the reason for both aging and age-related diseases. Errors in the organogenesis stage cause predisposed reduced redundancy of functional sub-component in the fault-tolerant living system. Although such influence can be transiently resolved inside of the system, the gradual reduction of fault-tolerance with time leads to late-onset pathological effects. In another word, there is probably a fatal origin of late-onset degenerative diseases and early life programming of late-life health and survival (Blackwell et al., 2001; Leon, 1998; Lucas, 1991). Therefore, the efforts to understand the routes and the early stages of aging and age-related diseases should not be discarded as irrelevant to understanding of the “true biological aging”. Early changes of system aging must be studied, and be integrated to prevention strategies of age-related diseases.

Reliability theory of aging provides an optimistic perspective on the opportunities for healthy life extension. According to reliability theory, human lifespan can be further increased through better early error prevention, body maintenances, repair and timely replacement of the failed body parts in the future. Such research should reveal ways in which aging populations can stay healthier and feel younger for longer.

6 Summary

Research on aging has obtained non-precedential importance due to the worldwide demographic structure transformation. The aim of the current work was to gain insight into the general mechanism of aging. Inspired by system engineering, we encountered the reliability theory as a promising theoretical framework. The applicability of this theory on biological systems was first verified. Next, a mathematical model was constructed in order to elucidate the impact of system redundancy on aging. The application of the reliability model on biological systems showed that redundancy in biological system leads to system reliability, but at the same time the aging phenotype. Implementation of this reliability model leads to three valuable insights: Firstly, it shows that there is common origin among aging and late-onset degenerative diseases. Secondly, it indicates that aging research should focus on quantitative aspects, as aging is a collective phenotypic expression of diverse error accumulations. Moreover, the reliability theory implies that aging can be retarded through constant subcomponent renewal. Following this view, we first strengthened to allocate essential quantitative alteration during aging and age-related diseases. This led us to the conclusion that lost of functional proteasome is most prominent aspect during aging. Through an in-depth analysis on the relation of cell volume regulation and proteasome function, we observed that one essential reason for the proteasome function decline in the aged could be the cellular dehydration due to the changed charge pattern of the proteome. Motivated by the reliability theory, several potential anti-aging strategies were discussed, where early-life intervention and body inbuilt repair and surveillance mechanism are stimulated to achieve the reduction of error accumulation.

7 Zusammenfassung

Die Alterungsforschung hat heute aufgrund der Verschiebung der demografischen Altersstruktur eine hohe Bedeutung. Ziel der Habilitationsschrift war es, Einblicke in die allgemeinen Mechanismen des Alterns zu erhalten. Inspiriert durch den Bereich des System-Engineering wurde die Reliabilitätsstheorie als eine vielversprechende Theoriebasis gewählt. Die Anwendbarkeit dieser Theorie auf biologische Systeme wurde zuerst überprüft. Weiterhin wurde ein mathematisches Modell konstruiert, um die Auswirkung der Systemredundanz auf die Alterung zu klären. Die Anwendung des Reliabilitätsmodells auf biologische Systeme hat gezeigt, dass die Redundanz zu einer hohen Zuverlässigkeit des Organismus führt, aber gleichzeitig auch das Alterungsphänomen erzeugt. Die Implementierung des Reliabilitätsmodells auf biologische Systeme führt zu drei wertvollen Erkenntnisse für die Alterungsforschung. Erstens zeigt sie, dass die Alterung und spät auftretende degenerative Erkrankungen eine gemeinsame Ursache haben. Zweitens zeigt sie, dass die Alterungsforschung sich mehr auf quantitative Aspekte fokussieren sollte, da die Alterung eine phänotypische Expression verschiedener Dimensionen von quantitativen Fehleransammlungen darstellt. Darüber hinaus sagt die Reliabilitätsstheorie aus, dass der Alterungsprozess durch ständige Erneuerung von Systemkomponenten sich verlangsamen lässt. Gemäß dieser Ansicht waren wir zunächst bestrebt, die wesentlichen quantitativen Veränderungen während der Alterung und während altersbedingter Krankheiten zu identifizieren. Dies führte zu der Erkenntnis, dass der Verlust des funktionellen Proteasoms ein wichtiger Aspekt des Alterungsprozesses ist. Die Analyse der Beziehung zwischen der Zellvolumenregulation und der Proteasomfunktion stellte fest, dass ein wesentlicher Grund für den altersbedingten Rückgang der Proteasomfunktion die zelluläre Dehydratation aufgrund eines veränderten zellulären Proteinladungsmuster ist. Verschiedene potentielle Anti-Aging-Strategien wurden diskutiert, durch die eine Schadensverminderung in frühen Lebensphasen sowie die Stimulierung von körpereigenen Reparatur- und Überwachungsmechanismen gefördert werden kann, um eine Reduzierung der Fehlerakkumulation zu gewährleisten.

8 Acknowledgments

The work with this habilitation has been extensive and trying, but in the first place exciting, instructive, and fun. Without help, support, and encouragement from some persons, I would never have been able to finish this work.

First of all, I would like to express my deep gratitude to the unselfish efforts of my mentors, Professor Ulf Stahl and Professor Dr. Karl Sperling, for their untiring guidance and help throughout the years.

I would like to thank my supervisor Prof. Dr. Dr. Joachim Klose for making possible the conduct of this research, for his inspiring and encouraging way to guide me to a deeper understanding of knowledge, and for his invaluable comments during the whole work.

I am also very grateful to everyone who has proofread parts of the manuscript, especially Albena Draycheva , Dr. Claus Zabel and Dr. Daniela Hartl, for their helpful advice and criticism throughout the course of this work. They are consistently appreciated for the exciting and endless discussions concerning the work.

My thanks also go to all my colleagues at the Institute of Human Genetics for providing a superior working atmosphere, especially Mrs. Grit Nebrich, Mrs. Andrea Koppelstätter and Ms. Oliver Klein in the core facility for their assistance of Mass spectrometry measurements. Mrs. Marion Herrmann is acknowledged for allowing the use of relevant data for this study. Mrs. Bettina Esch, and Mrs. Janine Stuwe are appreciated for their assistance of the laboratory works. Dr. Madeleine Diedrich is given thanks for sharing her valuable experimental data relating to this study and fruitful discussion.

At last, I wish to express my heartiest gratitude and respect to a special person who is always there for me: Mr. Rudi Beichel, to whom this work is dedicated.

9 References

Adelman, R., Saul, R. L., and Ames, B. N. (1988). Oxidative damage to DNA: relation to species metabolic rate and life span. Proc Natl Acad Sci U S A 85, 2706-2708.

Anderson, S., Bankier, A. T., Barrell, B. G., de Bruijn, M. H., Coulson, A. R., Drouin, J., Eperon, I. C., Nierlich, D. P., Roe, B. A., Sanger, F., et al. (1981). Sequence and organization of the human mitochondrial genome. Nature 290, 457-465.

Arendt, T. (2003). Synaptic plasticity and cell cycle activation in neurons are alternative effector pathways: the 'Dr. Jekyll and Mr. Hyde concept' of Alzheimer's disease or the yin and yang of neuroplasticity. Prog Neurobiol 71, 83-248.

Arendt, T. (2005). Alzheimer's disease as a disorder of dynamic brain self-organization. Prog Brain Res 147, 355-378.

Artandi, S. E., Alson, S., Tietze, M. K., Sharpless, N. E., Ye, S., Greenberg, R. A., Castrillon, D. H., Horner, J. W., Weiler, S. R., Carrasco, R. D., and DePinho, R. A. (2002). Constitutive telomerase expression promotes mammary carcinomas in aging mice. Proc Natl Acad Sci U S A 99, 8191-8196.

Barlow, R. E., and Proschan, F. (1996). Mathematical Theory of Reliability, In Classics in Applied Mathematics (Philadelphia: SIAM).

Blackwell, D. L., Hayward, M. D., and Crimmins, E. M. (2001). Does childhood health affect chronic morbidity in later life? Soc Sci Med 52, 1269-1284.

Blakemore, S. J. (2008). The social brain in adolescence. Nat Rev Neurosci 9, 267-277.

Boffoli, D., Scacco, S. C., Vergari, R., Solarino, G., Santacroce, G., and Papa, S. (1994). Decline with age of the respiratory chain activity in human skeletal muscle. Biochim Biophys Acta 1226, 73-82.

Bornemann, K. D., and Staufenbiel, M. (2000). Transgenic mouse models of Alzheimer's disease. Ann N Y Acad Sci 908, 260-266.

Brierley, E. J., Johnson, M. A., Lightowlers, R. N., James, O. F., and Turnbull, D. M. (1998). Role of mitochondrial DNA mutations in human aging: implications for the central nervous system and muscle. Ann Neurol 43, 217-223.

Bruno, C., Martinuzzi, A., Tang, Y., Andreu, A. L., Pallotti, F., Bonilla, E., Shanske, S., Fu, J., Sue, C. M., Angelini, C., et al. (1999). A stop-codon mutation in the human mtDNA cytochrome c oxidase I gene disrupts the functional structure of complex IV. Am J Hum Genet 65, 611-620.

Burns, J., Clarke, G., and Lumsden, C. J. (2002). Photoreceptor death: spatiotemporal patterns arising from one-hit death kinetics and a diffusible cell death factor. Bull Math Biol 64, 1117-1145.

Calabrese, B., Shaked, G. M., Tabarean, I. V., Braga, J., Koo, E. H., and Halpain, S. (2007). Rapid, concurrent alterations in pre- and postsynaptic structure induced by naturally-secreted amyloid-beta protein. Mol Cell Neurosci 35, 183-193.

Calne, D. B. (1994). Is idiopathic parkinsonism the consequence of an event or a process? Neurology 44, 5-10.

Cao, Z., Wanagat, J., McKiernan, S. H., and Aiken, J. M. (2001). Mitochondrial DNA deletion mutations are concomitant with ragged red regions of individual, aged muscle fibers: analysis by laser-capture microdissection. Nucleic Acids Res 29, 4502-4508.

Carey, J. R., Liedo, P., Orozco, D., and Vaupel, J. W. (1992). Slowing of mortality rates at older ages in large medfly cohorts. Science 258, 457-461.

Clarke, G., Collins, R. A., Leavitt, B. R., Andrews, D. F., Hayden, M. R., Lumsden, C. J., and McInnes, R. R. (2000). A one-hit model of cell death in inherited neuronal degenerations. Nature 406, 195-199.

Clarke, G., Lumsden, C. J., and McInnes, R. R. (2001). Inherited neurodegenerative diseases: the one-hit model of neurodegeneration. Hum Mol Genet 10, 2269-2275.

Crowder, M. J., Kimber, A. C., Smith, R. L., and Sweeting, T. J. (1991). Analysis of Reliability Data (London: Chapman and Hall).

Davies, K. J., Lin, S. W., and Pacifici, R. E. (1987). Protein damage and degradation by oxygen radicals. IV. Degradation of denatured protein. J Biol Chem 262, 9914-9920.

Demetrius, L., Gundlach, V. M., and Ochs, G. (2004). Complexity and demographic stability in population models. Theor Popul Biol 65, 211-225.

Diedrich, M., Mao, L., Bernreuther, C., Zabel, C., Nebrich, G., Kleene, R., and Klose, J. (2008). Proteome analysis of ventral midbrain in MPTP-treated normal and L1cam transgenic mice. Proteomics Mar;8(6):1266-75.

Eshleman, J. R., and Markowitz, S. D. (1996). Mismatch repair defects in human carcinogenesis. Hum Mol Genet 5 Spec No, 1489-1494.

Farmer, K. J., and Sohal, R. S. (1989). Relationship between superoxide anion radical generation and aging in the housefly, Musca domestica. Free Radic Biol Med 7, 23-29.

Fornai, F., Schluter, O. M., Lenzi, P., Gesi, M., Ruffoli, R., Ferrucci, M., Lazzeri, G., Busceti, C. L., Pontarelli, F., Battaglia, G., et al. (2005). Parkinson-like syndrome induced by continuous MPTP infusion: convergent roles of the ubiquitin-proteasome system and alpha-synuclein. Proc Natl Acad Sci U S A 102, 3413-3418.

Fraga, C. G., Shigenaga, M. K., Park, J. W., Degan, P., and Ames, B. N. (1990). Oxidative damage to DNA during aging: 8-hydroxy-2'-deoxyguanosine in rat organ DNA and urine. Proc Natl Acad Sci U S A 87, 4533-4537.

Garner, B., Shaw, D. C., Lindner, R. A., Carver, J. A., and Truscott, R. J. (2000). Non-oxidative modification of lens crystallins by kynurenine: a novel post-translational protein modification with possible relevance to ageing and cataract. Biochim Biophys Acta 1476, 265-278.

Gavrilov, L. A., and Gavrilova, N. S. (2002). Evolutionary theories of aging and longevity. ScientificWorldJournal 2, 339-356.

Gavrilov, L. A., and Gavrilova, N. S. (2004). Early-life programming of aging and longevity: the idea of high initial damage load (the HIDL hypothesis). Ann N Y Acad Sci 1019, 496-501.

Georgiadis, J., and J., K. (2002). Self-organising software architectures for distributed systems, Paper presented at: Proceedings of the first workshop on Self-healing systems (Charleston, South Carolina: ACM Press).

Ghosh, D., Sharman, R., Rao, H. R., and Upadhyaya, S. (2007). Self-Healing Systems, Survey and Synthesis. Decision Support Systems 42, 2164.

Gnedenko, B., Pavlov, I., and I., U. (1999). Statistical Reliability Engineering (New York: Wiley).

Gompertz, B. (1825). cited from Dictionary of Scientific Biography, (New York, 1970-1990).

Gouda, M. D., Singh, S. A., Rao, A. G., Thakur, M. S., and Karanth, N. G. (2003). Thermal inactivation of glucose oxidase. Mechanism and stabilization using additives. J Biol Chem 278, 24324-24333.

Gralle, M., and Ferreira, S. T. (2007). Structure and functions of the human amyloid precursor protein: the whole is more than the sum of its parts. Prog Neurobiol 82, 11-32.

Halliwell, B. (1989). Free radicals, reactive oxygen species and human disease: a critical evaluation with special reference to atherosclerosis. Br J Exp Pathol 70, 737-757.

Harley, C. B., Futcher, A. B., and Greider, C. W. (1990). Telomeres shorten during ageing of human fibroblasts. Nature 345, 458-460.

Harley, C. B., Vaziri, H., Counter, C. M., and Allsopp, R. C. (1992). The telomere hypothesis of cellular aging. Exp Gerontol 27, 375-382.

Harman, D. (1956). Aging: a theory based on free radical and radiation chemistry. J Gerontol 11, 298-300.

Harman, D. (1972). The biologic clock: the mitochondria? J Am Geriatr Soc 20, 145-147.

Harman, D. (1981). The aging process. Proc Natl Acad Sci U S A 78, 7124-7128.

Hartl, D., Irmler, M., Romer, I., Mader, M. T., Mao, L., Zabel, C., de Angelis, M. H., Beckers, J., and Klose, J. (2008a). Transcriptome and proteome analysis of early embryonic mouse brain development. Proteomics 2008 Mar;8(6):1257-65.

Hartl, D., Rohe, M., Mao, L., Staufenbiel, M., Zabel, C., and Klose, J. (2008b). Impairment of adolescent hippocampal plasticity in a mouse model for Alzheimer's disease precedes disease phenotype. PLoS ONE 2008 Jul 23;3(7):e2759.

Hayflick, L., and Moorhead, P. S. (1961). The serial cultivation of human diploid cell strains. Exp Cell Res 25, 585-621.

Hulley, P., Schachner, M., and Lubbert, H. (1998). L1 neural cell adhesion molecule is a survival factor for fetal dopaminergic neurons. J Neurosci Res 53, 129-134.

Joenje, H. (1989). Genetic toxicology of oxygen. Mutat Res 219, 193-208.

Jozwiak, Z., and Jasnowska, B. (1985). Changes in oxygen-metabolizing enzymes and lipid peroxidation in human erythrocytes as a function of age of donor. Mech Ageing Dev 32, 77-83.

Kasper, G., Mao, L., Geissler, S., Trippens, J., Kuehnisch, J., Tschirschmann, M., Kaspar, K., Perka, C., Duda, G. N., and Klose, J. (2009). Insights into mesenchymal stem cell ageing: involvement of antioxidant defense and actin cytoskeleton. Stem Cells 26;27, 1288-1297.

Khaitovich, P., Hellmann, I., Enard, W., Nowick, K., Leinweber, M., Franz, H., Weiss, G., Lachmann, M., and Paabo, S. (2005). Parallel patterns of evolution in the genomes and transcriptomes of humans and chimpanzees. Science 309, 1850-1854. Epub 2005 Sep 1851.

Khrapko, K., Bodyak, N., Thilly, W. G., van Orsouw, N. J., Zhang, X., Coller, H. A., Perls, T. T., Upton, M., Vijg, J., and Wei, J. Y. (1999). Cell-by-cell scanning of whole mitochondrial genomes in aged human heart reveals a significant fraction of myocytes with clonally expanded deletions. Nucleic Acids Res 27, 2434-2441.

Kopsidas, G., Kovalenko, S. A., Kelso, J. M., and Linnane, A. W. (1998). An age-associated correlation between cellular bioenergy decline and mtDNA rearrangements in human skeletal muscle. Mutat Res 421, 27-36.

Kowald, A., and Kirkwood, T. B. (1999). The mitochondrial theory of aging: do damaged mitochondria accumulate by delayed degradation? Exp Gerontol 34, 605-612.

Kowald, A., and Kirkwood, T. B. (2000). Accumulation of defective mitochondria through delayed degradation of damaged organelles and its possible role in the ageing of post-mitotic and dividing cells. J Theor Biol 202, 145-160.

Kundi, M. (1999). One-hit models for virus inactivation studies. Antiviral Res 41, 145-152.

Kuo, Y. M., Beach, T. G., Sue, L. I., Scott, S., Layne, K. J., Kokjohn, T. A., Kalback, W. M., Luehrs, D. C., Vishnivetskaya, T. A., Abramowski, D., et al. (2001). The evolution of A beta peptide burden in the APP23 transgenic mice: implications for A beta deposition in Alzheimer disease. Mol Med 7, 609-618.

Lang, F., Busch, G. L., Ritter, M., Volkl, H., Waldegger, S., Gulbins, E., and Haussinger, D. (1998). Functional significance of cell volume regulatory mechanisms. Physiol Rev 78, 247-306.

Lanz, T. A., Carter, D. B., and Merchant, K. M. (2003). Dendritic spine loss in the hippocampus of young PDAPP and Tg2576 mice and its prevention by the ApoE2 genotype. Neurobiol Dis 13, 246-253.

Leaman, B. M., and Beamish, R. J. (1984). Ecological and management implications of longevity in some northest Pacific ground-fishes. Bull Int N Pac Fish Commn, 85-95.

Leon, D. A. (1998). Fetal growth and adult disease. Eur J Clin Nutr 52 Suppl 1, S72-78; discussion S78-82.

Leskela, H. V., Risteli, J., Niskanen, S., Koivunen, J., Ivaska, K. K., and Lehenkari, P. (2003). Osteoblast recruitment from stem cells does not decrease by age at late adulthood. Biochem Biophys Res Commun 311, 1008-1013.

Linnane, A. W., Marzuki, S., Ozawa, T., and Tanaka, M. (1989). Mitochondrial DNA mutations as an important contributor to ageing and degenerative diseases. Lancet 1, 642-645.

Lopez, M. E., Van Zeeland, N. L., Dahl, D. B., Weindruch, R., and Aiken, J. M. (2000). Cellular phenotypes of age-associated skeletal muscle mitochondrial abnormalities in rhesus monkeys. Mutat Res 452, 123-138.

Lucas, A. (1991). Programming by early nutrition in man. Ciba Found Symp 156, 38-50; discussion 50-35.

Makeham, W. M. (1860). On the Law of Mortality and the Construction of Annuity Tables. J Inst Actuaries and Assur Mag, 301-310.

Mao, L., Hartl, D., Nolden, T., Koppelstatter, A., Klose, J., Himmelbauer, H., and Zabel, C. (2008). Pronounced alterations of cellular metabolism and structure due to hyper- or hypo-osmosis. J Proteome Res Sep;7(9):3968-83 Epub 2008 Jul 23.

Mao, L., Zabel, C., Herrmann, M., Nolden, T., Mertes, F., Magnol, L., Chabert, C., Hartl, D., Herault, Y., Delabar, J. M., et al. (2007). Proteomic shifts in embryonic stem cells with gene dose modifications suggest the presence of balancer proteins in protein regulatory networks. PLoS ONE 2, e1218.

Mao, L., Zabel, C., Wacker, M. A., Nebrich, G., Sagi, D., Schrade, P., Bachmann, S., Kowald, A., and Klose, J. (2006). Estimation of the mtDNA mutation rate in aging mice by proteome analysis and mathematical modeling. Exp Gerontol 41, 11-24. Epub 2005 Nov 2022.

Massof, R. W. (2002). The measurement of vision disability. Optom Vis Sci 79, 516-552.

Maynard Smith, J. (1987). On the equality of origin and fixation times in genetics. J Theor Biol 128, 247-252.

Medawar, P. B. (1952). An Unsolbed Problem of Biology (London: H.K. Lewis).

Medvedev, Z. A. (1990). An attempt at a rational classification of theories of ageing. Biol Rev Camb Philos Soc 65, 375-398.

Mitsumoto, Y., Watanabe, A., Mori, A., and Koga, N. (1998). Spontaneous regeneration of nigrostriatal dopaminergic neurons in MPTP-treated C57BL/6 mice. Biochem Biophys Res Commun 248, 660-663.

Myatt, S. S., and Lam, E. W. (2007). The emerging roles of forkhead box (Fox) proteins in cancer. Nat Rev Cancer 7, 847-859.

Nebrich, G., Herrmann, M., Hartl, D., Diedrich, M., Kreitler, T., Wierling, C., Klose, J., Giavalisco, P., Zabel, C., and Mao, L. (2009). PROTEOMER: A workflow-optimized laboratory information management system for 2-D electrophoresis-centered proteomics. Proteomics 3, 3.

Oeppen, J., and Vaupel, J. W. (2002). Demography. Broken limits to life expectancy. Science 296, 1029-1031.

Olovnikov, A. M. (1973). A theory of marginotomy. The incomplete copying of template margin in enzymic synthesis of polynucleotides and biological significance of the phenomenon. J Theor Biol 41, 181-190.

Pak, J. W., Herbst, A., Bua, E., Gokey, N., McKenzie, D., and Aiken, J. M. (2003). Mitochondrial DNA mutations as a fundamental mechanism in physiological declines associated with aging. Aging Cell 2, 1-7.

Peleg, M., Normand, M. D., and Campanella, O. H. (2003). Estimating microbial inactivation parameters from survival curves obtained under varying conditions--the linear case. Bull Math Biol 65, 219-234.

Petrelli, N. J., Valle, A. A., Weber, T. K., and Rodriguez-Bigas, M. (1996). Adenosquamous carcinoma of the colon and rectum. Dis Colon Rectum 39, 1265-1268.

Pichiorri, F., Ishii, H., Okumura, H., Trapasso, F., Wang, Y., and Huebner, K. (2008). Molecular parameters of genome instability: roles of fragile genes at common fragile sites. J Cell Biochem 104, 1525-1533.

Pryor, W. A. (1973). Free radical reactions and their importance in biochemical systems. Fed Proc 32, 1862-1869.

Rahman, S., Taanman, J. W., Cooper, J. M., Nelson, I., Hargreaves, I., Meunier, B., Hanna, M. G., Garcia, J. J., Capaldi, R. A., Lake, B. D., et al. (1999). A missense mutation of cytochrome oxidase subunit II causes defective assembly and myopathy. Am J Hum Genet 65, 1030-1039.

Readercomment (1993). A novel gene containing a trinucleotide repeat that is expanded and unstable on Huntington's disease chromosomes. The Huntington's Disease Collaborative Research Group. Cell 72, 971-983.

Richter, C. (1988). Do mitochondrial DNA fragments promote cancer and aging? FEBS Lett 241, 1-5.

Rodier, F., Campisi, J., and Bhaumik, D. (2007). Two faces of p53: aging and tumor suppression. Nucleic Acids Res 35, 7475-7484.

Sapolsky, R. M., and Finch, C. E. (2000). Alzheimer's disease and some speculations about the evolution of its modifiers. Ann N Y Acad Sci 924, 99-103.

Satoh, M., and Kuroiwa, T. (1991). Organization of multiple nucleoids and DNA molecules in mitochondria of a human cell. Exp Cell Res 196, 137-140.

Sawada, M., and Carlson, J. C. (1987). Changes in superoxide radical and lipid peroxide formation in the brain, heart and liver during the lifetime of the rat. Mech Ageing Dev 41, 125-137.

Schober, A. (2004). Classic toxin-induced animal models of Parkinson's disease: 6-OHDA and MPTP. Cell Tissue Res 318, 215-224.

Schulzer, M., Lee, C. S., Mak, E. K., Vingerhoets, F. J., and Calne, D. B. (1994). A mathematical model of pathogenesis in idiopathic parkinsonism. Brain 117, 509-516.

Shrestha, B. R., Vitolo, O. V., Joshi, P., Lordkipanidze, T., Shelanski, M., and Dunaevsky, A. (2006). Amyloid beta peptide adversely affects spine number and motility in hippocampal neurons. Mol Cell Neurosci 33, 274-282.

Smeyne, R. J., and Jackson-Lewis, V. (2005). The MPTP model of Parkinson's disease. Brain Res Mol Brain Res 134, 57-66.

Sohal, R. S., and Sohal, B. H. (1991). Hydrogen peroxide release by mitochondria increases during aging. Mech Ageing Dev 57, 187-202.

Spear, L. P. (2000). The adolescent brain and age-related behavioral manifestations. Neurosci Biobehav Rev 24, 417-463.

Suh, Y., and Vijg, J. (2006). Maintaining genetic integrity in aging: a zero sum game. Antioxid Redox Signal 8, 559-571.

Tanaka, Y., Engelender, S., Igarashi, S., Rao, R. K., Wanner, T., Tanzi, R. E., Sawa, A., V, L. D., Dawson, T. M., and Ross, C. A. (2001). Inducible expression of mutant alpha-synuclein decreases proteasome activity and increases sensitivity to mitochondria-dependent apoptosis. Hum Mol Genet 10, 919-926.

Thompson, I., and Jones, D. S. (1980). Annual internal growth banding and life history of the ocean quahog Artica islandica (Mollusca: Bivalvia). Marine Bilogogy, 25-34.

Turner, P. R., O'Connor, K., Tate, W. P., and Abraham, W. C. (2003). Roles of amyloid precursor protein and its fragments in regulating neural activity, plasticity and memory. Prog Neurobiol 70, 1-32.

Vacik, T., Ort, M., Gregorova, S., Strnad, P., Blatny, R., Conte, N., Bradley, A., Bures, J., and Forejt, J. (2005). Segmental trisomy of chromosome 17: a mouse model of human aneuploidy syndromes. Proc Natl Acad Sci U S A 102, 4500-4505.

Vasek, F. C. (1980). Creosote bush: Long-lived clones in the Mojave Desert. American J Botany, 246-255.

Wallace, D. C. (1997). Mitochondrial DNA in aging and disease. Sci Am 277, 40-47.

Watson, J. D. (1972). Origin of concatemeric T7 DNA. Nat New Biol 239, 197-201.

Wexler, N. S., Rose, E. A., and Housman, D. E. (1991). Molecular approaches to hereditary diseases of the nervous system: Huntington's disease as a paradigm. Annu Rev Neurosci 14, 503-529.

Willcox, B. J., Donlon, T. A., He, Q., Chen, R., Grove, J. S., Yano, K., Masaki, K. H., Willcox, D. C., Rodriguez, B., and Curb, J. D. (2008). FOXO3A genotype is strongly associated with human longevity. Proc Natl Acad Sci U S A 105, 13987-13992.

Williams, G. C. (1957). Pleiotropy, natural selection and the evolution of senescence. Evolution, 398-411.

Wolfer, D. P., Mohajeri, H. M., Lipp, H. P., and Schachner, M. (1998). Increased flexibility and selectivity in spatial learning of transgenic mice ectopically expressing the neural cell adhesion molecule L1 in astrocytes. Eur J Neurosci 10, 708-717.

Wright, W. E., and Shay, J. W. (1992). Telomere positional effects and the regulation of cellular senescence. Trends Genet 8, 193-197.

Zabel, C., Mao, L., Woodman, B., Rohe, M., Wacker, M. A., Klaere, Y., Koppelstaetter, A., Nebrich, G., Klein, O., Grams, S., et al. (2009). A large number of protein expression changes occur early in life and precede phenotype onset in a mouse model for Huntington's disease. Mol Cell Proteomics Apr;8(4):720-34.

Zabel, C., Sagi, D., Kaindl, A. M., Steireif, N., Klare, Y., Mao, L., Peters, H., Wacker, M. A., Kleene, R., and Klose, J. (2006). Comparative proteomics in neurodegenerative and non-neurodegenerative diseases suggest nodal point proteins in regulatory networking. J Proteome Res 5, 1948-1958.

Zakian, V. A. (1995). Telomeres: beginning to understand the end. Science 270, 1601-1607.

Tabellarischer Lebenslauf

Persönliche Angaben

Name:	Mao
Vorname:	Lei
Geboren:	29. April 1970 in Shanghai, China
Familienstand:	verheiratet (2 Kinder)

Bildungsweg

September 1976 bis Juli 1987	Besuch des Gymnasiums der Peking Universität in China **Abitur**
Oktober 1987 bis Juli 1991	Studium an der Beijing Agricultural University in China Studiengang: Laboratory Animal Sciences Thema der Abschlussarbeit: *Establishment of induced diabetics Animal model using Mini-pig* **Bachelor of Sciences in Veterinary Medicine**
Oktober 1996 bis Dez. 2001	Technischen Universität Berlin Studiengang: Biotechnologie Thema der Abschlussarbeit: *Simultaneous Isolation of Hepatocytes and Nonparenchymal Cells from Adult Rat and Human Liver* **Diplom Ingenieur**
März 2002 bis Februar 2005	Technische Universität Berlin Institut für Biotechnologie, Fakultät III - Prozesswissenschaften Biotechnologie mit Spezialisierung Proteomics Thema der Promotion: *The Mitochondrial Protein Profile Change during the Aging Process* **Promotion zum Dr. rer. nat.**
Oktober 2002 bis Juli 2004	Technische Fachhochschule Berlin Studiengang: Bioinformatik Thema der Abschlussarbeit: *Mathematical Modelling of the Accumulation of Defective Mitochondria during the Ageing Process* **Master of Computer Sciences in Bioinformatics**

Beruflicher Entwicklungsweg

August 1991 bis März 1996	Biotechnology Research Centre, Chinese Academy of Agriculture Sciences Projekt 1: Up-scaling der Monoklonalen Antikörper-Produktion. Projekt 2: Management der institutionellen SPF Versuchstieranlage.
Januar 1997 bis Februar 2002	Experimentelle Chirurgie, Charité-Universitätsmedizin Berlin, CVK AG PD. Dr. Jörg Gerlach Projekt: Primäre Leberzellkultur und Entwicklung eines Hepatozyten-Bioreaktors für Arztneimitteltests.
März 2002 bis Februar 2005	Institut für Humangenetik, Charité-Universitätsmedizin Berlin CVK AG Prof. Dr. Dr. Joachim Klose Promotion: Untersuchung des mitochondrialen Maus-Proteoms bei dem Alterungsprozess.
April 2004 bis Juli 2004	Institut für theoretische Biologie, Humboldt-Universität zu Berlin AG Prof. Dr. Peter Hammerstein Masterarbeit: Mathematical Modelling of the Accumulation of Defective Mitochondria during the Ageing Process
März 2005 bis Juni 2006	Gastwissenschaftlerin am Max Planck Institute for Molecular Genetics AG Dr. Heinz Himmelbauer Projekt: Genetische Manipulation von embryonalen Maus-Stammzellen mit für die Alzheimer und Parkinson Krankheit relevanten Transgenen.
Februar 2005 bis jetzt	Institut für Humangenetik, Charité-Universitätsmedizin Berlin CVK AG Prof. Dr. Dr. Joachim Klose Projekt 1: Proteomische Untersuchung von embryonalen Maus-Stammzellen und des Protein-Protein Interaktionsnetzwerkes Projekt 2: Proteomische Untersuchungen eines Mausmodells für das Downsyndrom.

Eigene Veröffentlichungen

1. Kasper G, Mao L, Geissler S, Trippens J, Kuehnisch J, Tschirschmann M, Kaspar K, Perka C, Duda GN, and Klose J. Insights into mesenchymal stem cell ageing: involvement of antioxidant defence and actin cytoskeleton. ***Stem Cells*** (2009) Feb 26;27(6): 1288-97. (IF 4.034)

2. Nebrich G, Herrmann M, Hartl D, Diedrich M, Kreitler T, Wierling C, Klose J, Giavalisco P, Zabel C, and Mao L. PROTEOMER: A workflow-optimized laboratory information management system for 2-D electrophoresis-centered proteomics. ***Proteomics*** (2009) Apr;9(7):1795-808. (IF 5.479)

3. Zabel C, Mao L, Woodman B, Rohe M, Wacker MA, Klaere Y, Koppelstaetter A, Nebrich G, Klein O, Grams S., et al. A large number of protein expression changes occur early in life and precede phenotype onset in a mouse model for Huntington's disease. ***Mol Cell Proteomics*** (2009) Apr;8(4):720-34. (IF 9.425)

4. Mao L, Hartl D, Nolden T, Koppelstätter A, Klose J, Himmelbauer H, Zabel C. Pronounced Alterations of Cellular Metabolism and Structure Due to Hyper- or Hypo-Osmosis. ***J Proteome Res***. (2008) Sep;7(9):3968-83. (IF 5,675)

5. Hartl D, Rohe M, Mao L, Staufenbiel M, Zabel C, Klose J. Impairment of adolescent hippocampal plasticity in a mouse model for Alzheimer's disease precedes disease phenotype. ***PLoS ONE***. (2008) Jul 23;3(7):e2759.

6. Zabel C, Andreew A, Mao L, Hartl D. Protein expression overlap: more important than which proteins change in expression? ***Expert Rev Proteomics***. (2008) Apr;5(2):187-205.

7. Diedrich M, Mao L, Bernreuther C, Zabel C, Nebrich G, Kleene R, Klose J. Proteome analysis of ventral midbrain in MPTP-treated normal and L1cam transgenic mice. ***Proteomics***. (2008) Mar;8(6):1266-75. (IF 5.479)

8. Hartl D, Irmler M, Römer I, Mader MT, Mao L, Zabel C, de Angelis MH, Beckers J, Klose J. Transcriptome and proteome analysis of early embryonic mouse brain development. ***Proteomics***. (2008) Mar;8(6):1257-65. (IF 5.479)

9. Mao L, Zabel C, Herrmann M, Nolden T, Mertes F, Magnol L, Chabert C, Hartl D, Herault Y, Delabar JM, Manke T, Himmelbauer H, Klose J. Proteomic shifts in embryonic stem cells with gene dose modifications suggest the presence of balancer proteins in protein regulatory networks. ***PLoS ONE***. (2007) Nov 28;2(11):e1218.

10. Diedrich M, Tadic J, Mao L, Wacker MA, Nebrich G, Hetzer R, Regitz-Zagrosek V, Klose J. Heart protein expression related to age and sex in mice and humans. ***Int J Mol Med***. (2007) Dec;20(6):865-74. (IF 1.847)

11. Mao L, Zabel C, Wacker MA, Nebrich G, Sagi D, Schrade P, Bachmann S, Kowald A, Klose J. Estimation of the mtDNA mutation rate in aging mice by proteome analysis and mathematical modeling. ***Exp Gerontol***. (2006) Jan;41(1):11-24. (IF 2.879)

12. Seefeldt I, Nebrich G, Romer I, Mao L, Klose J. Evaluation of 2-DE protein patterns from pre- and postnatal stages of the mouse brain. ***Proteomics***. (2006) Sep;6(18):4932-9. (IF 5.479)

13. Zabel C, Sagi D, Kaindl AM, Steireif N, Klare Y, Mao L, Peters H, Wacker MA, Kleene R, Klose J. Comparative proteomics in neurodegenerative and non-neurodegenerative diseases suggest nodal point proteins in regulatory networking. ***J Proteome Res***. (2006) Aug;5(8):1948-58. (IF 5.675)

14. Zeilinger K, Sauer IM, Pless G, Strobel C, Rudzitis J, Wang A, Nussler AK, Grebe A, Mao L, Auth SH, Unger J, Neuhaus P, Gerlach JC. Three-dimensional co-culture of primary human liver cells in bioreactors for in vitro drug studies: effects of the initial cell quality on the long-term maintenance of hepatocyte-specific functions. ***Altern Lab Anim***. (2002) Sep-Oct;30 (5):525-38.

15. Zeilinger K, Auth SH, Unger J, Grebe A, Mao L. Standardisierung eines Hepatozytenbioreaktorsystemes für in vitro-Metabolismusstudien als Alternative zum Tierversuch. In: Schöffl H, Spielmann H, Tritthart HA, eds. ***Ersatz- und Ergänzungsmethode zu Tierversuchen***. *Springer-Verlag*. (2000): 1-7.

16. Zeilinger K, Auth SHG, Unger J, Grebe A, Mao L, Petrik M, Holland G, Appel K, Nüssler AK, Neuhaus P, Gerlach JC. Leberzellkultur in Bioreaktoren für in vitro Studien zum Arzneimittelmetabolismus als Alternative zum Tierversuch. ***ALTEX*** (2000); 17: 3-10.

17. Mao L, Zeilinger K, Roth S, Gerlach JC, Neuhaus P. Gleichzeitige Isolierung von Hepatozyten, Itozellen und Simusendothelzellen der Leber aus demselben Organ. ***Z. Gastroenterol***. (2000); 39: 94. (IF 1.026)

18. Mao L, Zeilinger K, Auth SH, Grebe A, Petrik M, Appel D, Schonoy N, Holland G, Jennings G, Gerlach JC. Zukunftsmodell zum Ersatz von Metabolismusstudien am Tier? In: Schöffl H, Spielmann H, Tritthart HA, eds. Ersatz- und Ergänzungsmethode zu Tierversuchen. ***Springer-Verlag***. (2000): 450.

19. Grebe A, Zeilinger K, Auth SHG, Mao L, Schonoy N, Holland G, Appel D, Jennings G, Gerlach JC. Kultur primärer und immortalisierter humaner Hepatozyten in einem Bioreaktor-Perfusionssystem. ***Z. Gastroenterol***. (1999); 37:71. (IF 1.026)

Semesterweise Auflistung der Lehrleistung:

1. Praktikum „Biologie für Medizinen“ 2009 SS (7x5=35 h).

2. Praktikum „Biologie für Medizinen“ 2008/2009 WS (7x5=35 h).

3. Vorlesung “Biologie des Alters”, Fernstudiumsgang Medizinische Pädagogik, 2008/2009 WS (2h).

4. Praktikum „Biologie für Mediziner“ 2008 SS (7x5=35 h).

5. Praktikum „Biologie für Zahnmediziner“ 2008 SS (2x2,5=5h).

6. Ringseminar „Cell biology” für Berlin-Brandenburg School for Regenerative Therapies (BSRT): März 2008: “Aging Mechanism and Mitochondria” (2h).

7. Vorlesung “Biologie des Alters”, Fernstudiumsgang Medizinische Pädagogik. 2008 SS, (2h).

8. Ringseminar SFB Graduate school GK 754 “Myocardial Gene Expression and myocardial Hypertrophy”: 2007 “In-vitro differentiation of mouse ES cells to cardiomyocytes” (2h).

9. Praktikum “Biologie für Zahnmedizinen”, WS 2007 block V „Populationsgenetik: Hardy Weinberg Gesetz“ (2h).

10. Ringseminar SFB Graduate school GK 754 “Myocardial Gene Expression and myocardial Hypertrophy”: März 2006 “Mitochondrial aging” (2h).

Eingeworbene Drittmittel:

Title	Bezeichnung	Principle Investigators	Umfang (T Euro)	Förderungsperiode
AnEUploidy: Understanding gene dosage imbalance in human health using genetics, functional genomics and systems biology	**EU**: LSHG-CT-2006-037627	Prof. Joachim Klose und Dr. Lei Mao	250	12.2006-11.2010
Die Wirkung von Mutationen auf die Funktionsweise des Proteomnetzwerkes	**DFG:** SFB577-A3	Prof. Joachim Klose und Dr. Lei Mao	126	06.2008-06.2009
Zentrallabor für Proteomanalyse Service und Kooperation innerhalb des SFBs	**DFG:** SFB577-Z2	Prof. Joachim Klose und Dr. Lei Mao	57	06.2008-06.2009
Die Wirkung von Polymorphismen auf die Variabilitaet im Netzwerk des Proteoms: Proteine als Modifier komplxer Krankheiten (Alzheimer-Krankheit)	**DFG:** KL 237/12-1	Prof. Joachim Klose und Dr. Lei Mao	340	06.2009-06.2011

STEM CELLS

STEM CELL EPIGENETICS, GENOMICS, AND PROTEOMICS

Insights into Mesenchymal Stem Cell Aging: Involvement of Antioxidant Defense and Actin Cytoskeleton

GRIT KASPER,[a,b] LEI MAO,[c] SVEN GEISSLER,[a,b] ALBENA DRAYCHEVA,[a,c] JESSICA TRIPPENS,[a] JIRKO KÜHNISCH,[d] MIRIAM TSCHIRSCHMANN,[e] KATHARINA KASPAR,[a] CARSTEN PERKA,[a,b] GEORG N. DUDA,[a,b] JOACHIM KLOSE[b,c]

[a]Julius Wolff Institute and Center for Musculoskeletal Surgery Berlin; [b]Berlin-Brandenburg Center for Regenerative Therapies; [c]Institute for Human Genetics; [d]Institute of Medical Genetics, Charité—Universitätsmedizin Berlin, Berlin, Germany; [e]Department of Medical Biotechnology, Berlin University of Technology, Berlin, Germany

Key Words. Aging • Mesenchymal stem cells • Gene expression • Tissue regeneration

ABSTRACT

Progenitor cells such as mesenchymal stem cells (MSCs) have elicited great hopes for therapeutic augmentation of physiological regeneration processes, e.g., for bone fracture healing. However, regeneration potential decreases with age, which raises questions about the efficiency of autologous approaches in elderly patients. To elucidate the mechanisms and cellular consequences of aging, the functional and proteomic changes in MSCs derived from young and old Sprague–Dawley rats were studied concurrently. We demonstrate not only that MSC concentration in bone marrow declines with age but also that their function is altered, especially their migratory capacity and susceptibility toward senescence. High-resolution two-dimensional electrophoresis of the MSC proteome, under conditions of in vitro self-renewal as well as osteogenic stimulation, identified several age-dependent proteins, including members of the calponin protein family as well as galectin-3. Functional annotation clustering revealed that age-affected molecular functions are associated with cytoskeleton organization and antioxidant defense. These proteome screening results are supported by lower actin turnover and diminished antioxidant power in aged MSCs, respectively. Thus, we postulate two main reasons for the compromised cellular function of aged MSCs: (a) declined responsiveness to biological and mechanical signals due to a less dynamic actin cytoskeleton and (b) increased oxidative stress exposure favoring macromolecular damage and senescence. These results, along with the observed similar differentiation potentials, imply that MSC-based therapeutic approaches for the elderly should focus on attracting the cells to the site of injury and oxidative stress protection, rather than merely stimulating differentiation. *STEM CELLS 2009;27:1288–1297*

Disclosure of potential conflicts of interest is found at the end of this article.

INTRODUCTION

Mesenchymal stem cells (MSCs) have gained increasing interest for application in cell-based therapies and tissue engineering approaches [1]. This is based on their potential for self-renewal, as well as multilineage differentiation, combined with an easy accessibility [2]. MSCs reside in several tissues, e.g., bone marrow, fat, and muscle tissue, and contribute to physiological regeneration in organs such as bone, skin, liver, and muscle. However, clinical experience as well as animal studies prove that the regeneration potential of bone and other tissues declines with age [3]. Consequently, treatment with MSCs from older donors appears to be less effective than application of their younger counterparts [4]. If the age-dependent decrease in regenerative potential is caused by intrinsic changes in MSCs themselves, autologous approaches are prone to be suboptimal in elderly patients, who have the most need for such therapies. Understanding the underlying mechanisms of the age-associated decrease in regeneration potential might pave the way for the development of innovative treatment strategies, e.g., for bone defect healing.

Age-related changes in MSCs may not only account for delayed regeneration in the case of an acute trauma but also for a limited quality of the regenerated tissue. Indeed, aging of stem and progenitor cells was suggested to account for aging of tissue and whole organisms [5]. In principle, MSCs from aged individuals may be altered in quality or quantity (for details see review [6]). However, studies investigating the influence of age on MSCs are contradictory, probably due to differences in experimental parameters such as donor species, sex, age, cell isolation, and cell culture protocols. For example, most studies point to a decrease in MSC number with age [7–9], whereas others find no changes [10, 11]. Concerning the differentiation potential of MSCs, it has been demonstrated that MSCs lose osteogenic in favor of adipogenic potential (the so-called "adipogenic

Author contributions: G.K., C.P., G.N.D., and J.K.: designed research; L.M., S.G., J.T., M.T., A.D., and K.K.: performed research; L.M., S.G., J.T., A.D., and J.K.: analyzed data; G.K.: wrote paper.

Correspondence: Georg N. Duda, Ph.D., Julius Wolff Institute and Center for Musculoskeletal Surgery Berlin, Charité—Universitätsmedizin Berlin, Berlin, Germany. Telephone: ++49-30-450659079; Fax: ++49-30-450559969; e-mail: georg.duda@charite.de Received September 25, 2008; accepted for publication February 5, 2009; first published online in STEM CELLS *EXPRESS* February 26, 2009. 1066-5099/2009/$30.00/0 doi: 10.1002/stem.49

switch") [12], while others show the opposite [13]. Regarding growth rates, a significant decrease in MSCs from older donors was reported [14, 15], while another study shows an increase of more than three times in the proliferation rate of MSCs from older animals [16]. Further characteristics, such as number of colony-forming units (CFUs), telomere length, and telomerase activity, have been examined with a similar heterogeneity [6]. In conclusion, the impact of age on MSC behavior and availability is still controversial. Furthermore, the molecular basis for potential functional changes remains even more elusive.

However, there are some insights into adult stem cell aging from the hematopoietic stem cell (HSC) system. For these cells, the numbers do not necessarily decline with age, but for that cellular function is clearly compromised, for example with regard to mobilization, homing, and lineage choice [5, 17, 18]. Cellular aging of HSCs has been attributed to various mechanisms that exhibit a partial cause and effect relationship to each other. For example, telomere shortening, as a cell-intrinsic trigger for replicative senescence, was shown to be associated with impaired HSC function due to reduced long-term repopulation capacities and increased genetic instability [19].

Furthermore, abundant evidence in different model systems supports a connection between oxidative metabolism, stress resistance, and aging. It has been shown that lifelong dietary restriction increases HSC frequencies and improved HSC function. The self-renewal capacity of HSCs depends on the control of oxidative stress [20], and additionally, progressive bone marrow failure is associated with elevated reactive oxygen species (ROS). Concordantly, treatment with antioxidative agents has prevented bone marrow failure and restored the reconstitutive capacity of HSCs deficient of *Atm*, whose gene product inhibits oxidative stress.

Recently, proteomic approaches analyzing the MSC membrane fraction by mass spectrometry revealed novel MSC-specific markers [21] In a another study, PI3K was discovered as a control point for osteogenic differentiation of MSCs [22]. Thus, proteomics was considered in this study as valuable tool to investigate stem cell aging and molecular changes altering cellular behavior. By employing MSCs from young (yMSCs) and old (oMSCs) murine donors, it was demonstrated that a decrease in cell number with donor age is paralleled by increased senescence and decreased migration capacity. A high-resolution large-gel two-dimensional electrophoresis (2DE) screen, performed concurrently, revealed several candidate proteins for mediating these changes. Functional annotation clustering of proteins differently expressed with age and subsequent in vitro assays indicated that processes related to cytoskeleton organization and antioxidant defense are important cellular mechanisms associated with MSC aging.

Materials and Methods

MSC Culture

MSCs were isolated from the tibial and femoral bone marrow of 83-week- and 12-month-old Sprague–Dawley rats (Fa. Harlan Winkelmann, Eystrup, Germany, http://www.harlan-winkelmann.de). Male animals were chosen to avoid potential influences of estrogen levels. Isolated cells were cultured in standard expansion medium (EM) [23]. For flow cytometry the following antibodies were employed: mouse (α-rat CD44) (Serotec, Oxford, U.K., http://www.serotec.com), mouse (α-rat CD45) (Acris Antibodies, Herford, Germany, http://www.acris-antibodies.com), mouse (α-rat CD73) (BD Biosciences, San Diego, CA, http://www.bdbiosciences.com), mouse (α-rat CD90) (Acris Antibodies), rat(α-mouse IgG):PE (BD Biosciences).

Functional Assays

All assays were carried out with cells in passage two (P2). Senescence was additionally investigated in P6. Senescence: At a confluence of 80%–90%, cells were stained by the Senescent Cells Staining Kit (Sigma-Aldrich, St. Louis, MO, http://www.sigmaaldrich.com) according to manufacturer's instructions. Migration: A modified Boyden chamber assay was used. MSCs (1×10^4) were seeded and incubated for 5 hours at 37°C. Migrated cells were stained with 10 μg/ml Hoechst. Differentiation: Confluent MSCs were exposed to osteogenic and adipogenic differentiation media [2]. Alkaline phosphatase (AP) activity was detected colorimetrically by para-nitrophenylphosphate and mineralization by Alizarin red staining. Adipogenic differentiation was visualized by Sudan IV staining. Proliferation: Short-term proliferation assays were carried out for 3 days before measuring cell numbers by CellTiter 96 AQueous test (Promega, Madison, WI, http://www.promega.com). Population doubling times were determined by seeding 3,000 cells/cm^2 and determination of cell numbers after reaching 80% confluence.

2DE and Mass Spectrometry

For 2D gel electrophoresis, MSCs from young and old animals (passage 2) were cultivated to 80% confluence. For osteogenic stimulation, cells were additionally incubated with osteogenic medium (OM) for 5 days. Subsequent to washing cells with phosphate-buffered saline (PBS), they were harvested with PBS/5 mM EDTA by cautious scraping on ice. Cells were washed again with PBS and the remaining buffer was quantitatively removed before shock freezing of cells in liquid nitrogen. Seventy micrograms of protein lysates were separated by 2DE as described previously [24]. Gel evaluation was performed using Delta2D (version 3.4, Decodon, Greifswald, Germany, http://www.decodon.com) [25]. Briefly, corresponding gel images were first warped using "exact mode". A fusion image was subsequently generated. Spot detection was carried out on this fusion image automatically, followed by manual spot editing. Subsequently, spots were transferred from the fusion image to all gels. The signal intensities (volume of each spot) were computed as a weighted sum of all pixel intensities of each protein spot. Percent volume of spot intensities to the total spot volume of the parent gel was used for quantitative analysis of protein expression level. 2DE was repeated seven times for EM and eight times for OM. For protein identification, spots of interest were in-gel trypsin digested and analyzed by LCQ Deca XP nano HPLC/ESI ion trap mass spectrometer (Thermo Fisher Scientific, Waltham, MA, http://www.thermofisher.com). Monoisotopic mass values of peptides were searched against NCBInr sequence database (taxonomy: *Mus musculus*), allowing one missed cleavage [26]. To conduct functional categorizing, all differentially expressed proteins were submitted to the Database for Annotation, Visualization and Integrated Discovery [27].

Western Blot

The Novex system was employed according to the Invitrogen NuPAGE protocol. Primary antibodies were mouse (α-human calponin) (1:1,000; Sigma-Aldrich), mouse (α-human galectin-3) (1:1,000, Biozol, Eching, Germany, http://www.biozol.de), goat (α-human transgelin) (1:200, Santa Cruz Biotechnology, Santa Curz, CA, http://www.scbt.com), mouse (α-human peroxiredoxin-5) (1:5,000, Biozol) and mouse (α-rabbit glyceraldehyde-3-phosphate dehydrogenase) (1:10,000, Biozol). Secondary antibodies were donkey (α-goat IgG) peroxidase and goat (α-mouse IgG) peroxidase. Band intensities were quantified by NIH ImageJ software package (http://rsb.info.nih.gov/ij).

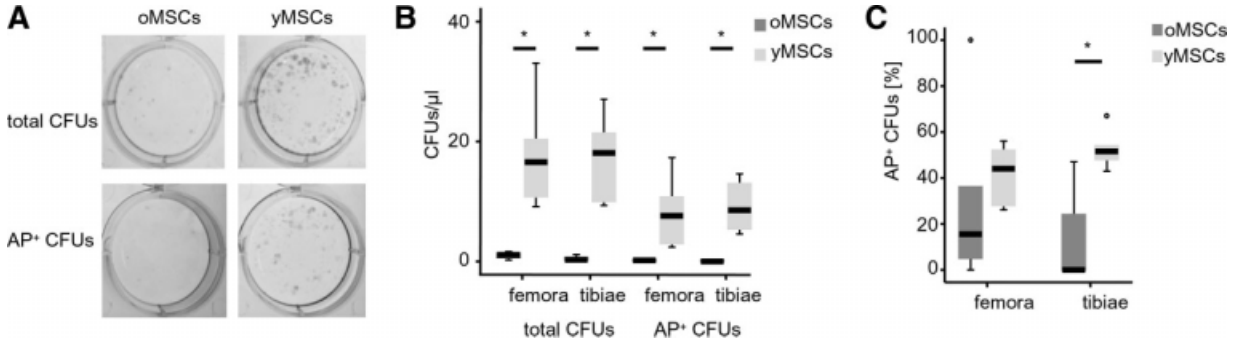

Figure 1. Quantity of total and AP-positive CFUs is decreased in oMSCs. **(A):** Typical photographs of CFUs derived from bone marrow of old and young animals. **(B):** Absolute numbers of CFUs and of AP-positive CFUs per volume of bone marrow. **(C):** Percentage of AP-positive CFUs relative to total CFUs. CFUs were considered as AP-positive when more than 50% of cells stained AP. *, indicates statistical significance. Abbreviations: AP, alkaline phosphatase; CFU, colony-forming unit; oMSC, old mesenchymal stem cell; yMSC, young mesenchymal stem cell.

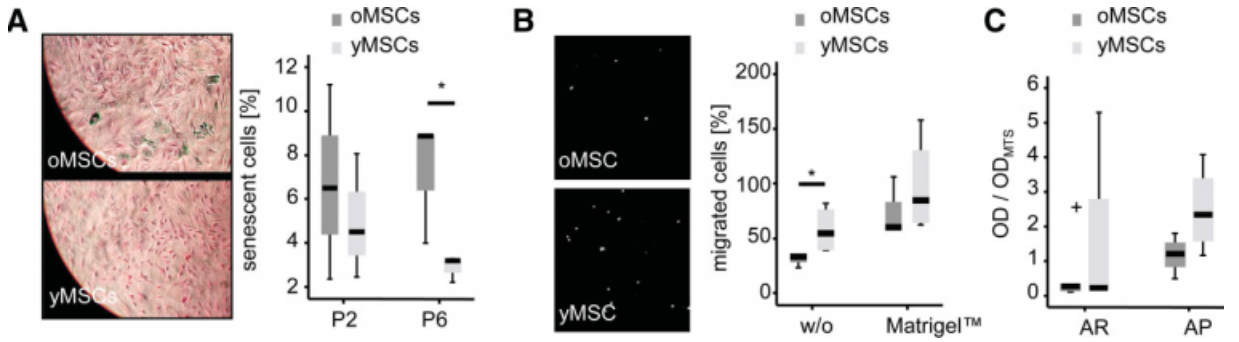

Figure 2. Number of senescent cells and migratory capacity of mesenchymal stem cells (MSCs) depends on donor age. **(A):** Photographs of ß-galactosidase staining (blue) of MSCs in passage 6 and the percentage of senescent cells in MSC populations from passage 2 and 6 in relation to total cell numbers. **(B):** Two representative Transwell filters with migrated cells and the ratio of migrated cells (after 5 hours) normalized to the internal standard (number migrated after 32 hours). Filters were either untreated or coated with Matrigel. **(C):** Osteogenic differentiation determined by matrix mineralization (Alizarin Red) and AP activity. Values were normalized to optical density values from CellTiter 96 AQueous assay. At least three independent experiments were carried out for all assays. *, indicates statistical significance. Abbreviations: AP, alkaline phosphatase; oMSC, old mesenchymal stem cell; P, passage; yMSC, young mesenchymal stem cell.

Antioxidant Activity and Cytoskeleton Dynamics

Cell lysates were investigated by the Antioxidant Assay Kit (Sigma-Aldrich) following manufacturer's instructions. Staining of actin fibers of (para)formaldehyde-fixed and permeabilized cells was achieved by an incubation with Alexa 488-conjugated phalloidin (6.6 nM; Invitrogen, Carlsbad, CA, http://www.invitrogen.com). Nuclei were counterstained with DAPI (4′,6-diamidino-2-phenylindole). Jasplakinolide (Merck, Darmstadt, Germany, http://www.merck.de) was delivered at a final concentration of 250 nM. Confocal fluorescence imaging used an LSM 510 META microscope system (Carl Zeiss, Jena, Germany, http://www.zeiss.de) under identical excitation and exposure conditions.

Statistics

Functional data were analyzed by Mann–Whitney U test. Results from expression analysis were tested by the Student's t test. All tests were analyzed two-sided and at a significance level of $p < .05$.

Results

The Number of MSCs Is Reduced in Aged Animals

To investigate the age-dependent variation of osteoprogenitor cells in bone marrow, CFUs were determined (Fig. 1). As bone, and hence bone marrow, volume is smaller in young animals (bone marrow volume femur: $\text{median}_{\text{oMSCs}} = 180\ \mu\text{l}$, $\text{median}_{\text{yMSCs}} = 40\ \mu\text{l}$; bone marrow volume tibia: $\text{median}_{\text{oMSCs}} = 78\ \mu\text{l}$ $\text{median}_{\text{yMSCs}} = 30\ \mu\text{l}$), results were normalized to the corresponding bone marrow volume. The total number of CFUs was significantly lower in bone marrow of old animals compared with younger ones (femora: $n_{\text{oMSCs}} = 1.1/\mu\text{l}$, $n_{\text{yMSCs}} = 16.7/\mu\text{l}$, $p = .004$; tibiae: $n_{\text{oMSCs}} = 0.3/\mu\text{l}$, $n_{\text{yMSCs}} = 18.0/\mu\text{l}$, $p = .003$). Similarly, the number of AP-positive CFUs was reduced in aged animals (femora: $n_{\text{oMSCs}} = 0.2/\mu\text{l}$, $n_{\text{yMSCs}} = 7.6/\mu\text{l}$, $p = .004$; tibiae: $n_{\text{oMSCs}} = 0.0/\mu\text{l}$, $n_{\text{yMSCs}} = 8.6/\mu\text{l}$, $p = .003$). In addition to the absolute number, the ratio of AP-positive CFUs in relation to total CFU numbers was significantly decreased in bone marrow from tibiae of aged animals ($\text{ratio}_{\text{oMSCs}} = 0.0\%$, $\text{ratio}_{\text{yMSCs}} = 51.2\%$, $p = .006$). A similar tendency could be observed in femora ($\text{ratio}_{\text{oMSCs}} = 15.3\%$, $\text{ratio}_{\text{yMSCs}} = 44.1\%$, $p = .109$). Subsequent to the finding that the quantity of MSCs is diminished with age, we pursued the question of functional alterations in the following experiments.

Aged MSCs Are More Susceptible Toward Senescence and Display a Lower Migratory Capacity

Senescence is a phenomenon of cellular aging, which can be monitored by β-galactosidase activity. MSC populations showed no difference in the proportion of senescent cells in

Table 1. Proteins age-dependently expressed under expansion as well as osteogenic conditions

NCBI acc	Protein name	Gene symbol	Expression ratio EM (oMSC/yMSC)	*p* value EM	Expression ratio OM (oMSC/yMSC)	*p* value OM	Expression ratio yMSC (EM/OM)	*p* value yMSC	Expression ratio oMSC (EM/OM)	*p* value oMSC
gil13516471	Beta-actin FE-3	Actg1	3.27	.019	1.53	.001				
gil6978589	Caldesmon 1	Cald1	1.11	.009	2.13	.035				
gil584951	Calponin-1 (Calponin H1, smooth muscle) (Basic calponin)	Cnn1	0.69	<.001	0.29	.003				
gil1706754	E-FABP (C-FABP)	Fabp5	1.40	<.001	1.82	.004	1.41	.008	1.41	<.001
gil13929190	Galectin 3	LGALS3	1.46	.036	1.49	<.001	0.65	.003	0.71	.011
gil41059678	Gamma synuclein	Sncg	1.85	<.001	6.31	<.001			0.77	.002
gil4504445	Heterogeneous nuclear ribonucleoprotein A1 isoform a[a]	HNRPA1	1.09/0.92	.002 .032	0.59/0.68	<.001 <.001	1.17	.042	1.42	<.001
gil4504447	Heterogeneous nuclear ribonucleoprotein A2/B1 isoform A2[a]	Hnrpa2b1	0.55/0.95	.002 0.035	0.51/4.31	.027 <0.001				
gil27229055	Huntingtin interacting protein K	HYPK	1.84	<.001	4.25	<.001				
gil8393781	Myosin light chain, regulatory B[a]	Mrlcb	0.61	.001	0.40/1.37	<.001 0.015	1.52	.001	2.07	<.001
gil16758404	Peroxiredoxin 5 precursor	Prdx5	1.43	.001	1.45	.004	1.44	<.001	1.42	<.001
gil34869683	Predicted: similar to purine-nucleoside phosphorylase	punA	1.96	.042	1.61	<.001				
gil18152793	Pyruvate dehydrogenase (lipoamide) beta	PDHB	0.84	.033	0.73	.016	1.24	.005	1.31	.011
gil13928744	Transgelin[a]	Tagln	1.49 0.68 1.23	<.0010 .007 0.016	2.36 0.59 1.56 2.64	0.002 >0.001 0.025 <.001	1.83	<.001	2.77	<.001

[a]More than one isoform of this protein was altered.

Abbreviations: C-FABP, Cutaneous fatty acid-binding protein; E-FABP, Fatty acid-binding protein, epidermal; EM, expansion medium; OM, osteogenic medium; oMSCs, old mesenchymal stem cell; yMSCs, young mesenchymal stem cells.

Table 2. Age-dependently expressed proteins associated with cytoskeleton and antioxidant defense

NCBI acc	Protein name	Gene symbol	Culture condition	Expression ratio (oMSC/yMSC)	*p* value
Cytoskeletal protein binding					
gil13928744	Transgelin[a]	Tagln	EM	1.49/0.68/1.23	<.001/.007/.016
gil61556900	Capping protein (actin filament), gelsolin-like	CAPG	EM	1.75	.015
gil6978589	Caldesmon 1	Cald1	EM	1.11	.009
gil13516471	Beta-actin FE-3	Actg1	EM	3.27	.019
gil34851815	Predicted: similar to coactosin-like 1	Cotl1	EM	2.25	.007
gil584951	Calponin-1 (Calponin H1, smooth muscle; Basic calponin)[b]	Cnn1	EM	0.69	<.001
gil31543942	Vinculin[a,b]	VCL	EM	1.37/1.61	.018/<.001
gil14389299	Vimentin[b]	Vim	EM	1.35	.032
gil50190	Beta-tropomyosin[b]	TPM2	EM	0.81	.024
gil8393781	Myosin light chain, regulatory B[b]	Mrlcb	EM	0.61	.001
gil61557028	Transgelin 2[b]	Tagln2	EM	1.06	.011
gil13928744	Transgelin[a]	Tagln	OM	2.36/0.59/1.56/2.64	.002/<.001/.025/<.001
gil6978589	Caldesmon 1	Cald1	OM	2.13	.035
gil78000192	Tropomyosin 1, alpha isoform c	TPM1	OM	0.76	.001
gil13516471	Beta-actin FE-3	Actg1	OM	1.53	.001
gil9506501	Calponin 3, acidic[a]	CNN3	OM	1.28/1.89	.002/.041
gil4758018	Calponin 2 isoform a[a,b]	Calponin 2	OM	1.98/2.71	<.001/<.001
gil584951	Calponin-1 (Calponin H1, smooth muscle; Basic calponin)[b]	Cnn1	OM	0.29	.003
gil4826659	F-actin capping protein beta subunit[b]	Capzb	OM	0.81	.010
gil193761	Alpha-globin[b]	Hba1	OM	10.00	.022
gil49864	Alpha-actin (aa 40–375)[b]	Acta2	OM	2.89	.002
gil8393781	Myosin light chain, regulatory B[a,b]	Mrlcb	OM	0.40/1.37	<.001/.015
gil543113	Smooth muscle protein SM22 homolog–bovine (fragments)[b]	Tagln2	OM	0.59	<.001
Antioxidant activity					
gil16758644	Thioredoxin	Txn1	EM	1.23	.005
gil8394432	Peroxiredoxin 2	Prdx2	EM	1.20	.026
gil16758404	Peroxiredoxin 5 precursor	Prdx5	EM	1.43	<.001
gil203658	Cu–Zn superoxide dismutase (EC 1.15.1.1)	SOD1	OM	1.24	.030
gil13928688	Glutathione S-transferase A5	GSTA5	OM	1.58	.006
gil16758404	Peroxiredoxin 5 precursor	Prdx5	OM	1.45	.004

[a]More than one isoform of this protein was altered.
[b]These proteins were added manually in addition to automatic annotation of DAVID.
Abbreviations: EM, expansion medium; OM, osteogenic medium; oMSCs, old mesenchymal stem cell; yMSCs, young mesenchymal stem cells.

second passage ($ratio_{oMSCs} = 6.5\%$, $ratio_{yMSCs} = 4.5\%$, $p = .827$, Fig. 2A). However, after six passages in vitro, a significantly higher percentage of oMSCs were β-galactosidase positive compared with cultures of yMSCs ($ratio_{oMSCs} = 8.8\%$, $ratio_{yMSCs} = 3.2\%$, $p = .0495$).

To investigate age-dependent changes in functional behavior of MSCs, their migration speed, differentiation, and proliferation was analyzed. Motility of oMSCs was lower relative to yMSCs on uncoated filters (migrated $cells_{oMSCs} = 32.7\%$, migrated $cells_{yMSCs} = 54.4\%$, $p = .031$, Fig. 2B). However, in the presence of Matrigel, oMSCs and yMSCs exhibited slightly elevated, but comparable, migration rates (migrated $cells_{oMSCs} = 59.7\%$, migrated $cells_{yMSCs} = 84.5\%$, $p = .289$). Both oMSCs and yMSCs responded similarly to osteogenic stimulation, as determined by the amount of matrix mineralization as well as cellular AP activity (Fig. 2C). There was a trend toward lower AP activities in oMSCs (oMSCs: $OD_{AP}/OD_{MTS} = 1.2$, yMSCs: $OD_{AP}/OD_{MTS} = 2.3$, $p = .157$). However, this tendency did not reach statistical significance, possibly due to the high interindividual variations that were generally observed in differentiation assays. In addition, there was a similar capability of oMSCs and yMSCs to differentiate into adipocytes ($percentage_{oMSCs} = 13.2\%$, $percentage_{yMSCs} = 14.3\%$, $p = .275$, data not shown). Furthermore, their proliferative capacity was unaffected by donor age. This was deduced from results of short-term proliferation assays ($OD_{oMSCs} = 2.4$, $OD_{yMSCs} = 2.0$, $p = .827$, data not shown) as well as by determining the population doubling time over a culture period of about 10 weeks.

To clarify whether alterations in the functional behavior of aged MSCs are due to changes in the composition of the MSC populations, their cell surface marker protein expression [2] was determined and found to be similar on cells from young and old rats ($CD44^+$, $CD73^+$, $CD90^+$, $CD45^-$, data not shown). Further, the pattern remained stable over serial passaging (analyzed until passage 17). In addition, oMSCs and yMSCs displayed a similar and typical fibroblastic morphology. Having established that old MSCs show increased susceptibility to senescence and decreased motility, we aimed to determine candidate proteins responsible for these cell physiological alterations.

Aging Alters the Cellular Proteome of MSCs

Lysates from MSCs with and without osteogenic stimulation were resolved by high-resolution 2DE. Around 5,000 protein spots were detected. Among the detected proteins, 10 were significantly and reproducibly downregulated and 26 upregulated under EM (Table 1, supporting information). In OM, 29 proteins were decreased and 40 proteins increased in their expression. Taken together, 14 proteins were age-dependently expressed under both conditions (Table 1). Differences between oMSCs and yMSCs were more prominent after

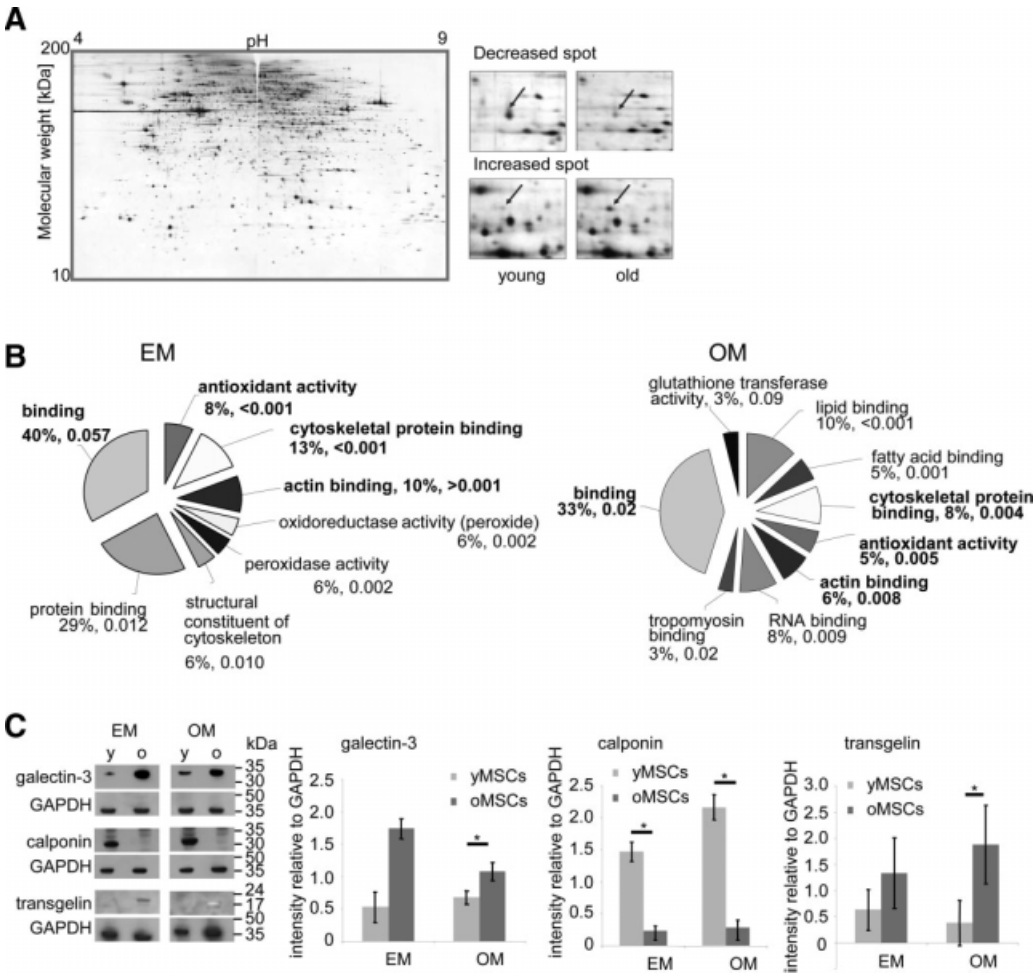

Figure 3. Age-related proteomic changes in mesenchymal stem cells (MSCs). **(A):** Representative two-dimensional protein pattern of MSCs. Enlarged insets show examples of upregulated and downregulated protein spots. **(B):** Pie charts depicting functional annotation clustering of age-affected proteins in EM and OM. Common proteins between OM and EM are indicated by bold font. Two-dimensional polyacrylamide gel electrophoresis was repeated seven times for EM and eight times for OM. **(C):** Representative Western blots for galectin-3, calponin, transgelin, and the corresponding GAPDH control blots and quantified signal intensities normalized to GAPDH. Data were determined from four animals. *, indicates statistical significance. Abbreviations: EM, expansion medium; GAPDH, glyceraldehyde-3-phosphate dehydrogenase; O, oMSC; OM, osteogenic medium; oMSC, old mesenchymal stem cell; Y, yMSC; yMSC, young mesenchymal stem cell.

osteogenic stimulation, reflected by a higher number of affected proteins (64 vs. 34), higher ratios of differential expression ($max_{EM} = 6.94$, $max_{OM} = 10.00$, $min_{EM} = 0.55$, $min_{OM} = 0.29$) and lower p values (median p $value_{EM} = .013$, median p $value_{OM} = .004$).

From all detected protein spots, roughly 3% (140 of 5,000) were differentially expressed under conditions of osteogenic stimulation. In contrast, from the detected age-affected protein spots, 57% (8 of 14) were altered after osteogenic stimulation (Table 2), indicating that a high number of proteins affected by aging of MSCs are also regulated during osteogenic differentiation of the cells. Among these proteins regulated in response to an osteogenic stimulus, pyruvate dehydrogenase (lipoamide) beta has already been described as related to osteogenic differentiation of MSCs [28]. The high-resolution 2DE could additionally identify fatty acid-binding protein 5, galectin-3, γ-synuclein, heterogeneous nuclear ribonucleoprotein A1, myosin light chain, regulatory B, peroxiredoxin 5 precursor, and transgelin as responding to osteogenesis. These proteins have not been detected previously in other proteomic studies investigating osteogenic differentiation of MSCs [21, 28, 29].

Functional annotation clustering of the differentially expressed proteins in oMSCs versus yMSCs revealed that processes altered, with and without osteogenic stimulation, seem to be related to antioxidant defense and cytoskeleton organization (Fig. 3B, Table 2): antioxidant activity ($p_{EM} < .001$, $p_{OM} = .005$), cytoskeletal protein binding ($p_{EM} < .001$, $p_{OM} = .004$), and actin binding ($p_{EM} < .001$, $p_{OM} = .008$). Furthermore, age-affected proteins seem to be involved in lipid binding, fatty acid binding, and RNA binding. Interestingly, age-associated proteins were not clustered to biological processes of cell cycle regulation or cell proliferation. This is in line with our functional analysis, demonstrating no age-dependent changes in the proliferative capacity of MSCs.

Differentially expressed proteins, involved in bone physiology or aging, were validated by Western blotting of whole cell lysates (Fig. 3C). Age-dependent expression of galectin-3 and calponin-1 was confirmed in EM and OM and of transgelin in OM (EM: $ratio_{galectin\text{-}3} = 3.33$, $p_{galectin\text{-}3} < .001$, $ratio_{calponin\text{-}1} = 0.17$, $p_{calponin\text{-}1} < .001$, $ratio_{transgelin} = 2.12$, $p_{transgelin} = .122$; OM: $ratio_{galectin\text{-}3} = 1.60$, $p_{galectin\text{-}3} = .003$, $ratio_{calponin\text{-}1} = 0.14$, $p_{calponin\text{-}1} < .001$, $ratio_{transgelin} = 4.94$, $p_{transgelin} = .014$). However, peroxiredoxin-5 was not found to be differentially

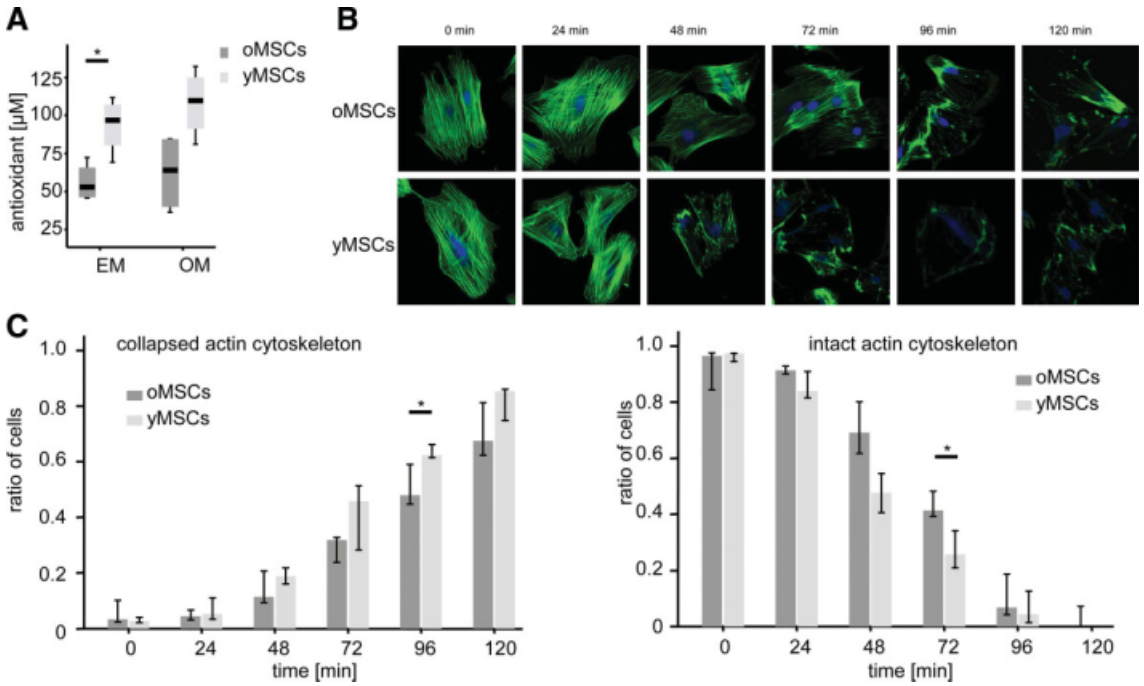

Figure 4. Antioxidant power and cytoskeleton kinetics are decreased with mesenchymal stem cell (MSC) aging. **(A):** Concentration of antioxidant activity in lysates of MSCs, according to a Trolox standard, investigated in four independent samples. **(B):** Representative images of phalloidin labeling in oMSCs and yMSCs after jasplakinolide application over a time series. **(C):** Cells containing a completely intact or a fully destroyed actin cytoskeleton were counted at different time points after Jasplakinolide application. Original magnification of fluorescence microscopy is ×630. Samples from three young and old animals were investigated. *, indicates statistical significance. Abbreviations: EM, expansion medium; OM, osteogenic medium; oMSC, old mesenchymal stem cell; yMSC, young mesenchymal stem cell.

expressed (EM: $\text{ratio}_{\text{peroxiredoxin-5}} = 1.01$, $p_{\text{peroxiredoxin-5}} = .897$; OM: $\text{ratio}_{\text{peroxiredoxin-5}} = 0.94$, $p_{\text{peroxiredoxin-5}} = .380$), probably due to the detection of different isoforms in Western blotting versus 2DE.

The mRNA amounts of the age-dependently expressed genes galectin-3, calponin-1, and transgelin were similar in young and old MSCs (Fig. 1, supporting information), indicating an age-associated regulation of protein levels by post-transcriptional mechanisms.

MSC Aging Affects Antioxidant Defense and Cytoskeleton Turnover

To further investigate the ontology-based association of aging and antioxidant defense in MSCs, the antioxidant power of old and young MSCs was determined under different culture conditions (Fig. 4A). Lysates from oMSCs cultured in EM exhibited a significantly reduced antioxidant activity compared with those from young cells ($\text{antioxidant}_{\text{oMSC}} = 56\ \mu\text{M}$, $\text{antioxidant}_{\text{yMSC}} = 94\ \mu\text{M}$, $p = .043$). A similar trend was observed after the application of an osteogenic stimulus, but did not reach statistical significance ($\text{antioxidant}_{\text{oMSC}} = 62\ \mu\text{M}$, $\text{antioxidant}_{\text{yMSC}} = 108\ \mu\text{M}$, $p = .083$).

The second major group of proteins over-represented in ontology analysis was related to cytoskeleton organization. To further validate these in silico data, actin fibers were labeled by phalloidin. Micrographs showed that both old and young MSC populations had no gross abnormalities in their actin filament content and organization. As it is known that aging affects the cytoskeletal dynamics, we further investigated the actin cytoskeleton remodeling by applying the actin-stabilizing drug Jasplakinolide in a time-dependent manner (Fig. 4B, 4C). The mean ratio of cells responding with a fully collapsed actin cytoskeleton was lower in oMSCs than in yMSCs at all five time points investigated reaching statistical significance at 96 minutes after Jasplakinolide supplementation ($\text{mean}_{\text{oMSCs}} = 51\%$, $\text{mean}_{\text{yMSCs}} = 63\%$, $p = .049$). Furthermore, the ratio of cells maintaining an intact actin cytoskeleton was higher in oMSCs compared with yMSCs at all time points and reached the significance level at 72 minutes ($\text{mean}_{\text{oMSCs}} = 43\%$, $\text{mean}_{\text{yMSCs}} = 27\%$, $p = .028$). Thus, oMSCs seem to respond to Jasplakinolide in a delayed manner indicating a decelerated actin turnover. Likely, the effect of Jasplakinolide was highest between 72 and 96 minutes after application due to its uptake or degradation kinetics, thereby reaching statistical significance at these time points, while at the other time points, a similar trend was observed.

Finally, it was investigated, whether the detected age-dependent alterations also occur in sexual matured animals by investigating MSCs from 3-month-old animals. CFU numbers, migratory capacity, and antioxidant power as well as cytoskeleton dynamic of MSCs have a similar qualitative tendency of elevation in these cells like MSCs from 3-weeks-old animals. However, the quantitative effects were more prominent in the youngest age group (Fig. 2, supporting information), indicating a gradual loss of number and function of MSCs with the age of the animal.

Discussion

We demonstrated that the age-related decrease in MSC number is paralleled by alterations in the functionality of oMSCs. Moreover, the proteome of MSCs undergoing aging was profiled for the first time, thereby uncovering age-affected proteins that are potentially causative for the described functional changes. Functional annotation clustering pointed to age-

dependent alterations in cytoskeleton organization and antioxidant defense in MSCs.

Potential Relevance of Age-Affected Proteins in Bone Physiology

Several proteins belonging to the actin-binding protein family of calponins were age-dependently expressed. Studies of the calponin-1 (CNN-1) knockout mouse revealed early onset of cartilage formation, premature ossification, increased postnatal bone formation, and accelerated fracture healing [30]. These observations were explained by the enhanced response to bone morphogenetic proteins (BMP). Therefore, by blocking BMP signaling, CNN-1 was established as negative regulator of bone formation [30]. As BMP levels decrease with age [30], downregulation of CNN-1 might be compensatory to maintain BMP signaling and thus osteogenesis.

Galectin-3 is a multifunctional protein regulation extracellular matrix adhesion, growth factor activity, intracellular signaling, and nuclear transcription. In murine bone development, loss of galectin-3 has been associated with altered Indian hedgehog expression pattern at the growth plate, increased cell death of hypertrophic chondrocytes, and uncoupling of growth plate vascularization [31–33]. The important role of galectin-3 in osteoblast differentiation and chondrocyte maturation is strengthened as its expression is controlled by Runx2/Cbfa1 [34]. Thus, galectin-3 might be involved in the regulation of MSC differentiation or fate determination. However, as galectin-3 is a multifunctional protein and its biological role seems to be defined by its subcellular localization [35], it will be crucial for further studies to investigate its age-dependent concentrations in different cellular compartments. For example, the identified intracellular upregulation of galectin-3 in aged MSCs indicate either intracellular retention due to an insufficient secretion and accumulation in the nucleus or a general increase in expression affecting all cellular compartments. As one of the extracellular functions of galectin-3 is to enhance migration, increased expression might be required to maintain normal MSC migration.

Osteogenesis by Aged MSCs

Although the number of AP-positive CFUs declined with age, the osteogenic differentiation capacity of the whole population, detected by matrix mineralization as well as AP activity was not affected. This is in concordance with other in vitro studies demonstrating the maintenance of the osteogenic capacity in aged MSCs [10]. However, opposite findings might account for analyzing different species (rat, human), variable output parameter (total AP activity, AP-positive cells, matrix mineralization, ectopic bone formation), and importantly different culture conditions (2D vs. 3D, dexamethasone, or calcitriol supplementation) [6, 7, 36]. Hence, the nonconformity of results could be caused by a potential effect of age on the regulation and timing of the osteogenic process. Apart from the intrinsic alterations identified in this in vitro study, an aged systemic environment providing altered biochemical stimuli has to be considered for interpretations in vivo. Indeed, MSCs under standard in vitro culture conditions have displayed a similar adipogenic and osteogenic potential [37], whereas under similar experimental conditions, MSCs exposed to serum from old donors are actually inhibited in their osteoblastic but not adipocytic differentiation, compared with those cultured with serum from young donors [38].

ROS Defense

We identified the age-dependent upregulation of several proteins involved in antioxidant defense, along with a decreased antioxidant power in aged MSCs. This might represent a response of the cells to higher ROS levels, possibly resulting from age-associated altered metabolic activities, which however seems to be inadequate to defend effectively. These effects seem to occur also in other cells as the expression of peroxiredoxins increases with age in mouse embryonic fibroblasts [39]. Hence, although the differential expression of antioxidative proteins is not likely to be causative for aging phenomena in MSCs, the reduced ROS defense in oMSCs indicates that aging of these cells follows at least partially the oxidative stress theory, stating that oxidizing species cause molecular damage and, over time, cell and tissue dysfunction [40]. This is strengthened by our observation of higher susceptibility toward senescence in oMSCs, for which ROS are a major trigger.

Cytoskeleton Dynamics

On the basis of a proteome and ontology analysis, we establish that aging results in altered expression of actin cytoskeleton-associated proteins in MSCs accompanied by decreased actin turnover. The molecular mechanism of actin stabilization in oMSCs might be due to the increased levels of transgelin, which is an actin cross-linking protein already identified as biomarker of aging.

Also consistent with altered cytoskeletal dynamics is the lower migratory capacity of oMSCs, as cellular movement is tightly coupled to local actin organization and turnover [41]. According to the molecular function of the detected age-dependent proteins, such as calponin-1, transgelin, vinculin, caldesmon-1, myosin light chain regulatory B, and β-actin, virtually each step of the cellular migration cycle could be altered in oMSCs. Interestingly, the cellular migration speed of oMSCs analyzed on Matrigel was elevated up to the level of the young cells indicating (a) a severe influence of the cellular environment, and (b) that oMSCs are still able to respond to external stimuli. This finding supports the feasibility of potential therapeutic approaches focusing on in vivo mobilization of MSCs in elderly patients.

Studies on actin dynamics and life span in budding yeast revealed that a deletion of the transgelin homologue Scp1 leads to increased actin dynamics and cell viability [42]. Considering our results in MSCs that (a) transgelin is upregulated with age and (b) aged MSCs show decreased actin dynamics, along with the finding that transgelin is overexpressed in senescent cells [43], this coupling of actin dynamics and life span might be conserved in mammalian cells, and especially in MSCs, with transgelin as a potential regulator and linker of these processes.

Local remodeling of the actin cytoskeleton is responsible for translating and modifying external biochemical stimuli, via growth factors and extracellular matrix molecules, into internal signals. Thus, a less dynamic actin cytoskeleton would respond inadequately to such signals. In the case of bone, it is intriguing that mechanical signals, which are important regulators of tissue homeostasis as well as regeneration, are also transduced via the cytoskeleton [44]. This is particularly interesting when considering that in vivo age seems to affect mechanical requirements [45]. Hence, we would postulate that aged MSCs are less responsive to environmental cues (both biological and mechanical), due to their lower actin dynamic, and that this has negative effects on their regenerative potential.

The two main findings on MSC aging, namely decreased ROS defense and reduced actin dynamics, might well affect each other and could potentially act additively or even synergistically. In yeast it has been shown that actin dynamics and ROS production seem to be coupled inversely [42]. The underlying mechanisms remain elusive, but a conceivable linkage could be the regulation of ion channels within the

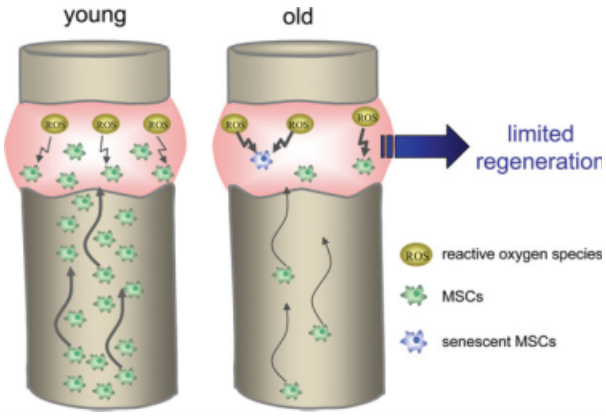

Figure 5. MSC-associated changes in aged individuals might cause a decrease in regeneration capacity. MSC numbers are reduced in the bone marrow of old individuals. Also, due to the lower migratory speed of old mesenchymal stem cells (oMSCs), fewer cells might be capable of homing to the site of injury, thereby further depleting their numbers in the hematoma. Reactive oxygen species, present especially in the early phases of healing, might affect oMSCs more dramatically than young mesenchymal stem cells, because of the age-related reduction in antioxidant power. A higher susceptibility toward senescence in oMSCs might additionally contribute to a shortage of functional progenitor cells able to augment a fast and uneventful regeneration. Abbreviation: MSC, mesenchymal stem cell.

mitochondrial membrane by actin remodeling, in turn affecting ROS release. On the other hand, increased oxidative stress could damage actin molecules themselves or their binding proteins, for example by irreversible carboxylation, thereby decreasing the kinetics of remodeling. Future studies will need to determine whether the two processes are linked to each other, and if so, which mechanisms are causative.

Aging Model

Aging can be defined as a progressive loss of function and thus increased risk of death with time. Decreased bone regeneration with age reflects the systemic aging phenomenon [46], which we hypothesize is due to (a) the number of MSCs lost over time and (b) the gradual accumulation of nonfunctional senescent MSCs. Aging of the MSC population does not necessarily mean that there is a qualitative decline of each individual MSC. Rather, our observations are quantitative expressions of the whole MSC population, potentially consisting of a mixture of nonfunctional and functional MSCs. Hence, it will be important to determine whether all cells in the MSC population age in a synchronized manner, to a similar extent, or whether all functional changes are attributable to a small number of cells. If the last point is the case, future studies will have to clarify questions such as: how can we identify the "bad guys?" Are there ideal cell surface markers distinguishing functional versus nonfunctional oMSCs?

Potential Clinical Relevance

The smaller number of MSCs observed in the bone marrow of old rats confirms observations from other studies, describing that aging of individuals is associated with a decrease in MSC quantity [6]. This shortage of progenitor cells could be exacerbated at the site of injury by the lower migratory potential of oMSCs. In addition, because oMSCs have a weaker capacity to defend against the reactive oxidant species especially prevalent in the initial phase of healing and are more susceptible to senescence, the pool of progenitor cells at regeneration sites could be further diminished (Fig. 5). This reduction in MSC number could account for the clinically recognized decrease in regeneration potential with age and might be overcome by cell therapies based on enrichment or ex vivo expansion of MSCs before retransplantation. Interestingly, there was no age-dependent change in adipogenic differentiation potential and only a mild trend in osteogenic differentiation. Based on these and the previously described observations, one could speculate that potential novel strategies for augmentation of regeneration should focus on attracting progenitor cells to the site of injury, e.g., by chemotactic agents, and/or on ROS protection, rather than simply to stimulate cell differentiation.

Conclusions

Results of this study are significant for the understanding of MSC aging, appearing to concur with current aging models involving ROS defense and cytoskeleton dynamics. Profound knowledge about these events might enable us to better understand age-related changes in tissue regeneration processes and thereby rationally design innovative approaches for regenerative therapies. Investigating stem cell aging might also give insights into organism aging and has been postulated as the other side of the coin in cancer protection [5]. This hypothesis aligns with our results because ROS protection and senescence control are two crucial physiological strategies of antitumor defense. A further understanding of the molecular basis of aging might allow for rational manipulation of cells, in a way that deleterious effects of aging are compensated without increasing the risk of tumorigenesis.

Acknowledgments

This study was supported by the Federal Ministry of Education and Research (BMBF) excellence cluster Berlin-Brandenburg Center for Regenerative Therapies and the German National Genome Research Network (NGFN) program established by the BMBF. We thank Marzena Princ for excellent technical assistance, Marion Herrmann for 2DE, and Silke Becker for technical assistance in mass spectrometric protein identification. They also thank Dr. C. Wilson for critical reading of the manuscript.

Disclosure of Potential Conflicts of Interest

The authors indicate no potential conflicts of interest.

References

1 Giordano A, Galderisi U, Marino IR. From the laboratory bench to the patient's bedside: An update on clinical trials with mesenchymal stem cells. J Cell Physiol 2007;211:27–35.
2 Pittenger MF, Mackay AM, Beck SC et al. Multilineage potential of adult human mesenchymal stem cells. Science 1999;284:143–147.
3 Meyer RA Jr, Meyer MH, Tenholder M et al. Gene expression in older rats with delayed union of femoral fractures. J Bone Joint Surg Am 2003;85-A:1243–1254.
4 Rauscher FM, Goldschmidt-Clermont PJ, Davis BH et al. Aging, progenitor cell exhaustion, and atherosclerosis. Circulation 2003;108:457–463.

5 Sharpless NE, Depinho RA. How stem cells age and why this makes us grow old. Nat Rev Mol Cell Biol 2007;8:703–713.
6 Sethe S, Scutt A, Stolzing A. Aging of mesenchymal stem cells. Ageing Res Rev 2006;5:91–116.
7 Quarto R, Thomas D, Liang CT. Bone progenitor cell deficits and the age-associated decline in bone repair capacity. Calcif Tissue Int 1995; 56:123–129.
8 Dobson KR, Reading L, Haberey M et al. Centrifugal isolation of bone marrow from bone: An improved method for the recovery and quantitation of bone marrow osteoprogenitor cells from rat tibiae and femurae. Calcif Tissue Int 1999;65:411–413.
9 Huibregtse BA, Johnstone B, Goldberg VM et al. Effect of age and sampling site on the chondro-osteogenic potential of rabbit marrow-derived mesenchymal progenitor cells. J Orthop Res 2000;18:18–24.
10 Stenderup K, Justesen J, Eriksen EF et al. Number and proliferative capacity of osteogenic stem cells are maintained during aging and in patients with osteoporosis. J Bone Miner Res 2001;16:1120–1129.
11 Oreffo RO, Bennett A, Carr AJ et al. Patients with primary osteoarthritis show no change with ageing in the number of osteogenic precursors. Scand J Rheumatol 1998;27:415–424.
12 Meunier P, Aaron J, Edouard C et al. Osteoporosis and the replacement of cell populations of the marrow by adipose tissue. A quantitative study of 84 iliac bone biopsies. Clin Orthop Relat Res 1971;80: 147–154.
13 Muraglia A, Cancedda R, Quarto R. Clonal mesenchymal progenitors from human bone marrow differentiate in vitro according to a hierarchical model. J Cell Sci 2000;113 (Part 7) :1161–1166.
14 Baxter MA, Wynn RF, Jowitt SN et al. Study of telomere length reveals rapid aging of human marrow stromal cells following in vitro expansion. Stem Cells 2004;22:675–682.
15 Park JS, Kim HY, Kim HW et al. Increased caveolin-1, a cause for the declined adipogenic potential of senescent human mesenchymal stem cells. Mech Ageing Dev 2005;126:551–559.
16 Bergman RJ, Gazit D, Kahn AJ et al. Age-related changes in osteogenic stem cells in mice. J Bone Miner Res 1996;11:568–577.
17 Xing Z, Ryan MA, Daria D et al. Increased hematopoietic stem cell mobilization in aged mice. Blood 2006;108:2190–2197.
18 Rossi DJ, Bryder D, Zahn JM et al. Cell intrinsic alterations underlie hematopoietic stem cell aging. Proc Natl Acad Sci USA 2005;102: 9194–9199.
19 Samper E, Fernandez P, Eguia R et al. Long-term repopulating ability of telomerase-deficient murine hematopoietic stem cells. Blood 2002; 99:2767–2775.
20 Ito K, Hirao A, Arai F et al. Regulation of oxidative stress by ATM is required for self-renewal of haematopoietic stem cells. Nature 2004; 431:997–1002.
21 Foster LJ, Zeemann PA, Li C et al. Differential expression profiling of membrane proteins by quantitative proteomics in a human mesenchymal stem cell line undergoing osteoblast differentiation. Stem Cells 2005;23:1367–1377.
22 Kratchmarova I, Blagoev B, Haack-Sorensen M et al. Mechanism of divergent growth factor effects in mesenchymal stem cell differentiation. Science 2005;308:1472–1477.
23 Kasper G, Dankert N, Tuischer J et al. Mesenchymal stem cells regulate angiogenesis according to their mechanical environment. Stem Cells 2007;25:903–910.
24 Klose J, Kobalz U. Two-dimensional electrophoresis of proteins: An updated protocol and implications for a functional analysis of the genome. Electrophoresis 1995;16:1034–1059.
25 Mao L, Zabel C, Wacker MA et al. Estimation of the mtDNA mutation rate in aging mice by proteome analysis and mathematical modeling. Exp Gerontol 2006;41:11–24.
26 Zabel C, Sagi D, Kaindl AM et al. Comparative proteomics in neurodegenerative and non-neurodegenerative diseases suggest nodal point proteins in regulatory networking. J Proteome Res 2006;5:1948–1958.
27 Dennis G Jr, Sherman BT, Hosack DA et al. DAVID: Database for Annotation, Visualization, and Integrated Discovery. Genome Biol 2003;4:P3.
28 Sun HJ, Bahk YY, Choi YR et al. A proteomic analysis during serial subculture and osteogenic differentiation of human mesenchymal stem cell. J Orthop Res 2006;24:2059–2071.
29 Salasznyk RM, Westcott AM, Klees RF et al. Comparing the protein expression profiles of human mesenchymal stem cells and human osteoblasts using gene ontologies. Stem Cells Dev 2005;14:354–366.
30 Moerman EJ, Teng K, Lipschitz DA et al. Aging activates adipogenic and suppresses osteogenic programs in mesenchymal marrow stroma/stem cells: The role of PPAR-gamma2 transcription factor and TGF-beta/BMP signaling pathways. Aging Cell 2004;3:379–389.
31 Fowlis D, Colnot C, Ripoche MA et al. Galectin-3 is expressed in the notochord, developing bones, and skin of the postimplantation mouse embryo. Dev Dyn 1995;203:241–251.
32 Aubin JE, Gupta AK, Bhargava U et al. Expression and regulation of galectin 3 in rat osteoblastic cells. J Cell Physiol 1996;169:468–480.
33 Colnot C, Sidhu SS, Balmain N et al. Uncoupling of chondrocyte death and vascular invasion in mouse galectin 3 null mutant bones. Dev Biol 2001;229:203–214.
34 Stock M, Schafer H, Stricker S et al. Expression of galectin-3 in skeletal tissues is controlled by Runx2. J Biol Chem 2003;278: 17360–17367.
35 Dumic J, Dabelic S, Flogel M. Galectin-3: An open-ended story. Biochim Biophys Acta 2006;1760:616–635.
36 Mueller SM, Glowacki J. Age-related decline in the osteogenic potential of human bone marrow cells cultured in three-dimensional collagen sponges. J Cell Biochem 2001;82:583–590.
37 Justesen J, Stenderup K, Eriksen EF et al. Maintenance of osteoblastic and adipocytic differentiation potential with age and osteoporosis in human marrow stromal cell cultures. Calcif Tissue Int 2002;71: 36–44.
38 Abdallah BM, Haack-Sorensen M, Fink T et al. Inhibition of osteoblast differentiation but not adipocyte differentiation of mesenchymal stem cells by sera obtained from aged females. Bone 2006;39: 181–188.
39 Kubo E, Miyazawa T, Fatma N et al. Development- and age-associated expression pattern of peroxiredoxin 6, and its regulation in murine ocular lens. Mech Ageing Dev 2006;127:249–256.
40 Harman D. Aging: A theory based on free radical and radiation chemistry. J Gerontol 1956;11:298–300.
41 Webb DJ, Parsons JT, Horwitz AF. Adhesion assembly, disassembly and turnover in migrating cells—Over and over and over again. Nat Cell Biol 2002;4:E97–E100.
42 Gourlay CW, Ayscough KR. The actin cytoskeleton: A key regulator of apoptosis and ageing? Nat Rev Mol Cell Biol 2005;6:583–589.
43 Gonos ES, Derventzi A, Kveiborg M et al. Cloning and identification of genes that associate with mammalian replicative senescence. Exp Cell Res 1998;240:66–74.
44 Banes AJ, Lee G, Graff R et al. Mechanical forces and signaling in connective tissue cells: Cellular mechanisms of detection, transduction, and responses to mechanical deformation. Curr Opin Orthopaedics 2001;12:389–396.
45 Strube P, Sentuerk U, Riha T et al. Influence of age and mechanical stability on bone defect healing: Age reverses mechanical effects. Bone 2008;42:758–764.
46 Gavrilov LA, Gavrilova NS. The reliability theory of aging and longevity. J Theor Biol 2001;213:527–545.

See www.StemCells.com for supporting information available online.

RESEARCH ARTICLE

PROTEOMER: A workflow-optimized laboratory information management system for 2-D electrophoresis-centered proteomics

Grit Nebrich[1], Marion Herrmann[1], Daniela Hartl[1], Madeleine Diedrich[1], Thomas Kreitler[2], Christoph Wierling[2], Joachim Klose[1], Patrick Giavalisco[3], Claus Zabel[1] and Lei Mao[1]

[1] Institute for Human Genetics, Charité – University Medicine Berlin, Berlin, Germany
[2] Max Planck Institute for Molecular Genetics, Berlin, Germany
[3] Max Planck Institute for Molecular Plant Physiology, Potsdam-Golm, Germany

Received: June 23, 2008
Revised: October 10, 2008
Accepted: October 22, 2008

In recent years proteomics became increasingly important to functional genomics. Although a large amount of data is generated by high throughput large-scale techniques, a connection of these mostly heterogeneous data from different analytical platforms and of different experiments is limited. Data mining procedures and algorithms are often insufficient to extract meaningful results from large datasets and therefore limit the exploitation of the generated biological information. In our proteomic core facility, which almost exclusively focuses on 2-DE/MS-based proteomics, we developed a proteomic database custom tailored to our needs aiming at connecting MS protein identification information to 2-DE derived protein expression profiles. The tools developed should not only enable an automatic evaluation of single experiments, but also link multiple 2-DE experiments with MS-data on different levels and thereby helping to create a comprehensive network of our proteomics data. Therefore the key feature of our "PROTEOMER" database is its high cross-referencing capacity, enabling integration of a wide range of experimental data. To illustrate the workflow and utility of the system, two practical examples are provided to demonstrate that proper data cross-referencing can transform information into biological knowledge.

Keywords:
Database / 2-D electrophoresis / Laboratory information management system / Mass spectrometry

1 Introduction

The importance of proteomics analysis, for both basic and clinical research, increased after the sequencing of many important genomes from yeast to humans is completed [1]. Proteomics describes the investigation of the entire collection of proteins of a given cell type or tissue under defined conditions [1]. A large-scale proteomics analyses is usually conducted in a two-step process. After protein extraction, separation of complex protein mixtures is achieved either by 2-DE [2], or different types of LC [3]. Subsequently, the separated proteins/peptides are identified by means of an array of diverse mass spectrometric (MS) technologies [4]. We use MS/MS identifications in many cases for our studies although some proteins are still identified by peptide mass fingerprint (PMS) [5–7]. The goal of many proteomics studies is to detect altered protein expression and modifications associated with disease [3, 8–10] or to find molecular targets for biomarkers and therapy which still

Correspondence: Dr. Claus Zabel, Charité – University Medicine Berlin, Augustenburger Platz 1, 13353 Berlin, Germany
E-mail: claus.zabel@charite.de
Fax: +49-30-566904

Abbreviations: LIMS, laboratory information management system; **PPI,** protein–protein interaction; **XML,** extensible mark-up language

remains as a major challenge [11]. To detect quantitative changes by LC/MS-based proteomics approaches is still difficult although novel techniques have improved this shortcoming considerably [12]. On the other hand, 2-DE-based proteomics which provides accessible qualitative and quantitative data, is difficult to automate and the processing and linking of 2-D gel image derived information to corresponding MS data is often associated with excessive manual labor [13].

In our proteomics core facility, large-gel 2-DE is the main protein separation technique employed. Due to its high reproducibility and resolution, up to 10 000 protein species can be analyzed using a single 2-D gel [2, 14]. In addition, the recent development of modern techniques such as multiplex fluorescence coloring using DIGE warrants a more precise gel-to-gel comparison and quantification of proteins separated by 2-DE [15, 16]. Moreover, we employed different protein staining methods, which allow us to identify distinct post-translational protein modifications such as phosphorylation [17, 18], glycosylation or protein carbonylation (oxidative stress) [5]. To gain expression information from complex protein patterns, two 2-D gel evaluation software packages (Delta2D, DECODON, Greifswald, Germany and Proteomweaver, BioRad, Munich, Germany) are used for 2-D image analysis. We decided upon using this specific evaluation software after extensively testing of many commercially available packages (Klose *et.al.* submitted). For protein identification by MS, two types of mass spectrometers are employed in our laboratory. For fast, high-throughput protein identification, a MALDI-TOF Reflex 4 mass spectrometer (Bruker Daltonics, Bremen, Germany) is used, while for more sophisticated identification tasks, an LCQ ESI ITs mass spectrometer (Thermo Finnigan, Waltham, MA, USA) equipped with a nano-HPLC system (Dinox, Idstein, Germany) is used. Currently, our proteomics platform allows us to process and analyze ~40 2-D gels and identify over 600 proteins *per* week. In parallel to our 2-DE-based proteomics, an increasing number of LC-based proteomic experiments had to be incorporated into our work flow.

This large number of protein identifications in our proteomics core facility generates huge amounts of data daily, which need to be properly processed to be useful. An additional problem of current proteomics analysis is the heterogeneity of datasets that result from the use of different experimental platforms (*i.e.*, 2-DE/MS or LC/MS data). Different data formats derived from different evaluation programs and MS instruments are used. Cross-platform datasets are therefore usually poorly comparable to each other without investing a tremendous effort by the user who adapts a diverse, nontransparent data structure. Therefore, the large amount of heterogeneous data imposes serious challenges for scientists that originally generated them, and thus preclude an efficient extraction of biologically relevant information [19–21]. Due to these difficulties, bioinformatics supported data mining and structuring is of utmost importance to proteome analyses, serving on the one hand to collect, unify and evaluate experimental data [19], and on the other hand to combine experimental data with biological information already available in public data bases (*e.g.*, NCBI, EMBL, Swiss-Prot) or in the literature [22].

Recently, bioinformatics tools have emerged that simplify data mining. Many tools [20, 21, 23, 24] such as PEDRo [25], PRIDE (www.ebi.ac.uk/pride), ProteinScape [26], HSC-2DPAGE [27] provide web interfaces to enable data retrieval and dissemination [28]. ProteinScape [26] is able to handle MS-based protein identification data [22]. A more recent version of ProteinScape has a very limited capability to integrate 2-DE data. Similar tools also exist from various suppliers (PRIDE, PEDRo). Unfortunately, most of them still put too little emphasizes on data generated by 2-DE. On the other hand, tools for 2-DE information annotation such as SWISS-2DPAGE (www.expasy.org) or 2-DE gel evaluation software tools are dedicated only to spot change data management (Delta2D, PDQuest, ProteomWeaver) but not to manage MS data. These systems export data on differentially regulated protein spots in either spreadsheet formats (Delta2D) or via an internal SQL database (*e.g.*, ProteomWeaver), where the protein expression information is assembled into match-sets consisting of spot information based on the comparison of a number of 2-D gels that belong to a specific project. However, most often, the assignment of protein identification data in 2-D evaluation software is restricted to manual annotation. Currently, there is still a lack of a flexible laboratory information management system (LIMS), which is capable of handling both MS and 2-DE data for academic users. Several examples of implemented LIMS are already reported in the literature but they focus either on non-2-DE proteomics approaches [29, 30] or are still incomplete [31]. In addition LIMS solutions for the research laboratory and pharmaceutical industry such as *Labvantage* (http://www.labvantage.com) and *Proteus* (Genologics, http://www.genologics.com/proteomics/) are also available. Especially *Labvantage* is a custom tailored for the requirements for LIMS in an industrial setting. *Proteus* provides a scalable laboratory and data management solution to integrate proteomics data from various platforms ranging from 2-D gel to LC proteomics experiments with their respective MS data.

An additional persisting problem of the currently available bioinformatics tools is the inability to cross-link data from our different proteomics projects and platforms. Frequently, cross-comparison of our different proteomics experiments is still limited to using protein or gene names supplied by MS identification data for manual comparison of protein or gene name lists. This precludes dynamic data inquiries guided by biological problems.

Here, we have developed the database and LIMS, PROTEOMER, to cope with the problems discussed above. The joint administration of experimental data from 2-DE analyses and MS with a suitable data infrastructure facilitates complex proteomic analyses across different projects.

2 Database design

PROTEOMER is a relational database for the management of comprehensive proteomic experimental data in our core facility. It stores relevant information on 2-DE such as protein expression changes under various conditions, as well as information on proteins identified using different MS techniques and instruments in an integrated data warehouse. One important feature of our database design is to use a wealth of experimental metadata, in order to provide users with the ability to retrieve cross-linked information (Fig. 1).

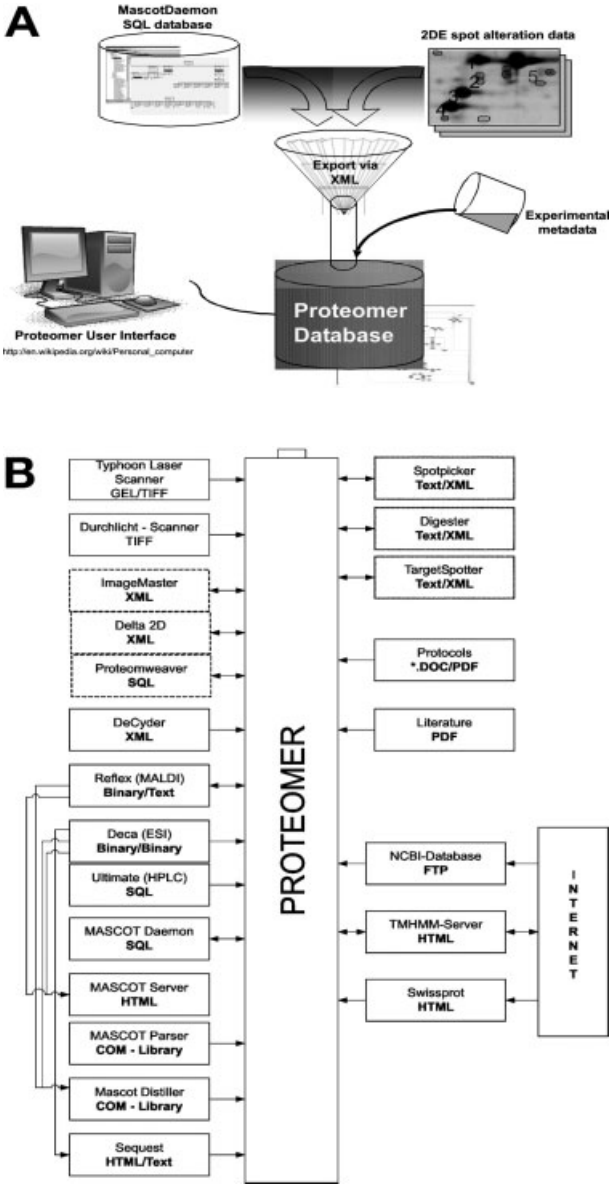

Figure 1. PROTEOMER LIMS database overview. (A) A simplified graphical representation of the PROTEOMER-centered laboratory information system structure is shown. (B) Dataflow chart representing the different components and modules of our proteomics core facility.

2.1 A laboratory-optimized workflow achieved by bench design

Unlike most other proteomic databases, PROTEOMER was developed in close cooperation with its users, taking our actual laboratory routine into consideration. Importantly, in order to determine the proper data structure of an LIMS, it is essential to carefully investigate the laboratory workflow in detail, *e.g.*, taking into account that protein identification data are generated by two MS instruments generating very different data formats and each is managed by different personnel. In order to generate a database optimized for 2-DE proteomics, we first trained some of its potential users in database techniques. Laboratory personnel from different backgrounds, technical assistances, engineers, bioinformaticians, and scientists, was selected and trained in database theory as well as programming language prior to the design phase. During bench design an even wider range of potential users was consulted frequently in order to optimize the workflow as much as possible. This approach was the starting point which allowed us to choose and combine suitable modules for the database.

The "data modeling" in PROTEOMER mimic the laboratory bench workflow established in our proteomics core facility. Figure 2 illustrates the abstract workflow of PROTEOMER. Here, nodes represent steps of analysis, while edges capture the flow of data along the processing pipeline. A more detailed representation of the workflow can be found as Supporting Information Fig. 1. The database focuses primarily on scientific users. Still, the integration of quality standards and standardization of procedures such as establishing standard operating procedures (SOPs) for ISO900 × certification may be feasible but this exceeds our resources and the scope of the database at present.

2.2 The PROTEOMER data structure

After completing bench design, the bench-routine adapted workflow was translated into a relational database structure. PROTEOMER comprises currently a total of 89 relational data tables to manage the entire range of our proteomics experimental data. The data tables representing modules were designed to centralize information obtained from 2-DE-based comparative proteomic experiments. Separate modules were established for the categories: projects, samples, protein extracts, electrophoresis run, gels, spots, proteins, measurements, identification method, MS-type, public sequence, literature, analytes. The stored information comprises all data related to our proteomics experiments, starting with the experimental setup, 2-DE run data, MS identification, statistical evaluation, and references for publication. Moreover, the information stored herein is organized in a way that reflects the structure of the actual experimental procedure that generated them.

The underlying criterion for each module is that it contains sufficient information to allow users to recreate any of

the experiments stored within it. This principle is now illustrated by looking at the "protein extracts" module. The sample preparation procedures and protocols [2, 32] are documented for each experiment [5, 8, 10, 17, 32]. This is essential since, the results of proteomics experiments have a tendency to strongly dependent on the method used for the experiment represented by a variety of factors such as sample treatment, sample preparation, staining method, electrophoresis and MS instrument parameters, and software used for 2-D gel evaluation. A schematic overview of part of the table structure for the modules is illustrated in Fig. 3. A detailed view of the complete data structure can be obtained at our website.

2.3 The flexibility of the data structure in the PROTEOMER database

Proteomics is a rapidly evolving field with a future holding the promise for even more efficient protein separation and identification methods [1, 12, 19]. However, the experimental window of all methods for proteome analysis is fundamentally restricted to subsets of a proteome. The 2-DE is only one method among a large number of complementary methods. Based on this consideration, we developed the abstract "Analyte" concept for our PROTEOMER data structure. Here, Analyte represents an abstract generic class, or a placeholder to be substituted by one of its subclasses (samples, fractions, band, spot, or something yet to emerge along with new techniques). Thereby samples from a large spectrum of proteomics methods can be included and PROTEOMER is not limited to storing protein spot data from 2-DE experiments. This supplies our LIMS with a generalized LIM design using inheritance abstract objects [33]. Adapting to this view, each 2-DE gel is now considered as a collection of "Analytes." Each single analyte of a 2-D gel is represented by a spot. Therefore a 2-D gel may consist of up to 10 000 analytes [2].

As detailed in Fig. 2A, the result of one Analyte processing step can be fed back into the cycle as a new Analyte. For example, after in-gel digestion of a spot (which is an Analyte), the peptide mixture is classified as another entity of type Analyte. This facilitates the intuitive integration of nongel analysis techniques, and also allows the description of rare or evolving techniques such like PF2D and iTRAQ samples into to our PROTEOMER database. This nested structure with meta entities enables a complex series of concatenated processes to be easily annotated [33].

The data structure of PROTEOMER can be divided into two general clusters. The first cluster *protein identification platform* handles automatic MS data evaluation and data transfer associated with protein identification. The second cluster, the *protein information network*, was designed to manage the entire protein information data. These two clusters are extensively linked to each other within the database.

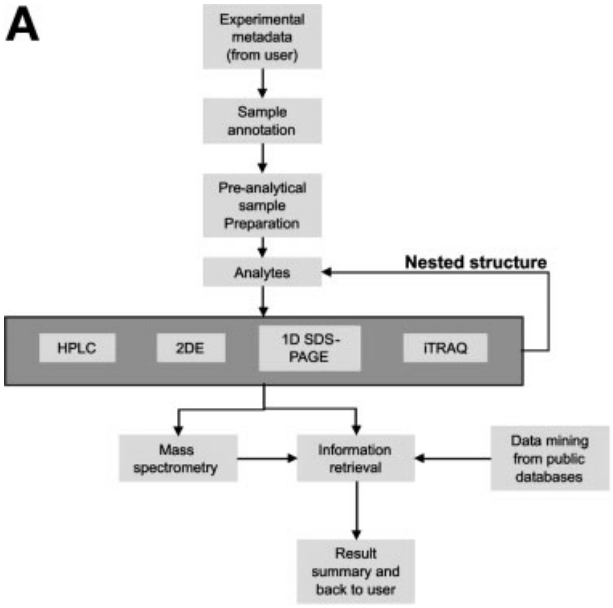

2.4 Protein identification platform

When using MS to identify proteins in a proteomics study, proteins are predominantly identified using the raw data files of mass spectrometric measurements and searching against sequence databases by software such as MASCOT (Matrixscience, www.matrixscience.com version 2.1). As a part of this software package, MASCOT server is currently used to manage our protein identification data. Both mass spectrometric raw data and MASCOT search results are by default stored in a MASCOT Daemon SQL server. The automatic retrieval of the protein identification data into PROTEOMER includes the export of protein identification results *via* extensible mark-up language (XML) from the MASCOT Daemon and the subsequent modification to fit the data structure of PROTEOMER. By this means, the system automatically takes unprocessed MS data files, identifies proteins *via* database searching, and then stores the processed search results into the relational database accordingly. This generates a detailed result table comprising comprehensive protein properties, such as the MOWSE score, sequence coverage, number of nonredundant peptides, possible peptide modifications, theoretical p*I*, molecular weight, NCBI, and UniProt accession numbers, as well as gene symbols. The generation of the table was realized by using an embedded Perl script.

Customized forms displaying the identification data in a user determined format may be generated thereafter. In addition, the raw mass spectra files are also stored as proprietary binary files in a high capacity data container. In this way, raw MS data are archived to allow for the sequence-based protein identification to be rerun in the future when more comprehensive protein databases appear. This feature

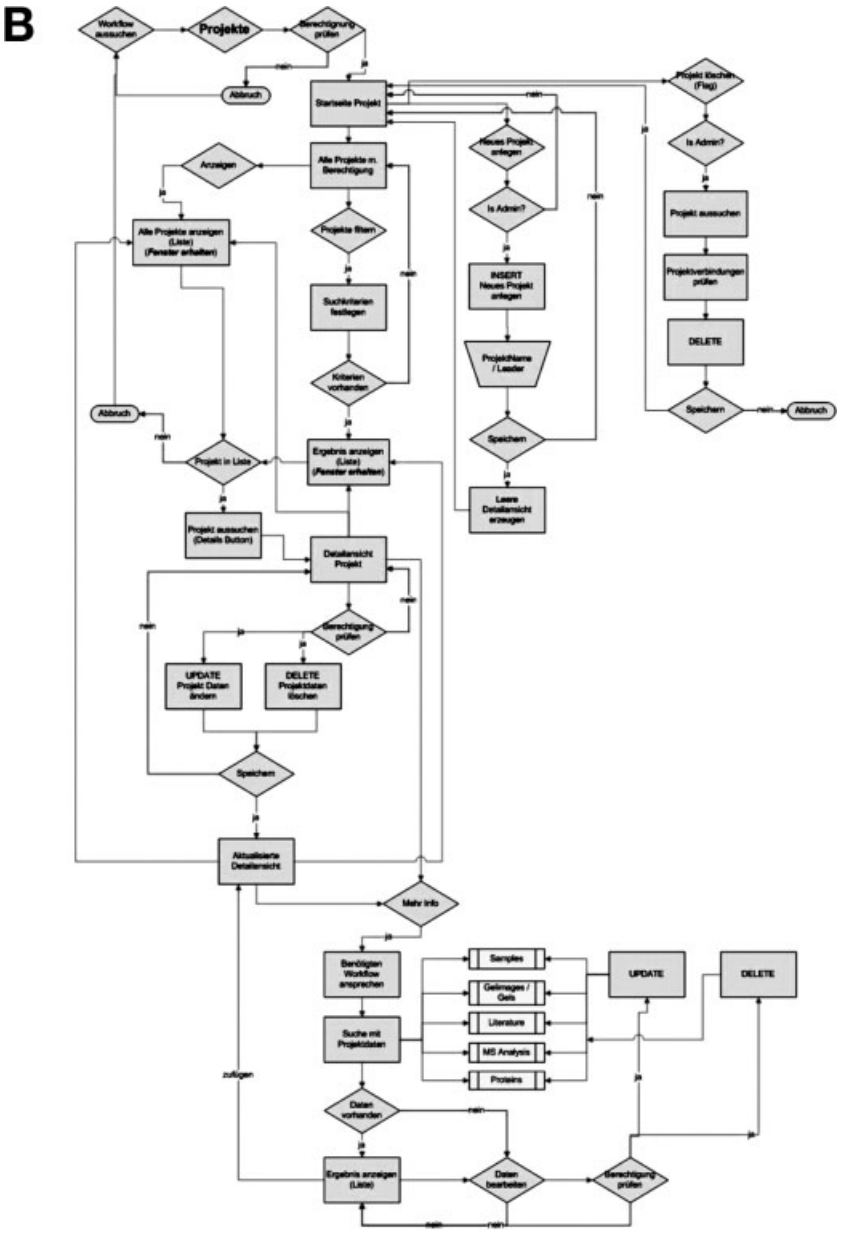

Figure 2. Representation of the optimized workflow for PROTEOMER modeled based on the laboratory routine in our 2-DE-centered proteomic core facility. (A) The overview of the processing pipeline of experimental data acquisition in our laboratory as implemented in PROTEOMER. (B) A detailed view of workflow cantered around the "Project" module. Each Project module represents an experiment or part thereof which was conducted in the laboratory.

is especially important when investigating species which are currently still without a completely sequenced genome such as potato, certain fish species and great apes such as chimpanzee. The *protein identification platform* ensures standardization during MASCOT searches and has substantially reduced the time needed to generate protein identification data in our proteomic core facility.

2.4.1 Protein information network

The protein information network is designed to store 2-DE spot evaluation data from 2-DE evaluation software. This includes, on the one hand, extensive protein expression alteration information derived from 2-DE evaluation sofware (Delta2D, DECODON; Proteomwaever, BioRad), and on the other hand the estimated protein p*I* and MW values according to where the spot is located on the 2D-gels. In addition, because of the complex relationships between protein, RNA expression in the cells, our database will also include mRNA expression data available to make these dynamic aspects accessible for user queries.

Each MASCOT search generates a large amount of data, which, in addition to peptide/protein assignments, include detailed information about protein structure, protein functional motifs, alternative splicing, as well as fragmentation data on the individual proteins identified. An extensible table

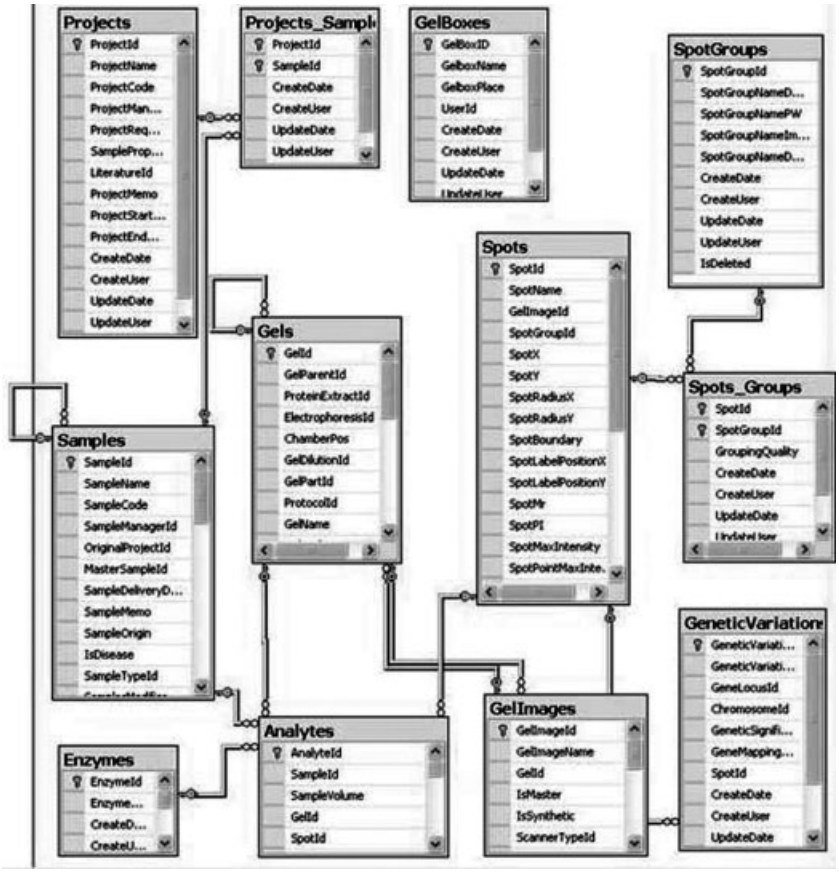

Figure 3. The data structure of PROTEOMER. Twelve out of over 80 representative linked data tables containing comprehensive information of proteomics experiments illustrate the data structure of PROTEOMER. The data tables shown demonstrate how information on project, samples, 2-D gels and other parameters are connected. The boxes represent data tables (entities). These are connected by various types of lines and arrows which signify the relationship between entities. Each class is described by its attributes, *e.g.*, a sample can be specified by its name, and date of creation.

structure has been designed in the protein information network to store this additional protein information, including link-outs to public protein databases (Swiss-Prot, NCBI, or Ensemble) based on MASCOT search results. In this way, linking protein data from MS identification and data from the biological database becomes possible.

2.4.2 Extensive cross-linking though multiple-level gels

In a 2-DE-based comparative proteomic experiments, protein expression differences are determined by comparing 2-DE gel images. Although different types of studies were conducted with protein alterations after various conditions/stimuli, the 2-D gel images generated when studying the same tissue are very similar. Therefore protein expression data from a large set of different experiments can be assigned to the same spot in a 2-D gel. This enables 2-D gel images to store information on protein expression alterations for later cross-referencing. By exploiting this 2-D gel-image centered information storage, we developed the "multiple-level gel" concept, which serves as scaffolding for the cross-linking capability of PROTEOMER. When considering the database structure, level-1 gels provide raw data from original comparisons between 2-D gels. Level-2 gels contain expression alterations shared by a predefined number of level-1 2-D gel comparisons. Level-3 gels summarize spots differentially expressed among different level-2 gels (Fig. 4A). In the following section, we will illustrate this concept with examples from practical applications in our laboratory.

When considering the simplest 2-DE-based comparative proteomics experiment, a comparison of two conditions is performed, *i.e.*, disease *versus* control samples. After generating sample pairs by running 2-D gels from controls and diseased animal in parallel, these sample pairs are compared and differences in expression between disease and controls are determined. The 2-D gels compared as sample pairs are called level-1 gels. Statistically significant spot alterations across sample pairs are registered on a level-2 2-D gel, which is typically a merged image of representative disease and control protein patterns. For this type of experiments where only two conditions (control *vs.* disease) are investigated, a level-2 gel is sufficient to represent the relevant data (Fig. 4B). When using a more sophisticated experimental setup, such as investigating different tissues at the same time or different time points in a disease, level 2 gels are no longer sufficient to represent all experimental results. When studying a mouse disease model at for time points, such as embryonic stage, newborn, adulthood, and end stage of a disease, se-

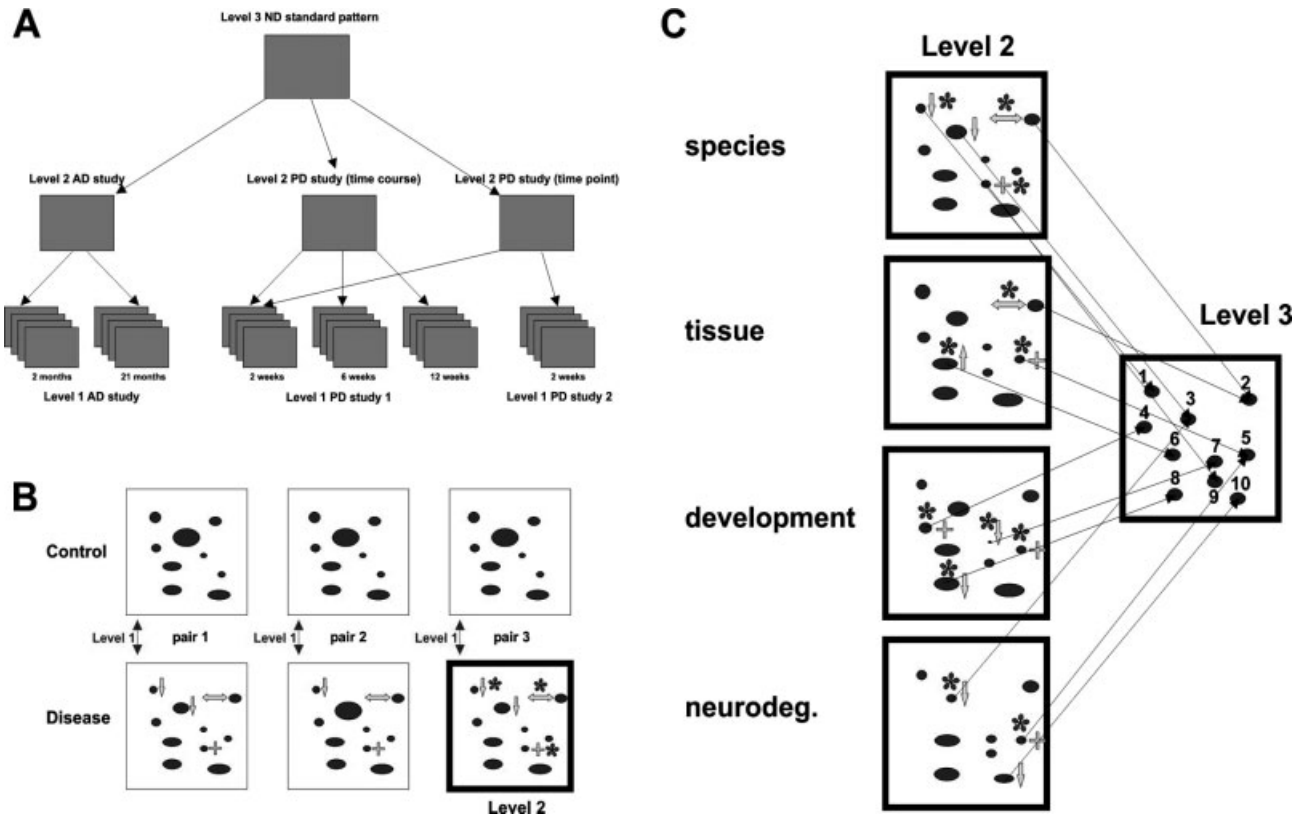

Figure 4. Three levels of data integration in PROTEOMER based on 2-D gels. (A) The three levels of data integration by 2-D gels are illustrated by various projects studying neurodegenerative diseases. Note that level-2 gels can summarize data from different experiments (see level-2 PD study (time point)). (B) The relationship between level-1 gels and level-2 gels in a proteomics experiment comparing two conditions, control, and disease. (C) A multiple experiment comparison combining several level-2 gels from different experiments.

veral level-2 gels are created from various sets of level-1 gel pairs, one for each time point investigated. In order to integrate protein spot alterations of the entire study, a synthetic gel from all level-2 gels has to be generated. This higher level synthetic gel is called level-3 gel (Fig. 4C).

In PROTEOMER, all three levels of gels are linked by parent–child relations (from level 3 to 2 to 1), generating a unidirectional acyclic graph. This ensures that each "real" 2-D gel comparison (level 1) can be oriented to its parent (level 2) and grandparent (level 3) gels unambiguously. The database is able to link related spots or proteins on level-1 gels by a fusion gel of all level 1 gels (level 2 gel), and link related protein spots on level-2 gels by creating level-3 gels (*i.e.*, standard gel of a disease time course experiment or standard gel after comparing protein alteration between various organs/tissues). Based on this hierarchical structure, database queries may reveal higher order information by recursively exploiting data along the tree of multiple levels of gels. Of course, more than three levels of data integration are needed at the core of our database to link results from all experiments. This higher level data organization is facilitated by experimental metadata rather than additional gel levels.

2.4.3 Graphical user interface of PROTEOMER

As probably the most important software element for potential users from the scientific community, a self-explanatory graphical user interface was implemented into PROTEOMER. This graphic interface guides a user through all steps of from uploading experimental data to import necessary metadata, select datasets for visualization, and perform database queries (Fig. 5). We aspired to create a graphical user interface which is as intuitive and user-friendly as possible. This goal was achieved by continuous end-user testing and feedback.

PROTEOMER may be searched using degenerated keywords or logical combinations thereof. This tool facilitates complex queries against interlaced data across different projects. Queries answerable by database inquiry include: was a protein-of-interest significantly altered in the contexts of experiments conducted? If the answer is yes, how does the protein-of-interest behave in the context of other experimental settings (other diseases, other disease models)? What is the expression spectrum of the protein-of-interest in multiple organs or tissues? How many isoforms of this protein have already been detected on a 2-D gel? Does the number of

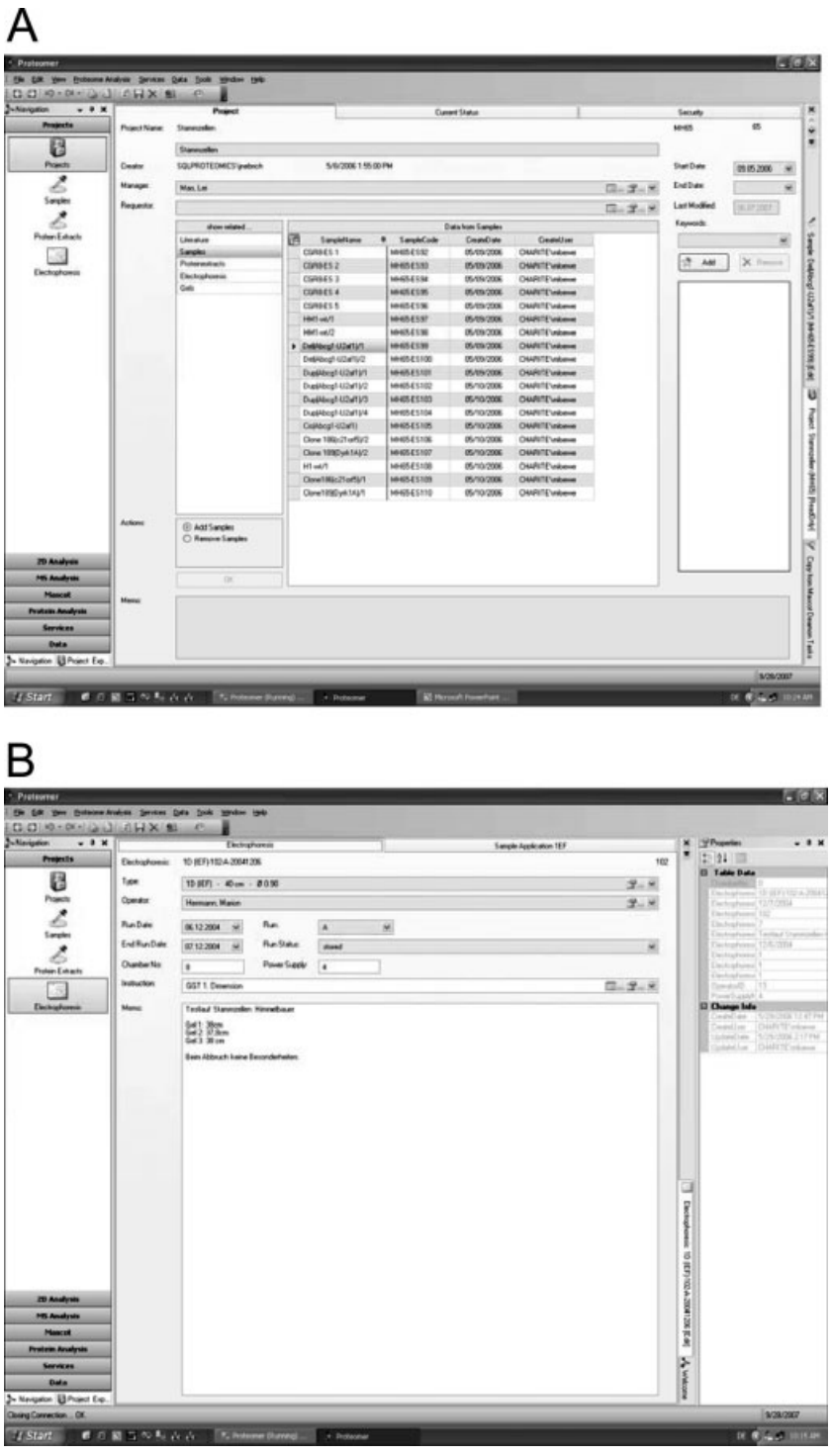

Figure 5. The graphical user interface of PROTEOMER. (A) The project navigation interface of the PROTEOMER database. (B) Example of the graphical interface when technical parameters of 2-D-electrophoresis are queried.

isoforms change with experimental settings? Which properties are so far assigned to a protein-of-interest in public databases?

In addition to the graphical interface for queries, a manual editing tool for 2-D gel images was integrated into PROTEOMER. The integration of this tool became necessary after evaluating our user feedback (Fig. 6). This *gel editor* module facilitates standard image handling tasks such as spot annotation, spot integration, gel warping, and image zooming. A user is enabled to dynamically display the entire uploaded 2-D gel images or parts thereof along with theoretical MW and p*I*. Additional features of the gel editor include: simulta-

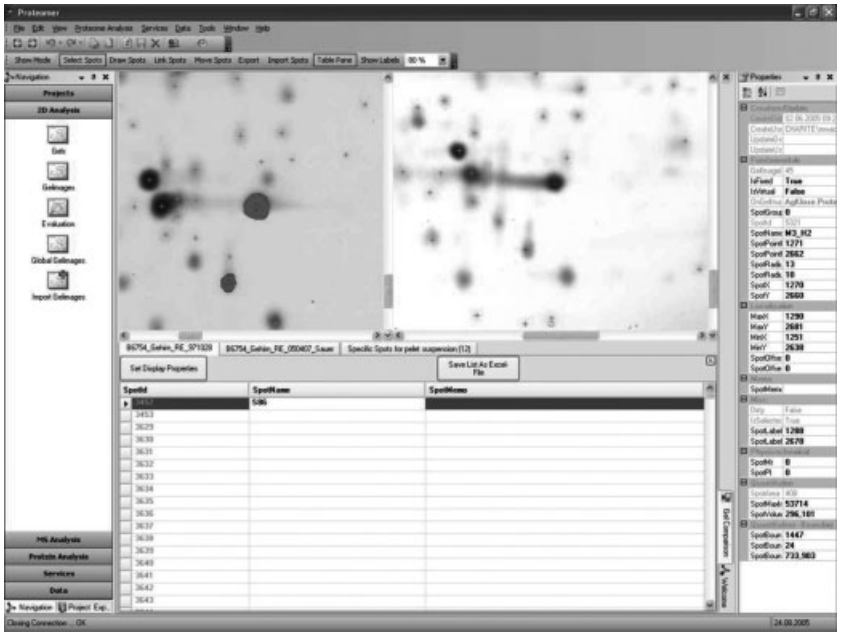

Figure 6. Simultaneous display of two gel sections and manual spot annotations using the *gel editor*. A screen shot of the editing tool displaying options for spot annotation such as spot ID, spot name and spot memo. Spot memo may include user defined information with no specific format.

neous display of several 2-D gel images, automatic gel/spot matching by cross-comparison, automatic spot annotation, calculation of spot border and volume, and relative intensity. Importantly, our 2-D gel editor is not intended to replace any 2-D image evaluation software, but rather to facilitate post-evaluation 2-DE gel annotation for the different levels of 2-D gel based of data integration (Fig. 4). This is mandatory especially for cross-project comparison. Therefore, this gel matching is mainly focused on finding the same spots on different gels without aiming for a totally correct overlap or exact quantification.

2.4.4 Integration of PROTEOMER into the framework of other databases

In order to make a database viable, it is important to link its input (upstream) and output (downstream) to facilitate proper information flow [34]. In order to achieve this goal, PROTEOMER is envisioned as a part of a more complex metadata model. It will be linked to the international database BrainProfile (HUPO organization) [35]. Currently, we are developing suitable data-exchange protocols and parsers that enable communication between both databases.

2.5 Technical platform

PROTEOMER database was programmed using the relational database management and analysis platform SQL server 2005 (Microsoft, Unterschleißheim Germany), an affordable, yet reliable database platform. Import and export into the SQL database structure *via* XML files (extensible mark-up language) was implemented with the SQL Server Integration Services platform (SSIS) of the Microsoft SQL server 2005 platform. The programming environment DOT-NET-framework (Microsoft, version 2.0) was employed to support the implementation of graphical user interfaces for all software tools. Instead of a common web interface, a rich client solution was preferred as a graphical interface for PROTEOMER. This shifts the data processing burden away from shared network and server resources onto client computers and warrants a better overall performance. Using these tools, end users are equipped with a fast and efficient graphic interface for even more sophisticated graphical applications. In addition, we incorporated a collection of flexible and efficient control elements (Infragistics NetAdvantage of 2005 volume 2, Zoschke Data GmbH, Selent, Germany; and ComponentOne, Pittsburgh, USA), which are in many ways superior to standard components of the DOT-NET framework. These additional control elements enhance graphical applications, while at the same time reducing programming time.

In order to enable efficient data exchange, PROTEOMER adheres to the minimum information required to unambiguously interpret, reproduce and verify experiment (MIAPE) standard to include sufficient information to reproduce each experiment [36]. This information content is subsequently enriched by additional data which we consider to be important based on our own laboratory expertise and experience.

2.6 Examples for applications of PROTEOMER

We will subsequently provide two examples of how to use our PROTEOMER database on actual problems occurring in the context of scientific investigation.

2.6.1 Example 1: Comparison of different 2-D-based proteomics studies carried out in our laboratory

Our PROTEOMER software solution has been used to integrate the data obtained from different comparative proteomic studies carried out in our core facility. As a case study for the cross-linking functionality of PROTEOMER, we developed a strategy that compares four different neurodegenerative disease projects based on information on six projects stored in the PROTEOMER database. Data on four neurodegenerative diseases, Alzheimer's, Huntington's, Parkinson's disease, and a mouse model for variant Creutzfeld–Jakob disease carried out by different users in our laboratory were searched for overlapping protein expression changes. In total the projects contained proteomics data on 25 conditions (age stages), extracted from over 200 single 2D-gel images spanning over four different brain regions and six time-points of investigation (from embryonic stage to end stage of disease). Using the query tool of PROTEOMER, we automatically compared 3 991 identified protein spots in the data base.

The query result reported by PROTEOMER comprises 858 different protein isoforms, which could be assigned to 690 nonredundant genes that co-changed in at least two disease conditions. This result illustrates the differential protein expression behavior of a large number of proteins in different disease models, brain regions, and time-points of investigation (Fig. 7). One hundred and eighty-six co-changed

A

Gene Symbol of Proteins	Number of disease affected
Tpm1	4
Anxa3	3
Apoe	3
Ca2	3
Cplx2	3
Cryab	3
Dpysl2	3
Eef1d	3
Hadhb	3
Mdh1	3
Prdx1	3
Prdx2	3
Prdx6	3
Taldo1	3
Tpm3	3
Acads	2
Acp6	2
Actg1	2
Actl6a	2
Adrm1	2
Ak5	2
Alad	2
Alb	2
Aldoa-ps1	2
Als2cr8	2
Amt	2
Apc2	2
Arhgdia	

B

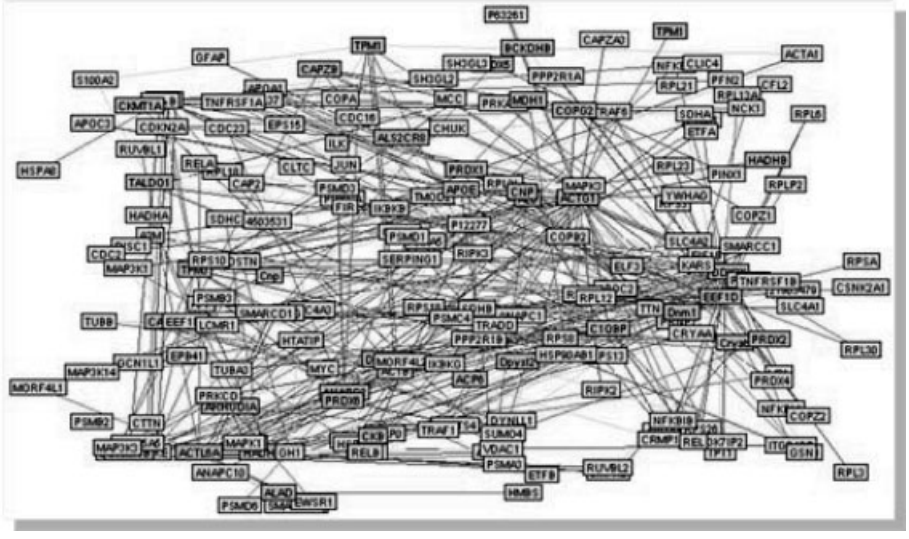

Figure 7. Investigation of protein expression overlap between four different neurodegenerative diseases using PROTEOMER revealed over 800 co-changed proteins. (A) An abbreviated list of gene symbols representing the co-changed proteins. (B) PPI network created by a publicly available online tool UniHI to find PPIs (http://theoderich.fb3.mdc-berlin.de:8080/unihi/home).

proteins with an overlap in at least three disease models investigated suggest that many changes are facilitated by the protein–protein interaction (PPI) network, presumably due to proteomic network effect [9, 17, 37, 38].

Another useful application of PROTEOMER is to determine the number of isoforms a proteins is expressed on a 2-D gel. The protein represented by the gene name Stmn1 occurs in sixteen protein isoforms that changed in eight different disease conditions tested and Dpysl2 was represented by ten isoforms, changed in seven conditions.

The results discussed above demonstrate that users can utilize the PROTEOMER database to search proteins overlapping in differential expression across different proteomics experiments.

2.6.2 Example 2: Detection of polymorphic proteins

Next, we investigated the possible influence of genetic polymorphisms on the protein expression profile using PROTEOMER. For this purpose, we semi-automatically compared the protein expression patterns of two mouse strains (*Mus musculus* and *Mus spretus*) and their F1-generation in three different tissues: brain [39], liver, and heart. The 2-D gels were originally generated in the context of different projects to answer distinct biological questions. Using a level-3 gel generated by PROTEOMER, fusing the brain protein expression patterns of *M. musculus* and *M. spretus* (Fig. 8A) the isoforms of same protein could be successfully annotated by PROTEOMER based on the protein identifica-

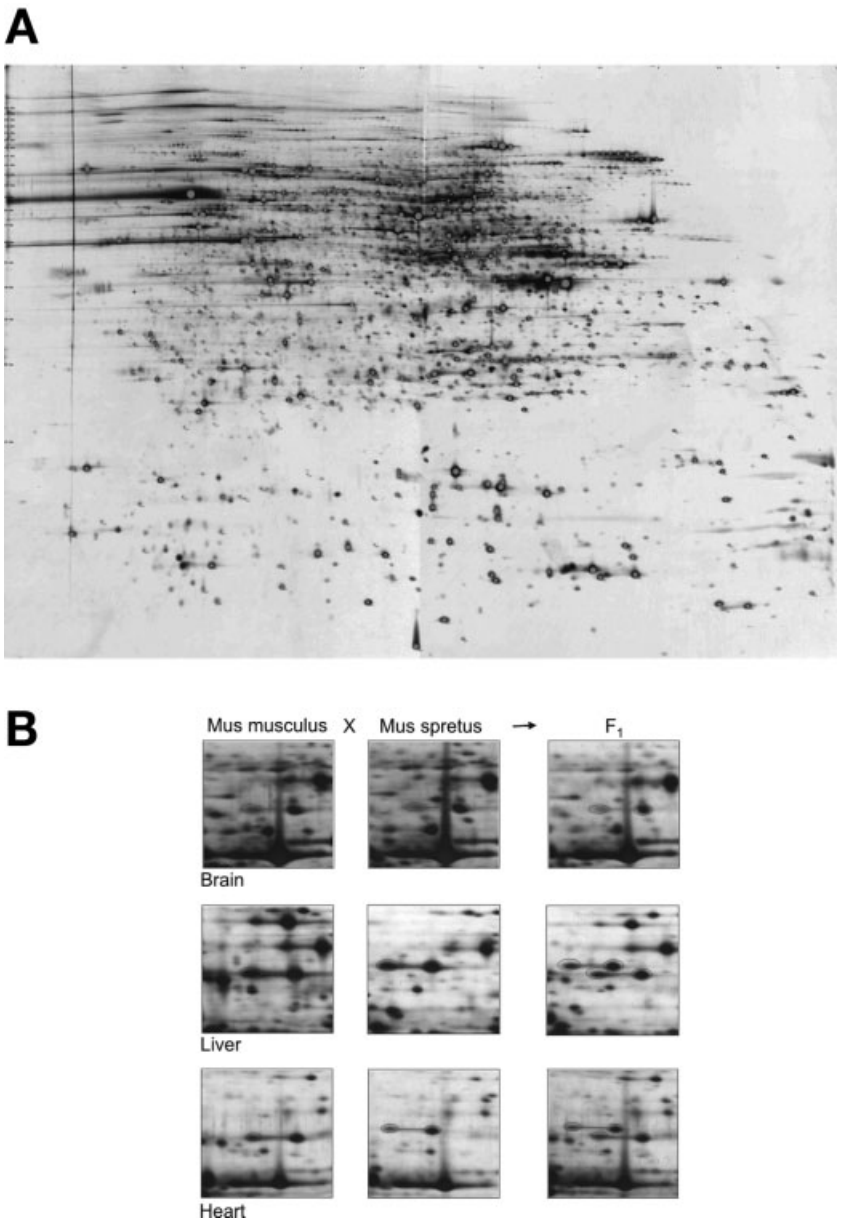

Figure 8. Identification of mouse protein polymorphisms using PROTEOMER. (A) The level-3 gel "mouse cross-tissue protein pattern" was exported by PROTEOMER based on a fusion brain protein expression pattern of *M. musculus* and *M. spretus*. Protein spots with annotation in the PROTEOMER database are marked green. (B) As shown on 2-D gel sections, the protein "Aldehyde dehydrogenase member A1 (*Aldh*)" shows a polymorphic expression pattern in liver and heart, but not in brain.

tion information and protein spot localization on the 2-D gel images. PROTEOMER was able to generate a list of proteins with polymorphic expression behavior, despite the dissimilarity of the 2D-gel images between different tissue types. Protein spots where identification resulted in the same gene name, but differ significantly in spot position on the 2-D gel (by p*I*, MW, or both) were characterized as protein polymorphisms by PROTEOMER [39]. Intrinsically, the results of this comparison showed that the penetration of genetic polymorphisms on protein expression appears to be tissue-specific (Fig. 8B and Klose *et.al.*, submitted). Results from the study on genetic polymorphisms which will be presented in detail elsewhere (Klose *et.al.*, submitted) will be illustrated here by a representative protein. One example of a protein polymorphic between species and tissues is aldehyde dehydrogenase (*Aldh*). The oxidation of ethanol generates toxic acetaldehyde which is mainly catabolized and thereby detoxified by NAD+ -dependent *Aldh*. In addition, *Aldh* metabolizes also many other aldehydes generated from diverse metabolic pathways. Some aldehydes are intermediates from the metabolism of amino acids, biogenic amines, steroids, vitamins, and generated by the biotransformation of drugs and environmental agents [40–42]. A number of isoenzymes of *Aldh* coded by different gene loci have been detected in human organs and tissues which differ in their electrophoretic mobility, kinetic properties and in their cellular, and tissue distribution [42]. Here, PRPTEOMER enabled us to access directly the organ-specific PTM pattern of *Aldh* at the protein level (Fig. 8B). Interestingly, by using PROTEOMER we found much more isoforms of *Aldh* in liver and heart than in brain. This example demonstrated the ability of PROTEOMER to extract protein expression data on protein isoforms from different tissues and determining polymorphisms using already available experimental data from earlier experiments.

3 Discussion

Due to our extensive experience accumulated during many years working in our proteomics core facility, we are aware that providing protein identification data from MS alone is by far not sufficient to answer complex biological questions of today. We are constantly confronted with specific *post hoc* queries from scientists inquiring about protein properties and cross-project comparisons of protein expression important to their projects. This clearly demonstrates that in present proteomics research, data sorting using specific criteria and comparisons pose significant challenges, especially when simultaneously analyzing multiple experiments. This led us to create a suitable cross-link competent LIMS that is able to handle heterogeneous data formats.

Several years ago, Taylor *et.al.* proposed two general criteria for proteomics data storage systems: sufficiency and natural organization [23]. Taylor *et al.* developed an advanced infrastructure for capture, storage, and dissemination strategies for proteomics data. Their PEDRo serves as a good example for the combination of 2-DE experiments with mass spectrometric analysis into an integrated XML-based format. Due to its flexibility granted by semi-structured characteristics, XML represents the most popular resource for the exchange of both formats and data, and thus is well suited for biological data [43–46]. Defined XML schemata act as mediator, allowing multiple input formats to be subjected to a common data analysis pipeline (mzXML) [47]. Since then, several proteomics toolkits, such as OpenMS [48] or the software collection from the "Trans-Proteomic Pipeline" (http://tools.proteomecenter.org/software.php) provide a set of computational tools for gel-free proteomics [47].

To complement currently available bioinformatics tools, and especially to improve the quality and efficiency of the service of our core facility, an LIMS was developed in-house to streamline our data throughput and reporting processes in a standardized format, so that proteomics data become portable and linked to facilitate the transformation of protein information into biological knowledge. For this purpose, we developed interfaces among special programs in order to enable flexible data exchange and complex inquiries. In this way, data from different analysis methods, as well as data generated in the context of a variety of proteomics studies conducted to answer highly diverse biological questions can be linked to one another.

3.1 Bench design ensures the viability of a database

Creating a database and making sure people use it are two quite distinct challenges. During the design stage of LIMS, the most commonly observed error is usually that database users are excluded from designing the LIMS. This is especially detrimental since, an average software professional does not always have the necessary background knowledge to predict a laboratory's requirements correctly and in detail. This communication problem may manifest itself in a badly designed system which does not easily fit into an existing laboratory operation. Frequently, a laboratory facility must significantly alter its workflow in order to compensate for this discrepancy forcing users to adjust their work habits. This requirement for global alterations of how users work significantly complicates LIMS operation. In addition, complaints about the LIMS are usually not communicated but obstacles in the workflow are rather worked around. This could ultimately make users abandon the application of a specific LIMS. This was the primary cause why many previously designed LIMS did not survive implementation in the laboratory. As a "laboratory-born" system, PROTEOMER was co-designed by users of highly diverse areas of research such as technical assistants, postdoctoral fellows of various backgrounds and also bioinformaticians. During the relatively long design phase, we paid special attention to its laboratory-adaptability, and most importantly the overall system speed in the human-PC environment, instead of the speed of certain particular database tasks. The co-design by multiple

members of the core facility and associated work groups as well as intensive documentation also ensured that many users are familiar with our database design concept and its internal structure and therefore know how to use it. This warrants that the maintenance of the PROTEOMER database is more intuitive and does not largely dependent on a small group of specialists, therefore ensuring its continuity.

3.2 Cross-referencing can generate new information

The power of a database lies in its ability to reveal hidden patterns across a variety of different datasets. Processed sets of 2-D gels containing differentially regulated protein spots obtained by comparative 2-DE experiments are stored at different locations. Proteins identifications are assigned in various ways using different tools, including identification by MS, 2-D gel image comparison, or *de novo* sequencing. Our database structure using the "multiple-level gel" design enables different investigators to compare the results from their experiments. In addition, the results from an investigator's own experiments can be put into a larger context. This allows a sophisticated meta-analysis that ultimately yields insights into the complexity of biological systems. When using a cross-project query, we are able to find additional information on disease-specificity of protein expression alterations, or the influence of polymorphisms on protein expression patterns. We have already found additional information on the frequency of polymorphic proteins which appear to be organ-dependent. This demonstrates that the PROTEOMER database helps to extract biological knowledge from laboratory information.

3.3 Limitations of the PROTEOMER database

One clear limitation of PROTEOMER is that it is programmed with nonopen-source software. To reduce the programming expenditure, we decided to realize PROTEOMER with commercial software development solutions (Microsoft Dot-NET programming environment). This means that the source code of our LIMS is not publicly available. In addition, the rich client solution is only fully functional when using Internet Explorer 6.0 or higher, but not with many other web browsers. Still, our aim with this study was to improve the performance of our proteomic core facility, and in addition, to share our experience on 2-DE-based database design, which can still benefit the scientific community. We think that using our expertise with a 2-DE centered proteomic core facility, which was in our opinion more important than informatics know-how alone, we were able to generate an integrated data modeling scheme and a valuable database structure.

In summary, we have constructed a software solution which is designed to administrate and cross-reference raw, processed and final proteomics data while linking them at multiple levels. Our aim was not to generate an omnipotent database system that is able to engineer every step perfectly, but rather to link different available modules/software and implement their inherent competence, which will ultimately convert raw protein expression data into biological information, and facilitate the generation of knowledge. We anticipate that PROTEOMER will assist a large number of scientists and bioinformaticians alike in their effort to obtain a deeper understanding of their area of research from the research data available.

This work is dedicated to the memory of Maik Wacker. We are grateful for the assistance of Jörg Nebrich with the programming of the PROTEOMER database. We also appreciate the contributions of Nicole Steireif, Dijana Sagi, and Jadranka Tadic and for their permission to use their experimental data for our meta-analysis. We also express our appreciation for Perl script programming and patching by Axel Fischer.

The authors have declared no conflict of interest.

4 References

[1] Tyers, M., Mann, M., From genomics to proteomics. *Nature* 2003, *422*, 193–197.

[2] Klose, J., Kobalz, U., Two-dimensional electrophoresis of proteins: An updated protocol and implications for a functional analysis of the genome. *Electrophoresis* 1995, *16*, 1034–1059.

[3] Wang, H., Qian, W. J., Chin, M. H., Petyuk, V. A. *et al.*, Characterization of the mouse brain proteome using global proteomic analysis complemented with cysteinyl-peptide enrichment. *J. Proteome Res.* 2006, *5*, 361–369.

[4] Aebersold, R., Mann, M., Mass spectrometry-based proteomics. *Nature* 2003, *422*, 198–207.

[5] Kaindl, A. M., Sifringer, M., Zabel, C., Nebrich, G. *et al.*, Acute and long-term proteome changes induced by oxidative stress in the developing brain. *Cell Death Differ.* 2006, *13*, 1097–1109.

[6] Hartl, D., Rohe, M., Mao, L., Staufenbiel, M. *et al.*, Impairment of adolescent hippocampal plasticity in a mouse model for Alzheimer's disease precedes disease phenotype. *PLoS One* 2008, *3*, e2759.

[7] Mao, L., Hartl, D., Nolden, T., Koppelstatter, A. *et al.*, Pronounced alterations of cellular metabolism and structure due to hyper- or hypo-osmosis. *J. Proteome Res.* 2008, *7*, 3968–3983.

[8] Diedrich, M., Mao, L., Bernreuther, C., Zabel, C. *et al.*, Proteome analysis of ventral midbrain in MPTP-treated normal and L1cam transgenic mice. *Proteomics* 2008, *8*, 1266–1275.

[9] Zabel, C., Andreew, A., Mao, L., Hartl, D., Protein expression overlap: More important than which proteins change in expression? *Expert Rev. Proteomics* 2008, *5*, 187–205.

[10] Zabel, C., Chamrad, D. C., Priller, J., Woodman, B. *et al.*, Alterations in the mouse and human proteome caused by Huntington's disease. *Mol. Cell. Proteomics* 2002, *1*, 366–375.

[11] Henley, S. M., Bates, G. P., Tabrizi, S. J., Biomarkers for neurodegenerative diseases. *Curr. Opin. Neurol.* 2005, *18*, 698–705.

[12] Ong, S. E., Mann, M., Mass spectrometry-based proteomics turns quantitative. *Nat. Chem. Biol.* 2005, *1*, 252–262.

[13] Issaq, H., Veenstra, T., Two-dimensional polyacrylamide gel electrophoresis (2D-PAGE): Advances and perspectives. *Biotechniques* 2008, *44*, 697–698.

[14] Klose, J., Large-gel 2-D electrophoresis. *Methods Mol. Biol.* 1999, *112*, 147–172.

[15] Unlu, M., Morgan, M. E., Minden, J. S., Difference gel electrophoresis: A single gel method for detecting changes in protein extracts. *Electrophoresis* 1997, *18*, 2071–2077.

[16] Alban, A., David, S. O., Bjorkesten, L., Andersson, C. *et al.*, A novel experimental design for comparative two-dimensional gel analysis: Two-dimensional difference gel electrophoresis incorporating a pooled internal standard. *Proteomics* 2003, *3*, 36–44.

[17] Zabel, C., Sagi, D., Kaindl, A. M., Steireif, N. *et al.*, Comparative proteomics in neurodegenerative and non-neurodegenerative diseases suggest nodal point proteins in regulatory networking. *J. Proteome Res.* 2006, *5*, 1948–1958.

[18] Steinberg, T. H., Agnew, B. J., Gee, K. R., Leung, W. Y. *et al.*, Global quantitative phosphoprotein analysis using Multiplexed Proteomics technology. *Proteomics* 2003, *3*, 1128–1144.

[19] Palagi, P. M., Hernandez, P., Walther, D., Appel, R. D., Proteome informatics I: Bioinformatics tools for processing experimental data. *Proteomics* 2006, *6*, 5435–5444.

[20] Pleissner, K. P., Schmelzer, P., Wehrl, W., Jungblut, P. R., Presentation of differentially regulated proteins within a web-accessible proteome database system of microorganisms. *Proteomics* 2004, *4*, 2987–2990.

[21] Pleissner, K. P., Eifert, T., Buettner, S., Schmidt, F. *et al.*, Web-accessible proteome databases for microbial research. *Proteomics* 2004, *4*, 1305–1313.

[22] Lisacek, F., Cohen-Boulakia, S., Appel, R. D., Proteome informatics II: Bioinformatics for comparative proteomics. *Proteomics* 2006, *6*, 5445–5466.

[23] Taylor, C. F., Paton, N. W., Garwood, K. L., Kirby, P. D. *et al.*, A systematic approach to modeling, capturing, and disseminating proteomics experimental data. *Nat. Biotechnol.* 2003, *21*, 247–254.

[24] Wilke, A., Ruckert, C., Bartels, D., Dondrup, M. *et al.*, Bioinformatics support for high-throughput proteomics. *J. Biotechnol.* 2003, *106*, 147–156.

[25] Garwood, K., McLaughlin, T., Garwood, C., Joens, S. *et al.*, PEDRo: A database for storing, searching and disseminating experimental proteomics data. *BMC Genomics* 2004, *5*, 68.

[26] Dowsey, A. W., English, J., Pennington, K., Cotter, D. *et al.*, Examination of 2-DE in the Human Proteome Organisation Brain Proteome Project pilot studies with the new RAIN gel matching technique. *Proteomics* 2006, *6*, 5030–5047.

[27] Dunn, M. J., Corbett, J. M., Wheeler, C. H., HSC-2DPAGE and the two-dimensional gel electrophoresis database of dog heart proteins. *Electrophoresis* 1997, *18*, 2795–2802.

[28] Binz, P. A., Muller, M., Hoogland, C., Zimmermann, C. *et al.*, The molecular scanner: Concept and developments. *Curr. Opin. Biotechnol.* 2004, *15*, 17–23.

[29] Droit, A., Hunter, J. M., Rouleau, M., Ethier, C. *et al.*, PARPs database: A LIMS systems for protein-protein interaction data mining or laboratory information management system. *BMC Bioinformatics* 2007, *8*, 483.

[30] Voegele, C., Tavtigian, S. V., de Silva, D., Cuber, S. *et al.*, A Laboratory Information Management System (LIMS) for a high throughput genetic platform aimed at candidate gene mutation screening. *Bioinformatics* 2007, *23*, 2504–2506.

[31] Tchuvatkina, O., Shimoni, L., Ochs, M. F., Moloshok, T., Proteomics LIMS: A caBIG project, year 1. *AMIA Annu. Symp. Proc.* 2006, 1116.

[32] Hartl, D., Irmler, M., Romer, I., Mader, M. T. *et al.*, Transcriptome and proteome analysis of early embryonic mouse brain development. *Proteomics* 2008, *8*, 1257–1265.

[33] Wendl, M. C., Smith, S., Pohl, C. S., Dooling, D. J. *et al.*, Design and implementation of a generalized laboratory data model. *BMC Bioinformatics* 2007, *8*, 362.

[34] Appel, R. D., Bairoch, A., Sanchez, J. C., Vargas, J. R. *et al.*, Federated two-dimensional electrophoresis database: A simple means of publishing two-dimensional electrophoresis data. *Electrophoresis* 1996, *17*, 540–546.

[35] Schuchhardt, J., Glintschert, A., Hartl, D., Irmler, M. *et al.*, BrainProfileDB – a platform for integration of functional genomics data. *Proteomics* 2008, *8*, 1162–1164.

[36] Taylor, C. F., Paton, N. W., Lilley, K. S., Binz, P. A. *et al.*, The minimum information about a proteomics experiment (MIAPE). *Nat. Biotechnol.* 2007, *25*, 887–893.

[37] Mao, L., Zabel, C., Herrmann, M., Nolden, T. *et al.*, Proteomic shifts in embryonic stem cells with gene dose modifications suggest the presence of balancer proteins in protein regulatory networks. *PLoS One* 2007, *2*, e1218.

[38] Zabel, C., Mao, L., Woodman, B., Rohe, M. *et al.*, A larger number of protein expression changes occur early in life and precede phenotype onset in a mouse model of Huntington's disease. *Mol. Cell Proteomics* 2009, in press.

[39] Klose, J., Nock, C., Herrmann, M., Stuhler, K. *et al.*, Genetic analysis of the mouse brain proteome. *Nat. Genet.* 2002, *30*, 385–393.

[40] Lindahl, R., Aldehyde dehydrogenases and their role in carcinogenesis. *Crit. Rev. Biochem. Mol. Biol.* 1992, *27*, 283–335.

[41] Vasiliou, V., Pappa, A., Polymorphisms of human aldehyde dehydrogenases. Consequences for drug metabolism and disease. *Pharmacology* 2000, *61*, 192–198.

[42] Agarwal, D. P., Genetic polymorphisms of alcohol metabolizing enzymes. *Pathol. Biol. (Paris)* 2001, *49*, 703–709.

[43] Patton, W. F., Detection technologies in proteome analysis. *J. Chromatogr. B Analyt. Technol. Biomed. Life Sci.* 2002, *771*, 3–31.

[44] Scheler, C., Lamer, S., Pan, Z., Li, X. P. *et al.*, Peptide mass fingerprint sequence coverage from differently stained proteins on two-dimensional electrophoresis patterns by matrix assisted laser desorption/ionization-mass spectrometry (MALDI-MS). *Electrophoresis* 1998, *19*, 918–927.

[45] Orchard, S., Hermjakob, H., Apweiler, R., The proteomics standards initiative. *Proteomics* 2003, *3*, 1374–1376.

[46] Webb-Robertson, B. J., Cannon, W. R., Current trends in computational inference from mass spectrometry-based proteomics. *Brief. Bioinform.* 2007, *8*, 304–317.

[47] Keller, A., Eng, J., Zhang, N., Li, X. J., Aebersold, R., A uniform proteomics MS/MS analysis platform utilizing open XML file formats. *Mol. Syst. Biol.* 2005, *1*, 0017.

[48] Mayr, B. M., Kohlbacher, O., Reinert, K., Sturm, M. *et al.*, Absolute myoglobin quantitation in serum by combining two-dimensional liquid chromatography-electrospray ionization mass spectrometry and novel data analysis algorithms. *J. Proteome Res.* 2006, *5*, 414–421.

research articles Journal of proteome research

Pronounced Alterations of Cellular Metabolism and Structure Due to Hyper- or Hypo-Osmosis

Lei Mao,[†,‡] Daniela Hartl,[†] Tobias Nolden,[‡] Andrea Koppelstätter,[†] Joachim Klose,[†] Heinz Himmelbauer,[‡] and Claus Zabel*[,†]

Institute for Human Genetics, Charité-University Medicine Berlin, Germany, and Max Planck Institute for Molecular Genetics, Berlin, Germany

Received April 2, 2008

Cell volume alteration represents an important factor contributing to the pathology of late-onset diseases. Previously, it was reported that protein biosynthesis and degradation are inversely (trans) regulated during cell volume regulation. Upon cell shrinkage, protein biosynthesis was up-regulated and protein degradation down-regulated. Cell swelling showed opposite regulation. Recent evidence suggests a decrease of protein biodegradation activity in many neurodegenerative diseases and even during aging; both also show prominent cell shrinkage. To clarify the effect of cell volume regulation on the overall protein turnover dynamics, we investigated mouse embryonic stem cells under hyper- and hypotonic osmotic conditions using a 2-D gel based proteomics approach. These conditions cause cell swelling and shrinkage, respectively. Our results demonstrate that the adaption to altered osmotic conditions and therefore cell volume alterations affects a broad spectrum of cellular pathways, including stress response, cytoskeleton remodeling and importantly, cellular metabolism and protein degradation. Interestingly, protein synthesis and degradation appears to be cis-regulated (same direction) on a global level. Our findings also support the hypothesis that protein alterations due to osmotic stress contribute to the pathology of neurodegenerative diseases due to a 60% expression overlap with proteins found altered in Alzheimer's, Huntington's, or Parkinson's disease. Eighteen percent of the proteins altered are even shared with all three disorders.

Keywords: aging • cell volume regulation • mouse embryonic stem cells • neurodegenerative disorders • osmotic stress • protein degradation • protein biosynthesis • proteomics

Introduction

Changes in intracellular or extracellular osmolarity result in a rapid transmembrane flow of water to reestablish an osmotic equilibrium. Cells respond to osmotic perturbation by activation of cell volume sensitive flux pathways for small ion and organic osmolytes to restore their original volume and thus maximize their probability of survival. Such cell volume regulatory mechanisms are associated with a wide range of physiological activities such as mitogenesis, differentiation, hormonal action, as well as neuronal excitation (reviewed in ref 1). In single cellular organisms, such as yeast, hyperosmolarity and therefore transient cell volume reduction, causes a broad spectrum of global responses, including transient stimulation of glucose uptake, inhibition of translation initiation, repression of ribosomal proteins, and transient inhibition of uracil uptake.[2] Higher, multicellular organisms are in general characterized by a metastable osmolarity of body fluid, strictly regulated by diuretic hormones secreted by the hypothalamus.[3] Hyperosmolarity treatment of eukaryotic cells results in rapid activation of multiple, highly conserved mitogen-activiated protein kinase (MAPK) cascades, also known as stress-activated MAPKs.[4] These complex regulatory mechanisms activated upon cell volume changes evidently require coordinated protein expression for adjustment.

About a decade ago, Haussinger and Lang reviewed that cell shrinkage could lead to a general down-regulation of protein synthesis, which is accompanied by simultaneous up-regulation of protein degradation.[5,6] An opposite trans-regulation of protein synthesis and degradation was proposed for cells upon swelling. This rational fits intuitively the strategy of a cell to maintain a constant cellular protein concentration. Recently, a considerable body of literature suggests that impaired cell volume regulation may contribute significantly to the pathology of many late-onset diseases such as Alzheimer's[7] and Huntington's[8] disease, which are studied extensively in our laboratory.[9–12] A decrease of proteasomal activity during aging[13–15] and in neurodegenerative diseases (ND) such as Alzheimer's (AD),[16] Parkinson's (PD), and Huntington's disease (HD)[17] is already well-established. Since a perturbation of the proteasome and ubiquitin system-related protein degradation is a hallmark of ND pathology (these alterations may results in, e.g., amyloid plague formation in Alzheimer's disease), it is

* Corresponding author: Claus Zabel, Institute for Human Genetics, Charité-University Medicine Berlin, Augustenburgerplatz 1, 13353 Berlin, Germany; Tel., +49-30-450-566258; fax, +49-30-566904; e-mail, claus.zabel@charite.de.

† Charité-University Medicine Berlin.

‡ Max Planck Institute for Molecular Genetics.

10.1021/pr800245x CCC: $40.75
Published on Web 07/23/2008

of utmost importance to clarify whether the dysregulation of protein degradation pathways in NDs is disease-specific or if a change in cellular osmolarity can trigger the same pathways. To clarify this issue, we subjected embryonic stem (ES) cells to osmotic stress and evaluated the alterations in protein expression profile. Our results suggest that, contrary to previous findings, there could rather be a cis-regulation between protein biosynthesis and degradation upon osmotic stress-induced cell volume alteration.

Materials and Methods

Composition of Hyper- and Hypo-Osmotic Cell Culture Media. High glucose (4.5 g/L D-glucose) Dulbecco's modified Eagle's medium (DMEM, 155 mM total Na^+, 110 mM NaCl) and DMEM with modified sodium-concentration were custom-made by Biochrom (Berlin, Germany). The cell culture medium with modified tonicity was designed based on previously published formulations.[18,19] Hyperosmotic medium contained 250 mM total Na^+ (205 mM NaCl) to obtain 500 mOsm (actual measured value: 498 mOsM), while hypo-osmotic medium contained 85 mM total Na^+ concentration (40 mM NaCl), to get a 200 mOsm (measured value: 206 mOsm) culture medium.

Maintenance of ES Cells. Mouse ES cell line CGR8 was maintained on gelatin-coated (0.1% v/v) cell culture dishes in either standard or customized DMEM (Biochrom, Berlin, Germany) supplemented with 10% fetal calf serum (PAN Biotech, Aidenbach Germany), 2 mM L-glutamine (PAA Laboratories GmbH, Pasching, Austria), 0.1 mM nonessential amino acids (PAA Laboratories GmbH, Pasching, Austria), 1 mM sodium pyruvate (PAA Laboratories GmbH, Pasching, Austria), 0.1 mM 2-mercaptoethanol (PAA Laboratories GmbH, Pasching, Austria) and 100 U/mL leukemia inhibitory factor (LIF, Chemicon, Hampshire, U.K.) under standard cell culture conditions (37 °C, 5% CO_2, 95% humidity). Upon thawing, CGR8 ES cells were passaged three times every other day until shortly before reaching confluence in standard DMEM (340 mOsm). Cells were subsequently cultured for an additional 48−144 h in either hypo-osmotic (200 mOsm), hyperosmotic (500 MOsm), or iso-osmotic (control) DMEM. Isotonic, hyper-, and hypo-treated cells were always cultured in parallel. Cells were grown to 70−90% confluence and met morphological criteria for undifferentiated ES cells at the time of harvest. ES cells were gently harvested by scraping in ice-cold PBS isotonic for the respective culture medium containing 5 mM EDTA. Typsinization was avoided to preclude protein alteration artifacts. The medium cell size was calculated using the average diameter of at least 100 cells. Dissociated cells were pelleted by centrifugation at 1000*g* for 5 min before snap freezing in liquid nitrogen and storage at −80 °C.

Two-Dimensional Gel Electrophoresis (2-DE). ES cell total protein extraction was performed using a protocol developed in our laboratory.[20,21] A total of 70 μg of protein was separated in each 2-DE run as described previously.[21−23] Osmotically stressed ES and control cells were always run in parallel. All experiments were repeated thrice using a fresh batch of ES cells (three biological replicates). In addition, two technical repeats were conducted for each protein extract. Proteins were visualized employing a highly sensitive silver staining protocol.[23,24] All altered protein spots were primarily detected by manual gel image evaluation using a conventional light box. 2D-gels were then scanned at high resolution (600 dpi) (Microtek TMA 1600, UMAX Systems GmbH, Willich, Germany). Computer-assisted 2D-gel evaluation by Delta2D (version 3.4) software (Decodon, Greifswald Germany) was conducted as described previously.[22,25−28] Corresponding gel images were warped by Delta2D using "exact mode". A fusion gel image was subsequently generated using union mode, which is a weighted arithmetic mean across the entire gel series. Spot detection was carried out on the fusion image using detection parameters suggested by the software, followed by manual spot editing. In total, more than 5000 protein spots could be detected on 2-D gels of both stressed and nonstressed cells. Spots were subsequently transferred from the fusion image to all gels. The signal intensities (volume of each spot) were calculated as weighted sum of all pixel intensities of each protein spot by Delta2D.[25] Calculations were based on spot intensity and spot area under local background removal. This was followed by a normalization procedure which uses the total pixel volume of all spots on the gel image as 100%. Subsequently, protein expression between osmotically stressed and control cells was compared as described in detail elsewhere.[25] Prenormalized values after local background subtraction were subsequently exported to spreadsheet format for statistical analysis. Therefore, protein spots found to be altered after visual inspection were now quantified and assigned to expression ratios and *p*-values. The cutoff was $p < 0.05$.

Protein Identification by Mass Spectrometry. For protein identification by mass spectrometry (MS), 40 μL (~20 μg/μL) of protein extract was separated on 1.5 mm diameter isoelectric focusing (IEF) and 1.0 mm (width) SDS-PAGE gels, and resulting 2-D gels were stained with a MS compatible silver staining protocol.[23,24] All protein spots of interest were excised from 2-D gels and subjected to in-gel trypsin digestion. Tryptic fragments were analyzed by liquid chromatography (LC)/electrospray ionization (ESI)-MS and -MS/MS on a LCQ Deca XP ion trap instrument (Thermo Finnigan, Waltham, MA). LC was directly coupled with ESI-MS analysis. Peptide eluates of 15 μL were loaded on a PepMap C18 Nano-Precolumn (5 μm, 100 Å, 300 μm i.d. × 1 mm; LC Packings, Amsterdam, Netherlands) using 0.1% (v/v) trifluoroacetic acid at a flow rate of 20 μL/min. Peptides were now separated by a PepMap C18 100 column (length 15 cm, i.d. 75 μm; LC Packings, Amsterdam, Netherlands). The elution gradient was created by mixing 0.1% (v/v) formic acid in water (solvent A) and 0.1% (v/v) formic acid in acetonitrile (solvent B) and run at a flow rate of 200 nL/ min. The gradient was started at 5% (v/v) solvent B and increased linearly up to 50% (v/v) solvent B after 40 min. ESI-MS data acquisition was performed throughout the LC run.

The ESI spray voltage was set to 4−5 kV. Three scan events, (i) full scan, (ii) zoom scan of most intense ion in full scan, and (iii) MS/MS scan of the most intense ion in full scan, were applied sequentially. No MS/MS scan for single charged ions was performed. The isolation width of precursor ions was set to 4.50 *m*/*z*, normalized collision energy at 35%, minimum signal required at 10 × 104 and zoom scan mass width low/high at 5.00 *m*/*z*. Dynamic exclusion was enabled; exclusion mass width low/high was set at 3.00 *m*/*z*. Raw data were extracted by a TurboSEQUEST algorithm, and trypsin autolytic fragments and known keratin peptides were subsequently filtered. All DTA files generated by TurboSEQUEST were merged and converted to MASCOT generic format files (MGF). Mass spectra were analyzed using our MASCOT in-house license (version 2.1.0, Matrix Science, London, U.K.) with automatic searches in NCBInr database (version 20061206, taxonomy: *Mus musculus*). MS/MS ion search was performed with the following set of parameters: (i) taxonomy, *Mus*

musculus; (ii) proteolytic enzyme, trypsin; (iii) maximum of accepted missed cleavages, 1; (iv) mass value, monoisotopic; (v) peptide mass tolerance, 0.8 Da; (vi) fragment mass tolerance, 0.8 Da; and (vii) variable modifications, oxidation of methionine and acrylamide adducts (propionamide) on cysteine. Criteria for positive identification of proteins were set according to the scoring algorithm delineated in Mascot,[29] with an individual ion score cutoff threshold corresponding to $p < 0.05$. The MOWSE score cutoff was 36.

Protein Expression Overlap Analysis of Osmotic Stress with ND Data. Protein expression data from three different ND studies, (AD),[26,30–34] (HD)[12,28,35,36] and (PD),[9,37–39] were compared to our osmotic stress data. Most of this data set was already analyzed previously,[27] but two recent studies from our laboratory were added to increase the number of proteins differentially expressed in AD[26] and HD[35] and make the data set more homogeneous, to 367, 389, and 377 for AD, HD, and PD, respectively. Previously, there was a disproportionally large number of proteins available that were only altered in PD.[27] All proteins altered in a disease, regardless of species investigated, tissue, and time point were considered. The 92 proteins differentially expressed after osmotic stress were compared to 367, 389, and 377 nonredundant proteins from AD, HD, and PD, respectively. The proteins were compared at the level of gene symbols since protein names sharing the same gene symbol can be quite numerous.

To investigate an enrichment of specific pathways in the altered protein expression data set, we used the "WEB-based GEne SeT AnaLysis Toolkit" (WEBGESTALT) tool supplied by the Vanderbilt University at http://bioinfo.vanderbilt.edu/webgestalt/. We employed the "Gene set analysis tool" and selected the gene set analysis option "Function" and the category "KEGG table and maps". KEGG is the abbreviated form of Kyoto Encyclopedia of Genes and Genomes and is a bioinformatics database containing information on genes, proteins, reactions, and pathways. The following parameters were used to create the KEGG tables: Reference set, "WEBGESTALT_MOUSE"; significance level, $p < 0.01$; minimum number of genes, 2. Statistical methods available were "hypergeometric test" and "Fisher's exact test". For our data set, the results were the same with either test.

Mathematical Modeling. A Petri net is a bipartite graph structure consisting of "place" nodes, "transition" nodes and directed arcs connecting places with transitions.[40] In our model, we concentrate on the dynamics of protein metabolism pathways. For this purpose, cellular pathways involved in protein handling were dissected into four abstract modules: protein biosynthesis (in ribosomes), protein maturing, protein degradation and protein turnover. These four processes are represented by four different **transitions**. In addition, these processes link the cellular material pools, represented by four different **places**: free amino acid resources, functional cellular proteins, proteins targeted to the proteasome and proteins located in the ER. Different arcs (arrows) indicate the material flow through different cellular processes (For a detailed description on Petri net formalism, see ref 41). Petri net simulation and analysis were performed using the Snoopy (http://www-dssz.informatik.tu-cottbus.de/) and INA (http://www2.informatik.hu-berlin.de/~starke/ina.html) software packages. To access quantitative properties of the abstract protein metabolic network, a mathematical model employing ordinary differential equations based on the Petri net model was constructed employing Cell Designer (www.celldesigner.org). In this kinetic model, five species (cellular proteins, ribosomes, ER, proteasome and resource) are interconnected by state transition reactions as described in the Petri net formalism above. To cope with the lack of data on kinetic parameters, we restricted our model to a very abstract and descriptive level. For this purpose, the overall reaction rates originating from a certain species was set to one. Specifically, since both material flows streaming to cellular proteins and ER come from proteins synthesized in the ribosome, the reaction rate of "ribosome" → cellular proteins", and "ribosome" → ER" were both set to 0.5. This is based on the consideration that about 50% of all synthesized protein undergo ER-processing.[42] In case of ER-processing in swollen (hyperosmotic) ES cells, the "overrun" from ER to proteasome "x" was defined as a fraction between 0 and 1 ($x \in (0, 1)$), whereas the kinetic parameter of the state transition reaction "ER → cellular proteins" was set to $1 - x$.

Statistical Evaluation of Data. To determine the statistical significance of expression differences between osmotic-treated and control cell lines, Student's t test was used for control versus osmotic-treated groups (pairwise, two sided, $n = 6$). $P < 0.05$ was used as statistical significance threshold. To reduce the influence of noise on the data set, only protein expression changes over 20% compared to control were retained for further analysis. Protein expression alterations (Table 1, expression fold change) are reported as standard error of means (SEM). As a post hoc control for false positives, protein expression data generated by 2-DE were analyzed using the "Significance Analysis of Microarrays" tool (SAM 3.0, www-stat.stanford.edu) to ensure a false positive rate of below 1%.[43]

Results

In this study, mouse ES cells cultured under different osmotic conditions affecting cell volume, were investigated using a 2-DE/MS based comparative proteomic approach to study the effect of modified tonicity on cell morphology and cellular protein expression profiles. For this purpose, mouse ES cells were exposed to culture media with osmolarities of 200 mOsM (hypoosmotic), 340 mOsm (standard cell culture medium) or 500 mOsm (hyperosmotic). ES cells were used since they represent progenitors to all somatic cells of an organism. Therefore, cell type specific changes caused by osmosis such as seen in spleen were excluded and more general responses of a cell/tissue were accessible to investigation.

Cell Morphology. During a cultivation time of 144 h, ES cells showed no significant morphological alteration due to altered tonicity. The vast majority of cells showed typical ES cell morphology with tightly packed cells forming round colonies (Figure 1).

Cell Growth. Cellular growth rates were considerably different under modified osmotic conditions, with the slowest growth rate observed in cells cultivated in hyperosmotic conditions. When compared to isotonically treated controls, which reached 90% confluency after 48 h of cultivation, the ES cells grown in hypo-osmotic medium reached 70% and cells in hyperosmotic culture medium only 40% confluency (Figure 1). This was also reflected by the pH value of the culture medium after 2 days: isotonic pH 4.7, hypotonic pH 5.5, and hypertonic pH 6.5. Therefore, prolonged exposure (144 h) to osmotic stress reduced the cellular growth rate, with hyperosmotic conditions showing the most drastic effect.

Cell Size. When considering cell size, slight differences could be observed in aniso-osmotically as compared to iso-osmotically cultured cells. On average, there was a clear cell swelling

Table 1. Osmotic Stress-Induced Protein Expression Alterations[a]

Spot ID	Protein name	Gene symbol	iMowse Score	Seq.ence Cov.erage (%)	# of Pepides	# of nonredundant Pep.	Molecular Weight (theo.) [Da]	pI (theoretical.)	NCBI Acc.	Expression fold change (Hyper)	Statistical significance (Hyper)	Expression fold change (Hypo)	Statistical significance (Hypo)
B018	Acetyl-Coenzyme A acyltransferase 2	Acaa2	816	41	29	15	41803	8.33	gi|29126205	1.82 ± 0.19	7.97E-04	0.79 ± 0.03	2.62E-04
S039	A-X actin	Actb	189	10	6	4	41667	5.21	gi|309090			0.54 ± 0.33	3.87E-02
B129	Put. beta-actin (aa 27-375)	Actg1	152	8	8	4	39161	5.78	gi|49868			0.42 ± 0.12	5.27E-04
S030	Put. beta-actin (aa 27-375)	Actg1	49	5	1	1	39161	5.78	gi|809561	1.23 ± 0.06	3.06E-03		
S047	Put. beta-actin (aa 27-375)	Actg1	328	22	11	6	39161	5.78	gi|49868	2.06 ± 0.25	6.72E-03	0.56 ± 0.09	9.00E-04
S063	Gamma-actin	Actg1	115	7	5	2	41724	5.56	gi|809561	1.56 ± 0.11	5.17E-05	0.51 ± 0.08	1.39E-03
S064	Gamma-actin	Actg1	177	10	7	3	41724	5.56	gi|809561	1.26 ± 0.18	1.31E-02	0.76 ± 0.10	3.83E-02
S111	Alpha-fetoprotein	Afp	110		3	2	47195	5.47	gi|191765	0.47 ± 0.16	1.26E-02	3.87 ± 1.12	6.07E-03
B059	Adenylate kinase 2	Ak2	272		16	5	25589	6.97	gi|34328230			0.72 ± 0.07	2.91E-02
S153	Albumin 1	Alb	143		8	4	68648	5.75	gi|19353306			2.38 ± 0.32	4.62E-02
S154	Albumin 1	Alb	143		8	4	68648	5.75	gi|19353306			1.71 ± 0.48	4.17E-02
S080	Annexin A4	Anxa4	733	38	26	12	35907	5.43	gi|33416530	1.21 ± 0.12	3.51E-03	1.29 ± 0.25	2.82E-02
S108	Rho GDP dissociation inhibitor (GDI) alpha	Arhgdia	119		11	4	23393	5.12	gi|31982030	0.70 ± 0.08	4.56E-03	1.32 ± 0.14	2.25E-02
B105	Actin related protein 2/3 complex subunit 4 isoform a	Arpc4	268	27	13	5	19654	8.53	gi|5031595			1.32 ± 0.06	1.63E-02
S128	Actin-related protein 2/3 complex subunit 5	Arpc5	287	25	10	5	16278	5.47	gi|62510460	1.48 ± 0.22	6.48E-03		
B039	ATP synthase, H+ transporting, mitochondrial F1 complex, gamma subunit	Atp5c1	79	4	2	1	35703	9.06	gi|11602916	2.06 ± 0.93	3.53E-02		
S140	BAT2 domain containing 1	Bat2d	69	29	20	20	63?	5.7	gi|39793885			1.72 ± 0.33	1.99E-02
S089	Bactericidal/permeability-increasing protein-like 3, precursor	Bpil3	38		3	1	48870	6.87	gi|28856146			2.44 ± 1.03	4.18E-02
S086	Similar to: CGI-150 protein	C17orf25	70		6	2	30765	4.8	gi|12840311	0.76 ± 0.15	8.81E-03	1.78 ± 0.06	2.97E-05
S082	Capping protein (actin filament) muscle Z-line, beta	Capzb	627		18	8	30609	5.69	gi|6753262			1.48 ± 0.16	7.20E-03
S116	Chromobox homolog 1	Cbx1	537	29	16	7	21405	4.85	gi|5803076			0.75 ± 0.04	3.62E-03
B139	Coiled-coil domain containing 58	Ccdc58	411	53	14	7	16654	8.35	gi|38348528			0.37 ± 0.51	1.50E-02
B028	Hyperparathyroidism 2 homolog	cdc73	647	21	24	10	60539	9.63	gi|22122445			2.92 ± 0.52	3.72E-02
S107	UMP-CMP kinase	Cmpk	39	4	2	1	57807	8.13	gi|31981246			2.27 ± 0.27	2.05E-03

Table 1. Continued

S068	Chromosome X open reading frame 26	CXorf26	196		12	5	15650	4.38	gi|26345738			1.54 ± 0.12	4.19E-03
S022	Drebrin-like	Dbnl	88		7	4	48312	4.9	gi|28386239	1.30 ± 0.05	1.91E-03		
B066	3,2-Trans-enoyl-CoA isomerase, mitochondrial precursor	Dci	361	20	11	7	32058	8.87	gi|1169205	1.32 ± 0.14	3.58E-03	1.26 ± 0.04	9.50E-03
B091	Dodecenoyl-Coenzyme A delta isomerase	Dci	136	9	3	2	32230	9.12	gi|31981810			1.69 ± 0.15	1.22E-02
B024	Elongation factor Tu	Eef1a1	88		3	1	50132	9.1	gi|556301	2.57 ± 0.38	4.21E-03		
B042	Elongation factor Tu	Eef1a1	119	4	6	2	50018	9.1	gi|556301	6.25 ± 0.90	3.11E-05	0.47 ± 0.70	4.62E-02
B023	Elongation factor Tu	Eef1a1	243	9	10	4	50132	9.1	gi|556301	5.56 ± 1.32	6.71E-03		
B025	Elongation factor Tu	Eef1a1	374	15	17	7	50132	9.1	gi|556301	1.28 ± 0.19	2.81E-02		
S055	Eukaryotic translation elongation factor 1 delta isoform b	Eef1d	441	2	11	6	31273	4.96	gi|54287684	0.47 ± 0.09	2.34E-02		
S119	Eukaryotic translation initiation factor 1A, Y-linked	Eif1ay	43		2	1	16450	5.07	gi|31541824			0.64 ± 0.12	1.38E-02
S123	Eukaryotic translation initiation factor 1A, Y-linked	Eif1ay	43		2	1	16450	5.07	gi|31541824	0.69 ± 0.03	3.02E-02		
S124	Eukaryotic translation initiation factor 5A	Eif5a	170		13	5	16292	4.85	gi|56800106	0.68 ± 0.03	2.00E-04		
B106	Fatty acid-binding protein, hepatic - mouse (fragment)	Fabp1	43	11	2	1	10173	5.88	gi|90485			1.32 ± 0.06	1.63E-02
B132	FK506 binding protein 1a	Fkbp1a	188	40	5	3	11915	7.88	gi|6679803			1.97 ± 0.33	7.31E-03
B099	Glyceraldehyde-3-phosphate dehydrogenase	Gapdh	265	13	7	4	35751	8.38	gi|55153885			0.36 ± 0.18	1.98E-03
B096	Glyceraldehyde-3-phosphate dehydrogenase	Gapdh	63	5	2	1	35787	8.44	gi|6679937	3.73 ± 0.79	3.83E-04	0.46 ± 0.32	3.90E-02
B100	Glyceraldehyde-3-phosphate dehydrogenase	Gapdh	119	7	3	2	35787	8.44	gi|6679937			0.61 ± 0.19	5.02E-02
S132	Glyceraldehyde-3-phosphate dehydrogenase	Gapdh	128	8	3	2	35787	8.44	gi|6679937	3.32 ± 0.43	1.31E-03		
S110	Glyoxalase 1	Glo1	137	35	9		21000	5.1	gi|51859026	0.63 ± 0.13	2.36E-03	1.50 ± 0.20	2.05E-02
S032	Y box-binbing protein	Gss	64	4	1	1	35822	9.98	gi|55451			2.11 ± 0.41	1.65E-02
B131	Alpha-1-globin	Hba1	89	19	2	2	12899	6.78	gi|553919	2.71 ± 0.78	4.33E-03		
S067	Histone cell cycle regulation defective interacting protein 5	Hirip5	94		3	2	22126	4.23	gi|9910264			1.54 ± 0.59	4.05E-02
S099	Hspb1 protein	Hspb1	114	32	7	7	23000	6.1	gi|17390597	2.38 ± 0.52	2.95E-02		
S101	Heat-shock protein beta-1	HspB1	535	47	20	10	23000	6.12	gi|547679	6.63 ± 1.03	4.97E-04		

Table 1. Continued

B029	heat shock protein 1	Hspd1	43	1	1	1	60918	5.67	gi|31981679			2.92 ± 0.52	3.72E-02
B060	Galectin-3	Lgals3	231	13	7	3	27498	8.46	gi|126679	1.32 ± 0.11	7.83E-04		
B038	Galectin-6	Lgals6	187	11	5	3	34118	8.99	gi|3335391	3.38 ± 1.23	3.05E-03	1.33 ± 0.53	4.38E-02
B121	Macrophage migration inhibitory factor	Mif	61	9	3	1	12365	6.79	gi|6754696	0.70 ± 0.17	4.92E-02		
S138	Myotrophin	Mtpn	116		5	2	12853	5.27	gi|6679961			2.33 ± 0.30	4.59E-03
S059	Nucleophosmin 1	Npm1	81		2	2	3254	4.62	gi|6679108	0.52 ± 0.08	9.23E-05		
S148	Nucleophosmin 1	Npm1	66	4	3	1	32540	4.62	gi|6679108	0.68 ± 0.01	5.33E-05	1.43 ± 0.19	2.25E-02
S150	Nucleophosmin 1	Npm1	43	14	2	2	32540	4.62	gi|6679108			1.62 ± 0.43	1.71E-02
B027	Poly(A) binding protein	Pabpc1	117		4	3	70598	9.48	gi|53754			2.34 ± 0.55	2.51E-02
B006	Mitochondrial phosphoenolpyruvate carboxykinase 2	Pck2	642	19	18	10	70448	7.88	gi|16307539	0.58 ± 0.08	1.10E-02	0.63 ± 0.03	2.86E-02
B120	Procollagen C-endopeptidase enhancer 1 precursor	Pcolce	42	1	1	1	50136	8.73	gi|6919942	2.70 ± 0.29	2.67E-05		
B012	Pyruvate dehydrogenase E1 alpha 1	Pdha1	608	22	27	12	43204	8.49	gi|6679261			0.58 ± 0.07	3.43E-02
S114	Phosphatidylethanolamine binding protein	Pebp1	86		4	2	20847	5.19	gi|9256572			1.59 ± 0.28	4.81E-02
B118	Profilin 1	Pfn1	130	78	17	17	15000	9.4	gi|38382852			1.36 ± 0.12	5.72E-03
B086	Peroxiredoxin 1	Prdx1	459	44	14	8	22162	8.26	gi|6754976	1.91 ± 0.29	1.50E-03		
B087	Peroxiredoxin 4	Prdx4	64	4	3	1	31033	6.67	gi|7948999	1.91 ± 0.29	1.50E-03		
S085	Nonselenium glutathione peroxidase	Prdx6	542		18	9	24855	5.71	gi|2072655			1.42 ± 0.13	7.91E-03
B044	Phosphoserine aminotransferase 1	PSAT1	170	35	13	13	40000	7.7	gi|26354941	0.65 ± 0.08	2.12E-03		
B056	Proteasome (prosome, macropain) subunit, alpha type 1	Psma1	160	13	10	4	29528	6	gi|33563282			1.38 ± 0.04	2.07E-03
S087	Proteasome (prosome, macropain) subunit, alpha type 3	Psma3	681		21	11	28472	5.4	gi|31981534	0.72 ± 0.05	1.62E-05		
B079	Component C5 of proteasome	Psmb1	226	19	11	4	24664	8.29	gi|1165123	0.73 ± 0.02	1.31E-05	1.37 ± 0.11	2.85E-02
S102	Proteasome subunit beta type 4 precursor	Psmb4	130	9	7	3	29097	5.47	gi|3914439			1.85 ± 0.21	1.95E-02
B092	Proteasome subunit beta type 5 precursor	Psmb5	497	37	16	7	22952	8.65	gi|3914434			1.69 ± 0.15	1.22E-02
S113	Proteasome (prosome, macropain) subunit, beta type 6	Psmb6	113		6	2	21668	4.99	gi|984938			1.74 ± 0.29	3.83E-02

Table 1. Continued

B094	proteasome subunit MC13	Psmb8	45	6	2	1	23032	6.89	gi|673450			1.69 ± 0.15	1.22E-02
S096	Proteasome (prosome, macropain) 28 subunit, alpha	Psme1	74				28655		gi|6755212			2.11 ± 1.04	2.98E-02
B035	Polypyrimidine tract-binding protein 1	Ptbp1	63	2	2	1	56443	8.47	gi|131529	2.22 ± 0.23	2.29E-03	0.72 ± 0.17	1.73E-03
B004	Glutaminyl-tRNA synthetase	Qars	222	5	5	3	87621	7.04	gi|55741703	0.63 ± 0.09	4.78E-02		
S109	Ran/TC4-binding protein 1	Ranbp1	340		23	7	23568	5.15	gi|739241	0.68 ± 0.04	8.46E-04	1.27 ± 0.15	5.79E-03
B080	RNA binding protein with multiple splicing 2	Rbpms2	43	4	2	1	18283	8.5	gi|31980694	0.73 ± 0.02	1.31E-05	1.37 ± 0.11	2.85E-02
S027	Reticulocalbin 1	Rcn1	511	30	14	8	38090	4.7	gi|6677691			0.86 ± 0.08	8.38E-03
B021	ROD1 regulator of differentiation 1 isoform 1	Rod1	304	9	7	5	56346	9.21	gi|21450285	1.44 ± 0.28	4.55E-02		
S081	Replication protein A2	Rpa2	136	11	4	3	29700	5.76	gi|13435424			1.59 ± 0.19	5.54E-03
S024	Ribosomal protein L14	Rpl14	44		5	1	23579	11.03	gi|12841593	0.65 ± 0.14	9.36E-03		
S093	40S ribosomal protein SA (p40) (34/67 kDa laminin receptor)	Rpsa	195	12	7	3	32698	4.74	gi|125970			0.70 ± 0.18	8.10E-03
S134	S100 calcium binding protein A11	S100a11	128		3	1	11076	5.28	gi|21886811	1.81 ± 0.42	3.66E-03	1.66 ± 0.21	5.57E-03
S045	Septin 1	Sept1.	38	1	1	1	47509	5.7	gi|8567344			1.93 ± 0.18	1.99E-02
S095	SET translocation	Set	119		5	3	33358	4.22	gi|13591862			3.16 ± 0.76	1.29E-02
S112	Set beta isoform	Set	119		5	3	33358	4.22	gi|13591862	0.47 ± 0.16	1.26E-02	3.87 ± 1.12	6.07E-03
S072	stratifin	Sfn	251		17	3	27696	4.75	gi|9055338	0.74 ± 0.05	2.12E-04		
B001	Splicing factor proline/glutamine rich	Sfpq	662		40	16	75394	9.45	gi|23956214			2.01 ± 0.31	6.66E-03
B002	Splicing factor proline/glutamine rich	Sfpq	662		40	16	75394	9.45	gi|23956214			2.29 ± 0.47	6.49E-03
S035	SH3-domain GRB2-like 1	Sh3gl1	104		6	3	41492	5.53	gi|7305485			1.49 ± 0.38	2.89E-02
B107	Cu/Zn superoxide dismutase	Sod1	49		3	6	15955	6.23	gi|201006			1.51 ± 0.22	1.61E-02
B081	Manganese superoxide dismutase	Sod2	240		18	4	24662	8.8	gi|53450			0.79 ± 0.06	1.77E-02
S129	Stathmin 1	Stmn1	63	8	1	1	17264	5.76	gi|9789995			1.29 ± 0.11	1.28E-02
S097	Sulfatase-modifying factor 2 precursor	Sumf2	383	23	17	6	34685	7.03	gi|33301722			0.77 ± 0.67	2.47E-02
S157	SMT3 suppressor of mif two 3 homolog 1 isoform a precursor	Sumo1	171	35	10	4	11550	5.53	gi|4507801			0.77 ± 0.15	2.63E-02
S125	Small ubiquitin-like modifier 2 isoform b precursor	Sumo2	165		13	3	25012	7.57	gi|51710859	0.78 ± 0.06	2.81E-03		

Table 1. Continued

B030	tumor-associated calcium signal transducer 1	Tacstd1	43	1	1	1	34925	5.67	gi|193008			2.92 ± 0.52	3.72E-02
S049	Transaldolase 1	Taldo1	272		24	3	37363	6.57	gi|33859640			0.39 ± 0.39	2.80E-02
S141	Transcription elongation factor B (SIII), polypeptide 2	Tceb2	80				13162		gi|13385800			1.72 ± 0.33	1.99E-02
S060	Tropomyosin 1, alpha	Tpm2	244	13	7	4	32689	4.71	gi|73971296	1.56 ± 0.22	6.71E-04	1.35 ± 0.09	2.99E-03
S126	Tripartite motif-containing protein 28	Trim28	201	3	10	3	88790	5.52	gi|3183181	1.66 ± 0.24	6.33E-03	0.49 ± 0.10	1.08E-03
S130	Tripartite motif-containing protein 28	Trim28	48	1	3	1	88790	5.52	gi|3183181	1.50 ± 0.17	1.01E-03		
S136	Thioredoxin 1	Txn1	75				11668		gi|14789654	0.69 ± 0.03	1.27E-02		
S031	Thioredoxin domain containing 4	Txndc4	49	3	2	1	46823	5.09	gi|19072792			1.07 ± 0.05	3.06E-03
B124	Polyubiquitin	Ubc	77	45	5		12000	9.8	gi|91870			1.69 ± 0.25	1.59E-02
S002	Ubiquitin-activating enzyme E1, Chr X	Ube1x	248		13	7	117734	5.43	gi|6678483			13.60 ± 3.40	3.68E-02
S088	Ubiquitin carboxy-terminal hydrolase L1	Uchl1	159	13	6	3	24822	5.33	gi|6755929			1.52 ± 0.29	1.94E-02
S079	Ubiquitin carboxyl-terminal esterase L3	Uchl3	149		2	1	26162	5.08	gi|7710106	0.71 ± 0.04	9.45E-05	1.49 ± 0.26	3.55E-02
S071	14-3-3 eta	Ywhah	48		4		28181	4.76	gi|1526541	0.74 ± 0.05	2.12E-04		
B031	NI											3.08 ± 0.78	3.67E-02
B111	NI									0.64 ± 0.28	4.44E-02	1.70 ± 0.13	2.58E-03
B126	NI											1.46 ± 0.23	4.80E-02
S042	NI									0.41 ± 0.08	2.17E-02	2.30 ± 0.74	9.10E-03

[a] Data set is sorted according to gene symbol; proteins altered specifically by osmotic stress are highlighted dark gray and those altered by osmotic stress, AD, HD, and PD are highlighted red. Abbreviations: #, number; Pep., peptides. Alterations were quantified as fold change of protein spot pixel volume (osmotic treated vs control) and represented as standard error of mean (SEM, $n = 6$). *Spot ID corresponds to marked spots on Figure 2. #NI: not identified. §Student's T-test, one sided, unpaired, $n = 6$.

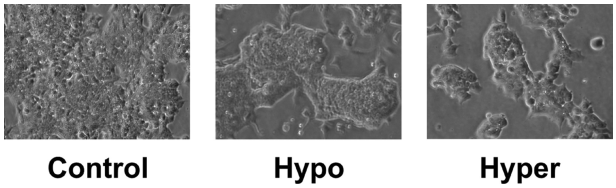

Figure 1. Representative micrographs of in vitro mouse embryonic stem cells after 48 h of cultivation in culture media of different osmolarities. (A) Cells in isotonic culture conditions reached 90% confluence. (B) Cells treated in hypo-osmotic medium reached 70% confluence. (C) Cells treated by hyperosmotic condition showed only 40% confluence.

or shrinkage under hypo-osmotic or hyperosmotic conditions, respectively, although statistical significance was not reached. After 48 h of cultivation, the cell diameters of isotonic, hypertonic or hypotonic treated ES cells were 36.97 ± 6.98 μm (26 457.38 ± 178.06 μm^3), 34.00 ± 4.86 μm (20 579.53 ± 60.10 μm^3) or 37.47 ± 5.35 μm (27 523.40 ± 80.18 μm^3), respectively. This suggests that the ES cells shrunk on average to 77.8% of

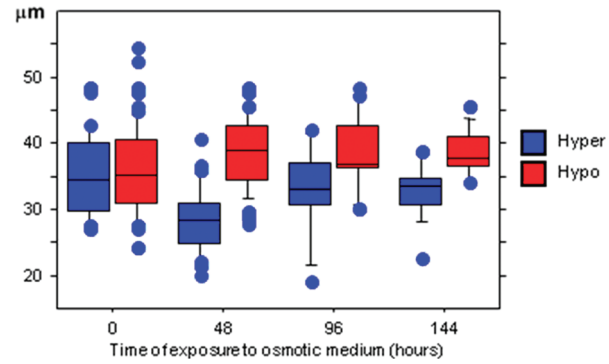

Figure 2. Effect of osmotic stress on ES cell size. Estimated cell size alteration after cultivating mouse ES cells 48, 96, and 144 h in isotonic (340 mOsm), hypertonic (500 mOsm) or hypotonic (200 mOsm) culture medium, respectively. Results are presented as box and whisker plots. The box indicates the interquartile range (25% and 75%) and the bold line within the median. Outliers are indicated by blue circles.

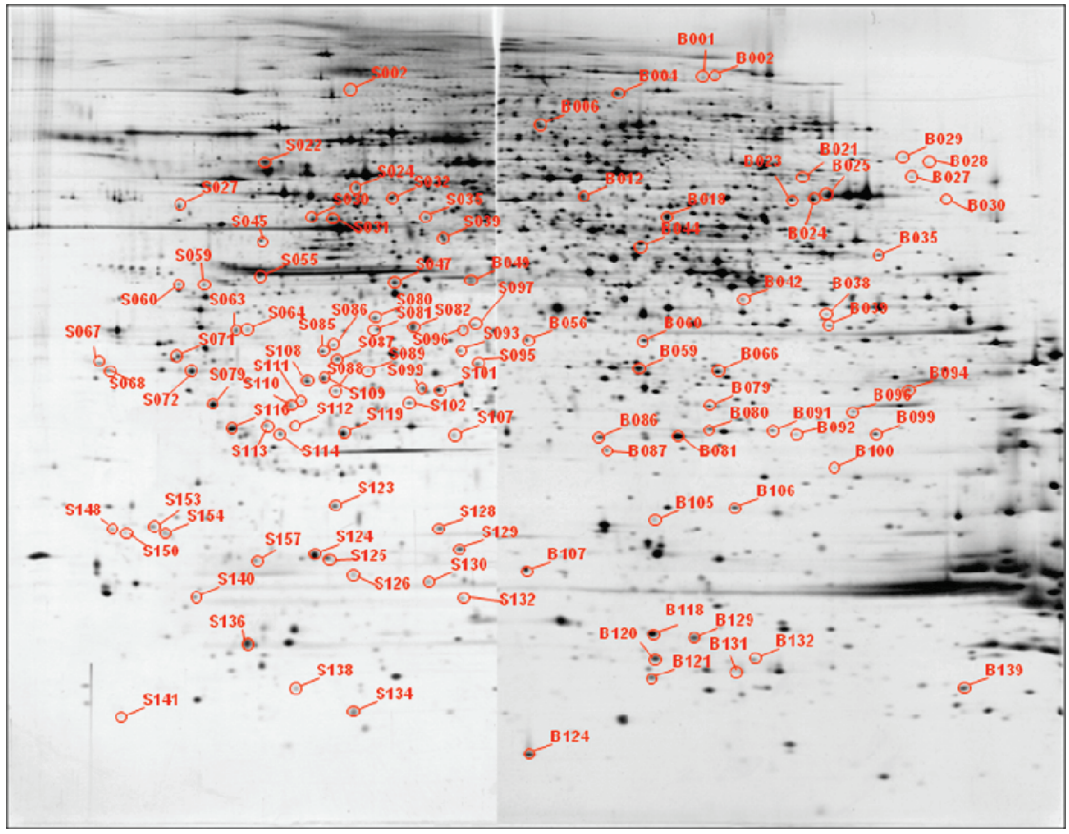

Figure 3. Representative protein expression patterns of mouse ES cells exposed to osmotic stress. Proteins (70 μg) were separated by 2-DE according to different isoelectric points and molecular masses. The protein spots were visualized by high sensitivity silver staining. Tagged spots (numbers) were differentially expressed after exposure to osmotic stress (see Table 1 for details).

their original volume in hypertonic conditions, whereas they expanded to 104% of their original volume during hypo-osmotic condition. Interestingly, cell size alteration was more drastic during hypertonic treatment (Figure 2).

Analysis of the ES Cell Proteome during Osmotic Stress. ES cells were treated by hyper-, hypo-, and normal osmosis. We found that the 2-D protein pattern of ES cells was very similar and well comparable for all three osmotic conditions (Figure 3). Visual and statistical examination of 2-D gels displaying 5000 separate protein spots revealed 114 significant differences between protein abundance of stressed and non-stressed cells. A false discovery rate of less than 1% was ensured by using the SAM software tool. Compared to isotonic controls, 30 protein spots increased and 26 decreased in expression under hyperosmotic conditions, while 62 were up and 22 down-regulated, under hypo-osmotic conditions. Among these, 26 proteins co-changed under both hyper- and hypo-osmotic conditions.

All protein spots found differentially expressed in osmotically stressed cells were analyzed by MS. A total of 110 out of 114 variant protein spots could be identified with high confidence. The identity of four protein spots remained unknown despite multiple identification efforts. According to spot appearance and location on the 2-D gel, the unidentified protein spots were either very faint (of low cellular abundance) or had extremely high or low isolelectric points. The 110 protein spots represent 92 nonredundant gene products.

Protein Expression Behavior during Osmotic Stress. The expression behavior of differentially expressed proteins was analyzed. Proteins with specific up-regulation or down-regulation under hyperosmotic conditions were found. *Eukaryotic translation elongation factor 1 alpha* (*Eef1a1*) was altered in expression only under hyperosmotic conditions (Figure 4A). *Eef1a1* was modestly expressed in nonstressed cells protein as two isoforms that differ slightly in their isoelectric points (Figure 4A). In hyperosmotic treated cells, this protein increased significantly in expression of both protein isoforms. In hypo-osmotic cells, the expression of both protein spots was unaltered (Figure 4A). A similar expression behavior was observed for *Cytoplasmic actin* (*Actg1*). A prominent protein spot was

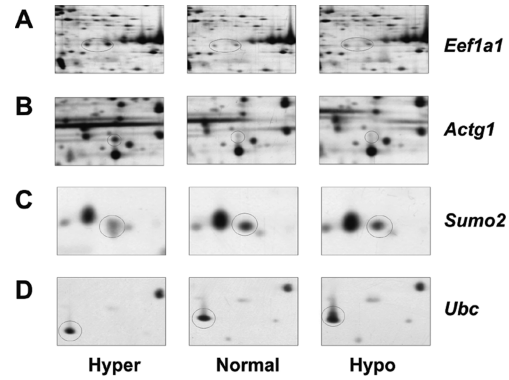

Figure 4. Representative protein spots showing differential expression after osmotic stress. Selective dysregulation after hyperosmotic treatment: (A) up-regulation of both protein isoforms of *Eef1a1*, (B) up-regulation of an isoform of *Actg1* and (C) down-regulation of *Sumo2*. Selective dysregulation after hypo-osmotic treatment: (D) up-regulation of *Ubc* in hypo-osmotic conditions (for fold expression changes, refer to Table 1.

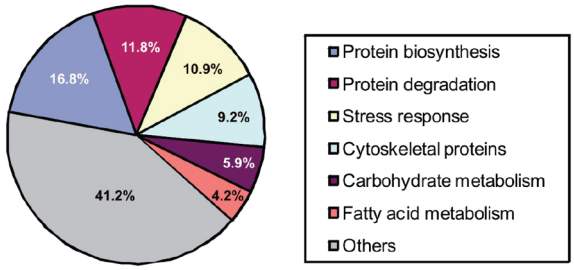

Figure 5. Functional categories of protein changes induced by oxidative stress. The protein which belong to a specific cellular function are shown as fractions of the total proteins changed by osmotic stress. Functional categories of proteins were selected according to keywords supplied by the EXPASY knowledgebase.[70]

exclusively observed on 2-D gels derived from hyperosmotically treated cells (Figure 4B). The opposite expression behavior was observed for *Small ubiquitin-like modifier 2* (*Sumo2*) (Figure 4C). It was decreased in expression after hyperosmotic stress (Figure 4C), while it remained at control levels during hypo-osmosis. *Polyubiquitin* (*Ubc*) was increased drastically in cells under hypo-osmotic treatment (Figure 4D). Therefore, the latter protein showed an inverse regulation pattern when compared to the three previous ones (Compare Figure 4A−C to Figure 4D). The detailed spot expression quantification data with fold-changes as compared to ES cells cultured in isotonic conditions are presented in Table 1. Spot pixel volumes including standard error of means (SEM) from three independent experiments and two technical repeats are shown (Table 1, $n = 6$ for each condition). All differentially expressed protein spots are numbered as highlighted in Figure 3.

Functional Categories of Variant Proteins: After identification of the proteins and determining their expression pattern, proteins bearing altered expression detected in this study were subjected to functional and structural category annotation. On the basis of gene ontology (GO) and UniProt Knowledgebase,[44] we estimated the percentage of changed proteins that belonged to a specific functional category among all changed proteins (Figure 5).

In terms of subcellular localization, one-fifth of all variant proteins (92) reside in the cytoplasm. This includes three mitochondrial and three endoplasmatic reticulum (ER) associated proteins. In terms of protein function, 13 distinct protein species are involved in cellular stress responses. This accounts for 14% of all variant proteins. A comparable fraction of variant proteins are involved in protein biosynthesis (20 proteins, 22%) and protein degradation (14 proteins, 15%), respectively. Among the proteins involved in protein degradation, eight were recognized as important components (subunits) of the proteasome complex, whereas six proteins are components of the ubiquitination system. Together, this accounts for 15% of total variant proteins (14/92). In addition, a significant amount of altered proteins (12%) are characterized as cytoskeletal proteins involved in cell structure maintenance. This includes nine cytoskeleton constituents and two actin-binding proteins. Moreover, seven and five proteins are involved in carbohydrate and fatty acid metabolism, respectively. The distribution of variant proteins over various functional categories of proteins is illustrated in Figure 5 and Table 2.

Integrating the protein expression alteration data according to their functional categories, we disclosed some consistent variation patterns at the level of protein metabolism functional modules in cells subjected to osmotic stress. On average, the protein expression for protein biodegradation (proteasome and ubiquitination system) was ***down-regulated*** to about 74% of isotonic levels after ***hypertonic treatment***, while there was a drastic ***up-regulation*** of protein degradation-related proteins (2.6-fold compared to isotonic controls) in cells under ***hypotonic conditions***. In addition, proteins involved in biosynthesis were decreased 0.8-fold and increased 1.7-fold in hyper- or hypotonic ES cells, respectively (Table 3). Therefore, biodegradation and biosynthesis were co-(cis) regulated. Moreover, an up-regulation (1.3-fold) of ER-bound proteins under hypo-osmotic conditions was observed, but no significant change was seen in hyperosmotic ES cells (Table 3 and Figure 6).

Protein Expression Overlap with Neurodegenerative Disorders. To investigate the specificity of the protein expression alteration during osmotic stress, we used differential expression data for AD,[26,30–34] HD[12,28,35,36] and PD[9,37–39] where a total of 367, 389 and 377 nonredundant proteins were differentially expressed. After comparing the 92 differentially expressed proteins using their gene symbols to the AD, HD and PD data sets, we found that 37 proteins were only altered during osmotic stress, while 17 proteins were altered in osmotic stress and all 3 ND investigated (Table 1). Specific proteins are labeled dark gray and proteins overlapping in osmotic stress, AD, HD and PD in red in Table 1. This means that only 40% of the nonredundant proteins altered by osmotic stress are specific. As much as an 18% expression overlap between all three ND investigated and osmotic stress was found. In addition, a total of 60% of the proteins altered by osmotic stress were altered in at least one ND investigated. A KEGG analysis of the specific as well as the unspecific data set revealed that "Glycolysis/Gluconeogenesis", "Proteasome" and "PD" proteins are enriched in the unspecific data set ($p < 0.01$), whereas only "Cell cyle" was enriched in the osmotic stress specific data set, although the former set contained only 17 and the latter 37 proteins. Proteins altered specifically by osmotic stress are therefore highly diverse in terms of cellular pathways, but there is a large overlap of proteins altered in osmotic stress and all ND studied.

Mathematical Modeling of the Effects of Osmotic Stress on ES Cells. To access the intrinsic relation between different modules of protein metabolic pathways, we employed a Petri net formalism to model the material flows within the protein metabolic pathways in an abstract but dynamic manner. In this reductionist view, cellular proteins are synthesized from cell free resources by ribosomes. Among the proteins synthesized, part of them (50%) are deposited as functional cellular proteins (maturing protein products), whereas the rest of the newly synthesized proteins are processed by the protein maturing pipeline in the endoplasmatic reticulum (ER), before they are released to the pool of functional proteins.[42] All cellular proteins undergo biodegradation at distinct rates as determined by their protein-specific half-life. To further reduce complexity, we assume that the entire protein degradation is carried out by the ubiquitin/proteasomal system. This pathway in turn facilitates the turnover of cellular proteins and the refilling of free amino acid resources (Figure 7A). Notice that here we consider the cellular protein metabolism system as a *closed* system. Therefore, the effect of cell volume alteration was exclusively modeled as an increment abundance of free cellular resources (5 tokens in the free resources place under isotonic condition, and 10 tokens in the swelled condition).

Table 2. Functional Categories of Altered Proteins Induced by Osmotic Treatments

Expasy keywords[a]	gene symbol
Cytoskeleton	Actb, Actg1 (5 isoforms), Arpc4, Arpc5, Pfn1, Dbnl, Tpm2
Endoplasmic reticulum	Rcn1, Txndc4, Sumf2
Mitochrondrion	Acaa2, C17orf25 (Glod4), Ak2
Fatty acid metabolism	Dci (2 isoforms), Fabp1, Pebp1, Acaa2
Carbohydrate metabolism	Gapdh (4 isoforms), Pdha1, Taldo1, Pck2
Proteasome	Psma1, Psma3, Psmb1, Psmb4, Psmb5, Psmb6, Psmb8, Psme1
Protein biosynthesis	Eef1a1 (4 isoforms), Eef1d, Eif1a, Eif1ay, Eif5a, Psat1, Qars, Rpl14, Rpsa, Sfpq (2 isoforms), Trim28 (2 isoforms), Npm1 (4 isoforms)
Stress response	Glo1, Gss, Hspb1 (2 isoforms), Hspd1, Prdx1, Prdx4, Prdx6, Sod1, Sod2, Txn1, Txndc4, St13
Ubl conjugation pathway	Ube1x, Uchl1, Uchl3, Sumo1, Sumo2, Tceb2

[a] Only Expasy keywords assigned with more than 3 distinct proteins (according to gene symbol) are included.

Table 3. Alterations in Protein Functional Modules during Osmotic Stress

	hypertonic	hypotonic
ER processing	1.0[a]	1.3
Proteasome	0.7	1.7
Ubiquitin proteins	0.8	3.8
Protein biodegradation	0.7	2.6
Protein biosynthesis	0.8	1.7

[a] The averaged fold-change expression of protein metabolic functional modules as deduced by the mean values of variant proteins that belong to the same functional module (expression fold-changes expressed as compared to isotonic controls).

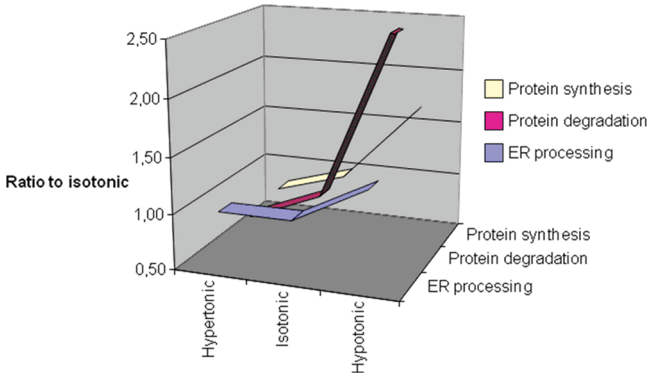

Figure 6. Changes in protein metabolism. Average fold change of protein degradation and ER-processing caused by osmotic stress in ES cell. We observed up-regulated protein degradation in hypo-osmotic culture conditions, and a down-regulation of protein degradation in hyperosmotic culture conditions. Similar but less drastic changes were observed for ER-processing proteins.

It is known that the ER is only able to process and mature proteins at a distinct maximal capacity,[45] which, according to our assumption, is reached at normal cellular operation. In case there is an increased amount of cellular resource due to cell swelling, the overload of proteins to be processed will lead to ER-stress.[46] Under such conditions, part of the proteins ("overrun") will be directed to the proteasome and ubiquitin system for degradation straight away. This generates an extra arc in the Petri net model (Figure 7B, red arrow).

Influence of Osmotic Stress on the Stationary (Static) Properties of Protein Metabolic Structure. At a first glance, the Petri nets of a normal and a swollen cell differ solely by an additional arrow in the swollen cell model under our current assumptions. Nevertheless, a topological and dynamic analysis of the Petri nets involved shows some distinct discrepancies between normal and swollen cellular conditions (Table 4). Compared to the isotonic state, the Petri net of swollen cells is no longer conservative, which means that the total number of tokens in this net no longer remains constant.[47] This shows that the protein resources in the normal, but not swollen cells are constant. Second, unlike the Petri net structure of normal cells, the Petri net of swollen cells is not bounded. "Boundedness" means that the token numbers of a Petri net will not exceed a certain upper value. This means that the network of normal cells is more stable as compared to swollen cells.

Another important difference is that the Petri net of swollen cells has neither place (p) nor transition (t) invariants (Table 4). In the Petri net theory, the presence and amount of p and t-invariants in a Petri net correlates positively with the stability and robustness of the network structure. The absence of structural invariants in the Petri net model of the swollen cells could suggest a reduced robustness of the metabolic protein network in swollen cells.

Next, we performed the dynamic simulation of these two Petri nets by random firing of enabled transitions. Starting with the respective initial markings, both the proteasome and functional protein places possess generally higher marking numbers along the time-dependent trajectory in the hypo-osmotic compared to normal (isotonic) condition (Figure 7C,D). Importantly, the up-regulation of biosynthesis occurs before that of protein degradation system. This implies that under our current assumptions, there is a cis up-regulation of protein biosynthesis and protein degradation in the swollen cells, among which the up-regulation of protein biosynthesis is more pronounced compared to that of protein degradation.

To access the quantitative aspects of our network structure, we transformed the Petri net model into a quantitative mathematical model represented by ordinary differentiation equations. According to the time evolutionary course of different species in our model, we could see that the effect of osmotic treatment on the cellular proteasome concentration could be directly influenced by the degree of "overflow", which is the material flow from ER-processing to the proteasome in case of ER-stress. Upon the increased overrun from ER, there was an initial drastic up-regulation of the cellular proteasome concentration, which is positively correlated with the degree of material flow from ER directly to proteasome. Along the entire time frame investigated, the proteasome concentration remains at a higher level in hypo-osmotic as compared to control cells under isotonic condition (Figure 8). This again

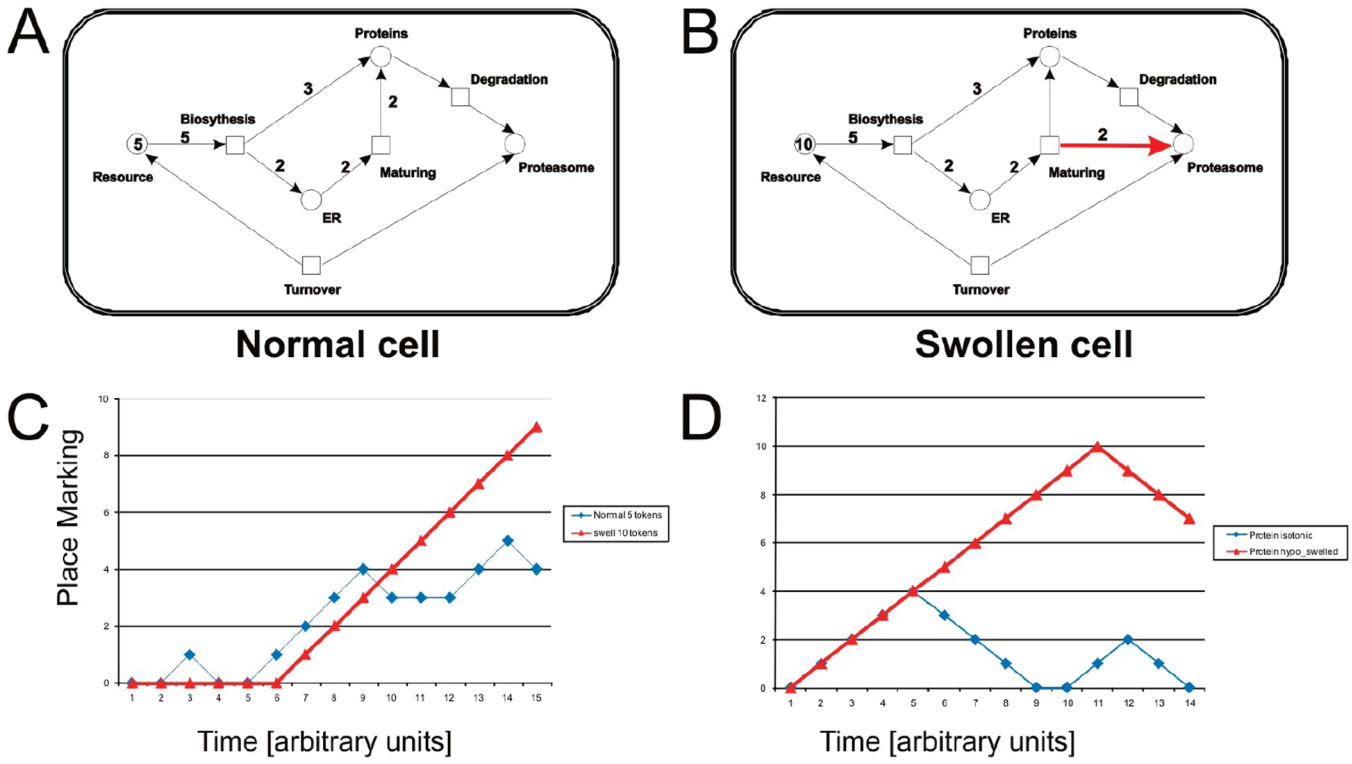

Figure 7. Petri net representation of protein metabolic pathways in normal and osmotically stressed cells. Cellular material pools and protein metabolic processes are represented by places (denoted by squares/circles) and transitions (arrows), respectively. Arrows denote flows between different martial pools via distinct metabolic processes (see Materials and Methods for detailed explanation). Protein metabolic networks of normal (isotonic) (A) and hypertonic (swollen) cells (B) are shown. A comparison of the cellular proteasome activity and amount of cellular proteins under (C) isotonic and (D) hypotonic conditions is presented.

Table 4. Comparison of Stationary Petri Net Properties for Protein Metabolic Flux under Isotonic (Normal) and Hypotonic (Swollen) Cells

isotonic	cell swelling (hypo-osmotic)
conservative	not conservative
bounded	not bounded
The net is covered by semipositive p-invariants	no place invariants
The net is covered by semipositive t-invariants	no transition invariants

establishes that there is an up-regulation of protein biodegradation upon cell swelling found in our study (Table 3).

Discussion

In the present study, we used a proteomic approach to investigate the impact of aniso-osmotic culture conditions on the protein expression pattern of mouse ES cells. For this purpose, ES cells were subjected to osmolarities of 200 mOsm (hypo-osmotic) and 500 mOsm (hyperosmotic) by altering sodium concentration in cell culture media. It was observed that, after 48 h of hyperosmotic treatment, cells shrunk by 22%, while hypo-osmolarity increased the cell volume by 4%. Therefore, altered osmotic conditions induced measurable cell volume changes in our experimental setting, with the effect of hyperosmolarity being more pronounced. Presumably, the coexistence of multiple mitotic phases in the cell population has precluded the access of statistical difference among cells under different osmotic conditions. These osmotic regulation effects might be due to increased or decreased water diffusion between cellular lumen and culture medium driven by osmotic gradients. On the other hand, except for cell volume alterations, ES cells incubated in aniso-osmotic medium showed similar cell morphology as compared to their isotonic-conditioned counterparts. This demonstrates a quick adaptation of ES cells to these adverse environmental changes.

To avoid an excessive alteration in cellular volume, cells have developed complex regulatory pathways during evolution. These include mechanisms that restore the cell volume by regulating intracellular salt and osmolyte concentrations and the development of temporal SOS-response mechanisms which help to sustain and withstand cell volume changes.[48] According to our current observations, proteins involved in stress response, cytoskeleton structure, fatty acid and carbohydrate metabolism, as well as protein metabolism were predominantly altered in ES cells subjected to osmotic stress.

Change in Oxidative Stress Related Proteins in Both Hyper- and Hypo-Osmotic Treated Cells. Increased peroxiredoxin activity was apparent in ES cells under both types of osmotic stress. Peroxiredoxin 1 (*Prdx1*) and Peroxiredoxin 4 (*Prdx4*) were altered during hyperosmotic conditions. In addition, Peroxiredoxin 6 (*Prdx6*) was up-regulated in cells under hypo-osmotic conditions. These observations suggest that oxidative stress may have been generally increased by osmotic stress. Another group of proteins found to be influenced by osmotic stress in ES cells were chaperones, which are a group of highly conserved proteins involved in protein folding and assembly.[49] *Hspb1* increased by hyperosmotic stress, while *Hspd1* increased in hypo-osmotic stress. Osmotic stress may lead to increased protein aggregation and denaturation.[50–52] The increased expression of these chaperones is likely to play an important role in stabilizing newly synthesized proteins, and

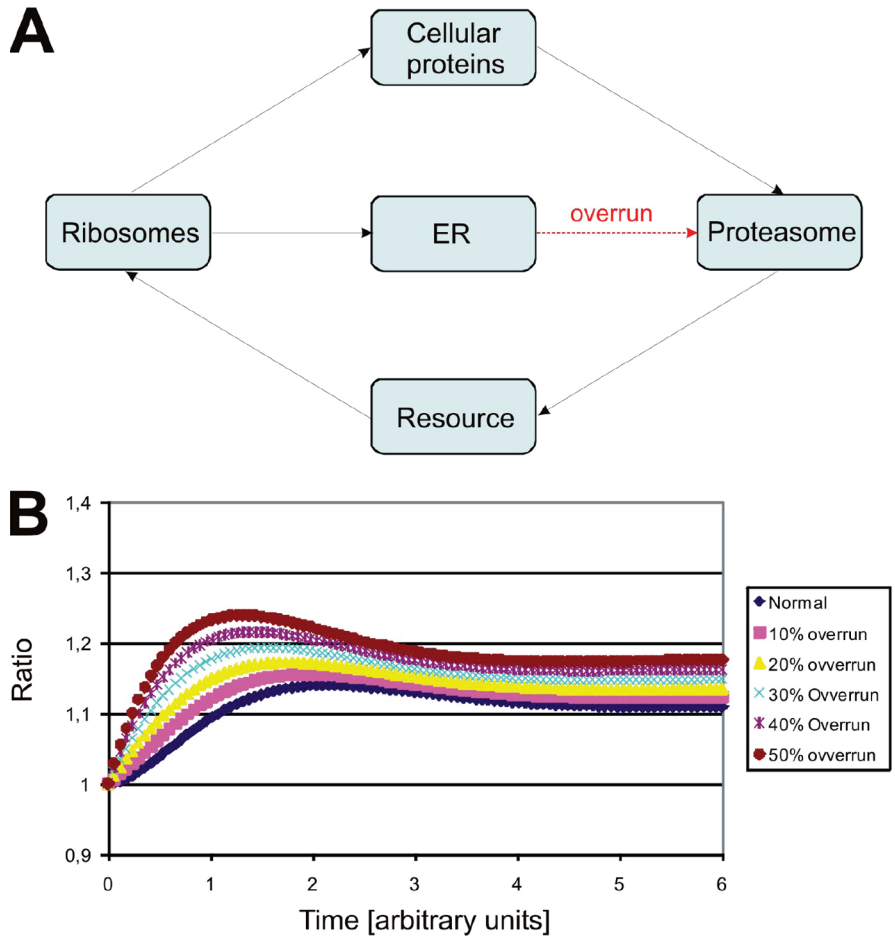

Figure 8. Mathematical modeling for the osmotic regulation of the protein metabolic network. The modeling was facilitated using Cell Designer software (see Material and Methods for details). (A) In this abstract model employing ordinary differential equation, the protein metabolic network differs between normal and swollen cells only by the absence or presence of a material flux ("overflow") between ER-processing and protein degradation.

facilitating the refolding of proteins that may have been denatured during exposure to osmotic stress in various intracellular compartments.[53]

Fatty Acid and Carbohydrate Metabolism. According to our current observations, osmotic stress by hyper- or hypo-osmolarity was accompanied by changes of proteins involved in fatty acid and carbohydrate metabolism. *Fatty acid binding protein 1* (*Fabp1*), a fatty acid transporter protein and *Dodecenoyl-CoA isomerase* (*Dci*), which is involved in β-oxidation, increased their expression in both hyperosmotic and hypo-osmotic conditioned ES cells, whereas *phosphatidylethanolamine binding protein 1* (*Pebp1*) *was up-regulated under* hypotonic conditions. Interestingly, *acetyl-Coenzyme A acyltransferase 2* (*Acaa2*), the key enzyme for fatty acid chain elongation, was increased in expression in hypertonic but decreased in hypotonic conditions. Alterations in fatty acid metabolism could be attributed to active osmoregulation in cells.[54,55]

Similarly, glucose metabolism related enzymes generally decreased in abundance under hypotonic conditions, while the opposite phenomenon was observed under hypertonic conditions. For instance, *Glyceraldehyde-3-phosphate dehydrogenase* (*Gapdh*), a key enzyme of glycolysis pathway, decreased significantly in its expression in hypo-osmotic-treated cells; whereas it was up-regulated in hyperosmotic condition. Moreover, the concentration of both *Pyruvate dehydradase* (*Pdha1*) and *Transaldolase 1* (*Taldo*) decreased by hypotonic treatment. This is in accordance with previous findings[5] and could suggest an increased glycolysis activity in hyperosmotic treatment, and a down-regulation of glucose catabolism in hypo-osmotic condition. Our finding regarding glucose metabolism could reflect an active regulation of cellular organic osmolytes production, which counteracts osmotic water diffusion. One of the most prevalent osmolytes, sorbitol, is synthesized from glucose in a chain of reactions involving glycolytic enzymes and gluconeogenic pathways.[56,57] Such protective mechanisms have been documented for renal cells, where the accumulation of organic osmolytes were observed under hyperosmotic condition.[58] These organic osmolytes act by maintaining cell volume without perturbing protein structure and function. Combined, our observations suggest that the up-regulation of glycolysis could be essential upon cell shrinkage to increase the production of organic osmolytes.

Cytoskeleton Remodeling. Cells possess adaptive responses that remodel and reinforce the cellular structure to withstand physical challenges.[59] Hyperosmotically induced cell shrinkage has been associated with a net increase in *F-actin* content in a variety of cells. Conversely, hypotonicity was accompanied by a decrease in *F-actin* in numerous cell systems (reviewed in ref 59). A similar behavior was observed in the current study: Increased cytoskeletal actin (*Actb, Actg1*) expression was observed in hyperosmotic ES cells. The *Drebrin-like actin binding protein* (*Dbnl*) was also observed to increase in its expression

under hyperosmotic condition. On the other hand, we observed a significant decrease of cellular *Actin* concentration (*Actb*, *Actg1*) in hypo-osmotic ES cells. In addition, the cytoskeleton *Actin*-filament stabilizing protein *Tropomyosin 1* (*Tpm2*) was up-regulated under both hyper- and hypotonic conditions. This could suggest that aniso-osmotic stress was accompanied by an active cytoskeletal remodeling processes.[60] According to previously published data, the *Actin-related protein 2/3* (*Arp2/3*) complex is a major osmotic-sensitive structural component of the *Actin* remodelling aparatus.[61,62] Activation of *Arp 2/3* complex is mediated by a direct molecular contact with various members of the *Wiskott-Aldrich syndrome protein* (*Wasp*) superfamily. These are in turn activated upstream by *Rho* family GTPases (*Cdc42* and *Rac*).[61,63] In the current study, we observed that two subunits of *Arp2/3* complex (*Arpc4* and *Arpc5*) were up-regulated in their expression under hyperosmotic conditions. On the other hand, the Rho *GDP-dissociation inhibitor 1* (*Arhgdia*), an inhibitor of *RhoGTPase* (by inhibiting nucleotide exchange of GTP/GDP), was decreased in abundance in hyperosmotic treated cells, whereas it was increased in hypo-osmotic condition. Taken together, the increase in cytoskeleton-associated protein expression may play a particularly important role in stabilization and reinforcement of the cellular scaffold in cells exposed to a hyperosmotic environment. A constant energy supply is required for *Actin* assembly,[64] and therefore, the increased Actin concentration and the up-regulation of glycolysis in hyperosmotic ES cells may act synergistically by stabilizing ES cells to adapt to adverse osmotic conditions.

Protein Synthesis and Degradation Appear To Be Cis-Regulated upon Cell Volume Alteration. When cell shrinkage by hyperosmosis was investigated, it was observed that protein catabolism (ubiquitination/proteasome) was generally decreased. This was evidenced by a consistent decrease of eight proteasome subunits (*Psma1*, *Psma3*, *Psmb1*, *Psmb4*, *Psmb5*, *Psmb6*, *Psmb8* and *Psme1*) and five ubiquitination-related proteins (*Ube1x*, *Uchl3*, *Sumo1*, *Sumo2* and *Tceb2*) (Table 1). It was described previously that an *increased* protein biosynthesis is accompanied by *decreased* proteolysis during cell swelling.[5] A similar *increase* of protein synthesis during ES cell swelling was also observed in the present study. Interestingly, there was also a prominent *increase* in abundance of proteasome and ubiquitination components after hypotonic treatment. *Psme1*, which acts as a proteasome activator, was increased in expression in hypo-osmotic ES cells. Moreover, there was an increased expression in *Ubiquitin carboxyl-terminal hydrolase activity* (*Uchl3*, *Uchl1*) in hypotonic ES cells (Table 1). In summary, this results in average (arithmetic mean) alteration of proteins involved in degradation of 0.7- and 2.6-fold by hyper- and hypotonic conditions, respectively, and shows clear cis-regulation (regulation in the same direction) of proteins biosynthesis and degradation. This is a clear *discrepancy* between previously published results and our current findings.

Another notable finding of our study is the consistent up-regulation of stress-response and endoplasmic reticulum (ER)-bound proteins in hyperosmotic ES cells. The latter include *Reticulocalbin 1* (*Rcn1*), a calcium-binding EF hand protein, *Thioredoxin domain containing 4* (*Txndc4*), which may control oxidative protein folding inside the ER, and *Sulfatase-modifying factor 2* (*Sumf2*). Combined, an average (arithmetic mean) 1.3-fold up-regulation of ER-processing proteins was determined. ER is the site of synthesis, folding and modification of secretary and cell-surface proteins.[45] The accumulation of unfolded proteins in the ER lumen due to disturbed protein biosynthesis induces a coordinated adaptive program called the unfolded protein response (UPR).[45] The UPR attempts to alleviate cellular stress, supporting protein refolding as well as increasing protein degradation.[46] As a large part of the cellular proteins undergo ER-processing,[45] an ER-processing module could be a key player in regulating the entire cellular protein metabolic network. We thus conclude that hypotonic ES cells show increased protein synthesis which evidently requires more free resources of the cell than used under normal osmolarity. Increased biosynthesis will require in turn an up-regulation of protein degradation to warrant a balanced protein turnover. This is opposite to the observation of Haussinger,[5] who reported a down-regulation of protein degradation during cell swelling. The effects on protein degradation studied by Haussinger were obtained using liver cells,[5,65–68] whereas in our study, we used ES cells. In addition, Häussinger did not study the expression alteration of a large number of proteins but proteolytic capacity by [^{3}H] leucine release.[5,65–68] Therefore, an increase in concentration of proteins involved in proteolysis might not mean an increased net proteolysis as measured by [^{3}H] leucine release.

Proteins Specifically Altered by Osmotic Stress. We found that only 37 of 92 proteins were specifically altered by osmotic stress. They show an enrichment of one pathway ("Cell cycle") when analyzed by KEGG, whereas the proteins altered in osmotic stress and all ND showed three enriched pathways, one of the "Proteasome". A vast majority of proteins (60%) are shared between ND and osmotic stress. Osmotic stress and therefore cell volume alteration which accompanies osmotic stress may play a significant role in ND. In addition, when looking at the individual proteins overlapping in all ND and osmotic stress, *Uchl1*, also known as *Park5*, is implicated in PD is one of them.[69] Therefore, mouse models transgenic for *Uchl1* may not be as specific for PD as formerly thought. It might more likely represent a protein the cell uses to fight cell volume alterations.

Mathematical Modeling of Cellular Protein Metabolic Flows. To access the dynamics of cellular protein metabolic flows and their possible disturbance caused by osmotic stimulation, we employed a mathematical modeling formalism. Using mathematical simulations considering the dynamic relation between different aspects of protein metabolism, we could show that both protein degradation and protein synthesis were up-regulated under hypotonic conditions. The up-regulation of protein synthesis was more pronounced than protein degradation. This suggests a positive nitrogen balance in case of cell swelling, which is in line with previous findings.[5] However, if we consider actual change of protein degradation, an up-regulation could be observed under swelling condition. This means that a comprehensive view, there appears to be a cis-regulation (regulation in the same direction) of protein biosynthesis and degradation upon cell volume alteration due to osmotic stress.

Conclusions

In summary, our results show that osmotic stress and therefore cell volume alteration influence a wide variety of cellular pathways, including stress response, cytoskeletal remodeling and metabolism. Interestingly, protein biosynthesis and degradation were cis-regulated in an altered osmotic environment, probably due to the modulating effect of ER function.

When comparing the proteins altered after osmotic stress to data sets of proteins altered in three different ND, we found that 60% of the proteins altered by osmotic stress were altered in at least one ND and 18% in all of them. Therefore, protein alterations caused by osmotic stress or cell volume alterations may contribute to the pathology of ND.

Abbreviations: 2-DE, 2-D electrophoresis; AD, Alzheimer's disease; ES cells, embryonic stem cells; ER, endoplasmatic reticulum; HD, Huntington's disease, MS, mass spectrometry; ND, neurodegenerative disease; PD, Parkinson's disease.

Acknowledgment. We thank Marion Herrmann for her excellent technical assistance and Pierre Savatier for the CGR8 ES cells. We are also indebted to Zhike Zi for his help with the mathematical model. This work was co-supported by the German National Genome Research Network (NGFN) program established by the German Ministry for Education and Research (BMBF), and by the EU grant 37627 "AnEUploidy", and SFB 577, "Molecular Basis of Clinical Variability in Mendelian Disorders".

References

(1) Okada, Y.; Maeno, E. Apoptosis, cell volume regulation and volume-regulatory chloride channels. *Comp. Biochem. Physiol., Part A: Mol. Integr. Physiol.* **2001**, *130* (3), 377–83.
(2) Kim, J. H.; Hong, J. A.; Pih, K. T.; Hwang, I. Identification and isolation of differentially expressed genes in osmotically stressed human oral keratinocytes. *Arch. Oral Biol.* **2001**, *46* (4), 335–41.
(3) Hatanaka, K.; Ikegami, K.; Takagi, H.; Setou, M. Hypo-osmotic shock induces nuclear export and proteasome-dependent decrease of UBL5. *Biochem. Biophys. Res. Commun.* **2006**, *350* (3), 610–5.
(4) de Nadal, E.; Alepuz, P. M.; Posas, F. Dealing with osmostress through MAP kinase activation. *EMBO Rep.* **2002**, *3* (8), 735–40.
(5) Haussinger, D. The role of cellular hydration in the regulation of cell function. *Biochem. J.* **1996**, *313* (3), 697–710.
(6) Lang, F.; Busch, G. L.; Ritter, M.; Volkl, H.; Waldegger, S.; Gulbins, E.; Haussinger, D. Functional significance of cell volume regulatory mechanisms. *Physiol. Rev.* **1998**, *78* (1), 247–306.
(7) Vogels, O. J.; Broere, C. A.; ter Laak, H. J.; ten Donkelaar, H. J.; Nieuwenhuys, R.; Schulte, B. P. Cell loss and shrinkage in the nucleus basalis Meynert complex in Alzheimer's disease. *Neurobiol. Aging* **1990**, *11* (1), 3–13.
(8) Loo, L. S.; McNamara, J. O. Impaired volume regulation is the mechanism of excitotoxic sensitization to complement. *J. Neurosci.* **2006**, *26* (40), 10177–10187.
(9) Diedrich, M.; Mao, L.; Bernreuther, C.; Zabel, C.; Nebrich, G.; Kleene, R.; Klose, J. Proteome analysis of ventral midbrain in MPTP-treated normal and L1cam transgenic mice. *Proteomics* **2008**, *8* (6), 1266–75.
(10) Zabel, C.; Sagi, D.; Kaindl, A. M.; Steireif, N.; Klare, Y.; Mao, L.; Peters, H.; Wacker, M. A.; Kleene, R.; Klose, J. Comparative proteomics in neurodegenerative and non-neurodegenerative diseases suggest nodal point proteins in regulatory networking. *J. Proteome Res.* **2006**, *5* (8), 1948–58.
(11) Zabel, C.; Klose, J. Influence of Huntington's disease on the human and mouse proteome. *Int. Rev. Neurobiol.* **2004**, *61*, 241–83.
(12) Zabel, C.; Chamrad, D. C.; Priller, J.; Woodman, B.; Meyer, H. E.; Bates, G. P.; Klose, J. Alterations in the mouse and human proteome caused by Huntington's disease. *Mol. Cell. Proteomics* **2002**, *1* (5), 366–75.
(13) Ding, Q.;.; Dimayuga, E.; Markesbery, W. R.; Keller, J. N. Proteasome inhibition induces reversible impairments in protein synthesis. *FASEB J.* **2006**, *20* (8), 1055–63.
(14) Zeng, B. Y.; Medhurst, A. D.; Jackson, M.; Rose, S.; Jenner, P. Proteasomal activity in brain differs between species and brain regions and changes with age. *Mech. Ageing Dev.* **2005**, *126* (6–7), 760–6.
(15) Shringarpure, R.; Davies, K. J. Protein turnover by the proteasome in aging and disease. *Free Radical Biol. Med.* **2002**, *32* (11), 1084–9.
(16) Upadhya, S. C.; Hegde, A. N. Role of the ubiquitin proteasome system in Alzheimer's disease. *BMC Biochem.* **2007**, *8* (Suppl. 1), S12.
(17) Rubinsztein, D. C. The roles of intracellular protein-degradation pathways in neurodegeneration. *Nature* **2006**, *443* (7113), 780–6.
(18) Anbari, K.; Schultz, R. M. Effect of sodium and betaine in culture media on development and relative rates of protein synthesis in preimplantation mouse embryos in vitro. *Mol. Reprod. Dev.* **1993**, *35* (1), 24–8.
(19) Petronini, P. G.; De Angelis, E. M.; Borghetti, P.; Borghetti, A. F.; Wheeler, K. P. Modulation by betaine of cellular responses to osmotic stress. *Biochem. J.* **1992**, *282* (1), 69–73.
(20) Klose, J. Large-gel 2-D electrophoresis. Fractionated extraction of total tissue proteins from mouse and human for 2-D electrophoresis. *Methods Mol. Biol.* **1999**, *112*, 147–72.
(21) Zabel, C.; Klose, J., Protein extraction for 2-D electrophoresis. *Methods Mol. Biol.* **2008**, in press.
(22) Mao, L.; Zabel, C.; Herrmann, M.; Nolden, T.; Mertes, F.; Magnol, L.;.; Chabert, C.; Hartl, D.; Herault, Y.; Delabar, J. M.; Manke, T.; Himmelbauer, H.; Klose, J. Proteomic shifts in embryonic stem cells with gene dose modifications suggest the presence of balancer proteins in protein regulatory networks. *PLoS One* **2007**, *2* (11), 1218.
(23) Zabel, C.; Klose, J. High resolution large gel 2-D electrophoresis. *Methods Mol. Biol.* **2008**, in press.
(24) Klose, J.; Kobalz, U. Two-dimensional electrophoresis of proteins: an updated protocol and implications for a functional analysis of the genome. *Electrophoresis.* **1995**, *16* (6), 1034–59.
(25) Berth, M.; Moser, F. M.; Kolbe, M.; Bernhardt, J. The state of the art in the analysis of two-dimensional gel electrophoresis images. *Appl. Microbiol. Biotechnol.* **2007**, *76* (6), 1223–43.
(26) Hartl, D.; Rohe, M.; Mao, L.; Staufenbiel, M.; Zabel, C.; Klose, J., Impairment of adolescent hippocampal pasticity in a mouse model for Alzheimer's disease precedes disease phenotype. *PLoS One* **2008**, in press.
(27) Zabel, C.; Andreew, A.; Mao, L.; Hartl, D. Protein expression overlap: more important than which proteins change in expression. *Expert Rev. Proteomics* **2008**, *5* (2), 187–205.
(28) Zabel, C.; Sagi, D.; Kaindl, A. M.; Steireif, N.; Klare, Y.; Mao, L.; Peters, H.; Wacker, M. A.; Kleene, R.; Klose, J. Comparative proteomics in neurodegenerative and non-neurodegenerative diseases suggest nodal point proteins in regulatory networking. *J. Proteome Res.* **2006**, *5* (8), 1948–58.
(29) Pappin, D. J. C.; Hojrup, P.; Bleasby, A. J. Rapid identification of proteins by peptide-mass fingerprinting. *Curr. Biol.* **1993**, *3* (6), 327–32.
(30) Butterfield, D. A.; Gnjec, A.; Poon, H. F.; Castegna, A.; Pierce, W. M.; Klein, J. B.; Martins, R. N. Redox proteomics identification of oxidatively modified brain proteins in inherited Alzheimer's disease: an initial assessment. *J. Alzheimers Dis.* **2006**, *10* (4), 391–7.
(31) David, D. C.; Ittner, L. M.; Gehrig, P.; Nergenau, D.; Shepherd, C.; Halliday, G.; Gotz, J. Beta-amyloid treatment of two complementary P301L tau-expressing Alzheimer's disease models reveals similar deregulated cellular processes. *Proteomics* **2006**, *6* (24), 6566–77.
(32) Sultana, R.; Boyd-Kimball, D.; Cai, J.; Pierce, W. M.; Klein, J. B.; Merchant, M.; Butterfield, D. A. Proteomics analysis of the Alzheimer's disease hippocampal proteome. *J. Alzheimers Dis.* **2007**, *11* (2), 153–64.
(33) Tsuji, T.; Shiozaki, A.; Kohno, R.; Yoshizato, K.; Shimohama, S. Proteomic profiling and neurodegeneration in Alzheimer's disease. *Neurochem. Res.* **2002**, *27* (10), 1245–53.
(34) Wilson, K. E.; Marouga, R.; Prime, J. E.; Pashby, D. P.; Orange, P. R.; Crosier, S.; Keith, A. B.; Lathe, R.; Mullins, J.; Estibeiro, P.; Bergling, H.; Hawkins, E.; Morris, C. M. Comparative proteomic analysis using samples obtained with laser microdissection and saturation dye labelling. *Proteomics* **2005**, *5* (15), 3851–8.
(35) Zabel, C.; Mao, L.; Woodman, B.; Rohe, M.; Klare, Y.; Koppelstatter, A.; Nebrich, G.; Kapferer, A.; Forsstrom-Olsson, O.; Grams, S.; Hartl, D.; Klose, J.; Bates, G. P. Early increase in protein expression changes during disease progression in a mouse model for Huntington's disease. *Mol. Cell. Proteomics* **2008**, submitted for publication.
(36) Zabel, C.; Klose, J. Influence of Huntington's disease on the human and mouse proteome. *Int. Rev. Neurobiol.* **2004**, *61*, 241–83.
(37) Basso, M.; Giraudo, S.; Corpillo, D.; Bergamasco, B.; Lopiano, L.; Fasano, M. Proteome analysis of human substantia nigra in Parkinson's disease. *Proteomics* **2004**, *4* (12), 3943–52.
(38) Leverenz, J. B.; Umar, I.; Wang, Q.; Montine, T. J.; McMillan, P. J.; Tsuang, D. W.; Jin, J.; Pan, C.; Shin, J.; Zhu, D.; Zhang, J. Proteomic identification of novel proteins in cortical lewy bodies. *Brain Pathol.* **2007**, *17* (2), 139–45.

(39) Periquet, M.; Corti, O.; Jacquier, S.; Brice, A. Proteomic analysis of parkin knockout mice: alterations in energy metabolism, protein handling and synaptic function. *J. Neurochem.* **2005**, *95* (5), 1259–76.
(40) Petri, C. A. *Kommunikation mit Automaten*; Rheinisch-Westfälisches Institut f. Instrumentelle Mathematik: Bonn, Germany, 1962.
(41) Koch, I.; Junker, B. H.; Heiner, M. Application of Petri net theory for modelling and validation of the sucrose breakdown pathway in the potato tuber. *Bioinformatics.* **2005**, *21* (7), 1219–26.
(42) Flanagan, J. J.; Chen, J. C.; Miao, Y.; Shao, Y.; Lin, J.; Bock, P. E.; Johnson, A. E. Signal recognition particle binds to ribosome-bound signal sequences with fluorescence-detected subnanomolar affinity that does not diminish as the nascent chain lengthens. *J. Biol. Chem.* **2003**, *278* (20), 18628–37.
(43) Tusher, V. G.; Tibshirani, R.; Chu, G. Significance analysis of microarrays applied to the ionizing radiation response. *Proc. Natl. Acad. Sci. U.S.A.* **2001**, *98* (9), 5116–21.
(44) Sanchez, J. C.; Golaz, O.; Frutiger, S.; Schaller, D.; Appel, R. D.; Bairoch, A.; Hughes, G. J.; Hochstrasser, D. F. The yeast SWISS-2DPAGE database. *Electrophoresis.* **1996**, *17* (3), 556–65.
(45) Lin, J. H.; Walter, P.; Yen, T. S. Endoplasmic Reticulum Stress in Disease Pathogenesis. *Annu. Rev. Pathol.* **2008**, *3*, 399–425.
(46) Rutkowski, D. T.; Kaufman, R. J. A trip to the ER: coping with stress. *Trends Cell Biol.* **2004**, *14* (1), 20–8.
(47) Priese, L.; Wimmel, H. *Theoretische Informatik—Petri Netze*; Springer Verlag: Berlin, 2008.
(48) Lang, M. A. Correlation between osmoregulation and cell volume regulation. *Am. J. Physiol.* **1987**, *252* (4 Pt 2), R768–73.
(49) Beck, F. X.; Neuhofer, W.; Muller, E. Molecular chaperones in the kidney: distribution, putative roles, and regulation. *Am. J. Physiol.: Renal Physiol.* **2000**, *279* (2), F203–15.
(50) Ignatova, Z.; Gierasch, L. M. Inhibition of protein aggregation in vitro and in vivo by a natural osmoprotectant. *Proc. Natl. Acad. Sci. U.S.A.* **2006**, *103* (36), 13357–61.
(51) Kanapathipillai, M.; Lentzen, G.; Sierks, M.; Park, C. B. Ectoine and hydroxyectoine inhibit aggregation and neurotoxicity of Alzheimer's beta-amyloid. *FEBS Lett.* **2005**, *579* (21), 4775–80.
(52) Liu, R.; Barkhordarian, H.; Emadi, S.; Park, C. B.; Sierks, M. R. Trehalose differentially inhibits aggregation and neurotoxicity of beta-amyloid 40 and 42. *Neurobiol. Dis.* **2005**, *20* (1), 74–81.
(53) van den Berg, B.; Ellis, R. J.; Dobson, C. M. Effects of macromolecular crowding on protein folding and aggregation. *EMBO J.* **1999**, *18* (24), 6927–33.
(54) Moffett, J. R.; Ross, B.; Arun, P.; Madhavarao, C. N.; Namboodiri, A. M. N-Acetylaspartate in the CNS: from neurodiagnostics to neurobiology. *Prog. Neurobiol.* **2007**, *81* (2), 89–131.
(55) Polakof, S.; Arjona, F. J.; Sangiao-Alvarellos, S.; Martin del Rio, M. P.; Mancera, J. M.; Soengas, J. L. Food deprivation alters osmoregulatory and metabolic responses to salinity acclimation in gilthead sea bream Sparus auratus. *J. Comp. Physiol., B* **2006**, *176* (5), 441–52.
(56) Jans, A. W.; Grunewald, R. W.; Kinne, R. K. Pathways for organic osmolyte synthesis in rabbit renal papillary tissue, a metabolic study using 13C-labeled substrates. *Biochim. Biophys. Acta* **1988**, *971* (2), 157–62.
(57) Jans, A. W.; Grunewald, R. W.; Kinne, R. K. Pathways for the synthesis of sorbitol from 13C-labeled hexoses, pentose, and glycerol in renal papillary tissue. *Magn, Reson, Med.* **1989**, *9* (3), 419–22.
(58) Dihazi, H.; Kessler, R.; Muller, G. A.; Eschrich, K. Lysine 3 acetylation regulates the phosphorylation of yeast 6-phosphofructo-2-kinase under hypo-osmotic stress. *Biol, Chem.* **2005**, *386* (9), 895–900.
(59) Di Ciano-Oliveira, C.; Thirone, A. C.; Szaszi, K.; Kapus, A. Osmotic stress and the cytoskeleton: the R(h)ole of Rho GTPases. *Acta Physiol.* **2006**, *187* (1−2), 257–72.
(60) Jaffe, A. B.; Hall, A. Rho GTPases: biochemistry and biology. *Annu. Rev. Cell Dev. Biol.* **2005**, *21*, 247–69.
(61) Millard, T. H.; Sharp, S. J.; Machesky, L. M. Signalling to Actin assembly via the WASP (Wiskott-Aldrich syndrome protein)-family proteins and the Arp2/3 complex. *Biochem. J.* **2004**, *380* (1), 1–17.
(62) Robinson, R. C.; Turbedsky, K.; Kaiser, D. A.; Marchand, J. B.; Higgs, H. N.; Choe, S.; Pollard, T. D. Crystal structure of Arp2/3 complex. *Science* **2001**, *294* (5547), 1679–84.
(63) Takenawa, T.; Miki, H. WASP and WAVE family proteins: key molecules for rapid rearrangement of cortical Actin filaments and cell movement. *J. Cell Sci.* **2001**, *114* (Pt 10), 1801–9.
(64) Marchand, J. B.; Moreau, P.; Paoletti, A.; Cossart, P.; Carlier, M. F.; Pantaloni, D. Actin-based movement of Listeria monocytogenes: Actin assembly results from the local maintenance of uncapped filament barbed ends at the bacterium surface. *J. Cell Biol.* **1995**, *130* (2), 331–43.
(65) Hallbrucker, C.; vom Dahl, S.; Lang, F.; Gerok, W.; Haussinger, D. Inhibition of hepatic proteolysis by insulin. Role of hormone-induced alterations of the cellular K+ balance. *Eur. J. Biochem.* **1991**, *199* (2), 467–74.
(66) Hallbrucker, C.; vom Dahl, S.; Lang, F.; Häussinger, D. Control of hepatic proteolysis by amino acids - The role of cell volume. *Eur. J. Biochem.* **1991**, *197*, 717–24.
(67) Haussinger, D.; Hallbrucker, C.; vom Dahl, S.; Decker, S.; Schweizer, U.; Lang, F.; Gerok, W. Cell volume is a major determinant of proteolysis control in liver. *FEBS Lett.* **1991**, *283* (1), 70–2.
(68) Haussinger, D.; Hallbrucker, C.; vom Dahl, S.; Lang, F.; Gerok, W. Cell swelling inhibits proteolysis in perfused rat liver. *Biochem. J.* **1990**, *272* (1), 239–42.
(69) Samii, A.; Nutt, J. G.; Ransom, B. R. Parkinson's disease. *Lancet* **2004**, *363* (9423), 1783–93.
(70) UniProt Knowledgebase (Swiss-Prot and TrEMBL). In Swiss Institute of Bioinformatics (SIB): 2008.

PR800245X

A Large Number of Protein Expression Changes Occur Early in Life and Precede Phenotype Onset in a Mouse Model for Huntington Disease*[S]

Claus Zabel‡§¶, Lei Mao‡§, Ben Woodman‖, Michael Rohe, Maik A. Wacker‡, Yvonne Kläre‡, Andrea Koppelstätter‡, Grit Nebrich‡, Oliver Klein‡, Susanne Grams‡, Andrew Strand‡‡, Ruth Luthi-Carter§§, Daniela Hartl‡, Joachim Klose‡, and Gillian P. Bates‖**

Huntington disease (HD) is fatal in humans within 15–20 years of symptomatic disease. Although late stage HD has been studied extensively, protein expression changes that occur at the early stages of disease and during disease progression have not been reported. In this study, we used a large two-dimensional gel/mass spectrometry-based proteomics approach to investigate HD-induced protein expression alterations and their kinetics at very early stages and during the course of disease. The murine HD model R6/2 was investigated at 2, 4, 6, 8, and 12 weeks of age, corresponding to absence of disease and early, intermediate, and late stage HD. Unexpectedly the most HD stage-specific protein changes (71–100%) as well as a drastic alteration (almost 6% of the proteome) in protein expression occurred already as early as 2 weeks of age. Early changes included mainly the up-regulation of proteins involved in glycolysis/gluconeogenesis and the down-regulation of the actin cytoskeleton. This suggests a period of highly variable protein expression that precedes the onset of HD phenotypes. Although an up-regulation of glycolysis/gluconeogenesis-related protein alterations remained dominant during HD progression, late stage alterations at 12 weeks showed an up-regulation of proteins involved in proteasomal function. The early changes in HD coincide with a peak in protein alteration during normal mouse development at 2 weeks of age that may be responsible for these massive changes. Protein and mRNA data sets showed a large overlap on the level of affected pathways but not single proteins/mRNAs. Our observations suggest that HD is characterized by a highly dynamic disease pathology not represented by linear protein concentration alterations over the course of disease. ***Molecular & Cellular Proteomics 8:720–734, 2009.***

Huntington disease (HD)[1] is an autosomal dominantly inherited disorder that usually presents in midlife and causes death 15–20 years after the first symptoms occur (1). The disease-triggering mutation consists of an unstable, elongated cytosine-adenine-guanine (CAG) trinucleotide repeat at the 5′-end of the *HD* gene in the first exon. The CAG repeat codes for a variable number of glutamines (2). The length of the polyglutamine repeat in the gene product of *HD*, Huntingtin (Htt), is one of the most important factors that determines the age of onset of the disorder (2). Individuals with 6–35 CAG repeats are not affected. Those with 36–39 CAG repeats have an increased risk of acquiring the disease, and repeats of 40 and above always cause disease (3–5). Onset of the motor disorder usually occurs between 35 and 45 years, but the age of onset can range anywhere from 2 to 80 years (2). In general, the larger the size of the polyglutamine repeat, the earlier the age of onset (6).

HD has been studied extensively at the level of single (interacting) proteins (7–9) and well characterized pathways, such as cell death (10–12). However, these experimental approaches have been rather limited in their identification of proteins that contribute to disease pathogenesis. Protein-protein interaction network studies have increased the num-

From the ‡Institute for Human Genetics, Charité-Universitätsmedizin Berlin, 13353 Berlin, Germany, ‖Department of Medical and Molecular Genetics, King's College London School of Medicine, Guy's Hospital London, London SE1 9RT, United Kingdom, **Molecular Cardiovascular Research, Max Delbrueck Center for Molecular Medicine, 13125 Berlin, Germany, ‡‡Division of Clinical Research, Fred Hutchinson Cancer Research Center, Seattle, Washington 98109, and §§Laboratory of Functional Neurogenomics, Ecole Polytechnique Fédérale de Lausanne, 1015 Lausanne, Switzerland

Received, June 19, 2008, and in revised form, November 24, 2008
Published, MCP Papers in Press, November 30, 2008, DOI 10.1074/mcp.M800277-MCP200

[1] The abbreviations used are: HD, Huntington disease; 2-D, two-dimensional; 2-DE, two-dimensional gel electrophoresis; Htt, Huntingtin; P, postnatal day; WEBGESTALT, Web-based gene set analysis toolkit; NCBInr, National Center for Biotechnology Information non-redundant; KEGG, Kyoto Encyclopedia of Genes and Genomes; MAPK, mitogen-activated protein kinase; E1, ubiquitin-activating enzyme; E2, ubiquitin carrier protein; E3, ubiquitin-protein isopeptide ligase; E, embryonic day; GnRH, gonadotropin-releasing hormone; Gapdh, glyceraldehyde-3-phosphate dehydrogenase.

ber of proteins available (13, 14). In addition, unbiased, large scale approaches have identified a large number of genes potentially involved in HD because microarrays probe a very large number of expression alterations simultaneously at the mRNA level (15, 16). Two-dimensional gel electrophoresis (2-DE)- (17, 18) or liquid chromatography-based proteomics approaches in combination with mass spectrometry are able to investigate many protein alterations at the same time (19, 20) increasing the number of proteins known to be involved in HD and complementing the protein interaction data.

HD has already been studied extensively at the transcriptomic level using brain tissue from a large number of mouse models (21–25) and humans (26) as well as human blood cells (27) using mostly late stages with visible disease phenotype. Proteome data on expression changes for HD are more scarce and so far only available for the R6/2 model (28–31). A common denominator of these studies is that only stages with disease phenotype were investigated (28–31). To understand the disease pathology in more detail, early changes need to be investigated. Here we present protein expression changes that occur at 2, 4, 6, 8, and 12 weeks of age in the well established R6/2 mouse model of HD representing the transition from the absence of disease-related phenotypes to a pronounced symptomatic disease state. Our results show that a large number of protein alterations are present prior to the developments of disease phenotypes. In addition most protein alterations were found to be disease stage-specific, and there were no proteins that were found to be altered at every stage investigated.

EXPERIMENTAL PROCEDURES

Experimental Animals—Hemizygous R6/2 transgenic mice (32) were bred and reared in our colony by backcrossing R6/2 males to CBA × C57BL/6 F1 females (B6CBAF1/OlaHsd, Harlan Olac, Bicester, UK). R6/2 mice were always housed with wild-type mice and were subject to a 12-h light:12-h dark cycle. All animals had unlimited access to water and breeding chow, and housing conditions and environmental enrichment were as described previously (33). R6/2 transgenic mice and wild-type littermate controls were sacrificed by cervical dislocation, and brains were rapidly removed, flash frozen in liquid nitrogen, and stored at −80 °C until use. We analyzed total brain from 2-, 4-, 6-, 8-, and 12-week-old R6/2 mice (n = 5–8). Genotyping and CAG repeat sizing were performed as described previously (34). Early changes in development at embryonic days 16 and 18; birth; and 1, 2, and 4 weeks were studied using brains of C57BL/6 mice (n = 3; Charles River WITA GmbH, Sulzfeld, Germany).

Protein Extraction Procedure—Total protein extracts were prepared from entire brains. The extraction procedure has been published previously and validated (30, 35). Frozen tissue, 1.6 parts (v/w) buffer P (50 mM Trizma® (Tris base) (Sigma-Aldrich), 50 mM KCl, and 20% (w/v) glycerol at pH 7.5) supplemented with a final CHAPS concentration of 4% (w/v) in the sample, 0.08 parts protease inhibitor solution I (one Complete™ tablet (Roche Applied Science) dissolved in 2 ml of buffer 1), and 0.02 parts protease inhibitor solution II (1.4 μM pepstatin A and 1 mM phenylmethylsulfonyl fluoride in ethanol) were ground to a fine powder in a mortar precooled in liquid nitrogen. The tissue powder was transferred into a 2-ml tube (Eppendorf, Hamburg, Germany), quickly thawed, and supplied with glass beads (0.034 units of glass beads/combined weight of tissue, buffers, and inhibitors in mg; glass beads, 2.5 ± 0.05-mm diameter; Worf Glaskugeln GmbH, Mainz, Germany). Each sample was sonicated six times in an ice-cold water bath for 10 s each with cooling intervals of 1 min 50 s in between. The homogenate was stirred for 30 min in buffer P without CHAPS at 4 °C in the presence of 0.025 parts (v/w) Benzonase (Merck) and a final concentration of 5 mM magnesium chloride in the sample. Subsequently 6.5 M urea and 2 M thiourea were added, and stirring was continued for 30 min at room temperature until urea and thiourea were completely dissolved. The protein extract was supplied with 70 mM dithiothreitol (Bio-Rad), 2% (v/w) ampholyte mixture (Servalyte pH 2–4, Serva, Heidelberg, Germany), corrected by the amount of urea added (correction factor = sample weight prior to addition of urea/sample weight after addition of urea), and stored at −80 °C. Protein concentrations were determined in sample aliquots without urea using Bio-Rad DC Protein Assay according to the protocol supplied by the manufacturer.

2-DE—After genotyping, mice were allocated to the HD or control group. Sample pairs were randomly selected choosing one mouse brain from each group. 2-D gels were run in batches of two. Sample pairs consisting of an HD and a control were run in parallel in both dimensions of 2-DE, IEF, and SDS-PAGE. Different sample pairs were processed at different days to avoid confounding of the experiment due to the same processing date. Protein samples were separated by the large gel 2-DE technique developed in our laboratory as described previously (17, 18). The gel format was 40 cm (isoelectric focusing) × 30 cm (SDS-PAGE) × 0.75 mm (gel width). For IEF using the carrier ampholyte technique, we applied 6 μl (20 μg/μl) of protein extract of each sample to the anodic end of an IEF gel (40 cm) and used a carrier ampholyte mixture to establish a pH gradient from 3 to 10. Proteins were visualized in SDS-PAGE polyacrylamide gels by high sensitivity silver staining (18, 36). For SDS-PAGE the IEF gels were cut in half and run as acidic and basic sides. 2-D gels were dried (described extensively in Ref. 36) and scanned at 300 dpi and 16-bit gray scale using a scanner (Microtek Scan Maker 9800XL, Evestar GmbH, Willich, Germany). The 2-D gel images were subsequently saved in Tiff format to avoid loss of quality due to compression.

Quantitative Analysis of Protein Expression—After uploading the 2-D gel images, protein spot patterns were evaluated by Delta2D imaging software version 3.5 (DECODON, Greifswald, Germany) as was already described recently in detail elsewhere (37). Delta2D is our standard 2-D gel evaluation software and was validated already in many of our studies (30, 35, 38–41). Briefly 2-D spot patterns of HD and control mouse brains were matched using the Delta2D "exact" mode matching protocol. First sample pairs (HD and control) were matched individually. Subsequently all HD gels were matched to create a "match link" between all 2-D spot patterns using match vectors (37). Using "union" mode a fusion image was generated, including the visible spots for each 2-D gel from each time point (2, 4, 6, 8, and 12 weeks) creating 10 fusion gels (five time points, one fusion gel for the acidic side and one for the basic side of 2-D gels). Only the fusion image was used for spot detection using the following settings for Delta2D: local background region, 100; average spot size, 1; and sensitivity, 100%. Spots were not edited manually after spot detection. About 2000 spots on the fusion image were transferred to all other 2-D gel images for each time point. This ensures that for each stage investigated the identity for each spot on a gel is identical. Relative spot volume intensities (fractions of 100%) were used for quantitative protein expression analysis. After background subtraction, normalized spot intensity values were copied into Excel spreadsheets for statistical analysis. Data sets were analyzed applying a Student's t test. In the case of HD *versus* control comparisons a paired t test was used to compare sample pairs run side by side during both electrophoresis runs. In longitudinal studies where differ-

ent age stages of HD or control were compared with one another, we used an unpaired *t* test because no natural pairing exists. Pairs were randomly selected from each group (time points) compared. The 2-D gel evaluation procedure by Delta2D remained the same as in HD *versus* control comparisons.

To determine changes in total protein concentration we determined the protein amount (gray value determined by Delta2D 2-D gel evaluation software) changed for all up- or down-regulated proteins for each stage. Now the sum of the protein amounts for *e.g.* all significantly up-regulated proteins from controls was subtracted from the sum of all HD proteins. Therefore we obtained the actual amount of changed protein. To determine the total protein amount changed we added the amount for up- and down-regulation. To determine whether total amount of protein changed was significantly different between stages we used an unpaired *t* test. The total amounts changed for each 2-D gel pair (five HD *versus* control repeats) were calculated separately. We subsequently compared the total amounts of each stage with its adjacent stages by *t* test. All protein amounts are relative as they are altered as compared with control, and although changes in gray scale value (spot volume) are proportional to protein concentration changes the absolute concentration values are not available. Sample size comprised at least five biological sample pairs. The Student's *t* test was used because the data investigated were normally distributed. The Kolmogorov-Smirnov *Z* test provided by the statistical analysis software SPSS 16.0 (SPSS Inc., Chicago, IL) was used to determine the "normal" distribution of our data. SPSS calculates a "two-tailed significance level," testing the probability that the observed distribution is significantly deviant from the expected normal distribution. That is, a finding of non-significance means that the sample distribution is normal. We used the data set of statistically significant protein isoforms ($p < 0.05$, paired Student's *t* test) at 8 weeks to check for normal distribution. This data (sub)set was chosen because (i) testing all data points (4816 spots) was very difficult using the program available (SPSS) and (ii) the significant changes were the relevant ones for this study. We investigated the up- and down-regulated spots separately. The two-tailed significance level for up- and down-regulated protein isoforms was on average 0.81 ± 0.21 and 0.86 ± 0.17, respectively. That is, the null hypothesis (normal distribution) is true ($p > 0.05$), and the data are therefore normally distributed. In addition, all protein isoform changes tested were distributed normally.

The rate of false positives was estimated according to the following equation for unpaired *t* tests.

$$Z = \frac{x_1 - x_2}{\sqrt{\frac{{s_1}^2}{n_1} + \frac{{s_2}^2}{n_2}}} \qquad \text{(Eq. 1)}$$

We assumed that the null hypothesis that there is no difference between samples tested is valid. In addition, x_1 and x_2 are the sample means of the distributions, and s_1 and s_2 are the corresponding standard deviations. n_1 and n_2 indicate the number of sample pairs used in our study. Because we assumed an equal standard normal distribution of both data sets to be tested for false positives we assume that the standard deviation $s_1 = s_2$. *Z* denotes the desired confidence and was determined to be 2.015 for $Q_{(0.95)}$ (0.95 quantiles) and $n = n_1 = n_2 = 5$ according to the "quantiles of Student's *t* distribution." The false positive rate was therefore determined to be smaller than 15% of the significant changes for an unpaired *t* test. This value is even smaller for paired *t* tests.

Evaluation of False Positive Protein Changes—To determine the reliability of the results obtained by our HD time course investigation it was important to establish a base line of protein alterations that occur even if no disease is present. Therefore we selected a representative time point, 8 weeks, and compared eight control gels with each other. We randomly allocated the eight 2-D gels into two groups of four each. Those groups were analyzed in the same way as HD and control gels were. We analyzed a total of 4031 protein spots by an unpaired Student's *t* test ($p < 0.05$) and found that 17 spots were up-regulated and 22 were down-regulated in expression. This makes a total of 39 spots changed at 8 weeks without disease present. When comparing this result with the changes obtained during our time course study where 205, 42, 40, 157, and 240 spots were altered between HD and control at 2, 4, 6, 8, and 12 weeks, respectively (Table I), we found a percentage of false positives of 19, 93, 98, 25, and 16%, respectively. In addition, a direct comparison of changes at 8 weeks (157 spots) shows that 25% of the proteins may be false positives, or at least 118 changes were identified correctly.

Protein Identification—For protein identification by mass spectrometry, 40 μl of extract was separated by 2-DE and stained using an MS-compatible silver staining protocol (42). Protein spots of interest were excised from 2-D gels and subjected to in-gel tryptic digestion. Tryptic fragments were analyzed by nanoflow HPLC (Dionex/LC Packings, Amsterdam, Netherlands)/ESI-MS and -MS/MS on an LCQ Deca XP ion trap instrument (Thermo Finnigan, Waltham, MA). Nanoflow HPLC was directly coupled to ESI-MS analysis. Protein spot eluates of 15 μl were loaded onto a PepMap100 C_{18} precolumn (5 μm, 100 Å, 300-μm-inner diameter × 5 mm; Dionex/LC Packings) using 0.1% (v/v) trifluoroacetic acid at a flow rate of 20 μl/min. Peptides were separated onto a PepMap100 C_{18} 100 column (3 μm, 100 Å, 75-μm-inner diameter × 15 cm; Dionex/LC Packings). The elution gradient was created by mixing 0.1% (v/v) formic acid in water (solvent A) and 0.1% (v/v) formic acid in acetonitrile (solvent B) and run at a flow rate of 200 nl/min. The gradient was started at 5% (v/v) solvent B and increased linearly up to 50% (v/v) solvent B after 40 min. ESI-MS data acquisition was performed throughout the LC run. Three scan events, (i) full scan, (ii) zoom scan of most intense ion in full scan, and (iii) MS/MS scan of the most intense ion in full scan, were applied sequentially. No MS/MS scan on single charged ions was performed. Raw data were extracted by the TurboSEQUEST algorithm, and trypsin autolytic fragments and known keratin peptides were subsequently filtered. All DTA (peak list files for mass spectrometry results generated by the SEQUEST search algorithm) files generated by BioWorks version 3.2 (Thermo Scientific, Waltham, MA) were merged and converted to MASCOT generic format files (MGF). Mass spectra were analyzed using our in-house MASCOT software package license version 2.1 automatically searching the NCBInr database for *Mus musculus* (house mouse) (NCBInr_20061206, 107,853 sequences). The *M. musculus* subset of the NCBInr database was used because only mouse samples were investigated. In rare cases, hits were researched using the Mammalia subset of the NCBInr database. All non-*M. musculus* proteins are indicated in supplemental Table 1 by addition of either "*Homo sapiens*" or "*Rattus norvegicus*" after their protein name. To reduce the length of the protein names for the large majority of *M. musculus* identifications because of space constraints the species label was omitted in many cases. MS/MS ion search was performed with the following set of parameters: (i) taxonomy, *M. musculus* (house mouse); (ii) proteolytic enzyme, trypsin; (iii) maximum of accepted missed cleavages, 1; (iv) mass value, monoisotopic; (v) peptide mass tolerance, 0.8 Da; (vi) fragment mass tolerance, 0.8 Da; and (vii) variable modifications, oxidation of methionine and acrylamide adducts (propionamide) on cysteine. No fixed modifications were considered. Only proteins with scores corresponding to $p < 0.05$ with at least two independent peptides identified were considered. The cutoff score for individual peptides using ESI identification was equivalent to $p < 0.05$ for each peptide and usually in a MOWSE (molecular weight search) score range from 32 to 37. This number was calculated by the MASCOT software. Furthermore the-

oretical and practical molecular weight and pI for each protein identified by database search were compared to remove proteins with deviating masses and pI values.

Pathway Enrichment Analysis in the Protein Data Set—Official gene symbols and gene names (Mouse Genome Informatics) were used to investigate similarities in protein expression alterations between stages. The gene names were retrieved using the GI numbers supplied by MASCOT after a database search. To investigate an enrichment of specific pathways in the altered protein expression data set, we used the "Web-based gene set analysis toolkit" (WEBGESTALT) tool supplied by Vanderbilt University. We used the "Gene set analysis tool" and selected the gene set analysis option "Function" and the category "KEGG table and maps." KEGG is the abbreviated form of Kyoto Encyclopedia of Genes and Genomes and is a bioinformatics database containing information on genes, proteins, reactions, and pathways. The following parameters were used to create the KEGG tables: reference set, "WEBGESTALT_MOUSE"; significance level, $p < 0.01$; and minimum number of genes, 2. Statistical methods available were "hypergeometric test" and "Fisher's exact test." For our data the results were the same with either test.

Analysis of mRNA Data Sets for Co-regulation with Protein Expression Data Sets—We used an mRNA data set for the R6/2 HD mouse model for 6, 9, and 12 weeks that had been published previously (22, 43). Only the striatal data set was utilized. The data sets were already analyzed for statistical significance in their respective studies (22, 43). Briefly Affymetrix microarrays were normalized using robust multiarray averaging. Analysis was performed using R version 2.3 and the Bioconductor packages Affy and Limma. Differential gene expression in each array set was assessed relative to unaffected controls using paired *t* tests. Random matching generated six HD-control sample pairs (43). The mRNA data set consists of 22,626 probe set identities. From the entire mRNA data set only genes with differential regulation at the protein level were selected for analysis. On the single mRNA/protein level we found that 88% of 371 altered proteins could be correlated to corresponding mRNA data. A common gene symbol (mouse variant) of protein and mRNA data was used as the selection criterion. We now had mRNA expression data for 328 of our proteins at 6, 9, and 12 weeks for HD and control at our disposal. We now determined whether any significant changes occurred in any of the 328 mRNAs at each of the three stages. The significance level for altered mRNA expression selected for our study was $p < 0.05$. If probe sets were not altered significantly in more than 66% of cases (note that more than one probe set per gene name is present on the mRNA chip) they were discarded. In the three data sets at 6, 9, and 12 weeks of age, one (*Rbmx*), three (*Eef1a2*, *Mapre2*, and *Nono*), and zero genes showed opposite regulatory behavior, respectively. Opposite regulatory behavior was present when individual probe sets coding for the same gene name on the mRNA array showed opposite expression behavior. The number of statistically significant mRNA alterations of the total of 328 was determined for each stage. The gene names for altered proteins were compared with the gene names of mRNAs to determine the overlap in expression changes between protein and mRNA on the single mRNA/protein level.

To investigate the overlap in cellular pathways between the mRNA and the protein data sets we used WEBGESTALT using the same parameters as already described earlier under "Pathway Enrichment Analysis in the Protein Data Set." To determine enriched pathways we used all significantly changed probe sets from the mRNA data sets at the stage investigated and not just those altered also in the protein data set.

RESULTS

We investigated the HD mouse model R6/2 for changes in the expression levels of proteins during phenotype onset and progression using a 2-DE gel-based proteomics approach. We observed two stages at which an extraordinarily large number of protein alterations had occurred. These peak alterations were present prior to onset and after the development of pronounced HD-related phenotypes. In addition, most of the changes were found to be stage-specific.

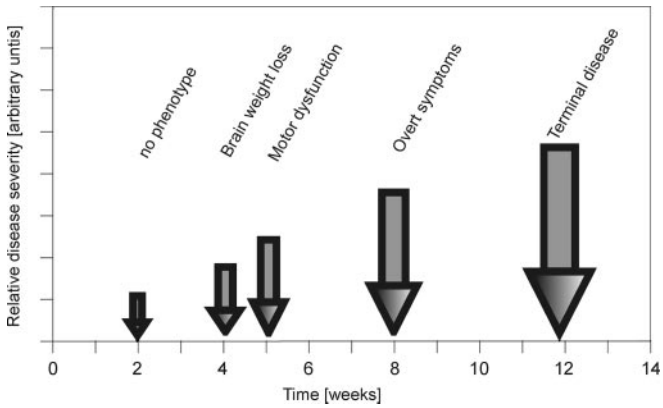

FIG. 1. **Scheme of disease progression in the HD mouse model R6/2.** Pathological hallmarks are marked on the time scale by *arrows*, and the observed phenotype is indicated on *top* of each *arrow*.

Altered Protein Expression during HD Progression in R6/2 Mice—To cover onset and all stages of disease progression in the well characterized R6/2 HD mouse model, we selected ages starting where no phenotype is present (2 weeks) and finishing where mice demonstrate pronounced symptoms (12 weeks). In our colony, disease end point is defined by 20% loss of body weight that occurs at 14–15 weeks of age. Further time points were selected to correspond to stages where hallmarks of disease progression appear. Loss of brain weight occurs from 4 weeks of age (44), an impairment of motor function as measured by RotaRod analysis is present from ~6 weeks (45), and a visible phenotype is present from ~8 weeks (45) (Fig. 1). After comparing R6/2 with control mice for 2, 4, 6, 8, and 12 weeks separately the number of differentially expressed proteins for each time point investigated was determined (Table I). For the 2-, 4-, 6-, 8-, and 12-week time points, a total of 3821, 4006, 4030, 4816, and 4283 protein isoforms were analyzed, respectively, to determine significant protein expression differences. As expected very few protein isoforms were altered in R6/2 mice at 4 (42 isoforms, 1.0% of total isoforms investigated at this age) and 6 weeks (40 isoforms, 1.0%) of age because the phenotype at these stages is very mild. The number of altered protein isoforms increased more than 3-fold at 8 weeks (157 isoforms, 3.3%) and a further 1.5-fold at 12 weeks (240 isoforms, 5.6%).

Unexpectedly we found a large number of protein isoforms altered at 2 weeks of age (205 isoforms, 5.4%). This number was almost as high as those detected at 12 weeks (Table I). We suspected that the number of protein isoforms changed at 2 weeks might not necessarily reflect a drastic change in the total amount of altered protein. Therefore, we determined the

TABLE I

Disease progression in the HD mouse model R6/2 is only reflected late in disease by altered protein isoforms

Shown is the number of differentially expressed protein spots. Only spots altered by >10% of spot volume and $p < 0.05$ are indicated. A paired Student's *t* test was used to determine statistical significance. All spots differentially expressed on the 2-D gels at each respective stage are listed.

Age	Number of differentially expressed spots		
	Up	Down	Total
weeks			
2	117	88	205
4	19	23	42
6	17	23	40
8	93	64	157
12	120	120	240

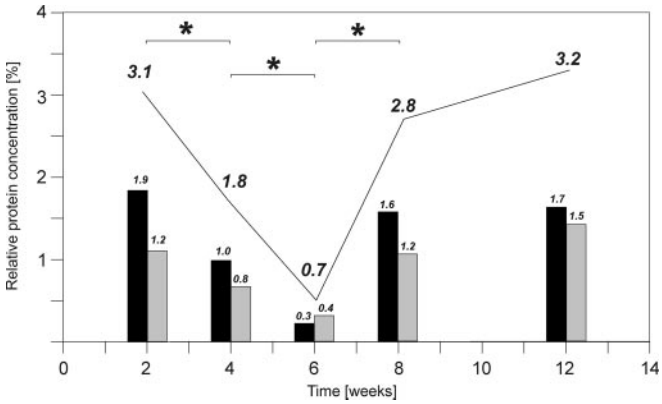

FIG. 2. **Relative protein concentration changes during HD progression.** Total brain extracts of R6/2 mice were studied at 2, 4, 6, 8, and 12 weeks of age. Protein concentration alterations were calculated for all significantly altered protein isoforms ($p < 0.05$, <0.9- or >1.1-fold change). The total spot volume (spot intensity × spot area) on each 2-D gel was set to 100%. The *y axis* indicates the amount of protein changed relative to a total protein concentration of 100%. *Asterisks* indicate statistical significance ($p < 0.05$). *Black bars* indicate up-regulated proteins, and *gray bars* indicate down-regulated proteins. The *numbers above* each *bar* indicate percentage of change. The *line above* the *bars* indicates the sum of up- and down-regulated protein concentration changes that is also indicated by *numbers*.

relative amount of protein changed (Fig. 2) and found that 3.1% of the total spot volume (protein concentration) was altered at 2 weeks comparable to 3.2% at 12 weeks of age. Again the values were almost identical. The *y axis* of Fig. 2 indicates the amount of protein changed relative to a total protein concentration of 100% for a 2-D gel.

We subsequently identified the altered protein isoforms by mass spectrometry. Table II shows the number of identified proteins for each stage separately. The identification rates were in general very high, ranging from 83 to 94% except for at 6 weeks (53%). However, at 6 weeks, only a very small number of proteins were altered (40), and therefore, the failure to identify specific proteins makes a huge difference to the

TABLE II

Number of identified proteins changed in R6/2 disease progression

Age	Identified differentially expressed spots		
	Up	Down	Total[a]
weeks			
2	91	80	171 (83%)
4	16	21	37 (88%)
6	10	11	21 (53%)
8	93	45	138 (88%)
12	114	112	226 (94%)

[a] The percentage of identified proteins as compared with the numbers in Table I is given in parentheses. The number of differentially expressed proteins is listed. Only proteins altered by >10% of spot volume and $p < 0.05$ are indicated. A paired Student's *t* test was used to determine statistical significance.

percentage identified. Because of the generally high identification ratio, the proteins changed represent the entire data set of altered protein spots (Table I). A low identification rate may leave an important subset of proteins beyond scrutiny and may bias the study for easily identifiable proteins. It is well established that a protein may be represented by more than one protein isoform (spot) on a 2-D gel. Therefore we determined the number of non-redundant proteins that were changed for each stage. We used the gene name as a selection criterion: proteins sharing the same gene name were considered as one non-redundant protein. Therefore, proteins with a different protein name but the same gene name and a protein altered in more than one isoform (seen on the 2-D gel as a protein spot (18)) on the 2-D gel were considered to be the same protein and counted only once per stage. Table IIIA shows the number of non-redundant proteins changed at each disease stage. As might have been expected, at each stage proteins were represented by more than one protein spot on the 2-D gel. The number of non-redundant proteins was 73, 89, 86, 77, and 70% of the total number of proteins identified at 2, 4, 6, 8, and 12 weeks, respectively. In total 371 individual, non-redundant proteins were identified. Interestingly almost all proteins represented by more than one spot showed the same regulatory pattern in all isoforms; that is, they were either up- or down-regulated (Table IIIB).

Drastic Protein Expression Changes Early in Disease Precede HD-related Phenotypes—The most unexpected observation was that an early peak in protein alterations in terms of numbers (Tables I–III) and amount (Fig. 1) was observed prior to phenotype onset, and we sought to identify the mechanism underlying this early peak. It is already known that protein changes related to development that are present at 2 weeks of age in the mouse are drastically reduced in adulthood (38). We investigated the longitudinal changes in R6/2 and wild-type mice to elucidate the magnitude of protein changes during development in the presence and absence of disease (Table IV). This means we compared each stage within a group (HD or control) with its adjacent stages. The number of

TABLE III
Number of non-redundant proteins changed at each stage during R6/2 disease progression

Age	A. Number of proteins		
	Up	Down	Total[a]
weeks			
2	65	59	124 (73%)
4	15	18	33 (89%)
6	10	8	18 (86%)
8	74	31	105 (77%)
12	84	74	158 (70%)

Age	B. Number of proteins with more than one spot		
	Same[b]	Different[b]	Total
weeks			
2	47	0	47
4	4	0	4
6	3	0	3
8	33	2	35
12	68	3	71

[a] The percentage of non-redundant proteins as compared with the number of proteins identified in Table II is indicated in parentheses.
[b] Regulation of redundant spots (up/down) is in the same or opposite direction. Only proteins altered by >10% of spot volume and $p < 0.05$ are indicated. A paired Student's *t* test was used to determine statistical significance.

TABLE IV
Longitudinal changes during wild-type and R6/2 development: number of proteins

Only proteins altered by >10% of spot volume and $p < 0.05$ are indicated. An unpaired Student's *t* test was used to determine statistical significance. Changes within the group of HD or control were considered. Adjacent age stages were compared with each other.

Age	Number of protein isoforms		
	Up	Down	Total
weeks			
A. R6/2			
2/4	137	181	318
4/6	39	36	75
6/8	26	105	131
8/12	66	23	89
B. Wild type			
2/4	162	136	298
4/6	30	80	110
6/8	78	230	308
8/12	110	32	142

protein isoform changes between 2 and 4 weeks, 318 in HD and 298 in wild type, were more numerous than all subsequent changes during longitudinal development and its interaction with HD disease progression. Interestingly the number of changes in wild-type and R6/2 mice reached another peak between 6 and 8 weeks (Table IV). These changes were reproduced when alterations in protein amount (concentration) were considered: again alterations were most dramatic between 2 and 4 weeks in HD and wild-type mice (16.3 and

TABLE V
Longitudinal changes during wild-type and R6/2 development: amount of protein

Only proteins altered by >10% of spot volume and $p < 0.05$ are indicated. An unpaired Student's *t* test was used to determine statistical significance. Changes within the group of HD or control were considered. Adjacent age stages were compared with each other.

Age	Amount of protein isoforms altered		
	Up	Down	Total
weeks		%	
A. R6/2			
2/4	8.5	7.8	16.3
4/6	0.9	1.2	2.1
6/8	2.7	3.2	5.9
8/12	2.2	2.0	4.2
B. Wild type			
2/4	6.8	6.5	13.3
4/6	0.8	2.2	3.0
6/8	8.0	6.1	14.1
8/12	3.4	2.8	6.2

TABLE VI
Longitudinal changes during C57BL/6 mouse development

Only proteins that are altered >10% of spot volume and $p < 0.05$ are indicated. An unpaired Student's T-test was used to determine statistical significance. E, embryonic day; P, postnatal day.

Age	A. Number of protein isoforms			
	Up	Down	Total	Total/day
weeks				
E16/E18 (−3 days)	52	87	139	70
E18/P0 (0 days)	37	57	94	31
P0/P7 (7 days)	157	170	327	47
P7/P14 (14 days)	245	181	426	61
P14/P28 (14 days)	155	197	352	25

Age	B. Amount of protein			
	Up	Down	Total	Total/day
weeks			%	
E16/E18 (−3 days)	2.6	2.3	4.9	2.5
E18/P0 (0 days)	1.1	1.8	2.9	1.0
P0/P7 (7 days)	4.8	4.3	9.1	1.3
P7/P14 (14 days)	7.7	9.6	17.3	2.5
P14/P28 (14 days)	8.8	5.4	14.2	1.0

13.3%, respectively) (Table V). All mice with nominal age 2 weeks were sacrificed exactly 14 days after birth, but to rule out a difference in "developmental age" between R6/2 and control mice at 2 weeks of age we compared the body weight of both groups. R6/2 mice had an average weight of 7.3 ± 0.75 g, and controls had an average weight of 7.54 ± 1.15 g. Brain weights were normally distributed and showed no statistically significant difference ($p = 0.814$, paired Student's *t* test).

Therefore, the number and extent of protein expression changes occurring between 2 and 4 weeks were large regardless of the presence of disease. We now used C57BL/6 mice to study expression changes during early development before 2 weeks of age (Table VI). When comparing the results for wild-type CBA × C57BL/6 and inbred C57BL/6 mice, we

found 298 *versus* 352 protein isoforms altered and 13.3 *versus* 14.2% changes in protein amount; this represents a very high degree of similarity (Tables IV, V, and VI). When looking at earlier changes it becomes clear that the amount of change is considerably higher between time points in earlier mouse developmental stages (35). We analyzed protein changes at embryonic days 16 and 18 and postnatal day (P) 0, P7, P14, and P28 ($n = 3$ per time point). We then calculated the number of isoforms and protein amount changed between consecutive time points and converted this to the average number of isoforms changed per day for comparison purposes (Table VI). A peak in the change in protein amount and isoform number was observed between P7 and P14 (1 and 2 weeks after birth; Table VI and Fig. 3). These data suggest that during normal development the changes in protein expression that occur at early stages (before 2 weeks) are already very pronounced. Generally the changes per day are very high except shortly before birth (Table VIB). A perturbation such as the expression of the transgenic fragment of the *HD* gene in R6/2 mice (32) may easily disturb a delicate equilibrium of expression changes during normal development. This may explain the large number of protein expression changes observed early in disease at 2 weeks (Tables I–III and Fig. 2).

Overlap of Protein Expression Changes between Different Stages of Disease Progression—After studying the possible causes of the protein expression overlap, the identity and properties of the proteins generating this early peak in differential expression were investigated. First the degree of similarity between the proteins that change in disease was investigated. We compared the gene names corresponding to the non-redundant proteins identified for each stage and found a protein expression overlap of 6–38% depending on the stages compared (Table VIIA). The protein expression overlap is defined as the percentage of gene names shared between two stages compared. Interestingly the overlap between 2 and 12 weeks of age was very high (38%). We then considered whether the direction of change in expression (*i.e.* up or down) was concordant or discordant between stages (Table VIIB). It became clear that even if the same proteins were differentially regulated at both 2 and 12 weeks the direction of expression was not necessarily the same. Correction for the direction of expression, that is the same genes in the stages compared with opposite regulation (*i.e.* up *versus* down) were removed, reduced the overlap to 27%. This means that 73% of the protein changes were specific for 2 and 12 weeks of age. The overlap in differentially expressed proteins was corrected to account for the direction of change for all comparisons and found to range from 0 to 29% with the lowest being between 6 and 8 weeks of age (Table VIIA). Although an expression overlap of up to 29% is still large, overall between 71 and 100% of the proteins that were differentially expressed were stage-specific (Table VII).

Early Changes in Energy Metabolism during HD Pathology—To obtain a deeper understanding of the processes involved in disease progression it is important to determine whether specific pathways are enriched within the altered protein data set for which we carried out a KEGG analysis (46). We analyzed all time points separately and only included pathways where at least three proteins were enriched. This cutoff was chosen to ensure that a reasonable number of proteins were altered for a given pathway thereby providing strong evidence for altered regulation. Pathways enriched in up-regulated and down-regulated proteins were identified (Table VIII). Interestingly glycolysis/gluconeogenesis was found to be at the top

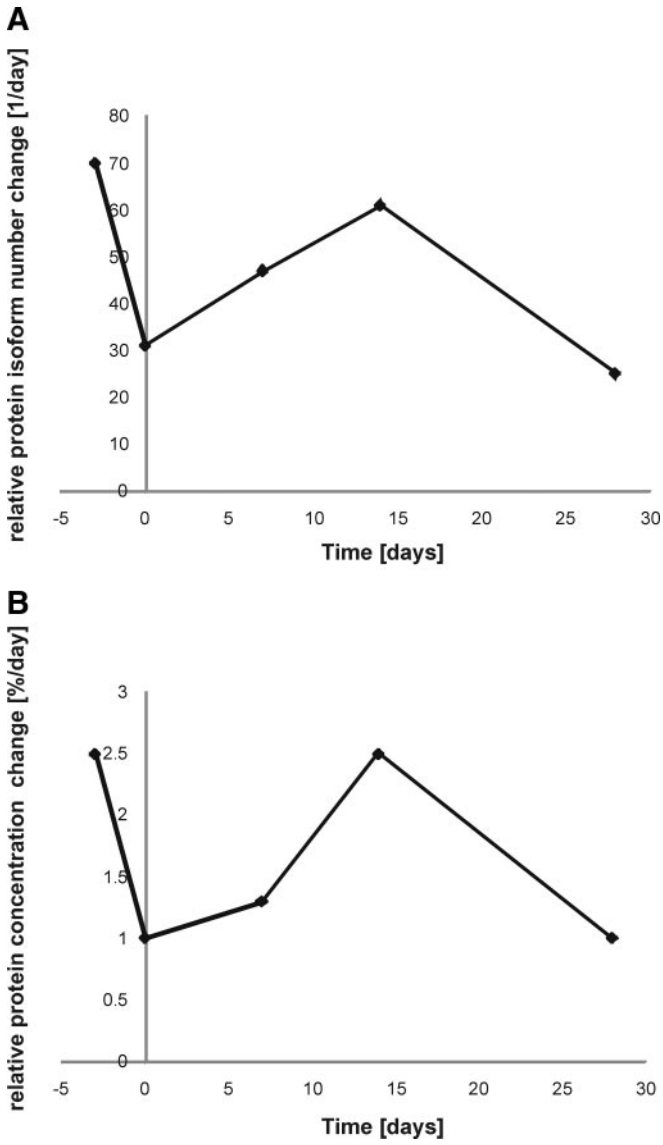

FIG. 3. **Longitudinal changes of protein expression during development.** Changes in protein expression per day in terms of number of proteins (*A*) and protein concentration (*B*) were determined. Total brain extracts of embryonic day 16 and 18 and neonate P0, P7, P14, and P28 wild-type C57BL/6 mice were compared. Altered protein numbers and concentration were calculated for all significantly altered protein isoforms ($p < 0.05$, <0.9- or >1.1-fold change). For a complete list of all alterations see Table VI.

TABLE VII

Protein expression overlap between R6/2 stages investigated

A, non-redundant proteins (Table III) were compared between the time points indicated. Note that the time point with the lower number of differentially expressed proteins was set to 100% to ensure that changes can reach 100%. B, the number of overlapping protein changes (A, overlapping) was investigated for changes sharing the same or opposite direction of expression (up/down). Only proteins altered by >10% of spot volume and $p < 0.05$ are indicated. An unpaired Student's *t* test was used to determine statistical significance.

Age	A. Number of non-redundant protein isoforms		
	Overlapping	Total	Relative overlap[a]
weeks			%
2/4	10	33	30 (18)
4/6	3	18	16 (11)
6/8	1	18	6 (0)
8/12	35	106	33 (29)
2/12	46	124	38 (27)

Age	B. Number of overlapping protein changes		
	Same	Opposite	Relative similarity
weeks			%
2/4	6	4	60
4/6	2	1	67
6/8	0	1	0
8/12	31	4	89
2/12	32	14	70

[a] The expression overlap corrected by the relative similarity of expression orientation between mRNA and protein datasets (number in parentheses).

TABLE VIII

Pathways enriched at each stage and during disease progression

A KEGG pathway analysis was carried out, and only pathways with three or more proteins and $p < 0.01$ were included. Pathways marked bold were altered in at least four of five time points studied.

Age	Pathways	Number of proteins
weeks		
A. Pathways up-regulated		
2	**Glycolysis/gluconeogenesis**	9
	Pentose phosphate pathway	4
	Citrate cycle (tricarboxylic acid cycle)	4
	Glutamate metabolism	4
4	**Glycolysis/gluconeogenesis**	3
	Oxidative phosphorylation	3
6	No pathways	
8	**Glycolysis/gluconeogenesis**	5
	Citrate cycle (tricarboxylic acid cycle)	4
	Proteasome	3
	Tryptophan metabolism	3
12	Proteasome	10
	Glycolysis/gluconeogenesis	5
	Citrate cycle (tricarboxylic acid cycle)	3
	Cell communication	3
B. Pathways down-regulated		
2	Regulation of actin cytoskeleton	3
	Proteasome	3
4	Gap junction	2
6	No pathways	
8	Oxidative phosphorylation	3
12	Regulation of actin cytoskeleton	6
	Glycolysis/gluconeogenesis	5
	Axon guidance	3
	Pyruvate metabolism	3

of the up-regulated categories at all stages except at 12 weeks of age when most up-regulated proteins were found in pathways involving proteasome function. In contrast some proteins involved in glycolysis/gluconeogenesis were down-regulated at 12 weeks. Of other down-regulated pathways, the "regulation of actin cytoskeleton" was at the top of the list at 2 and 12 weeks of age, and proteasome function was down-regulated at 2 weeks of age. In summary, "glycolysis/gluconeogenesis" was mostly up-regulated, whereas "regulation of cytoskeleton" was down-regulated. The regulation of proteasome function seems to be stage-specific.

When the overlap between proteins of altered expression was considered, those overlapping between 2 and 12 weeks of age (Table VII) belong to glycolysis/gluconeogenesis, the "pentose phosphate pathway," and "proteasome". In contrast, when the protein expression overlap from 8 and 12 weeks was compared, glycolysis/gluconeogenesis was still the top ranking enriched pathway followed by "Parkinson disease" (*Ube1x* and *Uchl1*), and "metabolism of xenobiotics by cytochrome P450" as well as "MAPK signaling pathway" were also included. At the level of individual proteins, only nine gene names, *Cops4*, *Efhd2*, *Mtpn*, *Phpt1*, *Sept7*, *Slc25a12*, *Stmn1*, *Tppp*, and *Uchl1*, were identified in the expression overlap data sets of 2 *versus* 12 weeks and 8 *versus* 12 weeks. Therefore, because a total of 49 genes overlapped between 2 and 12 weeks and 35 overlapped between 8 and 12 weeks, there is an overlap of 23% between both data sets at the individual protein level.

We now investigated the possibility that because some proteins within an altered pathway may be up-regulated and others may be down-regulated those pathways may be lost in an analysis that separates up- and down-regulated proteins. Table X shows that all pathways found with separate analysis (Table VIII) were also found when up- and down-regulated proteins were subjected to KEGG analysis simultaneously. Because some numbers of proteins of the pathways involved are higher in Table X, proteins of the same pathway show opposite regulation. Still most proteins were either up- or down-regulated. Still more altered pathways per stage were found with simultaneous analysis, and importantly in addition to glycolysis/gluconeogenesis, "oxidative phosphorylation" was found to be altered at all stages except 6 weeks (Table X).

This common enrichment in altered pathways is clearly contrasted by the fact that only two proteins, represented by the gene names glyceraldehyde-3-phosphate dehydrogenase (*Gapdh*) and pleckstrin homology (PH) and SEC7 domain-containing protein 3 (*Psd3*), were altered at four of the stages and that none were altered in all five stages. *Gapdh* catalyzes D-glyceraldehyde 3-phosphate, phosphate, and NAD^+ to 3-phospho-D-glyceroyl phosphate and NADH and is involved in glycolysis, but a nuclear function has also been described. *Psd3* acts as a guanine nucleotide exchange factor for ARF6 and is located at cell junctions, the presynapse, the postsynaptic cell membrane, and the postsynaptic density.

In summary, when analyzing our proteomics data set, we found two peaks in protein alteration, one early (5.4% of all protein isoforms changed, 2 weeks) and one late in disease (5.6%, 12 weeks). In addition, most changes at each time point investigated were stage-specific (71–100%; see Table VII).

Correlation of mRNA Expression Kinetics during HD Progression in R6/2 Mice—Recently mRNA expression data for R6/2 mice at 6, 9, and 12 weeks of age have been published (22, 47), and we used these data sets to compare mRNA and protein expression data to determine the degree by which altered mRNA regulates protein expression. The data sets were generated from the striatum of 6-, 9-, and 12-week-old R6/2 mice. Of the 371 non-redundant proteins that we identified, only 39 were not represented in the mRNA data. Therefore we were able to correlate the expression profiles of 328 mRNAs (88% of the proteins) with their protein expression. Only two of the stages studied at the mRNA level (6 and 12 weeks) coincided directly with the stages studied on the proteome level (2, 4, 6, 8, and 12 weeks). We compared the mRNA expression data with adjacent protein expression data on the single mRNA/protein level. 6-week mRNA expression data were compared with 4-, 6-, and 8-week protein data, the 9-week mRNA data were compared with 8- and 12-week protein data, and the 12-week mRNA data were compared with 8- and 12-week protein data.

The comparison of altered mRNAs and proteins at 6 weeks revealed an overlap of 3 of 13 (23%), and at 12 weeks the overlap was 42% when the direction of alteration was not taken into account. At 6 weeks all three mRNAs that showed a statistically significant alteration were regulated in the opposite direction to the alteration in protein expression (up/down). At 12 weeks this was the case for 16 of the 58 altered mRNAs. Interestingly this opposite regulation was lower, 3 of 31 (10%), when the 9-week mRNA data set was considered (Table IX). Because the pathways that are differentially regulated at 2 and 12 weeks of age are quite similar, mRNA alterations at 12 weeks were compared with the proteins that were altered at 2 weeks. 42% of the mRNAs altered at 12 weeks were also altered at the protein level at 2 weeks. If those changing in the opposite direction are excluded the overlap is still 23% (Table IX). Therefore although there is co-regulation between protein and mRNA expression it is generally low on the level of individual proteins/mRNA.

TABLE IX
Comparison of significantly altered protein with mRNA expression in R6/2 mice

Age	Number of mRNAs			
	Total mRNAs[a]	6 weeks[b]	9 weeks[b]	12 weeks[b]
weeks				
2	112 (12)	ND[c]	ND	47 (21)
4	33 (0)	5 (2)	ND	ND
6	13 (5)	3 (3)	6 (4)	ND
8	99 (7)	15 (5)	25 (10)	35 (6)
12	137 (21)	ND	31 (3)	58 (16)

[a] Total mRNAs were determined by using the number of non-redundant proteins (see also Table IIIA (Total)) minus the number that are not represented in the mRNA data set (parentheses).
[b] Number of mRNAs regulated in the opposite direction (up/down) to the proteins is indicated.
[c] ND, not done.

We now investigated the overlap between pathways of the mRNA and protein data sets. We determined the number of differentially expressed proteins considering mRNAs with $p < 0.05$. Subsequently we carried out a KEGG analysis using 2775, 4338, and 2940 significantly altered, non-redundant genes for 6, 9, and 12 weeks, respectively. We compared up- and down-regulated mRNAs and proteins for each stage together (Tables X and XI). Stage "8 weeks" of the protein data set was compared with "9 weeks" of the mRNA data set, and stage "12 weeks" of the protein data set was compared with 12 weeks of the mRNA data set. We found an overlap of 6 of 8 pathways at 8/9 weeks and 6 of 10 pathways at 12 weeks. No pathways were altered in the protein data set at 12 weeks. The top five pathways in Table XI are those listed at the top of a KEGG pathway analysis when using the mRNA datasets for each of the three age stages investigated. The additional pathways listed are altered in at least one of the stages from the protein data set. Interestingly the top scoring pathways of the mRNA data set such as oxidative phosphorylation and regulation of actin cytoskeleton were also altered in the protein data set (Tables X and XI).

DISCUSSION

In this study we investigated early changes in protein expression and followed these during disease progression in the R6/2 HD mouse model. We observed two peaks of altered protein expression, one at 2 weeks of age prior to the onset of phenotypes and one at 12 weeks when symptoms are pronounced. These changes corresponded to about 6% of the entire proteome (protein isoforms) studied. Although most alterations were stage-specific, in some cases *e.g.* proteins involved in glycolysis/gluconeogenesis were dysregulated at every stage. In addition there was a pronounced similarity between early and late changes at the protein and mRNA level. When comparing the mRNA and protein changes they showed a small overlap (<30%); that

TABLE X

Pathways enriched at each stage and during disease progression: all proteins

A KEGG pathway analysis was carried out, and only pathways with three or more proteins and $p < 0.01$ were included. Pathways marked bold were altered in at least four of five time points studied.

Age	Pathways	Number of proteins
weeks		
2	**Glycolysis/gluconeogenesis**	9
	Citrate cycle (tricarboxylic acid cycle)	6
	Regulation of actin cytoskeleton	5
	Proteasome	5
	Oxidative phosphorylation	5
	Pentose phosphate pathway	4
	Glutamate metabolism	4
	Propanoate metabolism	4
	Pyruvate metabolism	4
	Fructose and mannose metabolism	4
4	**Glycolysis/gluconeogenesis**	4
	Oxidative phosphorylation	4
6	No pathways	
8	**Glycolysis/gluconeogenesis**	6
	Oxidative phosphorylation	6
	Citrate cycle (tricarboxylic acid cycle)	5
	Glutathione metabolism	4
	Fatty acid metabolism	3
	MAPK signaling pathway	3
	Proteasome	3
	Valine, leucine, and isoleucine degradation	3
12	**Glycolysis/gluconeogenesis**	10
	Proteasome	10
	Regulation of actin cytoskeleton	7
	Pyruvate metabolism	6
	Fructose and mannose metabolism	5
	Axon guidance	4
	Cell communication	4
	Oxidative phosphorylation	3
	Focal adhesion	3
	Neurodegenerative disorder	3
	Parkinson disease	3

TABLE XI

Pathways enriched at each stage and during disease progression: mRNA

The first five pathways selected were the top pathways in the KEGG analysis of the mRNA data set. The following pathways are those that overlap with any pathway in the protein data sets. The cutoff for inclusion into the table for the mRNA data sets was 10 mRNAs. Pathways marked bold overlap with protein expression data at 8 weeks (mRNA at 9 weeks) and 12 weeks. Only pathways with three or more proteins and $p < 0.01$ were included. Numbers in parentheses were obtained from a second dataset for 12-week-old R6/2 mice.

Age	Pathways	Number of proteins
weeks		
6	MAPK signaling pathway	70
	Regulation of actin cytoskeleton	43
	Insulin signaling pathway	40
	Focal adhesion	40
	Neuroactive ligand-receptor interaction	38
	Axon guidance	27
	Oxidative phosphorylation	26
	Cell communication	15
	Glycolysis/gluconeogenesis	10
	Fatty acid metabolism	10
	Neurodegenerative disorders	10
	Proteasome	10
9	**MAPK signaling pathway**	102
	Focal adhesion	68
	Regulation of actin cytoskeleton	64
	Insulin signaling pathway	56
	Calcium signaling pathway	52
	Oxidative phosphorylation	49
	Axon guidance	44
	Cell communication	20
	Glycolysis/gluconeogenesis	16
	Citrate cycle (tricarboxylic acid cycle)	15
	Neurodegenerative disorders	14
	Glutamate metabolism	13
	Fatty acid metabolism	10
12	MAPK signaling pathway	64 (80)
	Focal adhesion	51 (50)
	Regulation of actin cytoskeleton	46 (55)
	Purine metabolism	41 (47)
	Cell cycle	39 (44)
	Axon guidance	32 (43)
	Oxidative phosphorylation	19 (23)
	Cell communication	17 (23)
	Valine, leucine, and isoleucine degradation	13 (17)
	Proteasome	14 (16)

is over 70% of the changes were specific to mRNAs or proteins.

The identification of early disease-related alterations will play a key role in our understanding of HD. However, most studies focus on late stages of disease in mouse models once an overt phenotype has occurred or study patients with manifest disease or postmortem brains of people who have died at late stage disease. In this study, we investigated the disease kinetics of altered protein expression levels, starting prior to phenotype onset and continuing through known stages of the disease.

Peak in Early Changes at 2 Weeks of Age—The most startling result of this study was the extent to which protein alterations had already occurred at 2 weeks of age. The number of protein alterations was almost equivalent to those found at a late stage of disease and showed a significant overlap in terms of gene names. The pathway identified using the KEGG database that is most altered during disease progression is glycolysis/gluconeogenesis. Interestingly at 2 weeks, almost all glycolytic enzymes (phosphofructokinase (*Pfkm*), aldolase (*Aldoa* and *Aldoc*), *Gapdh*, phosphoglycerate kinase 1 (*Pgk1*), and pyruvate kinase (*Pkm2*)) were up-regulated in their expression level (supplemental Table 1). In addition, an up-regulation of energy metabolism was further supported by up-regulation of key enzymes of the citrate

cycle: aconitase 2 (*Aco2*), fumarate hydratase 1 (*Fh1*), and malate dehydrogenase 2 (*Mdh2*). This is in accordance with a weight loss that occurs early in HD despite a high caloric intake (48). Weight loss has clearly been established in pre- and early symptomatic patients, and a significant reduction in the concentration of branched chain amino acids could be detected in their plasma by nuclear magnetic resonance spectroscopy suggesting that a perturbed mitochondrial energy metabolism is relevant to early pathogenesis (49). These changes are also consistent with an early disturbance of the transcription factor PGC-1α. The suppression of PGC-1α leads to mitochondrial dysfunction and therefore a dysfunction of the energy metabolism and neurodegeneration (50, 51).

At 2 weeks of age, an increase in "glutamate metabolism" was observed (Table VIIIA). Glutamate-ammonia ligase (*Glul*), glutamate dehydrogenase 1 (*Glud1*), glutamate oxalacetate transaminase 2 (*Got2*), and 4-aminobutyrate aminotransferase (*Abat*) were all up-regulated in expression. *Glul* converts glutamate to glutamine in astrocytes after glutamate-mediated neuronal signaling. Glutamate is removed by astrocytes after signaling from the synaptic cleft (52, 53), and glutamate conversion to glutamine is directly coupled to glutamate signaling (52, 53). Consequently this increased *Glul* activity may indicate an increase in glutamate signaling at a very early stage in HD progression at least in the R6/2 mouse model studied. Increased glutamate signaling at the *N*-methyl-D-aspartate subclass of ionotropic glutamate receptors has been linked to excitotoxicity, especially in striatal neurons, which has been proposed as a pathogenic disease mechanism for HD (54).

Furthermore at 2 weeks of age proteins involved in exo- and endocytosis were altered in expression. *Cplx1*, *Cplx2* (both down-regulated), *Syn1*, and *Syn2* (both up-regulated) are involved in exocytosis. *Pacsin1* (up-regulated; three isoforms) and *Dnm1* (down-regulated) are involved in endocytosis (55). In addition, *Arpc1a* and *Arpc5*, members of the Arp2/3 complex linking *Pacsin1* and *N-Wasp* to actin to ensure functional endocytosis (56), were up- and down-regulated, respectively. *Homer1* (two isoforms) located in the postsynaptic density (57) was up-regulated in expression. This dysregulation of proteins involved in exo- and endocytosis suggests that synapses are perturbed early in the R6/2 HD model. These changes were not detected by KEGG pathway analysis because up- and down-regulated proteins were investigated separately.

So far up- and down-regulated pathways were studied separately. Because proteins may be up- or down-regulated in the same pathways in disease we also considered pathway changes when up- and down-regulated proteins were subjected to KEGG analysis simultaneously. We found all pathways altered when we studied up- and down-regulated proteins separately. In addition we found that not only glycolysis/gluconeogenesis but also "oxidative phosphorylation" was altered at all stages except 6 weeks (Table X). In summary the changes observed may be due to a disturbance of the delicate equilibrium during development because of the large amount of changes naturally occurring at this time (Tables IV and V), or it is conceivable that the early changes act as a compensatory mechanism for early transgene Htt expression already in the absence of symptoms.

When considering the base-line level of false positives of 39 proteins per stage (see "Experimental Procedures" for more information) it becomes obvious that the protein alterations found at 4 and 6 weeks that are just above this level (Table I) should be treated with caution, whereas the other three time points that are more than 4-fold above this threshold are far more reliable. When considering this and the number of pathways altered at 2, 8, and 12 weeks in addition to confirmatory literature data the results of this study provide a valuable contribution to unraveling the dynamic protein changes in HD.

Changes Are Stage-specific on the Individual Protein Level but Overlapping in Terms of Metabolic Pathways—Unexpectedly we found that most of the changes identified at each stage were stage-specific. The degree of specificity ranged from 71 to 100% (Table VII). One important conclusion of this finding is that a disease is a complex process that is not represented by linear changes in protein expression starting early at low levels, *e.g.* 2 weeks, increasing steadily to high levels close to terminal disease (12 weeks; Fig. 1). However, the groups of metabolic pathways altered are relatively constant, especially glycolysis/gluconeogenesis and those involved in proteasome function. It is interesting that the number of changes varies considerably between stages ranging from 18 non-redundant proteins at 6 weeks to 158 at 12 weeks (Table III).

Proteasomal Alterations Dominate Late Changes—Alterations in the expression levels of proteins involved in proteasome function dominated at 12 weeks of age. Although proteasomal changes have already occurred at 2 weeks these were down-regulated. At 8 weeks they were up-regulated but less numerous, and at 12 weeks the following proteins represented by their gene names were up-regulated: PSMA3, PSMA5, PSMB1, PSMB3, PSMB4, PSMB5, PSMC3, PSMC5, PSMD4, and PSMD7. PSMA3 and PSMA5 are members of the 20 S proteasome α-subunits, whereas PSMB1, PSMB3, PSMB4, and PSMB5 are 20 S proteasome β-subunits (58). The β-subunits are catalytically active and responsible for proteasome specificity (58). So far 11 β-subunits have been identified in mice of which four were up-regulated in our study. In addition, all of the dysregulated subunits are essential subunits in yeast that are functionally conserved in humans (58). PSMC3, PSMC5, PSMD4, and PSMD7 belong to the regulatory or 19 S proteasome, which together with the 20 S complex forms the 26 S proteasome in eukaryotes (58–60). PSMA3, PSMB4, and PSMD4 were already up-regulated at 8 weeks of age. In contrast, PSMA5, PSMA6, and PSMB6 were down-regulated at 2 weeks. Only PSMA5 was later up-regulated at 12 weeks. Therefore, proteasomal changes are specific to certain stages of disease. Global changes to the

ubiquitin proteasome system have already been reported in HD at intermediate and late stages of disease at the functional level (61). In this context it is interesting that UBE1X (UBA1) was up-regulated in R6/2 mice at 8 and 12 weeks of age. UBE1X is currently thought to be the sole E1 for charging E2s with ubiquitin in mammals (62, 63). E1, E2, and E3 are enzymes that conjugate ubiquitin to cellular proteins in a multistep pathway prior to their degradation (64). In addition UCHL1, which has already been shown to be involved in the pathology of Parkinson disease and exhibits a ligase as well as a ubiquitin hydrolase activity, was down-regulated at 2 weeks of age but up-regulated at 8 and 12 weeks (supplemental Table 1). In summary components of the ubiquitin/proteasome pathway are up-regulated in symptomatic disease. This may reflect efforts to remove protein aggregates that are a hallmark of HD and other neurodegenerative diseases (65–67).

Relatively High Degree of Overlap between Early and Late Changes—When comparing changes at 2 and 12 weeks of age many of the protein changes can be observed at both stages (Table VIIB). It is interesting that this overlap exists at the level of pathways as well as at the level of individual proteins (Tables VIII and IX). However, the regulatory pattern of alterations is different at all stages (Tables VIIIB and IX). This may be caused by different types of perturbation in early and late stage disease that is reflected by the differential changes. This is supported by the changes observed in glycolysis/gluconeogenesis that were strictly up-regulated at 2 weeks of age but that were divided (five *versus* five proteins) at 12 weeks. An early effort to compensate for increased energy requirement early in disease (2 weeks) may be followed by a general deterioration of energy metabolism later prior to death.

No Protein Was Altered in All and Only Two Proteins Were Changed at Four Stages—After comparing the proteins changed at each stage it became obvious that only two proteins, *Psd3* and *Gapdh*, were changed at four of the five stages investigated, and none were altered at all five stages. Interestingly *Gapdh* has not only been reported to be involved in the pathology of HD (68, 69) but also in Alzheimer and Parkinson diseases (68). The number of proteins changed is therefore of more interest than the protein identities. The number of proteins investigated by a 2-DE proteomics approach is limited to up to 10,000 protein isoform spots depending on the application (18). The total number of proteins of the mouse proteome affected by HD is considerably larger than the number investigated in our study, but the ratio of changed proteins compared to unchanged proteins may remain approximately the same; that is the relative number of protein changes for each time point remains constant between our study and all proteins in the proteome. Therefore this study argues against a model in which there is a gradual increase in the number and magnitude of protein changes during disease progression and suggests a more dynamic regulatory pattern. We suggest that early changes affect late stage disease by changing processes in the mouse brain irreversibly. Our group has already shown that acute and long term proteome changes can be induced by oxidative stress in the developing brain (70). Oxidative stress has been proposed as a pathogenic mechanism for neurodegenerative disease in general. Early energy deficits or structural changes (Table VIII) may act in the same way.

High Correlation between Altered mRNA and Protein Expression on the Pathway Level—In the past, a large number of mRNA expression studies were done for HD mouse models (14, 21, 22, 43, 47, 71) as well as human tissue (26, 47) and blood samples (27). All studies so far used intermediate or late stage disease samples starting for the R6/2 mouse model used in our study at 6 weeks of age (22, 24). This means that the two earliest time points, 2 and 4 weeks, used in our study could not be correlated to mRNA expression, and it was not possible to investigate whether the early rise in differential protein expression was mirrored by a rise in altered mRNA expression. Still we found that the correlation between mRNA and protein expression changes was very low in our study on the level of individual proteins and did not exceed 30%, although 88% of the differentially expressed proteins were represented by mRNAs. This is consistent with previous studies in which mRNA data did not necessarily correlate well with protein data (72–76), although these studies did not investigate changes due to disease. In a recent study using brain cortex tissue, we found a 60–70% overlap between mRNA and protein changes during embryonic development where processes are highly predetermined and may be regulated to a large degree by mRNA expression with subsequent protein changes (35). Changes from three time points in embryonic development, embryonic days (ED) 9.5, 11.5, and 13.5, were compared with each other. Unfortunately the study investigates only changes up to ED 13.5, ending about 7 days before birth at ED 21 after gestation. Still during disease progression in contrast to development a cell or tissue may have to react to complex, unforeseen, and highly dynamic protein changes that are not predetermined by altered mRNA expression as they are in embryonic development. mRNA changes may be largely the result of pathological processes at the protein level such as protein aggregation or aberrant interactions of Htt that perturb transcription (77, 78).

After studying the overlap on the level of individual proteins we tested the pathway overlap between protein and mRNA data. We compared altered pathways at 8 and 12 weeks of the protein data set with 9 and 12 weeks of the mRNA data set (Tables X and XI). We found that the overlap of the pathways involved was actually very high. Therefore it is important to consider functional units such as pathways to measure the overlap between mRNA and protein data sets and not individual proteins or mRNAs.

In addition, a recent mRNA expression study of total brain extracts from R6/2 mice at 12 weeks of age revealed an alteration of 42 transcripts (see Fig. 1A of Ref. 79) that were all down-regulated in expression (79). When comparing the gene names from this study with our protein expression results we found no overlap on the single gene/protein or pathway level. Using the KEGG pathway analysis tool we found that the five most prominently altered pathways in the mRNA data set (79) were all related to neuronal signaling ("neuroactive ligand-receptor interaction" (six mRNAs), MAPK signaling pathway (six mRNAs), "cytokine-cytokine receptor interaction" (six mRNAs), "long term potentiation" (five mRNAs), and "GnRH signaling pathway" (five mRNAs)). Interestingly when considering the mRNA data investigated in this study (Table XI) we found that the MAPK signaling pathway was altered in both mRNA studies. Upon a more detailed inspection of the KEGG analysis of mRNA data for 12 weeks (data not shown), neuroactive ligand-receptor interaction (39 mRNAs), cytokine-cytokine receptor interaction (34 mRNAs), long term potentiation (22 mRNAs), and GnRH signaling pathway (25 mRNAs) were also altered on the mRNA level in our study. The most likely explanation for the discrepancy between mRNA and protein data is that most altered signaling mRNAs found in the study of Luthi-Carter *et al.* (79) are proteins that are either hydrophobic (receptors) and/or low in abundance (ligands) and can therefore not be detected by 2-DE. Importantly it would be of tremendous value to study mRNA and protein expression in the same tissue and time points in parallel because only then will we be able to determine the true correlation between differential mRNA and protein expression overlap without confounding influences such as different time points investigated (8 *versus* 9 weeks) or brain regions (total brain *versus* striatum).

In summary, we used a large 2-D gel/mass spectrometry-based proteomics approach to investigate HD-induced protein expression alterations and their kinetics prior to the onset of phenotypes and during the course of disease. Unexpectedly we found that protein changes were largely stage-specific (71–100%), and a drastic alteration (almost 6% of the proteome) in protein expression that occurred as early as 2 weeks of age predominantly included up-regulation of glycolysis/gluconeogenesis and down-regulation of the actin skeleton. This suggests a period of highly variable protein expression that precedes the visible HD phenotype. Although an up-regulation of glycolysis/gluconeogenesis-related protein alterations remained dominant during HD progression, late stage alterations at 12 weeks showed an up-regulation of proteins having proteasomal function. Our observations suggest that HD is characterized by a highly dynamic disease pathology not represented by linear protein concentration alterations over the course of the disease. Detailed time course studies for disease progression with emphasis on early and very early stages are important to understand disease pathology and determine the time for intervention when considering HD therapy.

Acknowledgments—We acknowledge the technical assistance by Janine Stuwe. We are indebted to Dr. Fanny Mochel for critically reading the manuscript and the valuable suggestions for improving the discussion of the data.

* This work was supported by the German Ministry for Education and Research (BMBF) within the National Genome Research Network (NGFN2) program.

This work is dedicated to the memory of our valued colleague and friend Maik A. Wacker who died too early in an accident.

S The on-line version of this article (available at http://www.mcponline.org) contains supplemental material.

§ Both authors contributed equally to this work.

¶ To whom correspondence should be addressed: Inst. for Human Genetics, Charité-Universitätsmedizin Berlin, Augustenburger Platz 1, 13353 Berlin, Germany. Tel.: 49-30-450-566258; Fax: 49-30-450-566904; E-mail: claus.zabel@charite.de.

REFERENCES

1. Wexler, N. S., Rose, E. A., and Housman, D. E. (1991) Molecular approaches to hereditary diseases of the nervous system: Huntington's disease as a paradigm. *Annu. Rev. Neurosci.* **14,** 503–529
2. The Huntington's Disease Collaborative Research Group (1993) A novel gene containing a trinucleotide repeat that is expanded and unstable on Huntington's disease chromosomes. *Cell* **72,** 971–983
3. McMurray, S. E., and McMurray, C. T. (2001) Huntington's disease. A sports star and a cook. *Lancet* **358,** (suppl.) S38
4. Rubinsztein, D. C., Leggo, J., Coles, R., Almqvist, E., Biancalana, V., Cassiman, J. J., Chotai, K., Connarty, M., Crauford, D., Curtis, A., Curtis, D., Davidson, M. J., Differ, A. M., Dode, C., Dodge, A., Frontali, M., Ranen, N. G., Stine, O. C., Sherr, M., Abbott, M. H., Franz, M. L., Graham, C. A., Harper, P. S., Hedreen, J. C., Jackson, A., Kaplan, J.-C., Losekoot, M., MacMillan, J. C., Morrison, P., Trottier, Y., Novelletto, A., Simpson, S. A., Theilmann, J., Whittaker, J. L., Folstein, S. E., Ross, C. A., and Hayden, M. R. (1996) Phenotypic characterization of individuals with 30–40 CAG repeats in the Huntington disease (HD) gene reveals HD cases with 36 repeats and apparently normal elderly individuals with 36–39 repeats. *Am. J. Hum. Genet.* **59,** 16–22
5. Bates, G. (2003) Huntingtin aggregation and toxicity in Huntington's disease. *Lancet* **361,** 1642–1644
6. Telenius, H., Kremer, H. P., Theilmann, J., Andrew, S. E., Almqvist, E., Anvret, M., Greenberg, C., Greenberg, J., Lucotte, G., Squitieri, F., Starr, A., Goldberg, Y. P., and Hayden, M. R. (1993) Molecular analysis of juvenile Huntington disease: the major influence on $(CAG)_n$ repeat length is the sex of the affected parent. *Hum. Mol. Genet.* **2,** 1535–1540
7. Waelter, S., Scherzinger, E., Hasenbank, R., Nordhoff, E., Lurz, R., Goehler, H., Gauss, C., Sathasivam, K., Bates, G. P., Lehrach, H., and Wanker, E. E. (2001) The huntingtin interacting protein HIP1 is a clathrin and α-adaptin-binding protein involved in receptor-mediated endocytosis. *Hum. Mol. Genet.* **10,** 1807–1817
8. Engelender, S., Sharp, A. H., Colomer, V., Tokito, M. K., Lanahan, A., Worley, P., Holzbaur, E. L., and Ross, C. A. (1997) Huntingtin-associated protein 1 (HAP1) interacts with the p150Glued subunit of dynactin. *Hum. Mol. Genet.* **6,** 2205–2212
9. Modregger, J., DiProspero, N. A., Charles, V., Tagle, D. A., and Plomann, M. (2002) PACSIN 1 interacts with huntingtin and is absent from synaptic varicosities in presymptomatic Huntington's disease brains. *Hum. Mol. Genet*. **11,** 2547–2558
10. Gervais, F. G., Singaraja, R., Xanthoudakis, S., Gutekunst, C. A., Leavitt, B. R., Metzler, M., Hackam, A. S., Tam, J., Vaillancourt, J. P., Houtzager, V., Rasper, D. M., Roy, S., Hayden, M. R., and Nicholson, D. W. (2002) Recruitment and activation of caspase-8 by the Huntingtin-interacting protein Hip-1 and a novel partner Hippi. *Nat. Cell Biol.* **4,** 95–105
11. Kim, Y. J., Yi, Y., Sapp, E., Wang, Y., Cuiffo, B., Kegel, K. B., Qin, Z. H., Aronin, N., and DiFiglia, M. (2001) Caspase 3-cleaved N-terminal fragments of wild-type and mutant huntingtin are present in normal and Huntington's disease brains, associate with membranes, and undergo calpain-dependent proteolysis. *Proc. Natl. Acad. Sci. U. S. A.* **98,** 12784–12789
12. Turmaine, M., Raza, A., Mahal, A., Mangiarini, L., Bates, G. P., and Davies,

S. W. (2000) Nonapoptotic neurodegeneration in a transgenic mouse model of Huntington's disease. *Proc. Natl. Acad. Sci. U. S. A.* **97,** 8093–8097
13. Goehler, H., Lalowski, M., Stelzl, U., Waelter, S., Stroedicke, M., Worm, U., Droege, A., Lindenberg, K. S., Knoblich, M., Haenig, C., Herbst, M., Suopanki, J., Scherzinger, E., Abraham, C., Bauer, B., Hasenbank, R., Fritzsche, A., Ludewig, A. H., Bussow, K., Coleman, S. H., Gutekunst, C. A., Landwehrmeyer, B. G., Lehrach, H., and Wanker, E. E. (2004) A protein interaction network links GIT1, an enhancer of huntingtin aggregation, to Huntington's disease. *Mol. Cell* **15,** 853–865
14. Kaltenbach, L. S., Romero, E., Becklin, R. R., Chettier, R., Bell, R., Phansalkar, A., Strand, A., Torcassi, C., Savage, J., Hurlburt, A., Cha, G. H., Ukani, L., Chepanoske, C. L., Zhen, Y., Sahasrabudhe, S., Olson, J., Kurschner, C., Ellerby, L. M., Peltier, J. M., Botas, J., and Hughes, R. E. (2007) Huntingtin interacting proteins are genetic modifiers of neurodegeneration. *PLoS Genet.* **3,** e82
15. Butte, A. (2002) The use and analysis of microarray data. *Nat. Rev. Drug Discov.* **1,** 951–960
16. Irizarry, R. A., Warren, D., Spencer, F., Kim, I. F., Biswal, S., Frank, B. C., Gabrielson, E., Garcia, J. G., Geoghegan, J., Germino, G., Griffin, C., Hilmer, S. C., Hoffman, E., Jedlicka, A. E., Kawasaki, E., Martinez-Murillo, F., Morsberger, L., Lee, H., Petersen, D., Quackenbush, J., Scott, A., Wilson, M., Yang, Y., Ye, S. Q., and Yu, W. (2005) Multiple-laboratory comparison of microarray platforms. *Nat. Methods* **2,** 345–350
17. Klose, J. (1999) Fractionated extraction of total tissue proteins from mouse and human for 2-D electrophoresis. *Methods Mol. Biol.* **112,** 67–85
18. Klose, J., and Kobalz, U. (1995) Two-dimensional electrophoresis of proteins: an updated protocol and implications for a functional analysis of the genome. *Electrophoresis* **16,** 1034–1059
19. Aebersold, R., and Mann, M. (2003) Mass spectrometry-based proteomics. *Nature* **422,** 198–207
20. Ong, S. E., and Mann, M. (2005) Mass spectrometry-based proteomics turns quantitative. *Nat. Chem. Biol.* **1,** 252–262
21. Chan, E. Y., Luthi-Carter, R., Strand, A., Solano, S. M., Hanson, S. A., DeJohn, M. M., Kooperberg, C., Chase, K. O., DiFiglia, M., Young, A. B., Leavitt, B. R., Cha, J. H., Aronin, N., Hayden, M. R., and Olson, J. M. (2002) Increased huntingtin protein length reduces the number of polyglutamine-induced gene expression changes in mouse models of Huntington's disease. *Hum. Mol. Genet.* **11,** 1939–1951
22. Kuhn, A., Goldstein, D. R., Hodges, A., Strand, A. D., Sengstag, T., Kooperberg, C., Becanovic, K., Pouladi, M. A., Sathasivam, K., Cha, J. H., Hannan, A. J., Hayden, M. R., Leavitt, B. R., Dunnett, S. B., Ferrante, R. J., Albin, R., Shelbourne, P., Delorenzi, M., Augood, S. J., Faull, R. L., Olson, J. M., Bates, G. P., Jones, L., and Luthi-Carter, R. (2007) Mutant huntingtin's effects on striatal gene expression in mice recapitulate changes observed in human Huntington's disease brain and do not differ with mutant huntingtin length or wild-type huntingtin dosage. *Hum. Mol. Genet.* **16,** 1845–1861
23. Luthi-Carter, R., Hanson, S. A., Strand, A. D., Bergstrom, D. A., Chun, W., Peters, N. L., Woods, A. M., Chan, E. Y., Kooperberg, C., Krainc, D., Young, A. B., Tapscott, S. J., and Olson, J. M. (2002) Dysregulation of gene expression in the R6/2 model of polyglutamine disease: parallel changes in muscle and brain. *Hum. Mol. Genet.* **11,** 1911–1926
24. Luthi-Carter, R., Strand, A., Peters, N. L., Solano, S. M., Hollingsworth, Z. R., Menon, A. S., Frey, A. S., Spektor, B. S., Penney, E. B., Schilling, G., Ross, C. A., Borchelt, D. R., Tapscott, S. J., Young, A. B., Cha, J. H., and Olson, J. M. (2000) Decreased expression of striatal signaling genes in a mouse model of Huntington's disease. *Hum. Mol. Genet.* **9,** 1259–1271
25. Luthi-Carter, R., Strand, A. D., Hanson, S. A., Kooperberg, C., Schilling, G., La Spada, A. R., Merry, D. E., Young, A. B., Ross, C. A., Borchelt, D. R., and Olson, J. M. (2002) Polyglutamine and transcription: gene expression changes shared by DRPLA and Huntington's disease mouse models reveal context-independent effects. *Hum. Mol. Genet.* **11,** 1927–1937
26. Hodges, A., Strand, A. D., Aragaki, A. K., Kuhn, A., Sengstag, T., Hughes, G., Elliston, L. A., Hartog, C., Goldstein, D. R., Thu, D., Hollingsworth, Z. R., Collin, F., Synek, B., Holmans, P. A., Young, A. B., Wexler, N. S., Delorenzi, M., Kooperberg, C., Augood, S. J., Faull, R. L., Olson, J. M., Jones, L., and Luthi-Carter, R. (2006) Regional and cellular gene expression changes in human Huntington's disease brain. *Hum. Mol. Genet.* **15,** 965–977
27. Runne, H., Kuhn, A., Wild, E. J., Pratyaksha, W., Kristiansen, M., Isaacs, J. D., Regulier, E., Delorenzi, M., Tabrizi, S. J., and Luthi-Carter, R. (2007) Analysis of potential transcriptomic biomarkers for Huntington's disease in peripheral blood. *Proc. Natl. Acad. Sci. U. S. A.* **104,** 14424–14429
28. Zabel, C., and Klose, J. (2004) Influence of Huntington's disease on the human and mouse proteome. *Int. Rev. Neurobiol.* **61,** 241–283
29. Zabel, C., Chamrad, D. C., Priller, J., Woodman, B., Meyer, H. E., Bates, G. P., and Klose, J. (2002) Alterations in the mouse and human proteome caused by Huntington's disease. *Mol. Cell. Proteomics* **1,** 366–375
30. Zabel, C., Sagi, D., Kaindl, A. M., Steireif, N., Klare, Y., Mao, L., Peters, H., Wacker, M. A., Kleene, R., and Klose, J. (2006) Comparative proteomics in neurodegenerative and non-neurodegenerative diseases suggest nodal point proteins in regulatory networking. *J. Proteome Res.* **5,** 1948–1958
31. Perluigi, M., Poon, H. F., Maragos, W., Pierce, W. M., Klein, J. B., Calabrese, V., Cini, C., De Marco, C., and Butterfield, D. A. (2005) Proteomic analysis of protein expression and oxidative modification in r6/2 transgenic mice: a model of Huntington disease. *Mol. Cell. Proteomics* **4,** 1849–1861
32. Mangiarini, L., Sathasivam, K., Seller, M., Cozens, B., Harper, A., Hetherington, C., Lawton, M., Trottier, Y., Lehrach, H., Davies, S. W., and Bates, G. P. (1996) Exon 1 of the HD gene with an expanded CAG repeat is sufficient to cause a progressive neurological phenotype in transgenic mice. *Cell* **87,** 493–506
33. Hockly, E., Woodman, B., Mahal, A., Lewis, C. M., and Bates, G. (2003) Standardization and statistical approaches to therapeutic trials in the R6/2 mouse. *Brain Res. Bull.* **61,** 469–479
34. Woodman, B., Butler, R., Landles, C., Lupton, M. K., Tse, J., Hockly, E., Moffitt, H., Sathasivam, K., and Bates, G. P. (2007) The Hdh(Q150/Q150) knock-in mouse model of HD and the R6/2 exon 1 model develop comparable and widespread molecular phenotypes. *Brain Res. Bull.* **72,** 83–97
35. Hartl, D., Irmler, M., Romer, I., Mader, M. T., Mao, L., Zabel, C., de Angelis, M. H., Beckers, J., and Klose, J. (2008) Transcriptome and proteome analysis of early embryonic mouse brain development. *Proteomics* **8,** 1257–1265
36. Klose, J. (1999) Large-gel 2-D electrophoresis. *Methods Mol. Biol.* **112,** 147–172
37. Berth, M., Moser, F. M., Kolbe, M., and Bernhardt, J. (2007) The state of the art in the analysis of two-dimensional gel electrophoresis images. *Appl. Microbiol. Biotechnol.* **76,** 1223–1243
38. Hartl, D., Rohe, M., Mao, L., Staufenbiehl, M., Zabel, C., and Klose, J. (2008) Impairment of adolescent hippocampal plasticity in a mouse model for Alzheimer's disease precedes disease phenotype. *PLoS ONE* **3,** e2759
39. Mao, L., Hartl, D., Nolden, T., Koppelstatter, A., Klose, J., Himmelbauer, H., and Zabel, C. (2008) Pronounced alterations of cellular metabolism and structure due to hyper- or hypo-osmosis. *J. Proteome Res.* **7,** 3968–3983
40. Mao, L., Zabel, C., Herrmann, M., Nolden, T., Mertes, F., Magnol, L., Chabert, C., Hartl, D., Herault, Y., Delabar, J. M., Manke, T., Himmelbauer, H., and Klose, J. (2007) Proteomic shifts in embryonic stem cells with gene dose modifications suggest the presence of balancer proteins in protein regulatory networks. *PLoS ONE* **2,** e1218
41. Diedrich, M., Mao, L., Bernreuther, C., Zabel, C., Nebrich, G., Kleene, R., and Klose, J. (2008) Proteome analysis of ventral midbrain in MPTP-treated normal and L1cam transgenic mice. *Proteomics* **8,** 1266–1275
42. Nebrich, G., Herrmann, M., Sagi, D., Klose, J., and Giavalisco, P. (2007) High MS-compatibility of silver nitrate-stained protein spots from 2-DE gels using ZipPlates and AnchorChips for successful protein identification. *Electrophoresis* **28,** 1607–1614
43. Strand, A. D., Baquet, Z. C., Aragaki, A. K., Holmans, P., Yang, L., Cleren, C., Beal, M. F., Jones, L., Kooperberg, C., Olson, J. M., and Jones, K. R. (2007) Expression profiling of Huntington's disease models suggests that brain-derived neurotrophic factor depletion plays a major role in striatal degeneration. *J. Neurosci.* **27,** 11758–11768
44. Davies, S. W., Turmaine, M., Cozens, B. A., DiFiglia, M., Sharp, A. H., Ross, C. A., Scherzinger, E., Wanker, E. E., Mangiarini, L., and Bates, G. P. (1997) Formation of neuronal intranuclear inclusions underlies the neurological dysfunction in mice transgenic for the HD mutation. *Cell* **90,** 537–548

45. Carter, R. J., Lione, L. A., Humby, T., Mangiarini, L., Mahal, A., Bates, G. P., Dunnett, S. B., and Morton, A. J. (1999) Characterization of progressive motor deficits in mice transgenic for the human Huntington's disease mutation. *J. Neurosci.* **19,** 3248–3257
46. Hoerndli, F., David, D. C., and Gotz, J. (2005) Functional Genomics meets neurodegenerative disorders. Part II: application and data integration. *Prog. Neurobiol.* **76,** 169–188
47. Strand, A. D., Aragaki, A. K., Baquet, Z. C., Hodges, A., Cunningham, P., Holmans, P., Jones, K. R., Jones, L., Kooperberg, C., and Olson, J. M. (2007) Conservation of regional gene expression in mouse and human brain. *PLoS Genet.* **3,** e59
48. Djousse, L., Knowlton, B., Cupples, L. A., Marder, K., Shoulson, I., and Myers, R. H. (2002) Weight loss in early stage of Huntington's disease. *Neurology* **59,** 1325–1330
49. Mochel, F., Charles, P., Seguin, F., Barritault, J., Coussieu, C., Perin, L., Le Bouc, Y., Gervais, C., Carcelain, G., Vassault, A., Feingold, J., Rabier, D., and Durr, A. (2007) Early energy deficit in Huntington disease: identification of a plasma biomarker traceable during disease progression. *PLoS ONE* **2,** e647
50. Cui, L., Jeong, H., Borovecki, F., Parkhurst, C. N., Tanese, N., and Krainc, D. (2006) Transcriptional repression of PGC-1α by mutant huntingtin leads to mitochondrial dysfunction and neurodegeneration. *Cell* **127,** 59–69
51. McGill, J. K., and Beal, M. F. (2006) PGC-1α, a new therapeutic target in Huntington's disease? *Cell* **127,** 465–468
52. Magistretti, P. J., Pellerin, L., Rothman, D. L., and Shulman, R. G. (1999) Energy on demand. *Science* **283,** 496–497
53. Rothman, D. L., Behar, K. L., Hyder, F., and Shulman, R. G. (2003) In vivo NMR studies of the glutamate neurotransmitter flux and neuroenergetics: implications for brain function. *Annu. Rev. Physiol.* **65,** 401–427
54. Fan, M. M., and Raymond, L. A. (2007) N-Methyl-D-aspartate (NMDA) receptor function and excitotoxicity in Huntington's disease. *Prog. Neurobiol.* **81,** 272–293
55. Li, J. Y., Plomann, M., and Brundin, P. (2003) Huntington's disease: a synaptopathy? *Trends Mol. Med.* **9,** 414–420
56. Weaver, A. M., Young, M. E., Lee, W. L., and Cooper, J. A. (2003) Integration of signals to the Arp2/3 complex. *Curr. Opin. Cell Biol.* **15,** 23–30
57. Li, Z., and Sheng, M. (2003) Some assembly required: the development of neuronal synapses. *Nat. Rev. Mol. Cell Biol.* **4,** 833–841
58. Coux, O., Tanaka, K., and Goldberg, A. L. (1996) Structure and functions of the 20S and 26S proteasomes. *Annu. Rev. Biochem.* **65,** 801–847
59. Voges, D., Zwickl, P., and Baumeister, W. (1999) The 26S proteasome: a molecular machine designed for controlled proteolysis. *Annu. Rev. Biochem.* **68,** 1015–1068
60. Zwickl, P., Voges, D., and Baumeister, W. (1999) The proteasome: a macromolecular assembly designed for controlled proteolysis. *Philos. Trans. R. Soc. Lond. B Biol. Sci.* **354,** 1501–1511
61. Bennett, E. J., Shaler, T. A., Woodman, B., Ryu, K. Y., Zaitseva, T. S., Becker, C. H., Bates, G. P., Schulman, H., and Kopito, R. R. (2007) Global changes to the ubiquitin system in Huntington's disease. *Nature* **448,** 704–708
62. Pickart, C. M. (2004) Back to the future with ubiquitin. *Cell* **116,** 181–190
63. Pickart, C. M., and Eddins, M. J. (2004) Ubiquitin: structures, functions, mechanisms. *Biochim. Biophys. Acta* **1695,** 55–72
64. Hershko, A., and Ciechanover, A. (1998) The ubiquitin system. *Annu. Rev. Biochem.* **67,** 425–479
65. Muchowski, P. J., and Wacker, J. L. (2005) Modulation of neurodegeneration by molecular chaperones. *Nat. Rev. Neurosci.* **6,** 11–22
66. Caughey, B., and Lansbury, P. T. (2003) Protofibrils, pores, fibrils, and neurodegeneration: separating the responsible protein aggregates from the innocent bystanders. *Annu. Rev. Neurosci.* **26,** 267–298
67. DiFiglia, M., Sapp, E., Chase, K. O., Davies, S. W., Bates, G. P., Vonsattel, J. P., and Aronin, N. (1997) Aggregation of huntingtin in neuronal intranuclear inclusions and dystrophic neurites in brain. *Science* **277,** 1990–1993
68. Zabel, C., Andreew, A., Mao, L., and Hartl, D. (2008) Protein expression overlap: more important than which proteins change in expression? *Expert Rev. Proteomics* **5,** 187–205
69. Burke, J. R., Enghild, J. J., Martin, M. E., Jou, Y. S., Myers, R. M., Roses, A. D., Vance, J. M., and Strittmatter, W. J. (1996) Huntingtin and DRPLA proteins selectively interact with the enzyme GAPDH. *Nat. Med.* **2,** 347–350
70. Kaindl, A. M., Sifringer, M., Zabel, C., Nebrich, G., Wacker, M. A., Felderhoff-Mueser, U., Endesfelder, S., von der Hagen, M., Stefovska, V., Klose, J., and Ikonomidou, C. (2006) Acute and long-term proteome changes induced by oxidative stress in the developing brain. *Cell Death Differ.* **13,** 1097–1109
71. Crocker, S. F., Costain, W. J., and Robertson, H. A. (2006) DNA microarray analysis of striatal gene expression in symptomatic transgenic Huntington's mice (R6/2) reveals neuroinflammation and insulin associations. *Brain Res.* **1088,** 176–186
72. Greene, N. D., Leung, K. Y., Wait, R., Begum, S., Dunn, M. J., and Copp, A. J. (2002) Differential protein expression at the stage of neural tube closure in the mouse embryo. *J. Biol. Chem.* **277,** 41645–41651
73. Zheng, P. Z., Wang, K. K., Zhang, Q. Y., Huang, Q. H., Du, Y. Z., Zhang, Q. H., Xiao, D. K., Shen, S. H., Imbeaud, S., Eveno, E., Zhao, C. J., Chen, Y. L., Fan, H. Y., Waxman, S., Auffray, C., Jin, G., Chen, S. J., Chen, Z., and Zhang, J. (2005) Systems analysis of transcriptome and proteome in retinoic acid/arsenic trioxide-induced cell differentiation/apoptosis of promyelocytic leukemia. *Proc. Natl. Acad. Sci. U. S. A.* **102,** 7653–7658
74. Mijalski, T., Harder, A., Halder, T., Kersten, M., Horsch, M., Strom, T. M., Liebscher, H. V., Lottspeich, F., de Angelis, M. H., and Beckers, J. (2005) Identification of coexpressed gene clusters in a comparative analysis of transcriptome and proteome in mouse tissues. *Proc. Natl. Acad. Sci. U. S. A.* **102,** 8621–8626
75. Gygi, S. P., Rochon, Y., Franza, B. R., and Aebersold, R. (1999) Correlation between protein and mRNA abundance in yeast. *Mol. Cell. Biol.* **19,** 1720–1730
76. Anderson, L., and Seilhamer, J. (1997) A comparison of selected mRNA and protein abundances in human liver. *Electrophoresis* **18,** 533–537
77. Steffan, J. S., Kazantsev, A., Spasic-Boskovic, O., Greenwald, M., Zhu, Y. Z., Gohler, H., Wanker, E. E., Bates, G. P., Housman, D. E., and Thompson, L. M. (2000) The Huntington's disease protein interacts with p53 and CREB-binding protein and represses transcription. *Proc. Natl. Acad. Sci. U. S. A.* **97,** 6763–6768
78. Dunah, A. W., Jeong, H., Griffin, A., Kim, Y. M., Standaert, D. G., Hersch, S. M., Mouradian, M. M., Young, A. B., Tanese, N., and Krainc, D. (2002) Sp1 and TAFII130 transcriptional activity disrupted in early Huntington's disease. *Science* **296,** 2238–2243
79. Luthi-Carter, R., Apostol, B. L., Dunah, A. W., DeJohn, M. M., Farrell, L. A., Bates, G. P., Young, A. B., Standaert, D. G., Thompson, L. M., and Cha, J. H. (2003) Complex alteration of NMDA receptors in transgenic Huntington's disease mouse brain: analysis of mRNA and protein expression, plasma membrane association, interacting proteins, and phosphorylation. *Neurobiol. Dis.* **14,** 624–636

DOI 10.1002/pmic.200700754 *Proteomics* 2008, *8,* 1266–1275

RESEARCH ARTICLE

Proteome analysis of ventral midbrain in MPTP-treated normal and L1cam transgenic mice

Madeleine Diedrich[1, 2], Lei Mao[1], Christian Bernreuther[3,4], Claus Zabel[1], Grit Nebrich[1], Ralf Kleene[5] and Joachim Klose[1]

[1] Institute for Human Genetics, Charité Universitätsmedizin Berlin, Berlin, Germany
[2] Freie Universität Berlin, Fachbereich Biologie, Chemie, Pharmazie, Germany
[3] Zentrum für Molekulare Neurobiologie, Institut für Biosynthese Neuraler Strukturen, Hamburg, Germany
[4] Institute for Neuropathology, University Medical Center Hamburg-Eppendorf, Hamburg, Germany
[5] Zentrum für Molekulare Neurobiologie, Universitätsklinikum Hamburg-Eppendorf, Hamburg, Germany

Treatment of mice by 1-methyl-4-phenyl-1,2,3,6-tetrahydropyridene hydrochloride (MPTP) is a well established animal model for Parkinson's disease (PD), while overexpression of L1 cell adhesion molecule (L1cam) has been proposed to attenuate the degeneration of dopaminergic neurons induced by MPTP. To gain insight into the role of L1cam in the pathomechanism of PD, we investigated protein expression patterns after MPTP-treatment in both C57BL/6 (wild-type) and transgenic mice overexpressing L1cam in astrocytes. Our results showed that during the acute phase, proteins in functional complexes responsible for mitochondrial, glycolysis, and cytoskeletal function were down-regulated in MPTP-treated wild-type mice. After a recovery phase, proteins that were down-regulated in the acute phase reverted to normal levels. In L1cam transgenic mice, a much higher number of proteins was altered during the acute phase and this number even increased after the recovery phase. Many proteins involved in oxidative phosphorylation were still down-regulated and glycolysis related protein were still up-regulated. This pattern indicates a lasting severely impaired energy production in L1cam mice after MPTP treatment.

Received: August 1, 2007
Revised: November 20, 2007
Accepted: November 21, 2007

Keywords:
MPTP / Parkinson disease / Transgene

1 Introduction

Parkinson's disease (PD) is one of the most common neurodegenerative disorders [1]. Approximately 3% of a population beyond the age of 65 years are affected by PD. One hallmark of PD is the degeneration of dopamine neurons in the *substantia nigra pars compacta*. An important clinical symptom is impaired motor function, manifested by resting tremor, rigidity, bradykinesia and postural instability [2]. Post mortem samples of affected brain areas of many affected individuals contain also Lewy bodies [1]. It has been demonstrated in previous studies that gene mutations in α-synuclein (PARK1), Parkin (PARK2), PTEN-induced kinase 1 (PINK1, PARK6) and DJ-1 (PARK7) lead to familial PD showing Mendelian inheritance patterns [3, 4]. However, the cause of sporadic PD, which accounts for 95% of all cases, is unknown.

1-Methyl-4-phenyl-1,2,3,6-tetrahydropyridene hydrochloride (MPTP) is a neurotoxin that causes PD-like symptoms in mammals and humans [5–9]. MPTP injection or consumption impairs motor function, decreases striatal dopamine levels as a result of degeneration and loss of dopaminergic neurons in the ventral mesencephalon (midbrain), predominantly in the *substantia nigra pars compacta* and ventral tegmental area. MPTP exerts its toxic effects on the

Correspondence: Professor Dr. Joachim Klose, Institut für Humangenetik, Charité – Universitätsmedizin Berlin, Augustenburgerplatz 1, D-13353 Berlin, Germany
E-mail: Joachim.klose@charite.de
Fax: +49-30-566904

Abbreviations: L1cam, L1 cell adhesion molecule; **MPTP,** 1-methyl-4-phenyl-1,2,3,6-tetrahydropyridene hydrochloride; **PD,** Parkinson's disease

dopaminergic nigrostriatal system by a cytotoxic metabolite, 1-methyl-4-phenylpridium ion (MPP^+), which is generated by monoamine oxidase B in astrocytes [6]. When delivered to neurons, MPP^+ is toxic to multiple types of neurons, among which dopaminergic neurons are the most susceptible. Within dopaminergic neurons, MPP^+ inhibits complex I of the mitochondrial electron transport chain and thus impairs oxidative phosphorylation. Impairment of oxidative phosphorylation results in leakage of ROS, and finally in the death of dopaminergic neurons [5–9].

L1 cell adhesion molecule (L1cam, L1) has been described to enhance neuronal survival and neurite outgrowth of dopaminergic neurons *in vitro* [10]. L1 acts as a homophilic cell adhesion molecule. When triggered by a *trans*-interacting L1 molecule from a neighbouring cell or in the extracellular matrix, L1 induces signal transduction in L1-expressing neurons, which results in cell survival and neuritogenesis [11, 12]. L1 is also involved in various aspects of synaptic plasticity. Defects in L1 expression cause reduced long-term potentiation and impaired learning and memory in transgenic mice [13]. Transgenic overexpression of L1 in astrocytes under the control of a murine glial fibrillary acidic protein (*GFAP*) promoter enhances homophilic interactions with neighbouring L1-expressing neurons, which in turn improved learning and memory [14].

Based on these findings we performed a proteome analysis [15–18] to identify differential protein expression in the acute phase of MPTP toxicity (1 day after MPTP injection) and after a recovery phase (7 days after MPTP treatment) by 2-DE and MS [19] using both C57BL/6 (wild-type) and L1cam transgenic C57BL/6 mouse midbrain samples. We were especially interested to identify how proteins were affected by MPTP treatment in these two different groups of mice and probe for a protective mechanism in L1cam mice.

2 Materials and methods

Animal experiments were carried out in accordance with State of Hamburg and European Community guidelines and were approved by University and State of Hamburg Animal Care Committees. Mice of C57BL/6J background (Charles River, Hanover, Germany) were used for this study. They were maintained in a 12 h light–dark cycle with free access to food and water.

2.1 Generation of transgenic mice

Standard molecular biology protocols were used for the generation of phGFAP-L1, a modified pKO-V924 plasmid (Lexicon genetics, The Woodlands, TX, USA) containing cDNA of murine full length L1 [20] controlled by a 2.2 kb fragment of the human glial fibrillary acidic protein promoter [21]. The 4.05 kb L1 cDNA contains the entire protein coding sequence and a 250 bp 3′-nontranslated region. A 6.5 kb fragment was excised from p924-hGFAP-L1 by *Not*I and *Hpa*I digestion, followed by electrophoresis and electroelution from an agarose gel. Purified DNA was diluted to a final concentration of 100 ng/mL in TE buffer (10 mM Tris-HCl, 0.2 mM EDTA, pH 7.5). Approximately 0.2 fg of DNA was injected into the male (strain CBA) pronucleus of fertilized (superovulated) C57BL/6J eggs. The eggs were subsequently transferred into oviducts of pseudopregnant foster mothers. The genotyping of transgenic mice was performed by PCR and Northern blot analysis. Before starting the experiments, heterozygous (CBAxC57BL/6J) females were backcrossed to C57Bl/6J for at least eight generations.

2.2 Drug treatment and tissue preparation

We used midbrain tissue from six male, 10–15-wk-old mice in each of the following groups: C57BL/6 1 day after treatment, C57BL/6 7 days after treatment, GFAP-L1 1 day after treatment and GFAP-L1 7 days after treatment. For drug treatment, MPTP hydrochloride (Sigma–Aldrich, Taufkirchen, Germany) was dissolved in saline and administered four times intraperitoneally at 2 h-intervals using 15 mg MPTP/kg body weight [8]. The control groups were matched for genetic background, sex and age and were injected with saline. Only L1cam transgene or wild type mice were compared to investigate how the introduction of a transgene affects MPTP treatment. Total brains were transferred into a mouse brain matrix (World Precision Instruments, Berlin, Germany) and two transversal cuts were performed through slots of the matrix that were 2 and 4 mm caudally from the optic chiasm. The tissue pieces were then placed on a precooled coverslip and the ventral midbrain was dissected from the 2-mm thick transverse slice by a horizontal cut along the middle of the midbrain. Subsequently, tissue sections were stored at –80°C until the protein extraction procedure was performed.

2.3 PCR analysis

Mice were tested for transgene integration by PCR analysis of genomic DNA isolated from tail biopsies. The PCR was performed using 5′-GTACCACCTGCCTCATGCAG-3′ and 5′-TCGTCCAGCGGAACTCCACT-3′ primers, which specifically recognize transgenic animals by amplifying a 500 bp fragment spanning the 3′-end of the human GFAP promoter and 5′-end of mouse L1 cDNA present only in transgenic animals. As internal control, a 1 kb fragment of genomic L1 DNA was amplified applying 5′-GGTAGGCAGGAGATAAGGTCA-3′ and 5′-CAGTCATTGATCCTGGAGTGC-3′ primers.

2.4 Northern blot analysis

Anesthetized adult mice (8-wk old) were sacrificed by a lethal dose of pentobarbital and brains were removed and immediately frozen in liquid nitrogen. Total cellular RNA was isolated applying RNeasy Mini kit (Qiagen, Hilden, Germany) according to manufacturer's instructions after pulverizing

the tissue in liquid nitrogen. RNA yields were estimated by absorbance at 260 nm. Fifteen micrograms of RNA were run on 1% agarose–formaldehyde gels for Northern blot analysis [22]. Randomly primed L1 cDNA probes were used to simultaneously detect endogenous L1 mRNA of 6 kb [23] and transgene-derived L1 mRNA of 4.2 kb. Human GFAP promotor drives expression in radial glia cells starting at day E13.5 and in astrocytes at later stages of development [21, 24]. We therefore used a glia cell specific promoter to direct expression of the neural cell adhesion molecule L1 to astrocytes and radial glia cells. Northern blot analysis of total RNA from the entire brain of transgenic animals revealed L1 transcripts of 4 kb for transgene-derived mRNA which are clearly distinct from the endogenous neuron-derived L1 mRNA of 6 kb (Fig. 1).

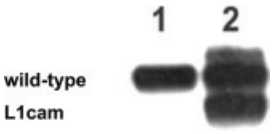

Figure 1. Northern blot analysis of an L1cam mouse showing transgene expression. Fifteen micrograms of total RNA from adult brains was loaded in each lane and probed with murine L1cam cDNA. Endogenous neuron-derived L1 mRNA resulted in a 6 kb band, whereas transgene-derived mRNA yielded a 4 kb signal. Lane 1, C57BL/6 wild-type (control); lane 2, L1cam transgenic animal.

2.5 Sample preparation for 2-DE

Midbrain total protein extracts for 2-DE were prepared for each sample separately as described previously ($n = 6$ for each group) [19]. Briefly, about 25 mg midbrain was ground in an Eppendorf tube submersed in liquid nitrogen adding 2.2 parts v/w of 50 mM Tris buffer (pH 70.5) containing 50 mM KCl, 20% v/v glycerol, 4% w/v CHAPS and a protease inhibitor cocktail (Complete™, according to manufacture's instruction, Roche Applied Science, Mannheim, Germany). Finally, a number of glass beads (1.5–1.7 mm diameter, Wolf Glaskugeln, Mainz, Germany) equivalent to 0.034 times of sample weight was added to the mixture and samples were sonicated six times (20 s each) in a water bath at 0°C. The resulting homogenate was stirred for 30 min at 4°C after adding 0.025 parts v/v DNase (Merck, Darmstadt, Germany). Subsequently, 6.5 mol/L urea and 2 mol/L thiourea was added to the sample. Total protein concentration was determined using a Roti-Nanoquant kit (Roth, Karlsruhe, Germany). Samples were stored at −80°C or analysed immediately.

2.6 2-D DIGE and protein pattern evaluation

Our sample labelling did not include Cy2. We labelled both our controls and treated samples with Cy3 and a pooled sample with Cy5. The pooled sample consisted of equal amounts of protein from each sample used in an experiment [25]. This control pool was used as internal standard to match controls to treated samples by our 2-D gel evaluation software. Cy3/Cy5 cross overlabelling was therefore unnecessary. Eighty micrograms control, treated and pooled protein samples were labelled for 2-D DIGE with Cy5 or Cy3 according the manufacturer's instructions for CyDye DIGE Flours minimal dyes for Ettan DIGE (GE Healthcare, Munich, Germany). Proteins were separated by 2-DE as described previously [19, 26]. The gel format was 40 cm (IEF) × 30 cm × 1.5 mm (SDS-PAGE). Capillary tube gels for IEF were prepared with a special mixture of carrier ampholytes covering a pH range of 3.5–9.5. The gels were scanned using a Typhoon 9400 laser scanner (GE Healthcare). Image analysis was performed with Delta2D software (version 3.4, DECODON, Greifswald, Germany). Sixteen bit tiff grey scale images were imported into the program. Delta2D software contains a special feature to handle DIGE gels which was employed to process the gels. Cy5 samples (pooled samples) were used as standard and matched to each other. A fusion image was generated and employed for spot detection. After manual spot editing to reduce the number of inaccurate spots, the spot pattern was transferred to all images in the project. Subsequently, Student's *t*-test (unpaired) was used to determine the significance of group-to-group difference. Differences were considered to be statistically significant when $p<0.05$. Only proteins with over 10% expression change compared to controls were used for further analysis. SD for relative spot intensities was reported in this study (Supporting Information Table S1).

2.7 Protein identification using MS

A total of 500 μg mouse midbrain protein was used for protein identification as described previously [16]. Briefly, proteins were separated by 2-DE and visualized using MS-compatible silver staining [27]. Protein spots of interest were excised from the 2-DE gel and in-gel trypsin digestion was performed. Tryptic fragments were analysed either by a Reflex IV MALDI-TOF mass spectrometer (Bruker Daltonics, Bremen, Germany) or LCQ Deca XP nano-HPLC/ESI IT mass spectrometer (Thermo Fisher Scientific, Waltham, MA, USA). Mass spectra were analysed using in-house licensed MASCOT (version 2.1, Matrix Science, London, UK) by automatic searches in NCBI nonredundant databases restricted to taxonomy *Mus musculus*. Search parameters allowed for one miscleavage, for oxidation of methionine and propionamidation of cysteine. Criteria for positive identification of proteins with MS were set according to the probability based MOWSE score algorithm delineated in MASCOT [28].

3 Results

In the current study, protein expression patterns of mouse midbrain at two different time points after MPTP-treatment were compared in wild-type and transgenic mice over-

expressing L1cam. Sham treated mice matched for age, sex and presence of transgene were used as controls. Differences in protein expression kinetics after MPTP treatment dependent on the L1cam transgene were determined. Both mouse models were of the same genetic background (C57BL/6). Around 4500 protein spots could be reproducibly detected in each 2-DE pattern. This enabled us to obtain genius expression alterations induced by MPTP between analytical time points and between mouse strains. In Fig. 2, representative 2-DE protein patterns of each of the experimental groups are shown in parallel.

A comparative proteomics approach across four different groups of mice revealed 459 protein spots-of-interests. All these protein spots were subjected to mass spectrometric protein identification. Among them, 118 protein spots contained more than one protein according to MASCOT evaluations. Although all protein identifications are presented in the Supporting Information table (Table S1) protein spots containing considerable protein mixtures were not taken into account in the subsequent analysis due to their ambiguous nature.

A comparison of MPTP- and saline-treated wild-type mice at 1 day after treatment revealed 153 differentially expressed protein spots. MPTP-treatment induced increased expression of 66 and decreased expression of 87 protein spots (Fig. 2a, Table 1). Among the variant spots, 102 were successfully identified and represent 36 distinct proteins (Table 1). Seven days after MPTP-application, 99 protein spots showed altered expression in treated wild-type mice. 45 protein spots increased and 54 decreased in their expression. Forty-eight of the differentially expressed protein spots were identified and constitute 30 distinct proteins.

L1cam transgenic mice showed 443 differentially expressed protein spots 1 day after MPTP treatment. Among them, 127 were increased and 316 decreased in expression as compared to untreated controls. A total of 114 protein spots were identified, representing 46 different proteins. Seven days after MPTP-treatment 665 differentially expressed spots were found in treated L1cam transgenic mouse. Two hundred and seventy-seven protein spots were up- and 388 down-regulated in expression. 195 protein spots could be identified. They represent 72 distinct proteins (Fig. 2d, Table 1). Figure 2e summarizes the number of up- or down-regulated proteins under different experimental conditions.

Figure 2e shows that wild-type mice of 1 day after MPTP-treatment displayed a considerable difference in the number of up- and down-regulated protein spots (66 up-regulated *vs.* 87 down-regulated protein spots). Interestingly, this difference was drastically reduced on day 7 after MPTP-treatment, accompanied by a drastic decline in the number of altered proteins (153 at 1 day *vs.* 99 at 7 days). Comparing the consequences of MPTP treatment for wild-type and transgenic mice it is obvious that significantly more proteins were altered in L1cam transgenic than in wild-type mice (252 *vs.* 1108 for wild-type and transgenic mice, respectively). Specifically, more than twice as much down-regulated than up-regulated protein spots were detected in treated L1cam mice. When comparing the two time points investigated, the number of variant proteins in transgenic mice continued to increase from days 1 to 7 after MPTP-treatment, with a persisting large difference in the number of up- and down-regulated proteins. A similar phenomenon was not observed in treated wild-type mice.

Subsequently, we examined whether there was an overlap in protein expression alteration between the different conditions (different time points after drug treatment, transgene yes/no). A comparison of both time points from both mouse strains to each other revealed no common protein alteration (Table 2, bottom). However, three proteins were consistently dysregulated in MPTP-treated wild-type

Table 1. Number of proteins differently expressed at 1 and 7 days after MPTP-treatment in wild-type and L1cam mice

Mouse model treated with MPTP ($n = 6$)		Number of altered spots	
Wild-type	1d	66	↑
		87	↓
	7d	45	↑
		54	↓
L1cam	1d	127	↑
		316	↓
	7d	277	↑
		388	↓

↓ down-regulation, ↑ up-regulation; sham treated control mice served as reference to determine up- or down-regulation of spot intensity.

Table 2. Number of protein spots with cochanged expression

Comparison	Number of altered spots
Between two models	
Wild-type 1d *vs.* wild-type 7d	3
Wild-type 1d *vs.* L1cam 1d	14
Wild-type 1d *vs.* L1cam 7d	11
Wild-type 7d *vs.* L1cam 1d	2
Wild-type 7d *vs.* L1cam 7d	8
L1cam 1d *vs.* L1cam 7d	49
Between three models	
Wild-type 1d *vs.* wild-type 7d *vs.* L1cam 1d	0
Wild-type 1d *vs.* wild-type 7d *vs.* L1cam 7d	1
Wild-type 1d *vs.* L1cam 1d *vs.* L1cam 7d	11
Wild-type 7d *vs.* L1cam 1d *vs.* L1cam 7d	2
Wild-type 1d *vs.* wild-type 7d *vs.* L1cam 1d *vs.* L1cam 7d	0

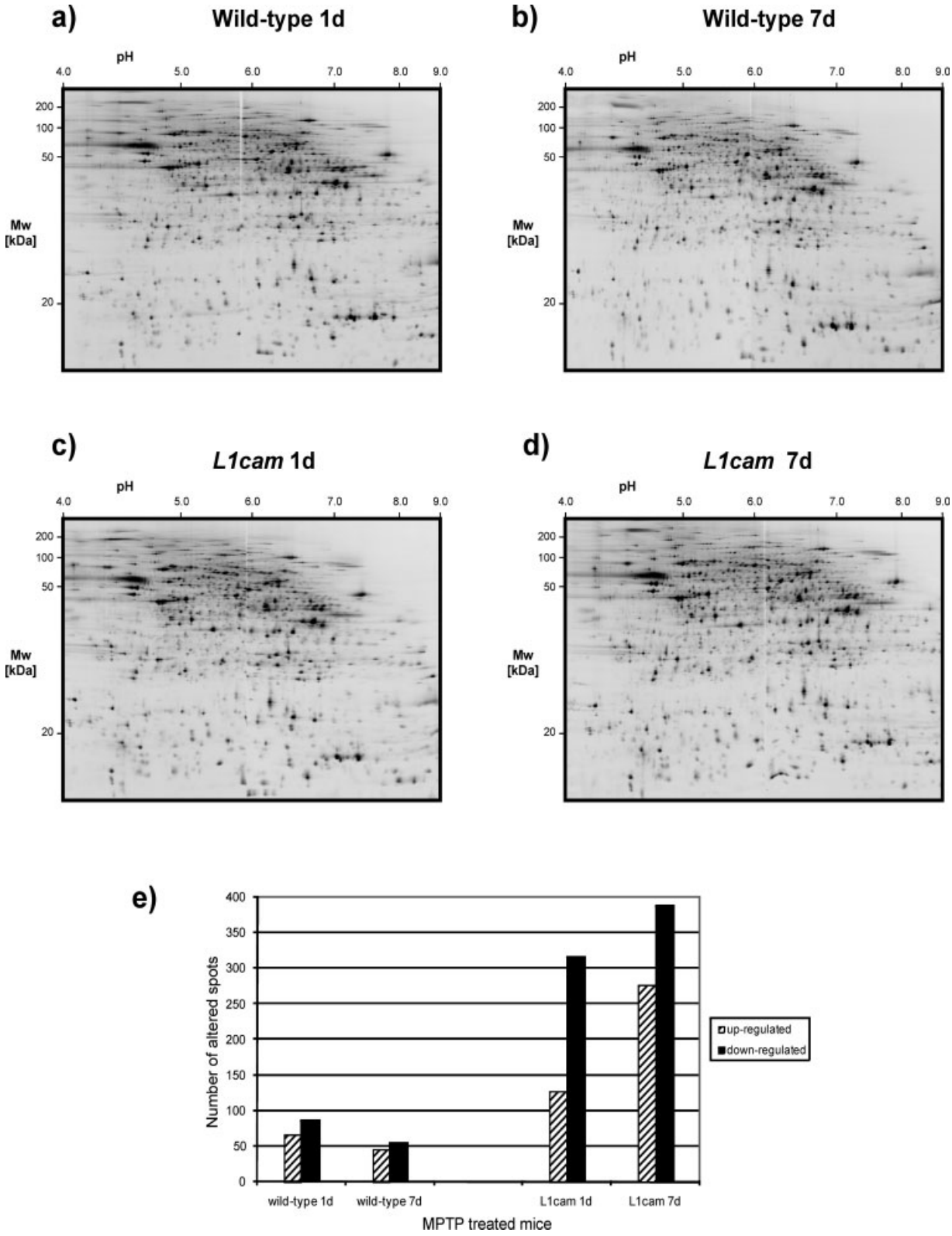

Figure 2. Large-gel 2-DE of the mouse midbrain proteome. Representative Cy3 stained 2-DE pattern of (a) a C57BL/6 mouse brain extract, 1 day and (b) 7 days after MPTP-treatment; (c) a L1cam transgenic mouse, 1 day and (d) 7 days after treatment are shown. (e) Bar charts showing the number of up- and down-regulated proteins on days 1 and 7 after MPTP-treatment in wild-type and L1cam transgenic mice. Saline-treated groups were used as control.

mice regardless of time point of investigation. More significantly, a much larger number of protein variants (49 protein spots) were commonly altered in MPTP-treated transgenic mice, independent of time after treatment. In addition, six distinct proteins cochanged in expression in the following three groups: L1cam transgenic mice 1 and 7 days after treatment, and wild-type mice 1 day after treatment (Tables 2 and 3). The expression fold changes of all altered protein spots are summarized in Table S1 of Supporting Information.

Differentially expressed proteins detected in this study were now subjected to an analysis determining their functional and structural category annotation [29]. Using the Uni-Prot Knowledgebase, we calculated the percentage of changed proteins that belonged to each category among all changed proteins. The following three categories were strongly enriched in our set of variant categories: 'mitochondrial proteins', 'cytoskeletal proteins' and 'proteins involved in neurogenesis' (Fig. 3). In wild-type mice, the fraction of mitochondrial proteins increased from 1 (13%) to 7 days after MPTP-treatment (27%). The percentage of cytoskeletal proteins decreased from 1 (7%) to 7 days after treatment (2%). In contrast, the percentages of proteins that are involved in neurogenesis remained constant at both time points (2%). Rather different results were obtained for L1cam transgenic mice: The percentage of mitochondrial proteins was similar at both days 1 (28%) and 7 (25%) after MPTP-treatment, The percentage of cytoskeletal proteins remained the same (5%) between the two time points investigated. However, proteins involved in neurogenesis increased from 1 to 3% as time after MPTP-treatment progressed.

4 Discussion

In an attempt to define the molecular targets of MPTP induced pathology at the protein expression level, and to investigate the effect of L1cam on the MPTP response, we investigated proteins that were dysregulated in ventral midbrain of MPTP-treated wild-type and transgenic mice. The transgenic mice neural cell adhesion molecule L1cam was overexpressed. Our high resolution large-gel 2-DE technique offered us a uniform and reproducible platform to investigate the extent to which MPTP modifies protein expression in these two mouse models. Importantly C57BL/6 mice but not L1cam transgenic mice did recover after MPTP treatment as determined by the number of differentially expressed proteins.

A standard MPTP injection protocol results in an acute reduction of locomotor activity in mice, which returns to normal levels after about 4 days [6, 7, 30]. This phenomenon has been attributed to a potential regeneration of the nigrostriatal dopaminergic system, despite a persistent reduction in the number of (TH positive) dopaminergic cell bodies [5]. In order to capture the kinetics of this process, we collected and analysed samples from both acute phase of impairment (1 day after injection) and after a recovery phase (7 days post-treatment). This approach gave us a novel opportunity to study the influence of a transgene on MPTP pathology at two different stages of pathology. At this point we did not focus on differences between C57BL/6 and L1cam mice since the aim of this study was to establish or refute differential protein expression kinetics after MPTP caused by L1cam.

Table 3. Overview of cochanged proteins in midbrain samples of MPTP-treated mice

Comparison	Protein name	Gene name	Expression
Wild-type 1d *vs.* 7d	Voltage-dependent anion channel 1	Vdac1	Higher
	Creatine kinase brain	Ckb	Higher
	Phosphofructokinase, platelet	Pfkp	Lower
L1cam 1d *vs.* 7d	Synuclein, beta	Sncb	Lower
	Peroxidase	Prdx2	Lower
	Pyruvate kinase muscle	Pkm2	Higher
	Phosphofructokinase, muscle	Pfkm	Higher
	Cytochrome *c* oxidase subunit 5A, mitochondrial precursor	Cox 5a	Lower
	ATP synthase, H^+ transporting, mitochondrial F1 complex, alpha subunit, isoform 1	Atp5a1	Lower
	Vacuolar H^+ ATPase E1	Atp6v1e1	Lower
	Atp5b protein	Atp5b	Lower
	ATPase, H^+ transporting, V1 subunit F	Atp6v1f	Lower
Wild-type 1d *vs.* L1cam 1d and L1cam 7d	Small nuclear ribonucleoprotein polypeptide F	Snrpf	Lower
	A-synuclein	Snca	Lower
	Stathmin1	Stmn1, 4 isoforms	Lower
	Actin related protein 2/3 complex, subunit 5-like	Arpc5l	Lower
	Transketolase	Tkt	Higher in L1cam Lower in wild-type
	Tubulin polymerization-promoting protein	Tppp, 3 isoforms	Lower

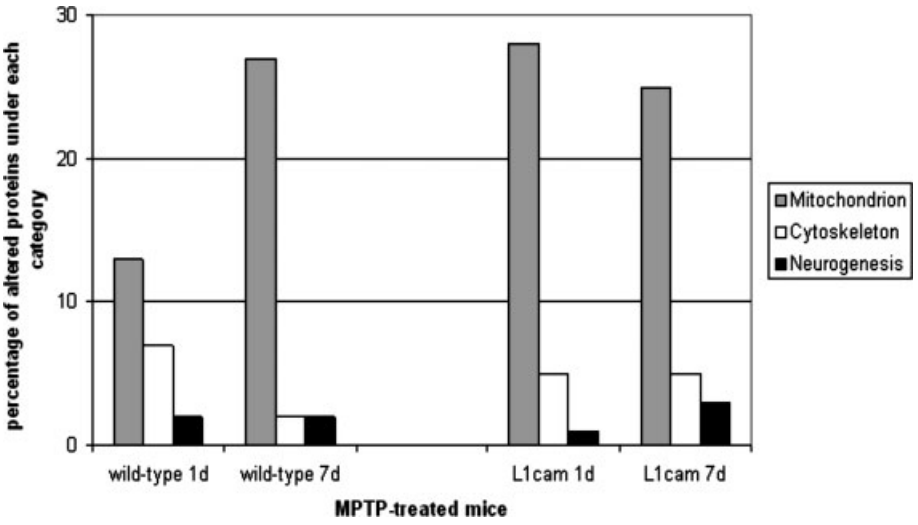

Figure 3. Percentage of proteins with altered expression profile in MPTP-treated mice assigned to different cellular compartmental and functional categories. 1d wild-type: C57BL/6 mice, 1 day after treatment; 7d wild-type: C57BL/6 mice, 7 days after treatment; 1d L1cam: L1cam transgenic mice, 1 day after treatment; 7d L1cam: L1cam transgenic mouse, 7 days after treatment.

In wild-type mice, there was a considerable difference in the numbers of up- and down-regulated proteins during the acute phase. However, 7 days after treatment, the total number of variant proteins decreased and the number of up- and down-regulated proteins was balanced again. This could be considered as an indication of a recovery, which is in line with previous observations on the regeneration of the nigrostriatal dopaminergic system during a recovery phase [5]. In contrast, the number of variant proteins in MPTP-treated transgenic mice was, at day 1, three-fold that of treated wild-type mice; and at day 7, even seven times higher compared to treated wild-type. Furthermore, the discrepancy between the number of up- and down-regulated proteins was much higher in treated transgenic than in wild-type mice. This discrepancy persisted throughout our investigation. These observations indicate a much stronger response to MPTP in transgenic than in wild-type mice. These transgenic mice showed virtually no tendency towards normalization within the recovery phase. In summary, our current observations clearly oppose previous descriptions on the protective effect of L1cam on PD pathology [14].

As has been described previously, overexpression of endogenous proteins alone could be sufficient to cause neurodegeneration [31], possibly due to a disturbed cellular homeostasis. The drug treatment on mice overexpressing L1cam could require additional compensatory efforts of the affected tissue. This may explain an exaggerated response of L1cam-transgenic mice to MPTP-treatment. In an alternative scenario, the increased number of differentially expressed proteins could be due to a protective response which does not manifest itself readily at the level of molecular phenotype – that is the identities of the proteins do not suggest the type of response. To gain insight into the molecular basis of this observation, we sorted the variant proteins according to their functional categories.

4.1 Mitochondrial dysfunction

In the transgenic as well as wild-type mice a significant number of mitochondrial proteins were down-regulated during the acute phase after MPTP-treatment. This confirms previous observations that MPTP targets predominantly mitochondrial proteins [4, 32]. This altered expression was much more pronounced in the L1cam transgenic mice, which showed a larger number of down-regulated mitochondrial proteins after MPTP-treatment. Specifically, a significant number of variant proteins detected in the transgenic mice during the recovery phase were involved in oxidative phosphorylation. Among them, *Atp5a1*, *Atp6v1e1*, *Atp5b* and *Atp6v1f* are subunits of the respiratory complex V, whereas *COX5a* is a component of complex IV. All five proteins, which are downstream to complex I (the primary target of MPTP) were decreased in expression compared to saline-treated controls. This may suggest that a decrease in ATP production by oxidative phosphorylation could be more prevalent in treated transgenic mice.

4.2 Glycolysis pathway

In MPTP-treated wild-type mice, numerous proteins of the glycolysis pathway were altered at both time points. For instance, *Pkm2* and *Pfkc* were both up-regulated after MPTP-treatment. Similar observations have already been made by Ryu *et al.* [33, 34], who reported previously that several glycolysis genes, including *G6pd*, *Pfkc*, *Pkm2* and *Ldha*, were up-regulated in a PD induced by 6-OHDA. These authors proposed that an up-regulation of glycolysis related genes compensates a decrease in ATP production, which is a result of mitochondrial dysfunction in PD. In the same line of evidence, the down-regulation of glycolysis after MPTP-treatment conforms well with a previous finding of Fornai, who observed that glucose uptake was increased in MPTP-treated

mice [35]. It is noteworthy that more proteins of the glycolysis pathway were up-regulated in transgenic mice than in wild-type mice during the recovery phase. This could indicate a stronger impairment of oxidative phosphorylation in these mice which will result in a decrease of ATP production.

4.3 Cytoskeleton

A substantial number of cytoskeletal proteins maintaining cell structure were down-regulated in the acute phases of both wild-type and transgenic mice. In contrast, a divergent regulation was observed during the recovery phase. For instance, tubulins (*Tuba2*, *Tuba4a* and *Tuba1a*) were consistently down-regulated in the acute phase of wild-type mice. During the recovery phase, *Tuba1c*, *Tuba1a* and a capping protein of actin filament (*Capzb*) were up-regulated. Contrary to this, tubulin proteins remained down-regulated in L1cam transgenic mice throughout the experiment. Tubulin is involved in microtubule-mediated cell movement [33]. Decreased expression of tubulin has also been described in the substantia nigra of human PD, postmortem brains [36, 37] or in dopaminergic cells after oxidative stress [38]. The up-regulation of tubulin in wild-type mice may be closely related to cytoskeleton mediated structural recovery mechanisms within the affected brain region after MPTP-treatment. This sign of recovery was absent in L1cam transgenic mice.

4.4 Ubiquitin pathway

One of the consistent findings across all MPTP-treated mice was a down-regulation of proteins involved in the ubiquitin pathway. Several genes causative for PD are tightly involved in the ubiquitin-proteasome pathway. Among them, *Parkin* and *UCH-L1* are two prominent examples which, when mutated, may cause familial PD [17, 39]. Here, we observed that alpha-synuclein, an interaction partner of *UCH-L1*, was down-regulated during the acute phase in wild-type mice and at both time points in L1cam transgenic mice. Alpha synuclein is known to be involved in the formation of Lewy bodies in PD [40]. Tanaka *et al.* [41] described that expression of a mutant alpha synuclein led to neuronal cell death through mitochondrial abnormalities. To our current knowledge, no Lewy-body related pathology has been described in PD models induced by transient MPTP-treatment. However, continuous administration of MPTP induced neuronal inclusions in substantia nigra and locus coeruleus that are characteristic of PD [35]. These authors suggested that chronic MPTP toxicity caused prolonged inhibition of the mitochondrial respiratory chain and ubiquitin-proteasome activity, which could be prerequisites for the formation of inclusion bodies. Down-regulation of alpha synuclein in MPTP-treated mice may suggest that the dysregulation of the ubiquitin-proteasome pathway in PD was common to both MPTP induced PD models investigated.

4.5 Neurogenesis

Several proteins that are important for neurogenesis (*e.g. Stmn1* and *Dpysl2*) were down-regulated at both time points in MPTP-treated wild-type mice. A more complicated phenomenon was observed in L1cam transgenic mice: in the acute phase, *Ulip2* was up-regulated and *Stmn1* down-regulated. During the recovery phase, three neurogenesis-associated proteins (*Stmn1*, *Ina* and *Gap43*) were down-regulated, whereas *Dpysl2* was up-regulated. Stathmin is necessary for tubulin polymerization and microtubule assembly, which is essential for mitosis-related processes [42]. If there is a decrease in microtubule growth and assembly, the mitotic spindle cannot be formed which results in cell cycle arrest [42]. In this study, four different isoforms of this protein detected on the 2-DE gels were persistently down-regulated in MPTP-treated mice. These findings are in line with the persistent reduction of dopaminergic cell bodies in MPTP-treated mice described previously [5]. Notice that stathmin is known to have at least 12 phosphorylated and unphosphorylated isoforms [43, 44]. This hints that MPTP might induce certain dysfunctions mediated by protein PTM, rather than at the level of transcription. Moreover, this reiterates the notion that all protein variations found in our 2-DE experiments could be the result of changes of protein isoforms and not the total protein.

In summary, MPTP-treatment disrupts multiple cellular pathways such as glycolysis, cytoskeleton, ubiquitin system and neurogenesis. Moreover, wild-type mice may be much better protected against a MPTP insult than L1cam mice. Apart from profound proteomic alterations, L1cam transgenic mice respond to MPTP with a stronger impairment of oxidative phosphorylation, and less apparent tubulin remodelling in the recovery phase. All these findings indicate that the transgenic mice are less efficient in coping with MPTP toxicity.

The authors acknowledge the excellent technical assistance of Bettina Esch and Andrea Koppelstätter. This work was cosupported by the German Ministry for Education and Research (BMBF) within the German National Genome Research Network 2 (NGFN2) program and by the German Research Foundation (DFG) SFB577.

The authors have declared no conflict of interest.

5 References

[1] Smeyne, R. J., Jackson-Lewis, V., The MPTP model of Parkinson's disease. *Brain Res. Mol. Brain Res.* 2005, *134*, 57–66.

[2] Dauer, W., Przedborski, S., Parkinson's disease: Mechanisms and models. *Neuron* 2003, *39*, 889–909.

[3] Bossy-Wetzel, E., Schwarzenbacher, R., Lipton, S. A., Molecular pathways to neurodegeneration. *Nat. Med.* 2004, *10*, S2–S9.

[4] Dawson, T. M., Dawson, V. L., Molecular pathways of neurodegeneration in Parkinson's disease. *Science* 2003, *302*, 819–822.

[5] Mitsumoto, Y., Watanabe, A., Mori, A., Koga, N., Spontaneous regeneration of nigrostriatal dopaminergic neurons in MPTP-treated C57BL/6 mice. *Biochem. Biophys. Res. Commun.* 1998, *248*, 660–663.

[6] Sedelis, M., Hofele, K., Auburger, G. W., Morgan, S. *et al.*, MPTP susceptibility in the mouse: Behavioral, neurochemical, and histological analysis of gender and strain differences. *Behav. Genet.* 2000, *30*, 171–182.

[7] Mori, A., Ohashi, S., Nakai, M., Moriizumi, T., Mitsumoto, Y., Neural mechanisms underlying motor dysfunction as detected by the tail suspension test in MPTP-treated C57BL/6 mice. *Neurosci. Res.* 2005, *51*, 265–274.

[8] Schober, A., Classic toxin-induced animal models of Parkinson's disease: 6-OHDA and MPTP. *Cell. Tissue Res.* 2004, *318*, 215–224.

[9] Ohashi, S., Mori, A., Kurihara, N., Mitsumoto, Y., Nakai, M., Age-related severity of dopaminergic neurodegeneration to MPTP neurotoxicity causes motor dysfunction in C57BL/6 mice. *Neurosci. Lett.* 2006, *401*, 183–187.

[10] Hulley, P., Schachner, M., Lubbert, H., L1 neural cell adhesion molecule is a survival factor for fetal dopaminergic neurons. *J. Neurosci. Res.* 1998, *53*, 129–134.

[11] Loers, G., Chen, S., Grumet, M., Schachner, M., Signal transduction pathways implicated in neural recognition molecule L1 triggered neuroprotection and neuritogenesis. *J. Neurochem.* 2005, *92*, 1463–1476.

[12] Maness, P. F., Schachner, M., Neural recognition molecules of the immunoglobulin superfamily: Signaling transducers of axon guidance and neuronal migration. *Nat. Neurosci.* 2007, *10*, 19–26.

[13] Law, J. W., Lee, A. Y., Sun, M., Nikonenko, A. G. *et al.*, Decreased anxiety, altered place learning, and increased CA1 basal excitatory synaptic transmission in mice with conditional ablation of the neural cell adhesion molecule L1. *J. Neurosci.* 2003, *23*, 10419–10432.

[14] Wolfer, D. P., Mohajeri, H. M., Lipp, H. P., Schachner, M., Increased flexibility and selectivity in spatial learning of transgenic mice ectopically expressing the neural cell adhesion molecule L1 in astrocytes. *Eur. J. Neurosci.* 1998, *10*, 708–717.

[15] Zabel, C., Chamrad, D. C., Priller, J., Woodman, B. *et al.*, Alterations in the mouse and human proteome caused by Huntington's disease. *Mol. Cell. Proteomics* 2002, *1*, 366–375.

[16] Zabel, C., Sagi, D., Kaindl, A. M., Steireif, N. *et al.*, Comparative proteomics in neurodegenerative and non-neurodegenerative diseases suggest nodal point proteins in regulatory networking. *J. Proteome Res.* 2006, *5*, 1948–1958.

[17] Palacino, J. J., Sagi, D., Goldberg, M. S., Krauss, S. *et al.*, Mitochondrial dysfunction and oxidative damage in parkin-deficient mice. *J. Biol. Chem.* 2004, *279*, 18614–18622.

[18] Zabel, C., Klose, J., Influence of Huntington's disease on the human and mouse proteome. *Int. Rev. Neurobiol.* 2004, *61*, 241–283.

[19] Klose, J., Kobalz, U., Two-dimensional electrophoresis of proteins: an updated protocol and implications for a functional analysis of the genome. *Electrophoresis* 1995, *16*, 1034–1059.

[20] Moos, M., Tacke, R., Scherer, H., Teplow, D. *et al.*, Neural adhesion molecule L1 as a member of the immunoglobulin superfamily with binding domains similar to fibronectin. *Nature* 1988, *334*, 701–703.

[21] Nolte, C., Matyash, M., Pivneva, T., Schipke, C. G. *et al.*, GFAP promoter-controlled EGFP-expressing transgenic mice: A tool to visualize astrocytes and astrogliosis in living brain tissue. *Glia* 2001, *33*, 72–86.

[22] Thomas, P. S., Hybridization of denatured RNA and small DNA fragments transferred to nitrocellulose. *Proc. Natl. Acad. Sci. USA* 1980, *77*, 5201–5205.

[23] Tacke, R., Moos, M., Teplow, D. B., Fruh, K. *et al.*, Identification of cDNA clones of the mouse neural cell adhesion molecule L1. *Neurosci. Lett.* 1987, *82*, 89–94.

[24] Malatesta, P., Hartfuss, E., Gotz, M., Isolation of radial glial cells by fluorescent-activated cell sorting reveals a neuronal lineage. *Development* 2000, *127*, 5253–5263.

[25] Kultima, K., Scholz, B., Alm, H., Skold, K. *et al.*, Normalization and expression changes in predefined sets of proteins using 2D gel electrophoresis: A proteomic study of L-DOPA induced dyskinesia in an animal model of Parkinson's disease using DIGE. *BMC Bioinformatics* 2006, *7*, 475.

[26] Klose, J., Genotypes and phenotypes. *Electrophoresis* 1999, *20*, 643–652.

[27] Nebrich, G., Herrmann, M., Sagi, D., Klose, J., Giavalisco, P., High MS-compatibility of silver nitrate-stained protein spots from 2-DE gels using ZipPlates and AnchorChips for successful protein identification. *Electrophoresis* 2007, *28*, 1607–1614.

[28] Pappin, D. J., Hojrup, P., Bleasby, A. J., Rapid identification of proteins by peptide-mass fingerprinting. *Curr. Biol.* 1993, *3*, 327–332.

[29] Boeckmann, B., Bairoch, A., Apweiler, R., Blatter, M. C. *et al.*, The SWISS-PROT protein knowledgebase and its supplement TrEMBL in 2003. *Nucleic Acids Res.* 2003, *31*, 365–370.

[30] Mitsumoto, Y., Mori, A., Ohashi, S., Nakai, M., Moriizumi, T., Differential effects of 1-methyl-4-phenyl-1,2,3,6-tetrahydropyridine in the olfactory bulb and the striatum in mice. *Neurosci. Res.* 2005, *51*, 111–115.

[31] Zoghbi, H. Y., Botas, J., Mouse and fly models of neurodegeneration. *Trends Genet.* 2002, *18*, 463–471.

[32] Beal, M. F., Experimental models of Parkinson's disease. *Nat. Rev. Neurosci.* 2001, *2*, 325–334.

[33] Kim, J. M., Lee, K. H., Jeon, Y. J., Oh, J. H. *et al.*, Identification of Genes Related to Parkinson's Disease Using Expressed Sequence Tags. *DNA Res.* 2006 *13*, 275–286.

[34] Ryu, E. J., Angelastro, J. M., Greene, L. A., Analysis of gene expression changes in a cellular model of Parkinson disease. *Neurobiol. Dis.* 2005, *18*, 54–74.

[35] Fornai, F., Schluter, O. M., Lenzi, P., Gesi, M. *et al.*, Parkinson-like syndrome induced by continuous MPTP infusion: Convergent roles of the ubiquitin-proteasome system and alpha-synuclein. *Proc. Natl. Acad. Sci. USA* 2005, *102*, 3413–3418.

[36] Grunblatt, E., Mandel, S., Jacob-Hirsch, J., Zeligson, S. *et al.*, Gene expression profiling of parkinsonian substantia nigra pars compacta; alterations in ubiquitin-proteasome, heat shock protein, iron and oxidative stress regulated proteins, cell adhesion/cellular matrix and vesicle trafficking genes. *J. Neural. Transm.* 2004, *111*, 1543–1573.

[37] Noureddine, M. A., Li, Y. J., van der Walt, J. M., Walters, R. *et al.*, Genomic convergence to identify candidate genes for Parkinson disease: SAGE analysis of the substantia nigra. *Mov. Disord.* 2005, *20*, 1299–1309.

[38] Yoo, M. S., Chun, H. S., Son, J. J., DeGiorgio, L. A. *et al.*, Oxidative stress regulated genes in nigral dopaminergic neuronal cells: Correlation with the known pathology in Parkinson's disease. *Brain Res. Mol. Brain Res.* 2003, *110*, 76–84.

[39] Mizuno, Y., Hattori, N., Yoshino, H., Hatano, Y. *et al.*, Progress in familial Parkinson's disease. *J. Neural. Transm. Suppl.* 2006, 191–204.

[40] Dawson, T. M., Parkin and defective ubiquitination in Parkinson's disease. *J. Neural. Transm. Suppl.* 2006, 209–213.

[41] Tanaka, Y., Engelender, S., Igarashi, S., Rao, R. K. *et al.*, Inducible expression of mutant alpha-synuclein decreases proteasome activity and increases sensitivity to mitochondria-dependent apoptosis. *Hum. Mol. Genet.* 2001, *10*, 919–926.

[42] Rubin, C. I., Atweh, G. F., The role of stathmin in the regulation of the cell cycle. *J. Cell. Biochem.* 2004, *93*, 242–250.

[43] Beretta, L., Dobransky, T., Sobel, A., Multiple phosphorylation of stathmin. Identification of four sites phosphorylated in intact cells and in vitro by cyclic AMP-dependent protein kinase and p34cdc2. *J. Biol. Chem.* 1993, *268*, 20076–20084.

[44] Munton, R. P., Tweedie-Cullen, R., Livingstone-Zatchej, M., Weinandy, F. *et al.*, Qualitative and quantitative analyses of protein phosphorylation in naive and stimulated mouse synaptosomal preparations. *Mol. Cell. Proteomics* 2007, *6*, 283–293.

RESEARCH ARTICLE

Transcriptome and proteome analysis of early embryonic mouse brain development

Daniela Hartl[1], Martin Irmler[2]*, Irmgard Römer[1], Michael T. Mader[3], Lei Mao[1], Claus Zabel[1], Martin Hrabé de Angelis[2, 4], Johannes Beckers[2, 4] and Joachim Klose[1]*

[1] Institute for Human Genetics, Charité – University Medicine Berlin, Berlin, Germany
[2] Institute for Experimental Genetics, Helmholtz Zentrum München, German Research Center for Environmental Health, Neuherberg, Germany
[3] Institute of Stem Cell Research, Helmholtz Zentrum München, German Research Center for Environmental Health, Neuherberg, Germany
[4] Technical University Munich, Center of Life and Food Sciences Weihenstephan Chair of Experimental Genetics, Weihenstephan, Germany

Received: July 26, 2007
Revised: October 26, 2007
Accepted: November 1, 2007

Mouse embryonic brain development involves sequential differentiation of multipotent progenitors into neurons and glia cells. Using microarrays and large 2-DE, we investigated the mouse brain transcriptome and proteome of embryonic days 9.5, 11.5, and 13.5. During this developmental period, neural progenitor cells shift from proliferation to neuronal differentiation. As expected, we detected numerous expression changes between all time points investigated, but interestingly, the rate of alteration remained in a similar range within 2 days of development. Furthermore, up- and down-regulation of gene products was balanced at each time point which was also seen at embryonic days 16–18. We hypothesize that during embryonic development, the rate of gene expression alteration is rather constant due to limited cellular resources such as energy, space, and free water. A similar complexity in terms of expressed genes and proteins suggests that changes in relative concentrations rather than an increase in the number of gene products dominate cellular differentiation. In general, expression of metabolism and cell cycle related gene products was down-regulated when precursor cells switched from proliferation to neuronal differentiation (days 9.5–11.5), whereas neuron specific gene products were up-regulated. A detailed functional analysis revealed their implication in differentiation related processes such as rearrangement of the actin cytoskeleton as well as *Notch*- and *Wnt*-signaling pathways.

Keywords:
Differentiation / Embryonic brain development / Neural progenitor cells / Transcriptome

1 Introduction

Neurons and glia located in the mammalian CNS are generated by neural progenitor cells (NPC) in a stepwise differentiation process. In early mouse brain development (expansion phase), NPCs increase in number by mitotic divisions. At embryonic day 11.5 (E11.5), NPCs make a switch from expansion to neurogenesis when an NPC subset starts to differentiate into neurons and self-renews simultaneously *via* asymmetric divisions. In later stages, NPCs switch to symmetrical divisions, producing only neurons. Glia cells are generated as early as E17 although the bulk of gliogenesis occurs after birth [1–3]. Thus, proliferation and neuronal differentiation occur simultaneously during the neurogenic phase whereas the former dominates in earlier stages. Proliferation of precursor cells is a key process nec-

Correspondence: Professor Joachim Klose, Institute for Human Genetics, Charité – University Medicine Berlin, Augustenburger Platz 1, D-13353 Berlin, Germany
E-mail: joachim.klose@charite.de
Fax: +49-30-450-566904

Abbreviations: GO, Gene Ontology; **NPC,** neural progenitor cells; **TCTP,** translationally controlled tumor protein

* These authors contributed equally to this work.

essary to produce a sufficient number of cells for brain development. Hence, many complex cellular mechanisms have been shown to be involved in the spatiotemporal orchestration of proliferation *versus* differentiation of NPCs (reviewed in Ref. [4]). However, our understanding of neuronal and glial differentiation is still limited.

The investigation of these mechanisms is of great interest, *e.g.*, because neurogenesis was shown to be implicated in neurodegenerative diseases such as Alzheimer's disease, Parkinson's disease, and Huntington's disease [5].

In this study, gene expression during early embryonic mouse brain development was investigated at the transcriptome and proteome level, focusing on the shift from NPC expansion to neurogenesis. For transcriptome analysis, we used whole genome Affymetrix GeneChips, containing about 45 000 probesets. For proteome analysis, two dimensional DIGE combined with MS was applied. We analyzed protein and mRNA abundance at E9.5 where mostly undifferentiated NPCs are present, E11.5 with NPCs starting to differentiate into neurons, and E13.5 when neurogenesis is peaking [1, 2]. Interestingly, we found that total protein concentration as well as the number of transcripts remained constant during differentiation. Moreover, the number of gene products altered in expression during 2 days of development was similar. Our results contribute to understanding the dynamic processes involved in neurogenesis.

2 Materials and methods

2.1 Embryonic tissue collection

Pregnant C57Bl/6 mice were sacrificed according to the German Animal Protection Act to obtain embryonic mouse brain tissue. Heads of embryos were cut following a straight line delineated by the following two positions: *postotocyst* until just past the *mandible anlage*. Embryonic head tissue was shock frozen in liquid nitrogen and stored at –80°C until protein or mRNA extraction was performed. Embryos were staged according to somite number and morphological criteria. For proteome analysis, two pooled samples containing 12 embryo heads each were prepared for E9.5, E11.5, and E13.5, respectively.

2.2 Transcriptome analysis

2.2.1 RNA isolation

Total RNA was isolated employing the Lipid Rich Tissue Mini kit (Qiagen). Briefly, Qiazol reagent was added to frozen tissue, followed immediately by Ultraturrax homogenization. After purification the RNA was incubated with DNase (turbo DNA-free, Ambion) and RNA quality was assessed using the RNA 600 Pico Assay (Agilent).

2.2.2 Expression profiling

High quality total RNA (1 μg) was amplified with the MessageAmp II-Biotin Enhanced Single Round aRNA Amplification kit (Ambion) according to manufacturer's instructions. Amplified aRNA (10 μg) was hybridized on Affymetrix MOE430 2.0 GeneChips® containing about 45 000 probesets. Staining and scanning were done according to the Affymetrix expression protocol. In total, 16 embryo heads distributed over three developmental stages (six heads at E9.5, four at E11.5, and six at E13.5) were analyzed.

2.2.3 Statistical transcriptome analysis

Statistical analysis of the microarrays was performed by utilizing the statistical programming environment R (R Development Core Team [6]), using packages available from http://cran.r-project.org and mips.gsf.de/mips/staff/mader/software. Briefly, probeset summaries were calculated according to RMA. A log-scale transformation (log, basis 2) using normalization against mean of all E9.5 samples employing the loess smoother [7] operating on M-A scale was carried out. Genewise testing for differential expression with Welch's *t*-test and Benjamini–Hochberg multiple testing correction (FDR$<$0.05), and application of nonstringent filters for basal expression and fold-change (mean$\geq$100, ratios of means$\geq$1.5, both on linear scale) was used.

2.3 cDNA synthesis and quantitative PCR analysis

cDNA was synthesized from the RNA samples used for microarray analysis using the SuperScript II First-Strand Synthesis System (Invitrogen). Real-time PCRs (qPCR) were performed according to the manufacturer's recommendations using Power SYBR Green PCR Master Mix (Applied Biosystems) on an Applied Biosystems 7300 System. Primer dimer melting temperatures were determined in order to exclude primer dimers from the analysis. The housekeeping gene Uqcrfs1 [8] was used for normalization of the target gene's expression. A second gene (Lrrc41) was selected as housekeeping gene based on its constant expression in our array data and performed similar to Uqcrfs (data not shown). Three biological replicates were used for each embryonic stage and typical ratios from multiple experiments are shown. Primer sequences are given for forward (F) and reverse (R) primers:

Uqcrfs1 (F: ACCTGTTCTGGATGTGAAGC, R: ACCTTGACATCTGTATGGGAAA), Lrrc41 (F: GAGGATTCTTCCTCTTCTCTCTGT, R: CAGTTCTGGAAGAGGCGTAG), *Notch1* (F: AACAAGGACATGCAGAACAAC, R: CAACACTTTGGCAGTCTCATAG), Rhoa (F: GACTCCAGAAGTCAAGCATTTC, R: ATCTCTGCCTTCTTCAGGTTTTAC), Cdc42 (F: ACAAACAGAAGCCTATTACTCCAG, R: ATTCTTTAGGCC-TTTCTGTGTGAG), Hes5 (F: GTCAGC-

TACCTGAAACACAGC, R: AGTAGCC-CTCGCTGTAGT-CCT), Neurog1 (F: CTTAAAAAGGAGCCACAAGGAGT, R: ATA-GCTATGCTAGCACTCAGGTTC), Neurog2 (F: CTCT-CTGATGTGCACTTTGTTT, R: ACTTCTAACCTGGCCCT-CTAAC).

2.4 Proteome analysis

2.4.1 Protein extraction and labeling

Protein extracts were prepared from individual embryo heads and pooled in two samples. Due to small sample size, E9.5 tissue material was pooled before protein extraction. Our published protein extraction procedure [9] was slightly altered. Briefly, tissue was ground to fine powder in a sample tube precooled in liquid nitrogen and only one part v/w of sample buffer (50 mM TRIZMA Base (Sigma–Aldrich, Steinheim, Germany), 50 mM KCl and 20% w/v glycerol at pH 7.5) was added. Samples were labeled by Cy3 minimal dye (GE Healthcare, Munich, Germany). An E11.5 pool sample aliquot was used as internal standard and labeled by Cy5 minimal dye (GE Healthcare). Labeling was carried out according to manufacturer's instructions adding 400 pmol fluorescent dye *per* 50 μg of protein. Each Cy3-labeled sample was mixed with the same amount of internal standard. The protein extracts were mixed with 70 mM DTT (BioRad, Munich, Germany), 2% v/w of ampholyte mixture Servalyte pH 2–4 (Serva, Heidelberg, Germany) and stored at −80°C. For protein spot counting in 2-D gels (Fig. 1), saturation dye labeled E9.5 and E11.5 samples were utilized (Cy3, GE Healthcare).

2.4.2 2-DE

Protein samples were separated by the large-gel 2-DE technique developed in our laboratory as described previously [10]. The gel format was 40 cm (IEF) × 30 cm (SDS-PAGE) × 1.0 mm (gel width). For visualization of protein spots, gels were scanned at a resolution of 100 μm using a 532 nm and 633 nm laser for Cy3 and Cy5 labeled samples, respectively (Typhoon 9400, GE Healthcare).

2.4.3 Spot evaluation procedure

Protein spot patterns were evaluated by Delta2D imaging software version 3.4 (Decodon, Greifswald, Germany). Briefly, spot patterns of in-gel standards were matched using the Delta2D "exact" mode matching protocol. Using "union" mode a fusion image was generated, including the visible spots from all 2-D gels within the project. The fusion image was used for spot detection (settings: local background region 100, average spot size 1, sensitivity 100%) followed by manual spot editing. A spot pattern containing 2004 protein spots was transferred from the fusion image to all other 2-D gel images to make sure that the spot identification number for each spot is the same for every gel in the project. Relative spot volume intensities (fractions of 100%) were used for quantitative protein expression analysis. After background extraction, normalized values were exported in spreadsheet format from Delta2D for statistical analysis. Data sets were analyzed applying a one-way ANOVA. Subsequently individual groups were compared by a Bonferroni *post hoc* test (SPSS version 14.0, Chicago, USA). Sample size comprised $n = 6$ for E9.5, $n = 8$ for E11.5, and $n = 5$ for E13.5.

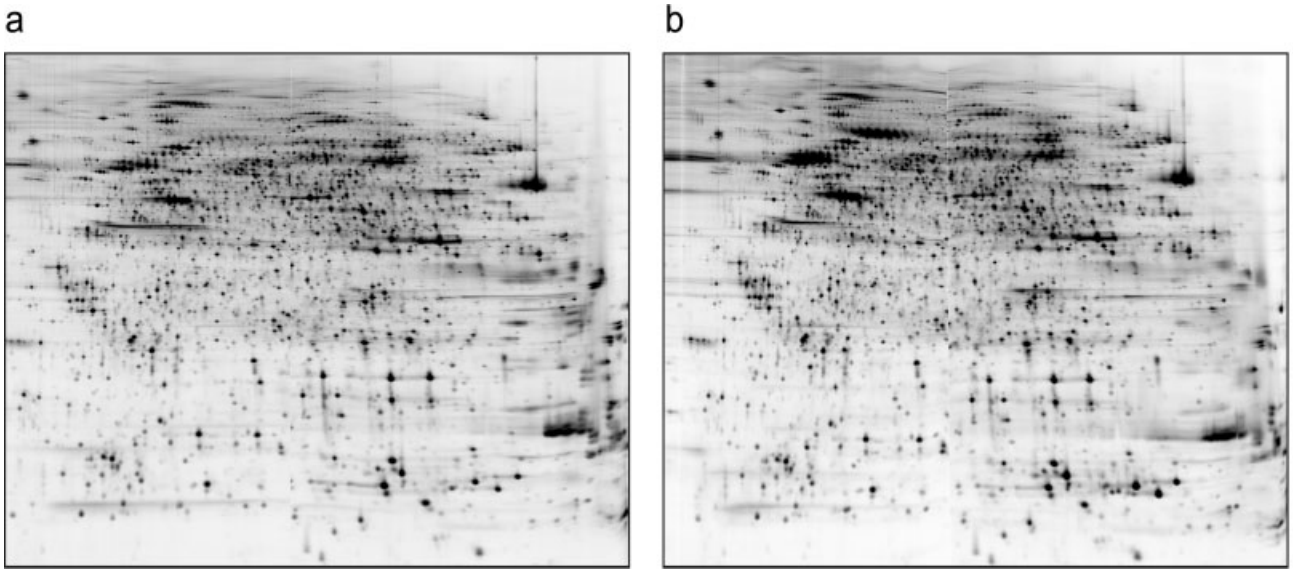

Figure 1. CyDye labeled 2-DE patterns of brain proteins from mouse embryos at stages E9.5 (a) and E11.5 (b). The complexity of the protein patterns is similar between stages; 3.350 protein spots are visible at E9.5 and 3.147 at E11.5, respectively.

2.4.4 Protein identification

For protein identification by MS, 40 μL extract was separated by 2-DE and stained using an MS-compatible silver staining protocol [11]. In order to assign corresponding protein spots from analytical fluorescent to quantitative silver stained 2-D gels, spot patterns were matched using Delta2D. Protein spots of interest were excised from 2-D gels and subjected to in-gel tryptic digestion. Peptides were analyzed by a Reflex 4 MALDI-TOF mass spectrometer (Bruker Daltonics, Bremen, Germany) as described previously [11]. Alternatively, ESI-MS and -MS/MS on an LCQ Deca XP ion trap (Thermo Finnigan, Waltham, MA) was applied. Mass spectra were analyzed using our in-house MASCOT software package license version 2.1 automatically searching NCBI databases. MS/MS ion search was performed with this set of parameters: (i) taxonomy: *Mus musculus,* (ii) proteolytic enzyme: trypsin, (iii) maximum of accepted missed cleavages: 1, (iv) mass value: monoisotopic, (v) peptide mass tolerance 0.8 Da, (vi) fragment mass tolerance: 0.8 Da, and (vii) variable modifications: oxidation of methionine and acrylamide adducts (propionamide) on cysteine. Only proteins with scores corresponding to $p<0.05$, with at least two peptides identified in two independent identifications were considered. Furthermore, theoretical and practical molecular weight and p*I* for each protein identified by database search were compared. Our results are summarized in Supporting Information Table 6.

2.4.5 Immunoblotting

Brain protein extracts were separated using 12% SDS-PAGE gels, blotted to PVDF membranes and probed with anti-TCTP; (Abcam, Cambridge, UK), anti-RhoA and anti-NICD (Cell Signaling, Danvers, MA, USA) antibodies according to standard immunoblotting procedures. Protein concentration was determined using a Roti-Nanoquant assay (Carl Roth, Karlsruhe, Germany).

2.4.6 Analysis of correlation and biological functions

Official gene symbols and gene names (MGI, http://www.informatics.jax.org/) were used to match our transcriptome and proteome datasets. Only differentially expressed probesets and protein spots (between embryonic stages) which were statistically significant were compared. CarmaWeb [12] was used for enrichment analysis of statistically significant Gene Ontology (GO) terms ($p<0.05$) for transcriptome data. Where indicated, groups of functionally related GO terms were defined with biological expert knowledge (Supporting Information Table1). Genes were tested for significant enrichment in a group by a hypergeometric distribution requiring that any of four entry counts was larger than two. For proteome data, GOTM [13] tools were used. To conduct hypergeometric probability analysis ($p\leq0.01$), protein groups were analyzed for the expected number of members as compared to a mouse genome reference gene set supplied by GOTM.

3 Results

3.1 Analysis of mRNA and protein abundance

Mouse brain development at embryonic stages E9.5, E11.5, and E13.5 was investigated using large-scale methods in mRNA and protein analysis. To study changes in gene expression at the transcriptome level, whole genome Affymetrix MOE 430 2.0 GeneChips were used. Cluster analysis of the data separated the three embryonic stages into three clusters according to their age (Supporting Information Fig. 1). Further statistical analyses to detect differentially expressed genes revealed 4311 significantly ($p<0.1$) regulated probesets between E9.5 and E11.5. These probesets accounted to about 10% of all probesets available on an array and correspond to 3426 individual genes. When comparing E11.5–E13.5 a similar number of alterations was found (4683 probesets; 12%; Table 1, Supporting Information Table 2).

To analyze overall signal distribution, we investigated the number of probesets detected at various expression levels. We observed that among embryonic stages, the expression distribution was remarkably similar (Fig. 2). We detected 7640, 7585, and 7592 probesets with an expression level higher than 250 arbitrary units for E9.5, E11.5, and E13.5, respectively. Probeset numbers with an expression level >2000 units were also very similar (821, 855, and 861) showing a maximum difference of $<5\%$. Therefore, we conclude that the complexity of the transcriptome was similar at all embryonic stages.

For proteome analysis, we used our large 2-DE method in combination with DIGE. First of all, the total number of protein spots on fluorescence stained 2-DE gels was counted (Fig. 1) to determine proteome complexity. We found similar spot numbers on gels of all three stages investigated (3560 ± 649 spots at E9.5, 3832 ± 166 spots at E11.5, and 3769 ± 107 spots at E13.5).

Using Delta2D, 2004 protein spots were quantified on every gel at stages E9.5, E11.5, and E13.5. Statistical analysis

Table 1. Numbers of proteins and mRNAs altered in expression among stages

Stages of development compared	% of protein spots altered in expression	
	Up-regulation	Down-regulation
E 9.5 *vs.* E 11.5	11.08	7.68
E 11.5 *vs.* E 13.5	7.88	7.19
E 16 *vs.* E 18	8.67	7.88
E 9.5 *vs.* E 13.5	15.42	13.92
	% of probesets altered in expression	
E 9.5 *vs.* E 11.5	5.70	3.88
E 11.5 *vs.* E 13.5	5.12	6.49
E 9.5 *vs.* E 13.5	7.51	6.49

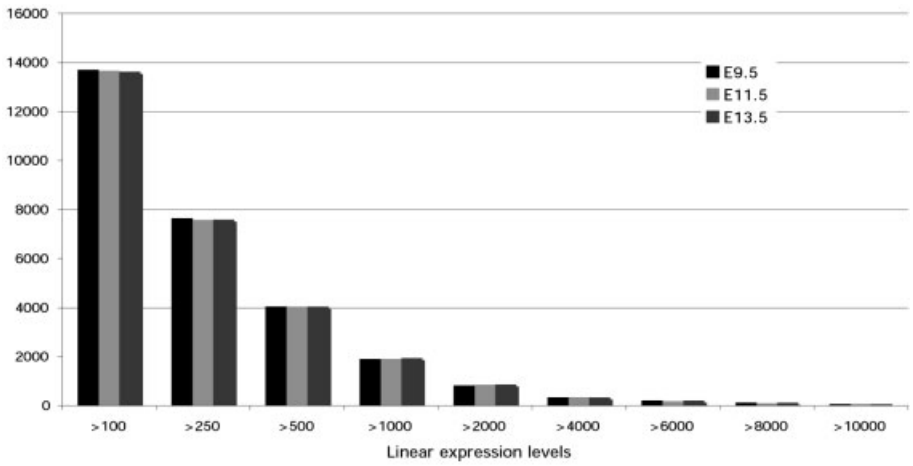

Figure 2. mRNA expression levels in mouse developmental stages E9.5, E11.5, and E13.5. Numbers of expressed probesets are shown. The *x*-axis indicates discrete, expression level cut-offs.

(one-way ANOVA, $p \leq 0.05$) revealed 379 (19%) proteins significantly altered in expression in E11.5 compared to E9.5; 302 (15%) altered proteins in E13.5 compared to E11.5; and 588 (29%) alterations in E13.5 compared to E9.5 (Table 1). Interestingly, we obtained similar results when we analyzed two additional stages, E16 and E18 (4430 protein spots were analyzed, 733 or 17% were altered in expression) using silver staining of gels and Proteomweaver (Definiens AG, Munich, Germany, version 3.2.0.5) analysis software (data not shown). In total, about 17% of all proteins were altered in expression within 2 days of embryonic development, which was consistently found between all time points investigated.

Then we determined spot volumes (relative quantity of a protein spot in gray units on the 2-DE gel without background noise) of all significantly altered protein spots. We found no statistically relevant difference (Students *t*-test; $p<0.05$) among total volumes (equivalent to the total protein amount) altered between E9.5 and E11.5 (48.8 $\pm$ 3.1 gray units at E9.5 *vs.* 52.2 $\pm$ 2.0 gray units at E11.5), indicating that up- and down-regulated proteins were in equilibrium. Similar results were obtained comparing E11.5–E13.5 (37.3 $\pm$ 1.9 gray units at E11.5 and 41.4 $\pm$ 2.6 gray units at E13.5) and E9.5–E13.5 (79.8 $\pm$ 4.8 gray units at E9.5 and 78.3 $\pm$ 3.3 gray units at E13.5), respectively. When total spot volumes altered in the first (E9.5–E11.5) and second (E11.5–E13.5) developmental step were considered, we found that a significantly higher spot volume was changed in the former compared to the latter step (50.5 $\pm$ 3.1 gray units or 13% at E9.5/E11.5 and 39.4 $\pm$ 3.0 gray units or 10% at E11.5/E13.5), although the number of altered proteins was similar. When comparing the sum of all spot volumes among embryonic stages, no significant difference was detected (400.9 $\pm$ 0.8 gray units). In summary, our results indicate that up- and down-regulation of protein expression was in equilibrium between all stages although total volume alteration was slightly larger between E9.5 and E11.5 than E11.5 and E13.5.

3.2 Correlation analysis of gene and protein expression

We randomly selected 300 protein spots from our 2-DE gels for identification by MS. Identified protein spots were equally distributed among p*I*-values and molecular masses on 2-DE gels and assigned to 213 different proteins (Supporting Information Table 6). Within this dataset, 72 proteins were significantly ($p<0.05$) altered in expression between E9.5 and E11.5 (21 up- and 51 down-regulated), 51 proteins (25 up- and 26 down-regulated) between E11.5 and E13.5 and 72 proteins (27 up- and 45 down-regulated) between E9.5 and E13.5 whereas 119 proteins remained unchanged.

Then it was determined if alterations in gene expression were consistent between protein and mRNA data (Fig. 3; details in Supporting Information Tables 3–5). Therefore, probesets were matched to proteins according to their gene names. We found a remarkable 60–70% coregulation between mRNA and protein data. Only 20–30% showed a clear opposite regulation. A small percentage of mRNAs and proteins showed ambiguous regulation, that is, two protein spots of the same protein showed opposite regulation and consequently a probeset and one or more protein spots but not all were coregulated.

3.3 Functional analysis of protein and mRNA data

GO term analysis was used to estimate biological functions of our mRNA/protein data. Comparison of mRNA expression between E9.5 and E11.5 revealed a prominent increase in GO terms associated with neurogenesis and associated functions, such as axon outgrowth, dendrite morphogenesis, and synapse formation among transcripts with higher abundance in E11.5. Pathways implicated in differentiation processes like *Notch*- and *Wnt*-signaling were also enriched in E11.5. In contrast, metabolic pathway and cell cycle associated GO terms were enriched among transcripts with increased abundance at E9.5 (Fig. 4a). Analysis of E13.5 *vs.*

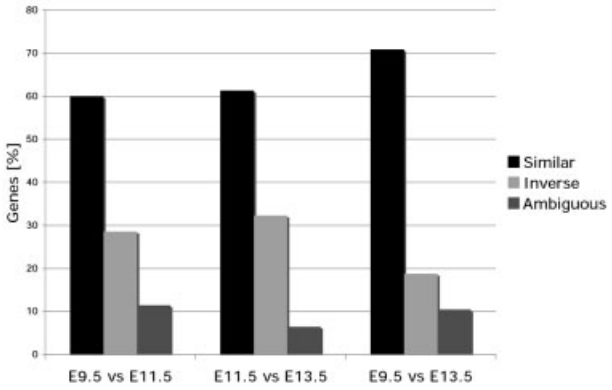

Figure 3. Comparison of transcriptome and proteome data. Mouse brains at E9.5, E11.5, and E13.5 were analyzed. Only expression ratios of significantly altered genes and proteins between embryonic stages indicated were used. In case of similar expression, all probesets and all protein spots corresponding to a gene were either both up-regulated (>1) or down-regulated (<1). Inverse: the ratios of all probesets were <1 and all protein spots were >1 (or the *vice versa*). Ambiguous: at least one probeset and protein spot had a similar ratio, but other probesets or protein spots were regulated in the opposite direction.

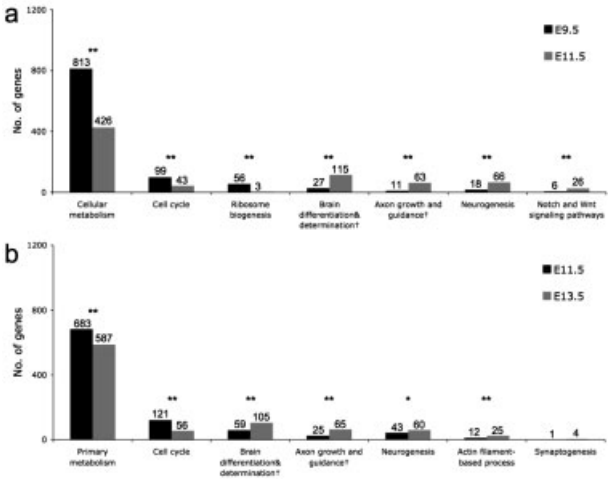

Figure 4. Analysis of enriched GO terms based on transcriptome data. Significantly altered genes from a comparison of (a) E9.5 *vs.* E11.5 and (b) E11.5 *vs.* E13.5 were used to analyze associated GO terms. Only significantly enriched GO terms are shown ($p<0.05$) and the number of genes (of our analysis) associated with each term is indicated. Black bars indicate higher gene expression at (a) E9.5 or (b) E11.5 and gray bars indicate higher gene expression at (a) E11.5 or (b) E13.5 (Chi test *p*-values are indicated as ** $p<0.05$, * $p<0.1$). † indicates the statistical analysis of grouped GO terms (see Section 2 details).

E11.5 (Fig. 4b) showed enrichment for similar biological functions, but the difference between the two stages was less pronounced.

Among significantly altered proteins (data of GO term analysis not shown), we found an enrichment of the GO term nervous system development within proteins stronger expressed at E13.5 compared to E11.5. When the earlier stages were analyzed (E9.5 *vs.* E11.5 and at E11.5 *vs.* E13.5), we found an enrichment of mainly metabolism related terms within proteins of increased expression. It is noteworthy that the same GO terms were enriched within unchanged proteins, indicating that with developmental progression, metabolism related proteins decrease in abundance whereas cell type specific proteins are up-regulated. In general, housekeeping proteins were either not changed in expression or down-regulated whereas neuron-specific proteins were up-regulated during development. In addition we found that many cytoskeleton related proteins were significantly altered in the course of development. Using GO term analysis of microarray data, we detected that genes related to the *Notch*- and *Wnt*-signaling pathways were enriched in the group of up-regulated genes at E11.5 compared to E9.5. A summary of selected key players in both processes is provided in Table 2. Altered expression of some key proteins was verified either by immunoblotting or quantitative PCR (Fig. 5).

4 Discussion

Microarray studies are widely used to investigate brain development [14–16]. However, gene expression at the mRNA level does not necessarily correlate with protein abundance, *e.g.*, due to post-transcriptional control mechanisms [17–19]. Combined transcriptome and proteome studies have previously shown that the degree of concordant regulation is highly dependent on the system under investigation, and can be as high as 80% [19]. Others reported little or no similarity between gene and protein expression, but did find significant similarity on the level of gene functions [20]. In the study presented here, we analyzed early embryonic brain development on the transcriptome and proteome level and found 60–70% concordant regulation of mRNAs and corresponding proteins, whereas only 20–30% showed clear opposite regulation.

Since alterations in protein expression and PTMs are ultimately responsible for changes in cellular phenotype and function, a proteome analysis is highly valuable to obtain insights into complex processes such as brain development. When investigating embryonic mouse brain development at stages E9.5, E11.5, and E13.5, we consistently found that 10–13% of all proteins (considering protein concentrations) and mRNAs were changed in expression during 2 days of development. This was confirmed on the proteome level for two additional stages of development, E16 and E18. We suggest that keeping the rate of expression alterations constant might restrict the ultimate speed of development. Comprehensive changes in gene expression have to occur during development in order to facilitate cellular differentiation. A high rate of alteration, however, requires a large amount of cellular resources such as energy, precursor molecules, space, and free water. We hypothesize that during embryonic

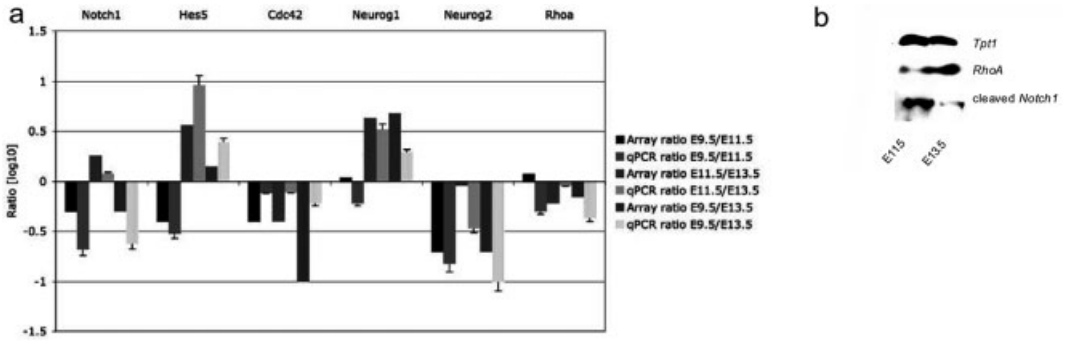

Figure 5. Expression patterns of key gene products analyzed by (a) quantitative PCR or (b) immunoblotting. (a) Comparison of expression ratios derived from microarray analyses and quantitative PCRs, (b) immunoblotting of E11.5 (left lane) and E13.5 (right lane) protein extracts confirmed results for proteins *TCTP* (gene name *Tpt1*), *RhoA*, and Notch intracellular domain (cleaved *Notch*).

development, the alteration of protein expression is restricted by the maximum rate still compatible with available cellular resources. Furthermore, we observed that up- and down-regulation of protein expression was always in equilibrium between stages. Since additional proteins have to be produced by the cell to promote differentiation, we suggest that the concentration of others must decrease in order to keep the total protein concentration constant. Protein overexpression at constant cell volume can result in conformational changes of proteins resulting in protein aggregation and loss of function, as observed in neurodegenerative diseases [21, 22]. Taken together, we propose that the overall rate of gene expression change might be one of the factors that determine developmental velocity, which would be therefore limited by the availability of cellular resources.

We found that the complexity (total number of gene products) of mRNAs and proteins was similar among stages. Therefore, we assume that differentiation is driven by cell type specific changes in protein concentrations rather than merely by an increase in the number of cell type specific proteins. To characterize functional changes during cellular differentiation, we analyzed our datasets for enriched GO terms associated with differentially regulated gene products. At E9.5 we observed a stronger expression of transcripts and proteins associated with the terms "metabolism" and "cell-cycle" compared to E11.5. This result is consistent with previous findings [1, 2] demonstrating that NPCs mainly proliferate at E9.5. Proteins associated with metabolism and cell cycle were also enriched in the group of unchanged proteins. In contrast, at E11.5 and E13.5, when a larger subset of NPCs differentiates into neurons [1, 2], we observed an enhanced abundance of mRNAs and proteins related to neuronal differentiation. A proteomics study, where *in vitro* cultured murine embryonic stem cells were compared to differentiated dopaminergic neurons, revealed similar results [23]. Consistent with this study we also observed a significant down-regulation of translationally controlled tumor protein (TCTP; gene name *Tpt1*) during development. The relevance of this finding is supported by a recent publication showing that mice deficient in TCTP were embryonic lethal. The authors suggested that TCTP plays a vital role in embryonic cell proliferation and is linked to the regulation of the cell cycle machinery [24].

Neuronal morphogenesis is mainly facilitated by a rearrangement of the actin cytoskeleton architecture [25, 26]. Newly generated neurons start to form neurites at thin actin-rich peripheral protrusions which then grow larger driven by a structure known as the "growth cone." Most of the motile activities of the growth cone are dependent on high actin turnover. Actin turnover is assisted by a variety of actin-binding proteins, not only their activity but also their expression levels are thought to be critical for neuronal morphogenesis [25, 27]. We found that actin-related protein 2/3 complex subunit 5 (gene name *Arpc5*) was significantly up-regulated in expression during development. *Arpc5* is known to be involved in the initiation of new filamental actin to grow as a branch on the side of an existing filament. Furthermore, we found that neuromodulin (gene name *Gap43*) and myristoylated alanine-rich C kinase substrate (gene name *Marcks*) were up-regulated during development. Together with brain acid soluble protein 1 (gene name *Basp1*), which was also up-regulated, all three proteins were recently described to regulate actin dynamics by a common mechanism [26]. In summary, we found that actin-binding proteins were up-regulated in expression during the developmental period E9.5–E13.5, a period where actin cytoskeleton rearrangements create the scaffolding for neuronal morphogenesis.

Actin cytoskeleton rearrangement is orchestrated by a number of signaling pathways. Key players that were shown to be involved in actin cytoskeleton regulation are largely members of the *Rho* family of small GTP-binding proteins (gene names *RhoA*, *Cdc42*, and *Rac1*) [28]. These signaling molecules couple cell surface receptor activation to actin cytoskeleton regulation. Indeed, we found that *RhoA* (protein name ras homolog gene family, member A) as well as *Cdc42* (protein name cell division cycle 42 homolog) expression was up-regulated during development, although *Rac1* (protein name RAS-related C3 botulinum substrate 1) expression was not significantly altered.

Table 2. Expression ratios of selected mRNAs and proteins among embryonic stages

Gene name	Expression ratio (mRNA)		
	E9.5/E11.5	E11.5/E13.5	E9.5/E13.5
Cytoskeleton			
Arpc5	0.9**	0.9	0.8
Marcks	0.4**	1.4	0.5**
Gap43	0.7	0.2**	0.2**
Basp1	0.6	0.8	0.5**
Tpt1	0.9	1.0	1.0
RhoA	1.2	0.6*	0.7
Cdc42	0.4*	0.4*	1.5*; 0.1*
Rac1	0.7	1.3	0.9
***Notch*- and *Wnt*-signaling**			
CtBP1	0.7	1.1	0.8
Notch1	0.5**	1.8**	0.5**
Hes5	0.4**	3.6**	1.4
Hes1	1.6**	0.6**	0.9
Rest	2.3**	0.4**	0.9
Neurog1	1.1	4.3**	4.8**
Neurog2	0.2	0.9	0.2**
	Expression ratio (protein)		
Cytoskeleton			
Arpc5	0.75*	1.01	0.76**
Marcks	0.52	0.48	0.25
Gap43	0.98	0.83	0.82**
Basp1	0.47**	0.82	0.38
Tpt1	1.43**	1.50**	2.15*
***Notch*- and *Wnt*-signaling**			
CtBP1	0.70*	1.15	0.8

* $p \leq 0.05$; ** $p \leq 0.1$.

Using GO term analysis, we found that mRNAs implicated in *Notch*- and *Wnt*-signaling pathways were altered in abundance during development. The *Notch*-signaling pathway plays an important role during the neurogenic phase of brain development [4] and *Notch1* (protein name *Notch1* protein) is a key component required for the maintenance of the NPC proliferative state. Loss-of-function mutations in *Notch1* result in precocious initiation of neurogenesis in the early embryonic neural tube at the expense of NPC proliferation and gliogenesis. For embryonic brain development, the most important downstream targets of *Notch* signaling are transcription factors of the *Hes* (Hairy and enhancer of split) family [29]. Their transcription is positively regulated by *Notch* and, in the nervous system, their predominant function seems to be the repression of proneurogenic basic helix-loop-helix (bHLH) genes such as Neurogenin 1, and 2 (gene names *Neurog1/2*) [29]. *Notch1*-expression is spatiotemporally correlated with neurogenesis and may be required for NPCs undergoing asymmetric but not symmetric divisions [29]. Consistent with this model, we found that *Notch1* (as well as the *Notch* intracellular domain, NICD, cleaved fragment of *Notch1*) and its downstream target *Hes5*, were up-regulated at E11.5, when NPCs start to divide asymmetrically. Both, *Notch1* and *Hes5* were down-regulated at E13.5, where neurogenesis is on its peak and NPCs divide symmetrically producing only neurons. Interestingly, we found that the expression of *Hes1* showed the opposite regulation, indicating that *Hes1* might have functions independent from *Notch*-signaling. Nevertheless, the controversial regulation of *Hes1* and *Hes5* might be of interest especially because it was shown that *Hes1* expression starts at the early neuroectoderm and might be involved in *Notch*-independent proliferation of NPCs *via* symmetric divisions. *Hes5* expression starts only later in development, between E8.5 and E9 and was shown to be directly correlated to *Notch1* expression [29, 30]. Furthermore, C-terminal binding protein 1 (gene name *CtBP1*) which acts as corepressor of the CSL family of transcriptional regulators (gene names *RBP-jk*, *Su(H)*, and *Lag-1*, downstream of *Notch* and other signaling pathways) was up-regulated at E11.5 as compared to E9.5. *CtBP1* also acts as repressor of the *Wnt*-signaling pathway and its up-regulation might be due to its general role in differentiation related processes [31].

Besides *Notch* signaling, canonical *Wnt* signaling has also been shown to spatiotemporally regulate brain development. It was reported to promote progenitor proliferation at early stages of brain development whereas at later stages (after murine E13.5), a shift in *Wnt*-signaling activity promotes neurogenesis instead [4]. It was shown *in vitro* that under conditions where NPC proliferation is favored, *Wnt*-signaling mediates the up-regulation of the neuron restrictive silencer factor/repressor element 1 transcription factor (gene name *Rest*) [32]. We found that *Rest* related mRNA was down-regulated from E9.5 to E11.5, indicating that its high expression might indeed play a role in NPC proliferation at E9.5. In contrast, *Wnt* signaling was also proposed to promote neuronal differentiation in an instructive way by controlling the expression of proneurogenic genes [4]. Proneurogenic genes, such as *neurogenin 1* and *2* were shown to be affected downstream of both, the *Notch*- and *Wnt*-signaling pathway. Moreover, overexpression of proneurogenic genes turned out to be sufficient to promote the differentiation of cultured NPCs into neurons. We found that *Neurog2* related mRNA was up-regulated from E9.5 until E11.5, the time period when the switch towards neurogenesis occurs. In contrast, *Neurog1* related mRNA was massively down-regulated at E13.5.

In summary, we used transcriptome and proteome analysis as complementary approaches to analyze early mouse brain development. Interestingly, we observed that the rate of gene expression alteration was almost constant and a balance in up- and down-regulation was observed between E9.5 and E13.5. Furthermore, the complexity (number of gene products) of mRNAs and proteins was similar among stages. When cytoskeleton reassembly or *Notch*- and *Wnt*-signaling pathways were analyzed in more detail, we found many similarities to published data, validating the significance of the large number of mRNA and protein changes found in our study.

We would like to thank Grit Nebrich, Ferdinand von Meyenn, Christiane Lach, Constanze König, Silke Becker, and Andrea Koppelstätter for excellent technical assistance. This work was supported by the German Ministry for Education and Research (BMBF) within the German National Genome Research Network (NGFN) program. The study was funded by BMBF through NGFN2 (Human Brain Proteome Project), subprojects FKZ 01GR0442 and FKZ 01GR0448.

The authors have declared no conflict of interest.

5 References

[1] Hirabayashi, Y., Gotoh, Y., Stage-dependent fate determination of neural precursor cells in mouse forebrain. *Neurosci. Res.* 2005, *51*, 331–336.

[2] Gotz, M., Huttner, W. B., The cell biology of neurogenesis. *Nat. Rev. Mol. Cell Biol.* 2005, *6*, 777–788.

[3] Qian, X., Shen, Q., Goderie, S. K., He, W., *et al.*, Timing of CNS cell generation: A programmed sequence of neuron and glial cell production from isolated murine cortical stem cells. *Neuron* 2000, *28*, 69–80.

[4] Guillemot, F., Cell fate specification in the mammalian telencephalon. *Prog. Neurobiol.* 2007, *134*, 3771–3780.

[5] Greenberg, D. A., Jin, K., Neurodegeneration and neurogenesis: Focus on Alzheimer's disease. *Curr. Alzheimer Res.* 2006, *3*, 25–28.

[6] Team, R. D. C., *R: A Language and Environment for Statistical Computing.* R Foundation for Statistical Computing, Vienna, Austria 2006.

[7] Cleveland, W. S., Grosse, E., Shy, W. M., in: Chambers, J. M., Hastie, T. J. (Eds.), *Statistical Models in S*, Chapman and Hall, New York 1992, pp. 309–376.

[8] Eisenberg, E., Levanon, E. Y., Human housekeeping genes are compact. *Trends Genet.* 2003, *19*, 362–365.

[9] Zabel, C., Klose, J., Protein extraction for 2-D electrophoresis. *Methods Mol. Biol.* 2007, *in press*.

[10] Zabel, C., Klose, J., High resolution large gel 2-D electrophoresis. *Methods Mol. Biol.* 2007, *in press*.

[11] Nebrich, G., Herrmann, M., Sagi, D., Klose, J., Giavalisco, P., High MS-compatibility of silver nitrate-stained protein spots from 2-DE gels using ZipPlates and AnchorChips for successful protein identification. *Electrophoresis* 2007, *28*, 1607–1614.

[12] Rainer, J., Sanchez-Cabo, F., Stocker, G., Sturn, A., Trajanoski, Z., CARMAweb: Comprehensive R- and bioconductor-based web service for microarray data analysis. *Nucleic Acids Res.* 2006, *34*, W498–W503.

[13] Zhang, B., Schmoyer, D., Kirov, S., Snoddy, J., GOTree Machine (GOTM): A web-based platform for interpreting sets of interesting genes using Gene Ontology hierarchies. *BMC Bioinformatics* 2004, *5*, 16.

[14] Abramova, N., Charniga, C., Goderie, S. K., Temple, S., Stage-specific changes in gene expression in acutely isolated mouse CNS progenitor cells. *Dev. Biol.* 2005, *283*, 269–281.

[15] Neidhardt, L., Gasca, S., Wertz, K., Obermayr, F., *et al.*, Large-scale screen for genes controlling mammalian embryogenesis, using high-throughput gene expression analysis in mouse embryos. *Mech. Dev.* 2000, *98*, 77–94.

[16] Machka, C., Kersten, M., Zobawa, M., Harder, A., *et al.*, Identification of Dll1 (Delta1) target genes during mouse embryogenesis using differential expression profiling. *Gene Expr. Patterns* 2005, *6*, 94–101.

[17] Greene, N. D., Leung, K. Y., Wait, R., Begum, S., *et al.*, Differential protein expression at the stage of neural tube closure in the mouse embryo. *J. Biol. Chem.* 2002, *277*, 41645–41651.

[18] Zheng, P. Z., Wang, K. K., Zhang, Q. Y., Huang, Q. H., *et al.*, Systems analysis of transcriptome and proteome in retinoic acid/arsenic trioxide-induced cell differentiation/apoptosis of promyelocytic leukemia. *Proc. Natl. Acad. Sci. USA* 2005, *102*, 7653–7658.

[19] Mijalski, T., Harder, A., Halder, T., Kersten, M., *et al.*, Identification of coexpressed gene clusters in a comparative analysis of transcriptome and proteome in mouse tissues. *Proc. Natl. Acad. Sci. USA* 2005, *102*, 8621–8626.

[20] Frey, I. M., Rubio-Aliaga, I., Siewert, A., Sailer, D., *et al.*, Profiling at mRNA, protein, and metabolite levels reveals alterations in renal amino acid handling and glutathione metabolism in kidney tissue of Pept2-/- mice. *Physiol. Genomics* 2007, *28*, 301–310.

[21] Ellis, R. J., Minton, A. P., Protein aggregation in crowded environments. *Biol. Chem.* 2006, *387*, 485–497.

[22] Zoghbi, H. Y., Botas, J., Mouse and fly models of neurodegeneration. *Trends Genet.* 2002, *18*, 463–471.

[23] Wang, D., Gao, L., Proteomic analysis of neural differentiation of mouse embryonic stem cells. *Proteomics* 2005, *5*, 4414–4426.

[24] Chen, S., Wu, P. S., Chou, C. H., Yan, Y. T., *et al.*, A knockout mouse approach reveals that TCTP functions as an essential factor for cell proliferation and survival in a tissue- or cell type-specific manner. *Mol. Biol. Cell* 2007, *18*, 2525–2532.

[25] Tojima, T., Ito, E., Signal transduction cascades underlying de novo protein synthesis required for neuronal morphogenesis in differentiating neurons. *Prog. Neurobiol.* 2004, *72*, 183–193.

[26] Laux, T., Fukami, K., Thelen, M., Golub, T., *et al.*, GAP43, MARCKS, and CAP23 modulate PI(4,5)P(2) at plasmalemmal rafts, and regulate cell cortex actin dynamics through a common mechanism. *J. Cell. Biol.* 2000, *149*, 1455–1472.

[27] Dent, E. W., Gertler, F. B., Cytoskeletal dynamics and transport in growth cone motility and axon guidance. *Neuron* 2003, *40*, 209–227.

[28] Watabe-Uchida, M., Govek, E. E., Van Aelst, L., Regulators of Rho GTPases in neuronal development. *J. Neurosci.* 2006, *26*, 10633–10635.

[29] Hatakeyama, J., Kageyama, R., Notch1 expression is spatiotemporally correlated with neurogenesis and negatively regulated by Notch1-independent Hes genes in the developing nervous system. *Cereb. Cortex* 2006, *16 Suppl 1*, i132–i137.

[30] Basak, O., Taylor, V., Identification of self-replicating multipotent progenitors in the embryonic nervous system by high Notch activity and Hes5 expression. *Eur. J. Neurosci.* 2007, *25*, 1006–1022.

[31] Chinnadurai, G., CtBP family proteins: more than transcriptional corepressors. *Bioessays* 2003, *25*, 9–12.

[32] Pinnoji, R. C., Bedadala, G. R., George, B., Holland, T. C., *et al.*, Repressor element-1 silencing transcription factor/neuronal restrictive silencer factor (REST/NRSF) can regulate HSV-1 immediate-early transcription via histone modification. *Virol. J.* 2007, *4*, 56.

OPEN ACCESS Freely available online

PLoS one

Impairment of Adolescent Hippocampal Plasticity in a Mouse Model for Alzheimer's Disease Precedes Disease Phenotype

Daniela Hartl[1], Michael Rohe[2], Lei Mao[1], Matthias Staufenbiel[3], Claus Zabel[1]*, Joachim Klose[1]

1 Institute for Human Genetics, Charité -University Medicine, Berlin, Germany, **2** Max-Delbrueck-Center for Molecular Medicine, Berlin, Germany, **3** Novartis Institutes for Biomedical Research, Basel, Switzerland

Abstract

The amyloid precursor protein (APP) was assumed to be an important neuron-morphoregulatory protein and plays a central role in Alzheimer's disease (AD) pathology. In the study presented here, we analyzed the APP-transgenic mouse model APP23 using 2-dimensional gel electrophoresis technology in combination with DIGE and mass spectrometry. We investigated cortex and hippocampus of transgenic and *wildtype* mice at 1, 2, 7 and 15 months of age. Furthermore, cortices of 16 days old embryos were analyzed. When comparing the protein patterns of APP23 with *wildtype* mice, we detected a relatively large number of altered protein spots at all age stages and brain regions examined which largely preceded the occurrence of amyloid plaques. Interestingly, in hippocampus of adolescent, two-month old mice, a considerable peak in the number of protein changes was observed. Moreover, when protein patterns were compared longitudinally between age stages, we found that a large number of proteins were altered in *wildtype* mice. Those alterations were largely absent in hippocampus of APP23 mice at two months of age although not in other stages compared. Apparently, the large difference in the hippocampal protein patterns between two-month old APP23 and *wildtype* mice was caused by the absence of distinct developmental changes in the hippocampal proteome of APP23 mice. In summary, the absence of developmental proteome alterations as well as a down-regulation of proteins related to plasticity suggest the disturbation of a normally occurring peak of hippocampal plasticity during adolescence in APP23 mice. Our findings are in line with the observation that AD is preceded by a clinically silent period of several years to decades. We also demonstrate that it is of utmost importance to analyze different brain regions and different age stages to obtain information about disease-causing mechanisms.

Citation: Hartl D, Rohe M, Mao L, Staufenbiel M, Zabel C, et al. (2008) Impairment of Adolescent Hippocampal Plasticity in a Mouse Model for Alzheimer's Disease Precedes Disease Phenotype. PLoS ONE 3(7): e2759. doi:10.1371/journal.pone.0002759

Editor: Ashley I. Bush, Mental Health Research Institute of Victoria, Australia

Received April 18, 2008; **Accepted** June 23, 2008; **Published** July 23, 2008

Funding: This work was supported by the German ministry for education and research (BMBF) within the German National Genome Research Network (NGFN2) program.

Competing Interests: The authors have declared that no competing interests exist.

* E-mail: claus.zabel@charite.de

Introduction

The *Amyloid precursor protein* (APP) plays a central role in Alzheimer's disease (AD) pathology. It was implicated in a variety of cellular processes such as axonal transport, cell adhesion, cholesterol metabolism or gene transcription and assumed to be an important neuro-morphoregulatory protein [1]. Furthermore, APP is already expressed at high levels in the developing nervous system where it is localized at regions of neuronal motility and synapse formation [2–4]. In addition, APP is also considered to act as a "molecular hub" protein in the cellular protein network [5]. According to scale-free interaction network theory, the disruption of a hub which possesses many connections will have a more drastic impact on the entire network than disruptions at sites with few connections. In line with this, mutations in APP or the APP-cleaving enzymes presenilin 1 and 2 are implicated in early-onset familial AD cases, whereas the numerous risk factors identified for non-familial AD cases characterize late onset disease.

In order to study AD, numerous mouse models are available. In these mice, a gene of particular interest such as APP is knocked out, mutated and/or overexpressed. When the effect of genome modifications is subsequently screened at the molecular level, usually a large number of mRNA and protein changes are observed [6–8]. The cellular proteome is a highly interconnected protein network that is among other restrictions dependent on resources such as space, metabolites and unbound water to allow protein diffusion. If the concentration of one protein or a larger number of proteins is altered, this affects functionally linked proteins by altering relative concentrations of those proteins to avoid macromolecular crowding [9,10].

When analyzing the proteome of human patients or animal models for neurodegenerative diseases, the specificity of a disease (i.e. Alzheimer's, Huntington's or Parkinson's disease) is more likely determined by the affected brain region and not by the identity of altered proteins in the brains of patients or genetically modified mice [11]. Moreover, massive proteome alterations occur during normal development and aging in the animal model studied. Therefore, the impact of mutations on the proteome might be strongly age-dependent. Disease models are conventionally investigated at age stages where the disease phenotype is prominent. However, these analyses may be already biased by secondary effects of pathogenesis and may therefore obscure the causative process for disease occurring earlier in development.

In the study presented here we investigated APP-transgenic mice (APP23) expressing human APP^{751} which contains the Swedish double mutation [12]. In APP23 mice, transgene expression is sevenfold higher than endogenous APP. APP23 mice develop an AD-like pathology (ß-amyloid depositions) at 6 months of age. Plaques increase dramatically in size and number at older stages, occupying a substantial area of the cerebral cortex and hippocampus at 24 months of age [13,14]. Furthermore, region-specific neuronal loss [7] and progressive age-related impairment of cognition [15–18] were observed with increasing age.

To analyze the age-specific impact of transgenic APP on the brain proteome, we designed a time course starting at very early stages where no phenotypes were reported so far. We investigated age-stages spanning adolescence (1 and 2 months of age) and adulthood (7 and 15 months of age) of mice [19]. Furthermore, the embryonic stage at day 16 *post coitum* (ED16) which represents late neurogenic phase of mouse brain development [20], was investigated. To analyze the tissue-specificity of transgenic APP in different brain regions, hippocampal (H) as well as cortical (C) proteomes of APP23 mice were investigated.

Our results show a large number of protein changes in the proteomes of APP23 mice at prenatal stages. However, the largest number of alterations was observed during adolescence in the hippocampal region, where brain plasticity is predominant. Together, our results indicate a perturbance of hippocampal plasticity in adolescent APP23 mice which may result in the development of memory deficits later during disease progression.

Results

In the study presented here, we analyzed the cortical and hippocampal proteomes of the AD mouse model APP23 using a 2-dimensional gel-electrophoresis (2-DE) based proteomics approach. Protein spot patterns of cortex and hippocampus obtained from transgenic and *wildtype* mice at 1, 2, 7 and 15 months of age as well as cortices of 16 days old embryos were investigated (n = 6).

We used our highly reproducible and extensively validated large-gel 2-DE technology [21] in combination with 2-D fluorescence difference gel electrophoresis (DIGE). *Wildtype* and transgenic samples were always labeled with the same dye (Cy3) to avoid dye-specific spot abundance variations (false positives). To allow data comparison among groups, we predefined a fixed group of 1769 spots (figure 1) that was analyzed at all age stages and brain regions. Thus, every protein spot had the same spot identification number (ID) on spot patterns of all stages and brain regions. Only 2-D patterns of embryonic day 16 brains were analyzed separately due to major differences of the embryonic compared to adult spot patterns.

Alterations in protein abundance

When comparing 2-DE spot patterns of APP23 versus *wildtype* brain tissues, we found that many protein spots were significantly ($p \leq 0.05$) altered in abundance in APP23 brain tissue even as early as in ED16. At this stage, expression of transgenic APP was already present (figure 2, figure 3A and B).

When comparing the total number of variant proteins at each stage, we made an interesting observation. A considerable peak in protein alterations was detected in hippocampus of 2 months old APP23 mice. At this stage, 140 protein spots (7.9%) were altered in contrast to 51 spots (2.9%) at 1 month, 72 spots (4.1%) at 7 months and 82 spots (4.6%) at 15 months (figure 3B). In cortex, a smaller peak of alterations was detected at the same age. 79 spots (4.5%) were altered at 2 months in contrast to 62 spots (3.5%) at 1 month and 63 spots (3.6%) at 7 and 15 months (figure 3A). Similar results were obtained when the relative protein concentration instead of the number of variant proteins was analyzed (figure 3C, 3D). Total protein amounts changed at each stage were calculated as sums of the spot volumes of all significantly altered spots. This sum corresponds to the total change in protein concentration.

When comparing the numbers of up- versus down-regulated protein spots (figure 3A and B) as well as their protein concentrations

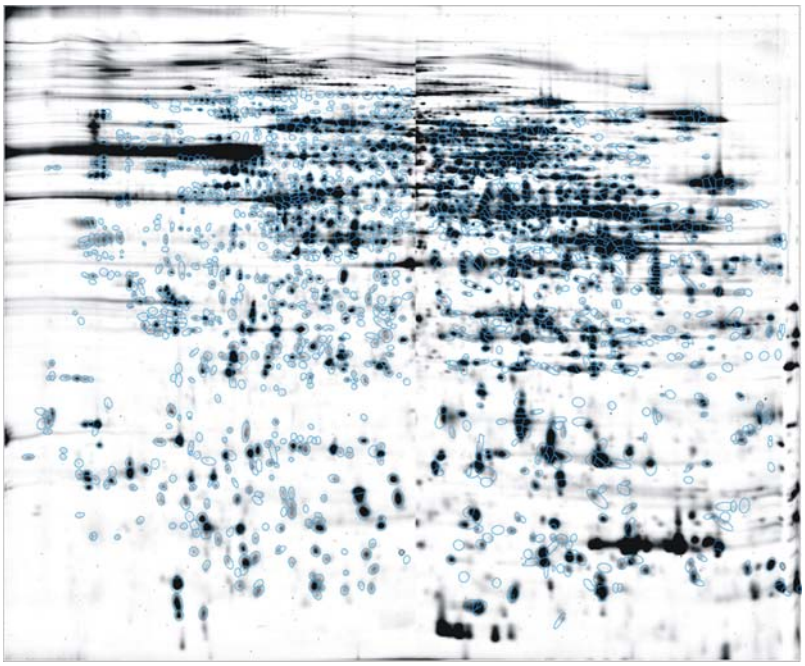

Figure 1. Standard pattern of protein spots analyzed. A protein spot pattern comprising 1769 spots (indicated with blue circles on a hippocampus spot pattern of a 7 months old *wildtype* mouse) was analyzed on all gels within this study.
doi:10.1371/journal.pone.0002759.g001

Figure 2. Trangenic APP expression at ED16. Immunoblot of human APP (antibody clone 6E10) with APP23 (Trans) and *wildtype* (WT) cortex tissue of 16 days old mouse embryos. A strong signal of human APP is seen on the left lane. This signal is absent in *wildtype* tissue (middle lane). The right lane shows the human APP-signal of a positive control sample (cortex tissue, 7 months, APP23-mouse).
doi:10.1371/journal.pone.0002759.g002

(figure 3C and D), we observed that down-regulation predominated up-regulation at early stages. In hippocampus, this was observed in 1, 2 and 7 months old APP23 mice. In cortex, predominant down-regulation was observed in ED16 and in 1 month old mice. In older stages, up- and downregulation was more balanced.

In order to monitor proteome alterations related to development, age stages 1 versus 2, 2 versus 7 and 7 versus 15 months were compared. Comparisons were made within *wildtype*, transgenic, cortex and hippocampus groups.

As shown in figure 4A, a higher number of proteins was generally altered within transgenic mice when compared to *wildtype* mice. However, in hippocampus, both stage comparisons including the 2 months-stage showed a remarkable exception to this rule. There the number of altered protein spots was considerably lower within the transgenic group (figure 4B). Only about 9% of investigated proteins were altered in APP23 mice whereas 23% of proteins were altered in *wildtypes* during the same period. In detail, 328 (*wildtype* mice) and 486 (APP23 mice) protein spots were altered in cortex between 1 and 2 months of age, respectively. During the same time period, 373 spots were altered in hippocampus of *wildtype* mice, but only 158 spots were altered in APP23 mice. Between 2 and 7 months of age, 615 (*wildtype* mice, cortex), 783 (APP23 mice, cortex), 437 (*wildtype* mice, hippocampus) and only 162 (APP23 mice, hippocampus) spots were altered. In the later time points studied (7 to 15 months), fewer proteins were altered in comparison to the younger stages. In cortex, 566 (*wildtype* mice) and 623 (APP23 mice) spots were altered and in hippocampus, 571 (*wildtype* mice) and 672 spots (APP23 mice) were altered, respectively.

Of the proteome alterations during development, 38% to 67% of proteins that were altered in APP23 mice during aging were also altered in *wildtype* mice (figure 4 C).

To exclude the possibility of systematic bias introduced by differences in spot pattern quality, mean standard deviations of spot volumes were compared between all groups. However, no significant differences were detected (data not shown).

In summary, when comparing cortex spot patterns of APP23 versus *wildtype* mice, we found that a fraction of 3.2% to 4.5% of investigated protein spots was significantly altered at all stages. In

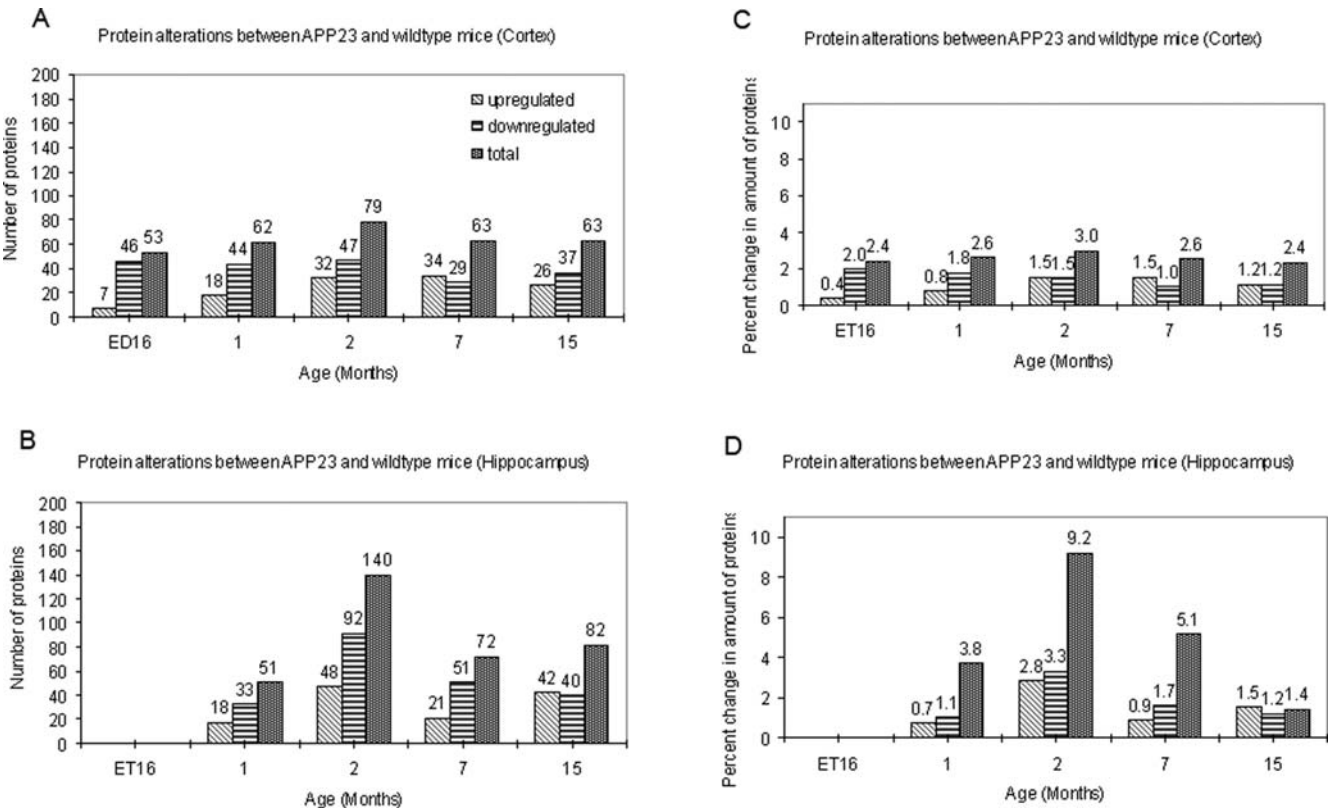

Figure 3. Alteration in protein number and concentration during disease progression in APP23 mice. Numbers (A and B) or volumes (corresponding to relative protein amounts; C and D) of protein spots significantly altered in APP23 mice are shown for different ages (x-axis) and brain regions (cortex: A and C; hippocampus: B and D) investigated. The values supplied represent the numbers of significantly changed spots (A and B) or a percentage of the spotvolume for 1769 spots (C and D). Upregulated spots are shown in cross striated bars, downregulated spots are shown in horizontally striated bars and the sum of both is shown by dotted bars. Many spots were altered at all stages but 2 months of age, where a peak in alteration was observed in hippocampus tissue.
doi:10.1371/journal.pone.0002759.g003

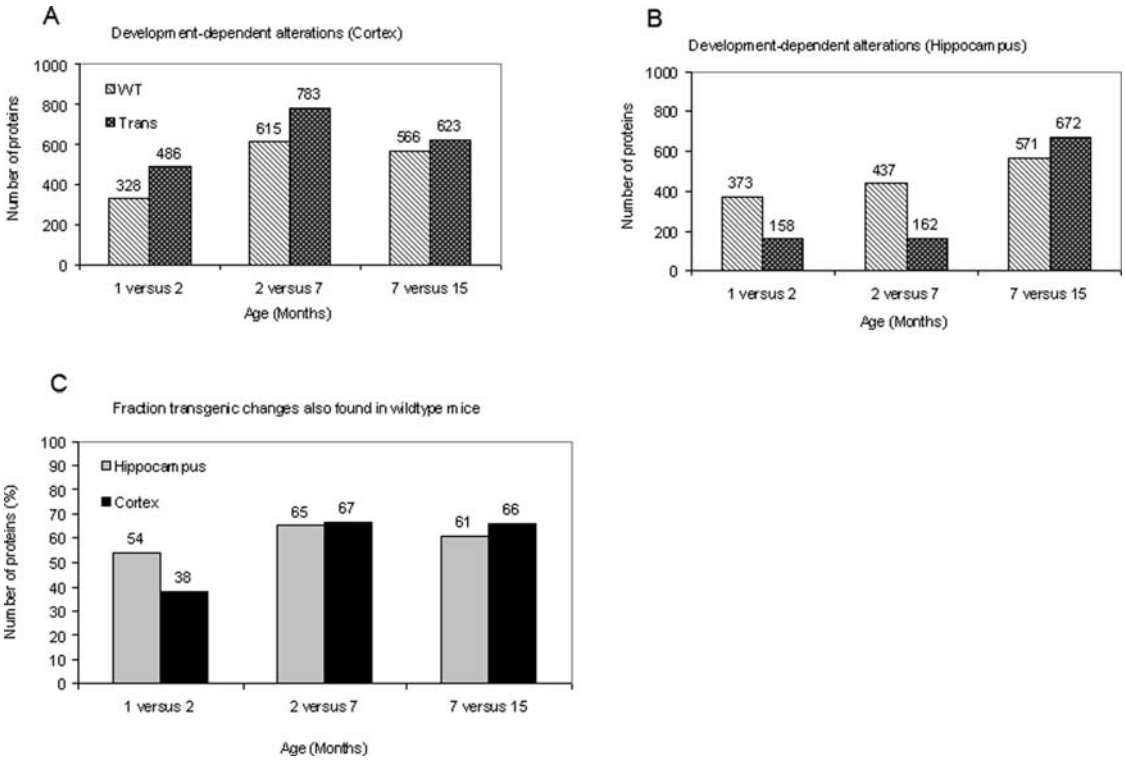

Figure 4. Developmental changes in APP23 and *wildtype* mice. Numbers of (y-axis) protein spot alterations associated to development are shown for *wildtype* (light grey bars) and transgenic (dark grey bars) cortex (A) and hippocampus (B) 2-D spot patterns. In (C), the fraction of proteins altered in transgenic mice that were also found in *wildtype* mice is shown. The x-axis indicated the age stages which were compared.
doi:10.1371/journal.pone.0002759.g004

hippocampus patterns, 2.9% to 7.9% of investigated protein spots were altered. Interestingly, in hippocampus of 2 months old mice, a significant peak in variant proteins was observed. When investigating proteome alterations related to development, we found that the observed peak in hippocampus of 2 months old mice was mainly caused by alterations in the proteome of *wildtype* mice during adolescence. These alterations were largely absent in APP23 mice.

Functional analysis of altered proteins

65% of the protein spots altered significantly between transgenic and *wildtype* mice were identified by mass spectrometry which amounts to 293 non-redundant proteins as determined by their different gene names (details in supplementary table S1).

About 90% of the identified proteins were subsequently grouped into seven functional categories. The categories were then hierarchically listed according to the percentage of altered proteins they include. This was possible since the distribution of proteins over categories was relatively similar among adult age stages. With the exception of ED 16, the most abundant category was "metabolism", followed by "cytoskeleton", "signal transduction", "transcription, translation and nucleotide metabolism", "degradation" and "folding, sorting". The last category was "cell growth and death" (table 1). Within proteins altered in ED16, the category "transcription, translation and nucleotide metabolism" accounted for the most pronounced protein group and no protein was included in the categories "cytoskeleton" and "cell growth and death".

Although the functional distribution was similar in different age stages and brain regions, most proteins (126 proteins) were altered only at a single stage and brain region, that is, they were stage specific. Only 80 proteins were altered in two conditions (stages and/or brain regions), 46 proteins were altered in three and 28 proteins were altered in four conditions. Only thirteen proteins were found to be altered in five or more conditions (table 2).

To test the impact of our results on human AD, we compared our data to three 2-DE-based proteomic studies of human AD. All three studies yielded a total of 30 disease-related proteins in human brain tissue of AD patients. We found 22 of the 30 proteins in our study (table 3).

Furthermore, since APP is thought to be involved in neuronal plasticity, we determined all proteins which were altered in APP23 mice and might indicate changes in neuronal plasticity. Proteins were selected if they are structural components of synapses or if they are implicated in the dynamics of neurogenesis and synaptogenesis (table 4). Those proteins were termed neuron-specific because they have neuron-specific functions in the brain and may thus help to identify the role of mutated APP towards neuronal plasticity.

Within neuron-specific proteins, twelve proteins were altered in hippocampus of two-month old APP23 mice. In cortex of two-month old APP23 mice, eight neuron-specific proteins were altered. In the cortex and hippocampus of the other age-stages, always four or five neuron-specific proteins were altered, respectively. In brain regions of all age-stages, down-regulation of neuron-specific proteins was predominant. In hippocampus of two-month old APP23 mice for example, nine proteins were down-regulated and only two proteins were up-regulated. One protein, *Synapsin Ib*, which occurred as more than one spot on the 2-DE pattern was up- and down-regulated depending on the protein isoform.

We analyzed the expression profiles of the two very important neuron-specific proteins *Neuromodulin* (*Gap43*) and *Post-synaptic density protein 95* (PSD95, *Dlg4*) in more detail. As shown in figure 5, the expression of Gap43 was significantly down-regulated during aging in hippocampus and cortex of *wildtype* mice from 2 to

Table 1. Percentages of proteins altered in hippocampus (H) and cortex (C) of ED16 or 1, 2, 7 and 15 months old transgenic mice, grouped into functional categories.

Functional category	1H	2H	7H	15H	ED16	1C	2C	7C	15C
1. Metabolism	**34**	**25**	**33**	**35**	**16**	**34**	**23**	**30**	**40**
1.1 CH Metabolism	13	9	15	19	10	16	7	10	13
1.2 Energy Metabolism	10	4	5	2	3	9	3	7	6
1.3 AA Metabolism	5	2	7	6	3	5	5	9	4
1.4 Lipid Metabolism	7	9	5	8	0	5	8	5	17
2. Cytoskeleton	**10**	**10**	**14**	**19**	**0**	**8**	**13**	**10**	**13**
3. Signal Transduction	**7**	**9**	**13**	**15**	**13**	**6**	**8**	**13**	**2**
4. Folding, Sorting	**7**	**11**	**7**	**8**	**3**	**9**	**12**	**9**	**8**
5. Transcription, Translation, Nucleotide Metabolism	**3**	**8**	**10**	**2**	**39**	**14**	**13**	**9**	**4**
6. Degradation	**5**	**8**	**8**	**6**	**19**	**8**	**0**	**10**	**10**
7. Cell Growth and Death	**2**	**2**	**3**	**4**	**0**	**6**	**2**	**2**	**6**

doi:10.1371/journal.pone.0002759.t001

7 ($p_{Hip} = 0.04$) as well as from 7 to 15 months of age ($p_{Hip} = 0.002$; $p_{Cor} = 0.005$). In APP23 mice, Gap43-expression was also down-regulated during aging (7 to 15 months) in both brain regions ($p_{Hip} = 0.001$; $p_{Cor} = 0.008$). It was also down-regulated between 1 and 2 months of age in cortex ($p = 0.025$) but not hippocampus. Moreover, Gap43 was down-regulated in hippocampus of one ($p = 0.03$) and two ($p = 0.004$) months old APP23 when compared to *wildtype* mice. Figure 5B shows the expression profile of PSD95 during disease progression. This protein was significantly down-regulated in the cortex of APP23 mice when comparing 1 and 2 months old mice ($p = 0{,}007$) and in the cortex of APP23 as well as *wildtype* mice when comparing 7 and 15 months old mice ($p_{APP23} = 0.032$; $p_{wt} = 0.017$). Furthermore, expression of PSD95 was significantly down-regulated in APP23 mice as compared to *wildtype* mice at 1 month in cortex ($p = 0.049$) and at 2 months of age in hippocampus ($p = 0{,}019$) and cortex ($p = 0.043$).

Discussion

In this study, the APP23 mouse model for AD was investigated using a 2-DE proteomics approach. We analyzed the neocortex and hippocampus of 1, 2, 7 and 15 months old mice. In addition, the neocortex of 16 days old mouse embryos was investigated.

When comparing the 2-DE protein patterns of APP23 mice against those of *wildtype* mice, we detected that about 4% (70 protein spots) of all protein spots were altered in abundance. This large number of protein expression changes was observed at all age stages and brain regions except for hippocampus of two-month old mice. Here, twice as many (8%) protein spots were altered. To elucidate this unexpected observation we compared protein patterns of APP23 or *wildtype* mice longitudinally between all ages investigated. Interestingly, we found a large number of proteome alterations related to development including the two-

Table 2. Proteins altered in five or more conditions (time points and tissues): cortex (C) or hippocampus (H) of ED16, 1, 2, 7 and 15 months old APP23 mice.

Protein name	Gene name	1H	2H	7H	15H	ED16	1C	2C	7C	15C
Apolipoprotein E precursor (Apo-E)	Apoe	▲		▲	▲			▲	▲	▲
ATP synthase subunit beta, mitochondrial [Precursor]	Atp5b	▼		■	▼				■	▼
ATP synthase D chain, mitochondrial	Atp5h			▲		▲	▲	▲	▲	
diazepam binding inhibitor isoform 2	Dbi	▲	▼		▼				▼	▲
Dihydropyrimidinase-related protein 2	Dpysl2	▲	▲	▲				▲		▼
enolase 2, gamma neuronal	Eno2	▼	▲	■	▲		▲		▲	▲
Guanine nucleotide-binding protein G(I)/G(S)/G(T) subunit beta 1	Gnb1	▼	▼	▼	▼			▼	▼	
L-lactate dehydrogenase B chain	Ldhb			▼	▼		▼		▼	▼
Phosphoglycerate kinase 1	Pgk1		▼	▼			▼	▼	▼	
protein (peptidyl-prolyl cis/trans isomerase) NIMA-interacting 1	Pin1		▲	▲	▼		▼			▲
Transcriptional activator protein Pur-alpha	Pura	▲		▲	▲		▲		▲	▲
Septin-7		▼	▼	▼	▲		▼		▲	
triosephosphate isomerase	Tpi1	▲	■		▲		▲		▼	▼

▲upregulated.
▼downregulated.
■up- and downregulated.

doi:10.1371/journal.pone.0002759.t002

Table 3. Proteins altered in APP23 mice (cortex (C) or hippocampus (H) of 1, 2, 7 or 15 months old mice) and human *post mortem* AD brains.

Reference	Protein name	Gene name	1H	2H	7H	15H	1C	2C	7C	15C
[35]	Gamma-actin	Actg1		▼	■	▼			▲	
[34]	Adenylate kinase 1	Ak1			▼					
[34]	Aldolase 1, A isoform	Aldoa	▲	▲	▲	▲				
[34]	Aldolase 3, C isoform	Aldoc			▼					
[33]	ATP synthase, H+ transporting, mitochondrial F1 complex, alpha subunit, isoform 1	Atp5a1					■			
[33]	ATP synthase subunit beta, mitochondrial	Atp5b	▼		■	▼			■	▼
[35]	NG,NG-dimethylarginine dimethylaminohydrolase 1	Ddah1		▼	▼	▼				
[34]	Dihydropyrimidinase-related protein 2	Dpysl2	▲	▲	▲			▲		▼
[34]	Enolase 1, alpha non-neuron	Eno1	▲	▲	▲	▲	▲			
[35]	Enolase 2, gamma neuronal	Eno2	▼	▲	■	▲	▲		▲	▲
[33]	Fatty acid-binding protein, heart	Fabp3		▼		▼				▲
[34]	Glyceraldehyde-3-phosphate dehydrogenase	Gapdh	▲		▼		▼		▼	
[33]	Glial fibrillary acidic protein	Gfap	▼			▲	▼			▲
[33]	Guanine nucleotide-binding protein G(I)/G(S)/G(T) subunit beta 1	Gnb1	▼	▼	▼	▼		▼	▼	
[34]	Heat shock protein 8	Hspa8		▲			▲			▲
[33]	Heat shock protein 65	Hspd1		▲	▲			▲	▲	
[33]	Alpha-Internexin	Ina							▼	
[34]	Pgam1 protein	Pgam1		▼						
[34]	Protein (peptidyl-prolyl cis/trans isomerase) NIMA-interacting 1	Pin1		▲	▲	▲	▼			▲
[34]	Peroxiredoxin-2	Prdx2							▼	▲
[34]	Triosephosphate isomerase	Tpi1	▲	■		▼	▲		▼	▼
[34,35]	Ubiquitin carboxy-terminal hydrolase L1	Uchl1		■	▼				▼	

▲up-regulated.
▼down-regulated.
■up- and down-regulated.
doi:10.1371/journal.pone.0002759.t003

month age stage in the *wildtype* hippocampus but not in the hippocampus of APP23 mice. This may indicate that impairment of brain maturation precedes the intrinsic disease process.

Beta-amyloid deposits first appear when APP23 mice are six months old. Deposits occupy a substantial area of the cerebral cortex and hippocampus at 21 months of age. In those old-aged animals, a very large number of protein expression differences can be observed (data not shown) but they might rather be the consequence of secondary alterations due to inflammatory reactions as well as neuritic and synaptic degeneration [22]. According to our results, brain maturation might be impaired at much younger age stages preceding beta-amyloid deposition. This is in line with findings that synaptic dysfunction, synaptic loss and learning deficits in transgenic mouse models of AD appear prior to amyloid plaque deposition [23–26].

The developmental period around two months of age represents adolescence in mice. During that age, mesocorticolimbic brain regions are exceedingly plastic in terms of synaptic reorganization and adult neurogenesis [27–29]. With the transition to adulthood and during subsequent aging, brain plasticity is gradually reduced. APP was assumed to be a neuron morphoregulatory protein and is therefore involved in plasticity associated dynamics [5,30]. This would imply that when APP function is disturbed, this might predominantly affect the brain during adolescence - the age phase of enhanced plasticity. Accordingly we observed a significant reduction in proteome alterations related to development which resulted in a large difference between the proteomes of APP23 and *wildtype* mice. Importantly, this was observed in adolescent but not in adult mice.

Processes that contribute to brain plasticity are the formation and degradation of synapses, modulation of synaptic strength as well as neurogenesis. Of all proteins changed in APP23 mice, those which are most likely involved in neuronal plasticity due to their selective expression at synapses or their up-regulation during neurogenesis were analyzed in more detail. Interestingly, the majority of these proteins were altered in hippocampus of two-month old APP23 mice. Furthermore, those proteins were predominantly down-regulated in APP23 mice. For example, *neuromodulin* (gene name *Gap43*), which is widely used as marker protein for neurogenesis and synaptic plasticity [31], was down-regulated in hippocampus of one and two-month old APP23 versus *wildtype* mice. During aging (7 to 15 months of age), neuromodulin expression was down-regulated to the same expression level in both, APP23 and *wildtype* mice. Another synaptic protein, PSD95 was down-regulated in hippocampus and cortex of APP23 mice during adolescence. In addition, this protein was later down-regulated after 7 months in cortex of both, APP23 and *wildtype* mice and was expressed on the same level in both mice. Therefore differential expression of PSD95 and Gap43 between APP23 and *wildtype* mice was specific to adolescence.

Taken together, the absence of developmental proteome alterations as well as the predominant down-regulation of neuron-specific proteins in APP23 mice indicate an interference of transgenic APP with mechanisms that generate the naturally

Table 4. Neuron-specific proteins altered in cortex (C) or hippocampus (H) of 1, 2, 7 or 15 months old APP23 mice.

Protein name	Gene name	Protein function in neurons	1H	2H	7H	15H	1C	2C	7C	15C
Brain abundant, membrane attached signal protein 1	Basp1	Regulation of the synaptic cytosceleton [42]						▼		▼
Complexin-1	Cplx1	Modulation of neurotransmitter release, more abundant in inhibitory synapses [43,44,45,46,47]		▼				▼		
Complexin-2	Cplx2	Modulation of neurotransmitter release, more abundant in excitatory synapses [43,44,45,46,47]						▲	▲	
Diazepam binding inhibitor isoform 2	Dbi	Modulation of the GABA(A) receptor, overexpression in mice is associated to deficits in hippocampal learning [48,49]	▲	▼		▲			▼	▲
Postsynaptic density protein 95	Dlg4	Structural component of the postsynaptic compartment [50]		▼			▼	▼		
Dihydropyrimidinase-related protein 2	Dpysl2	Regulation of microtubule assembly in neurons [51]	▲	▲	▲			▲		▼
Neuromodulin	Gap43	Regulation of the cytosceleton, marker for neurogenesis and synaptic plasticity [27]	▼	▼			▼	▼		
Beta-soluble NSF attachment protein	Napb	Component of the SNARE complex[52]			▼					
Gamma-soluble NSF attachment protein	Napg	Component of the SNARE complex[53]		▼		▼			▼	
Neuron derived neurotrophic factor	Nenf	Role in cell proliferation and differentiation during neurogenesis [54]		▼						
Protein kinase C and casein kinase substrate in neurons 1	Pacsin1	Role in endocytosis of synaptic vesicles [55]		▼	▼		▼			
Septin-7	Sept7	Structural component of dendritic spines [56,57]	▼	▼	▼	▼	▼		▲	
Synaptosomal-associated protein 25	Snap25	Component of the SNARE complex [58]			▼					
Syntaxin-binding protein 1	Stxbp1	Regulation of the SNARE complex [59]		▲		▼				▼
Synapsin I	Syn1	Synaptic protein, involved in synaptogenesis and neurotransmitter release [60]						▲		
Synapsin-2	Syn2		▲	▼			▲			
Synapsin Ib	Synl			■				■		▼

▲up-regulated.
▼down-regulated.
■up- and down-regulated.
doi:10.1371/journal.pone.0002759.t004

occurring peak in hippocampal plasticity during adolescence in *wildtype* mice.

Recently, it was reported that low concentrations of natural, soluble Aß (which is enhanced in many mouse models for AD, such as APP23) can alter dendritic spine number, morphology and dynamics in hippocampal neurons [32,33]. Accordingly *Lanz et al.* made an interesting observation when counting dendritic spines of hippocampal CA1-neurons in two different mouse models for AD. They observed the greatest loss of dendritic spines in adolescent transgenic mice. Differences in the number of dendritic spines then disappeared in older, plaque-bearing transgenic mice [25]. When the behavior of APP23 mice was investigated, major learning and memory deficits were found as early as 3 months [17]. Those results are quite compatible with our observations on the proteome level.

In the neocortex, we did not detect a general decrease in proteome alterations related to development in APP23 mice. In this brain region, progression of brain maturation during adolescence appears to be very region-specific. Moreover, differing types of neurons and synapses show differences in vulnerability to Aß-induced degeneration [34]. In line with this, a decrease in the total neocortical synapse number has not been detected in APP23 mice [35]. In contrast, only in neocortical pyramidal neurons has a decrease in spine density been demonstrated in mice carrying human APP bearing the Swedish mutation [36]. We therefore speculate, that since the neocortex is a very heterogenous brain region, observations concerning a disturbed plasticity might be hard to detect when the entire cortex is analyzed.

We identified 293 proteins altered in the APP23 mouse model for AD. Comparing our data to proteomic studies performed with *post mortem* human brain tissue of AD patients [37–39] we found that 22 out of 30 published proteins were altered in both, human AD patients and in our study of APP23 mice. In addition, we identified many proteins such as *Apolipoprotein E* (gene name *Apoe*) [40], *Peptidyl-prolyl cis/trans isomerase NIMA-interacting 1* (gene name *Pin1*) [41], and numerous other proteins that have already been implicated in AD. Although the distribution of altered proteins over functional categories was similar among all postnatal stages, most protein alterations were stage and/or brain region specific. The latter fact also demonstrates that the effect of a mutation on the proteome is highly age- and tissue- dependent.

In conclusion, we found a large number of protein expression differences throughout the entire lifespan of APP23 mice, beginning at ED16, a phase where neurogenesis is predominant in the developing mouse brain suggesting an early impact of transgenic APP. This finding correlates with the observation that APP has an important role during embryonic neurogenesis [30]. Interestingly, during adolescence, rather specific proteome alter-

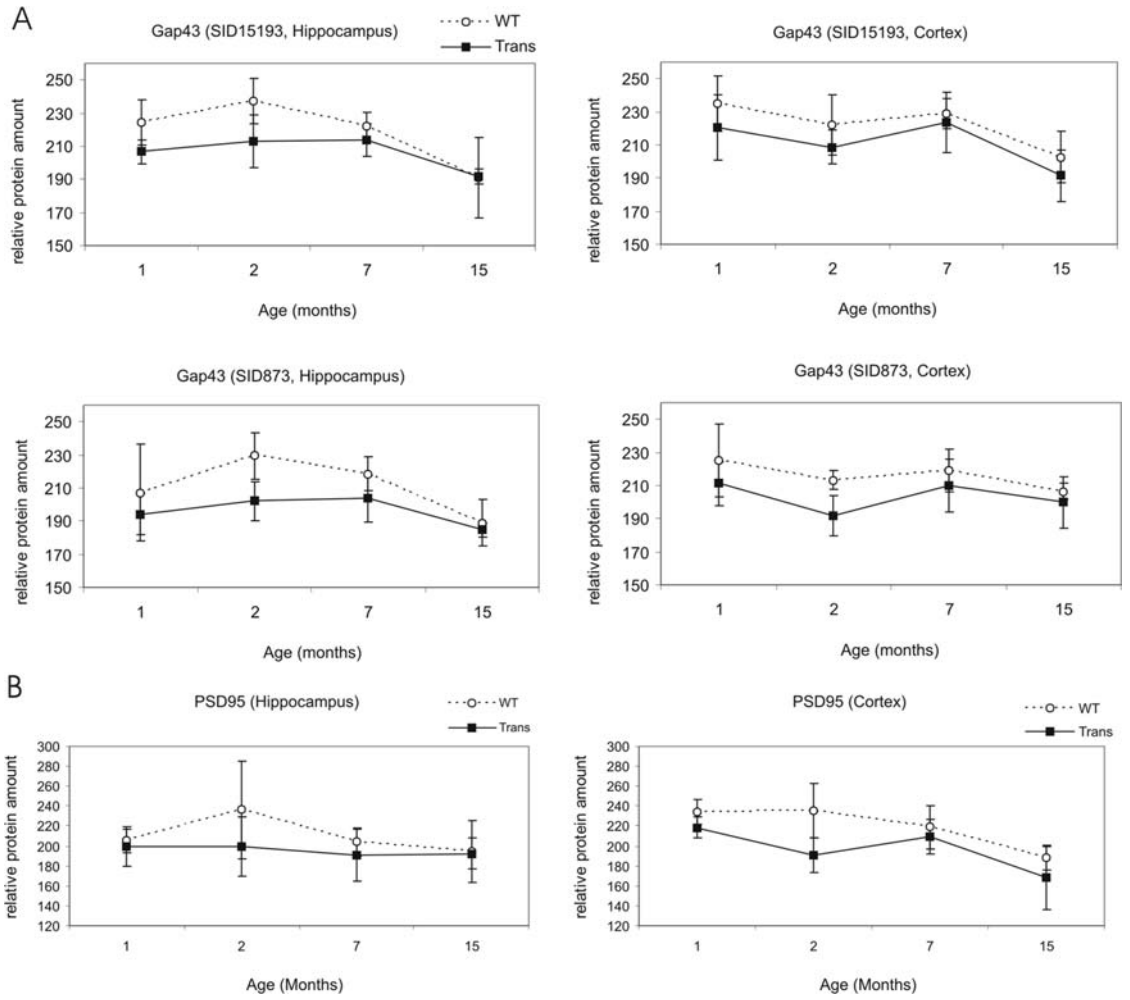

Figure 5. Expression levels of Neuromodulin (Gap43) and Post-synaptic density protein 95 (PSD95) during disease progression. Expression for APP23 (solid squares) and *wildtype* mice (open circles) is shown. A: Two Gap43 spots (Spots SID15193 and SID873) in hippocampus (left) and cortex (right) are shown. Significant differences ($p \leq 0.05$; Student's t-test) in spot abundance were observed in the hippocampus and cortex between 2 and 7 months of age (only *wildtype* mice) and between 7 and 15 months of age (*wildtype* and APP23 mice) as well as in the cortex between 1 and 2 months of age (only APP23 mice). Between *wildtype* and APP23 mice, significant differences in Gap43-expression were observed at 1 and 2 months of age in both brain regions. In general, expression of Gap43 was higher in younger *wildtype* as compared to APP23 mice. During aging, expression of Gap43 decreased in both, APP23 and *wildtype* mice and differences disappeared. B: Expression of PSD95 in hippocampus (left) and cortex (right). Significant differences in spot abundance were observed in the cortex between 1 and 2 (only APP23 mice) as well as between 7 and 15 months of age (*wildtype* and APP23 mice). Between *wildtype* and APP23 mice, significant differences in PSD95-expression were observed at 1 (only cortex) and 2 months (hippocampus and cortex) of age.
doi:10.1371/journal.pone.0002759.g005

ations were observed in the hippocampus. Based on the cellular localization of the proteins altered we conclude that a naturally occurring peak in hippocampal plasticity was absent in APP23 mice. This might be a transient effect of mutated APP on adolescent plasticity. Still, the deficiency may cause a longterm perturbance of the neuronal network finally resulting in memory impairment in aging APP23 mice.

Our findings illuminate the process during the clinically silent period of several years or decades in AD. Synaptic degeneration, which is the major structural correlate to cognitive dysfunction is a slow process initiated by a failure of local regulatory mechanisms of synaptic plasticity [42] which we demonstrated in adolescent APP23 mice. Nevertheless, we need more information to elucidate how exactly the changes found on the proteome level translate to alterations in cellular morphology and phenotype which finally lead to AD.

Materials and Methods

Mouse models and tissues

We investigated the APP23 mouse model for AD with a 7 fold over-expression of hAPP751 carrying the Swedish double-mutation [12]. These mice have been backcrossed to the C57Bl/6 strain for over 20 generations. We investigated cortices of mouse embryos (E16) as well as cortices and hippocampi of 1, 2, 7 and 15 months old male APP23 mice as well as *wildtype* littermates. Sample size was $n = 6$ (biological replicates) for all groups within the study.

Protein Extraction and Separation Procedure

Each protein extract was prepared from individual brain regions of single mice according to our updated protein extraction protocol [10]. Briefly, frozen tissue samples together with sample

buffer (50 mM TRIZMA Base (Sigma-Aldrich, Steinheim, Germany), 50 mM KCl and 20% w/v glycerol at pH 7.5) as well as a proteinase inhibitor cocktail (Complete, Roche Diagnostics) were ground to fine powder in liquid nitrogen and subsequently sonicated on ice (0°C). Afterwards, DNAse and urea were added to the samples. Individual transgenic and *wildtype* tissue samples were then labeled by Cy3 minimal dye (GE Healthcare, Munich, Germany). A pooled *wildtype* tissue sample of the relevant age and tissue was used as internal standard and labeled by Cy5 minimal dye (GE Healthcare). Labeling was carried out according to manufacturer's instructions (400 pmol fluorescent dye per 50 µg of protein). Each Cy3-labeled sample was mixed with the same amount of internal standard. The protein extracts were then supplied with 70 mM dithiothreitol (Biorad, Munich, Germany), 2% v/w of ampholyte mixture Servalyte pH 2–4 (Serva, Heidelberg, Germany) and stored at −80°C.

Two-Dimensional Gel Electrophoresis (2-DE)

Protein samples were separated by the large-gel 2-DE technique developed in our laboratory as described previously [43]. The gel format was 40 cm (isoelectric focusing)×30 cm (SDS-PAGE)×1.0 mm (gel width). Two dimensional fluorescent protein patterns were obtained by fluorescent image acquisition at a resolution of 100 µm (laser scanner Typhoon 9400, GE Healthcare).

Spot evaluation procedure

Protein spot patterns were evaluated by Delta2D imaging software (version 3.4 Decodon, Greifswald, Germany). Briefly, protein patterns of internal standards were matched to each other using "exact" mode of Delta2D. Subsequently, a fusion image was generated employing "union" mode, creating a protein pattern containing all spots from all 2D gels (cortex as well as hippocampus at all age stages except ED16, internal standard gels were not included) within the project. Digital spot detection was carried out on the fusion image, followed by manual spot editing. The spot pattern containing 1769 protein spots was then transferred from the fusion image to all other 2-DE images. In this way, each spot on every gel of the project had the same spot identification number.

Percent volume of spot pixel intensities was used for quantitative analysis of protein expression. Normalized values (after background extraction and normalization to internal standard) were exported from Delta2D in spreadsheet format for statistical analysis. Data sets were analyzed applying paired students t-test (*wildtype* and transgenic samples were handled in pairs from protein extraction to 2-D gel runs) when transgenic groups were compared to *wildtype* groups (n = 6). Unpaired students t-test was performed when *wildtype* or transgenic groups of different age stages were compared (n = 6). Only fold changes over 10% were considered for graphs shown but results were similar when all significantly altered spots were included. All significantly altered proteins that were identified by mass spectrometry are listed in supplementary table S1.

Protein Identification

For protein identification by mass spectrometry, 640 µg protein extract was separated on 2-D gels and stained with a mass spectrometry-compatible silver staining protocol [44]. In order to assign corresponding protein spots between analytical fluorescent and quantitative silver stained 2-D gels reliably, spot patterns of silver stained gels were matched to CyDye stained gels using Delta2D. Protein spots of interest were excised from 2-D gels and subjected to in-gel tryptic digestion. Peptides were analyzed by a Reflex 4 MALDI-TOF mass spectrometer (Bruker Daltonics, Bremen Germany) as described previously [44]. Alternatively, ESI-tandem -MS/MS on a LCQ Deca XP ion trap instrument (Thermo Finnigan, Waltham, MA, USA) was applied. Mass spectra were analyzed using our in-house MASCOT software package (version 2.1) automatically searching NCBI databases.

MALDIM-MS ion search was performed with this set of parameters: (I) taxonomy: Mus musculus, (II) proteolytic enzyme: trypsin, (III) maximum of accepted missed cleavages: 1, (IV) mass value: monoisotopic, (V) peptide mass tolerance 0.8 Da, (VI) fragment mass tolerance: 0.8 Da, and (VII) variable modifications: oxidation of methionine and acrylamide adducts (propionamide) on cysteine. Only proteins with scores corresponding to $p<0.05$, with at least two peptides identified by two independent identifications each were considered. Furthermore, the molecular weight and pI of each protein identified by database search was compared to values obtained from our 2-D patterns.

Analysis of biological functions

Gene symbols and SwissProt accession numbers were used to investigate proteins with altered expression profile in this study. Furthermore, proteins were grouped according to functional categories using parameters like GO and KEGG terms (retrieved by WEBGESTALT [45]) and by literature search.

Immunoblotting

Protein concentration was determined using a Roti-Nanoquant assay (Carl Roth, Karlsruhe, Germany). Brain protein extracts were separated using 12% SDS-PAGE gels, blotted to PVDF membranes and probed with human Aß-antibody (clone 6E10) (Abcam, Cambridge, UK) according to standard immunoblotting procedures.

Supporting Information

Table S1 Proteins significantly altered in transgenic mouse brain regions hippocampus (H) and cortex (C) of different ages (1, 2, 7 and 15 months) as well as in cortex of 16 days old APP23 mouse embryos (ED16).
Found at: doi:10.1371/journal.pone.0002759.s001 (2.33 MB DOC)

Acknowledgments

We would like to thank Bettina Esch, Marion Herrmann, Grit Nebrich, Silke Becker and Andrea Koppelstätter for excellent technical assistance.

Author Contributions

Conceived and designed the experiments: DH CZ JK. Performed the experiments: DH. Analyzed the data: DH MR LM CZ. Contributed reagents/materials/analysis tools: MS. Wrote the paper: DH MR LM CZ JK.

References

1. Arendt T (2005) Alzheimer's disease as a disorder of dynamic brain self-organization. Prog Brain Res 147: 355–378.
2. Masliah E, Mallory M, Ge N, Saitoh T (1992) Amyloid precursor protein is localized in growing neurites of neonatal rat brain. Brain Res 593: 323–328.
3. Loffler J, Huber G (1992) Beta-amyloid precursor protein isoforms in various rat brain regions and during brain development. J Neurochem 59: 1316–1324.
4. Small DH, Clarris HL, Williamson TG, Reed G, Key B, et al. (1999) Neurite-outgrowth regulating functions of the amyloid protein precursor of Alzheimer's disease. J Alzheimers Dis 1: 275–285.
5. Turner PR, O'Connor K, Tate WP, Abraham WC (2003) Roles of amyloid precursor protein and its fragments in regulating neural activity, plasticity and memory. Prog Neurobiol 70: 1–32.

6. Guerreiro N, Staufenbiel M, Gomez-Mancilla B (2008) Proteomic 2-D DIGE Profiling of APP23 Transgenic Mice Brain from Pre-plaque and Plaque Phenotypes. J Alzheimers Dis 13: 17–30.
7. Bondolfi L, Calhoun M, Ermini F, Kuhn HG, Wiederhold KH, et al. (2002) Amyloid-associated neuron loss and gliogenesis in the neocortex of amyloid precursor protein transgenic mice. J Neurosci 22: 515–522.
8. Diedrich M, Mao L, Bernreuther C, Zabel C, Nebrich G, et al. (2008) Proteome analysis of ventral midbrain in MPTP-treated normal and L1cam transgenic mice. Proteomics 8: 1266–1275.
9. Ellis RJ (2001) Macromolecular crowding: obvious but underappreciated. Trends Biochem Sci 26: 597–604.
10. Mao L, Zabel C, Herrmann M, Nolden T, Mertes F, et al. (2007) Proteomic shifts in embryonic stem cells with gene dose modifications suggest the presence of balancer proteins in protein regulatory networks. PLoS ONE 2: e1218.
11. Zabel C, Andreew A, Mao L, Hartl D (2008) Protein expression overlap: more important than which proteins change in expression? Expert Rev Proteomics 5: 187–205.
12. Sturchler-Pierrat C, Abramowski D, Duke M, Wiederhold KH, Mistl C, et al. (1997) Two amyloid precursor protein transgenic mouse models with Alzheimer disease-like pathology. Proc Natl Acad Sci U S A 94: 13287–13292.
13. Bornemann KD, Staufenbiel M (2000) Transgenic mouse models of Alzheimer's disease. Ann N Y Acad Sci 908: 260–266.
14. Kuo YM, Beach TG, Sue LI, Scott S, Layne KJ, et al. (2001) The evolution of A beta peptide burden in the APP23 transgenic mice: implications for A beta deposition in Alzheimer disease. Mol Med 7: 609–618.
15. Prut L, Abramowski D, Krucker T, Levy CL, Roberts AJ, et al. (2007) Aged APP23 mice show a delay in switching to the use of a strategy in the Barnes maze. Behav Brain Res 179: 107–110.
16. Vloeberghs E, Van Dam D, D'Hooge R, Staufenbiel M, De Deyn PP (2006) APP23 mice display working memory impairment in the plus-shaped water maze. Neurosci Lett 407: 6–10.
17. Van Dam D, D'Hooge R, Staufenbiel M, Van Ginneken C, Van Meir F, et al. (2003) Age-dependent cognitive decline in the APP23 model precedes amyloid deposition. Eur J Neurosci 17: 388–396.
18. Kelly PH, Bondolfi L, Hunziker D, Schlecht HP, Carver K, et al. (2003) Progressive age-related impairment of cognitive behavior in APP23 transgenic mice. Neurobiol Aging 24: 365–378.
19. Hefner K, Holmes A (2007) Ontogeny of fear-, anxiety- and depression-related behavior across adolescence in C57BL/6J mice. Behav Brain Res 176: 210–215.
20. Hirabayashi Y, Gotoh Y (2005) Stage-dependent fate determination of neural precursor cells in mouse forebrain. Neurosci Res 51: 331–336.
21. Klose J, Kobalz U (1995) Two-dimensional electrophoresis of proteins: an updated protocol and implications for a functional analysis of the genome. Electrophoresis 16: 1034–1059.
22. Sturchler-Pierrat C, Staufenbiel M (2000) Pathogenic mechanisms of Alzheimer's disease analyzed in the APP23 transgenic mouse model. Ann N Y Acad Sci 920: 134–139.
23. Hsia AY, Masliah E, McConlogue L, Yu GQ, Tatsuno G, et al. (1999) Plaque-independent disruption of neural circuits in Alzheimer's disease mouse models. Proc Natl Acad Sci U S A 96: 3228–3233.
24. Mucke L, Masliah E, Yu GQ, Mallory M, Rockenstein EM, et al. (2000) High-level neuronal expression of abeta 1–42 in wild-type human amyloid protein precursor transgenic mice: synaptotoxicity without plaque formation. J Neurosci 20: 4050–4058.
25. Lanz TA, Carter DB, Merchant KM (2003) Dendritic spine loss in the hippocampus of young PDAPP and Tg2576 mice and its prevention by the ApoE2 genotype. Neurobiol Dis 13: 246–253.
26. Jacobsen JS, Wu CC, Redwine JM, Comery TA, Arias R, et al. (2006) Early-onset behavioral and synaptic deficits in a mouse model of Alzheimer's disease. Proc Natl Acad Sci U S A 103: 5161–5166.
27. Spear LP (2000) The adolescent brain and age-related behavioral manifestations. Neurosci Biobehav Rev 24: 417–463.
28. Johnston MV (2004) Clinical disorders of brain plasticity. Brain Dev 26: 73–80.
29. Blakemore SJ (2008) The social brain in adolescence. Nat Rev Neurosci 9: 267–277.
30. Gralle M, Ferreira ST (2007) Structure and functions of the human amyloid precursor protein: the whole is more than the sum of its parts. Prog Neurobiol 82: 11–32.
31. Benowitz LI, Routtenberg A (1997) GAP-43: an intrinsic determinant of neuronal development and plasticity. Trends Neurosci 20: 84–91.
32. Shrestha BR, Vitolo OV, Joshi P, Lordkipanidze T, Shelanski M, et al. (2006) Amyloid beta peptide adversely affects spine number and motility in hippocampal neurons. Mol Cell Neurosci 33: 274–282.
33. Calabrese B, Shaked GM, Tabarean IV, Braga J, Koo EH, et al. (2007) Rapid, concurrent alterations in pre- and postsynaptic structure induced by naturally-secreted amyloid-beta protein. Mol Cell Neurosci 35: 183–193.
34. Capetillo-Zarate E, Staufenbiel M, Abramowski D, Haass C, Escher A, et al. (2006) Selective vulnerability of different types of commissural neurons for amyloid beta-protein-induced neurodegeneration in APP23 mice correlates with dendritic tree morphology. Brain 129: 2992–3005.
35. Boncristiano S, Calhoun ME, Howard V, Bondolfi L, Kaeser SA, et al. (2005) Neocortical synaptic bouton number is maintained despite robust amyloid deposition in APP23 transgenic mice. Neurobiol Aging 26: 607–613.
36. Alpar A, Ueberham U, Bruckner MK, Arendt T, Gartner U (2006) The expression of wild-type human amyloid precursor protein affects the dendritic phenotype of neocortical pyramidal neurons in transgenic mice. Int J Dev Neurosci 24: 133–140.
37. Tsuji T, Shiozaki A, Kohno R, Yoshizato K, Shimohama S (2002) Proteomic profiling and neurodegeneration in Alzheimer's disease. Neurochem Res 27: 1245–1253.
38. Sultana R, Boyd-Kimball D, Cai J, Pierce WM, Klein JB, et al. (2007) Proteomics analysis of the Alzheimer's disease hippocampal proteome. J Alzheimers Dis 11: 153–164.
39. Butterfield DA, Sultana R (2007) Redox proteomics identification of oxidatively modified brain proteins in Alzheimer's disease and mild cognitive impairment: insights into the progression of this dementing disorder. J Alzheimers Dis 12: 61–72.
40. Mahley RW, Huang Y, Weisgraber KH (2007) Detrimental effects of apolipoprotein E4: potential therapeutic targets in Alzheimer's disease. Curr Alzheimer Res 4: 537–540.
41. Balastik M, Lim J, Pastorino L, Lu KP (2007) Pin1 in Alzheimer's disease: multiple substrates, one regulatory mechanism? Biochim Biophys Acta 1772: 422–429.
42. Arendt T (2003) Synaptic plasticity and cell cycle activation in neurons are alternative effector pathways: the 'Dr. Jekyll and Mr. Hyde concept' of Alzheimer's disease or the yin and yang of neuroplasticity. Prog Neurobiol 71: 83–248.
43. Zabel C, Klose J (2007) High resolution large gel 2-D electrophoresis. Methods Mol Biol, in press.
44. Nebrich G, Herrmann M, Sagi D, Klose J, Giavalisco P (2007) High MS-compatibility of silver nitrate-stained protein spots from 2-DE gels using ZipPlates and AnchorChips for successful protein identification. Electrophoresis 28: 1607–1614.
45. Zhang B, Kirov S, Snoddy J (2005) WebGestalt: an integrated system for exploring gene sets in various biological contexts. Nucleic Acids Res 33: W741–748.

OPEN ACCESS Freely available online

PLoS one

Proteomic Shifts in Embryonic Stem Cells with Gene Dose Modifications Suggest the Presence of Balancer Proteins in Protein Regulatory Networks

Lei Mao[1,2]*, Claus Zabel[1], Marion Herrmann[1], Tobias Nolden[2], Florian Mertes[2], Laetitia Magnol[3], Caroline Chabert[4], Daniela Hartl[1], Yann Herault[3], Jean Maurice Delabar[4], Thomas Manke[2], Heinz Himmelbauer[2], Joachim Klose[1]

1 Institute for Human Genetics, Charité-University Medicine Berlin, Germany, **2** Max Planck Institute for Molecular Genetics, Berlin, Germany, **3** Institut de Transgénose, IEM, UMR6218, CNRS Uni Orléans, Orléans, France, **4** EA 3508, Université Paris Diderot-Paris 7, Paris, France

Large numbers of protein expression changes are usually observed in mouse models for neurodegenerative diseases, even when only a single gene was mutated in each case. To study the effect of gene dose alterations on the cellular proteome, we carried out a proteomic investigation on murine embryonic stem cells that either overexpressed individual genes or displayed aneuploidy over a genomic region encompassing 14 genes. The number of variant proteins detected per cell line ranged between 70 and 110, and did not correlate with the number of modified genes. In cell lines with single gene mutations, up and down-regulated proteins were always in balance in comparison to parental cell lines regarding number as well as concentration of differentially expressed proteins. In contrast, dose alteration of 14 genes resulted in an unequal number of up and down-regulated proteins, though the balance was kept at the level of protein concentration. We propose that the observed protein changes might partially be explained by a proteomic network response. Hence, we hypothesize the existence of a class of ''balancer'' proteins within the proteomic network, defined as proteins that buffer or cushion a system, and thus oppose multiple system disturbances. Through database queries and resilience analysis of the protein interaction network, we found that potential balancer proteins are of high cellular abundance, possess a low number of direct interaction partners, and show great allelic variation. Moreover, balancer proteins contribute more heavily to the network entropy, and thus are of high importance in terms of system resilience. We propose that the ''elasticity'' of the proteomic regulatory network mediated by balancer proteins may compensate for changes that occur under diseased conditions.

Citation: Mao L, Zabel C, Herrmann M, Nolden T, Mertes F, et al (2007) Proteomic Shifts in Embryonic Stem Cells with Gene Dose Modifications Suggest the Presence of Balancer Proteins in Protein Regulatory Networks. PLoS ONE 2(11): e1218. doi:10.1371/journal.pone.0001218

INTRODUCTION

Investigations of etiology and pathogenesis of human diseases are frequently performed using suitable animals as a model system. Most commonly mice are employed where a gene of particular interest is knocked out, mutated or overexpressed. When the effect caused by genome modification is subsequently studied in these mice at the molecular level, usually a large number of changes are observed on the mRNA and protein levels, in spite of the fact that only a single gene was altered. For example, in protein patterns obtained by two-dimensional gel electrophoresis (2-DE) of brain proteins from a mouse model for Parkinson's disease deficient of the parkin protein [1] and from a transgenic mouse model for Huntington's disease [2], we detected 15 and 40 variant proteins, respectively [3,4]. Using more sensitive protein detection methods, such as the differential in-gel electrophoresis (DIGE) technique and analyzing two different brain regions at two different age stages, 87 quantitatively variant proteins were detected in the parkin knock-out mouse [5]. In investigations of a transgenic mouse model for Alzheimer's disease that overexpressed mutated human amyloid precursor protein (*App*) [6] using our large-gel 2-DE [7,8] and DIGE technique, we detected more than one hundred variant proteins (Hartl D. et. al., unpublished results). On the mRNA level, Miller and colleagues observed over 600 changes in a single gene modified Parkinson disease mouse model [9]. Similar results were also obtained in other single gene knock-out mouse models [10].

Apparently, the molecular response to a single gene mutation is of considerable complexity, and certainly much more complex than detectable using current experimental approaches. We have previously compared the protein changes detected in mouse models for different neurodegenerative diseases and, in addition, mouse models of non-neurodegenerative disorders [11]. We found that up to 36% of variant proteins were shared among these different disease models and hypothesized that these protein alterations were not disease-specific. Unexpectedly, when we compared wild-type mice of different inbred strains, we found that most of these putative disease-unspecific protein alterations also occurred as polymorphisms that distinguished strains of mice. This suggested that some, if not most of the protein changes observed when investigating disease models might not be genuinely informative regarding etiology or pathogenesis of the disease under consideration.

To investigate the significance of protein changes under disease conditions, we have chosen a more systematic and simplified approach by using mouse embryonic stem (ES) cells with highly

Academic Editor: Sui Huang, Children's Hospital Boston, United States of America

Received July 2, 2007; **Accepted** November 1, 2007; **Published** November 28, 2007

Funding: This work was co-supported by the German National Genome Research Network (NGFN) program established by the German Ministry for Education and Research (BMBF), and by the EU grant 37627 ''AnEUploidy''. C. Chabert and L. Magnol were supported by a Lejeune foundation grant. T. Manke was supported by a grant from the Volkswagen Foundation.

Competing Interests: The authors have declared that no competing interests exist.

* **To whom correspondence should be addressed.** E-mail: lei.mao@charite.de

defined modifications in a controlled environment. Six mutant cell lines were investigated. All of them contained gene modifications relevant to neurodegenerative diseases. Four cell lines contained one single overexpressed gene, i.e. *App* (a cell surface receptor), *Snca* with changes relevant to Alzheimer's and Parkinson's disease, respectively [9,12] and *Dyrk1a* (a nuclear kinase) as well as *Dopey2* (a leucine zipper-like protein) both relevant to Down syndrome [13,14]. In two other cell lines, a segment encompassing 14 genes relevant to Down syndrome was duplicated (trisomic) in one case and deleted (monosomic) in the other [15]. The six mutant cell lines were investigated by 2-DE and altered protein expression was recorded by comparison with the respective parental lines. Many variant proteins showing up or down-regulation were observed. Profound quantitative analysis of protein changes led us to the hypothesis that the cellular proteome is kept quantitatively in balance by a particular class of proteins to which we refer as "balancer proteins". Accordingly, we assume that when the quantitative arrangement of the proteome is perturbed by gene dosage effects, it will be subjected to a rearrangement in order to achieve a new balance. Thus, the many protein changes observed may reflect the rearrangement of the proteome to protect the cell from deleterious effects of gene dosage mutations.

RESULTS

Proteins expressed in ES cells were separated by large-gel 2-DE. On a representative 2-DE pattern of total protein extract from ES cells, a total of 4958 protein spots could be scored visually (Figure 1). Using Delta2D imaging software (see Methods), over 5500 protein spots were detected. Six different transgenic cell lines were investigated in this study. These comprised two cell lines in which one single gene was duplicated (*mES_Dyrk1a_Tris* or *mES_Dopey2_Tris*), and two cell lines in which one gene was overexpressed (5.5 times more than wild-type in *mES_hAPP* or 1.6 times in *mES_Snca*). In two cell lines gene dosage was altered over a chromosomal region that spanned 14 genes on mouse chromosome 17. A hemizygous deletion line was monosomic for the interval (*mES_14_Mono*). The other line contained an engineered duplication of the segment, and thus was trisomic (*mES_14_Tris*). No difference was observed between transgenic and parental cell lines with respect to cellular morphology and growth behavior. The six cell lines were compared to their parental cell lines with regard to their protein expression profiles. The number of proteins that showed significantly increased or decreased expression, when compared to their expression in parental cell lines, was in the range of 70 to 110 variants per cell

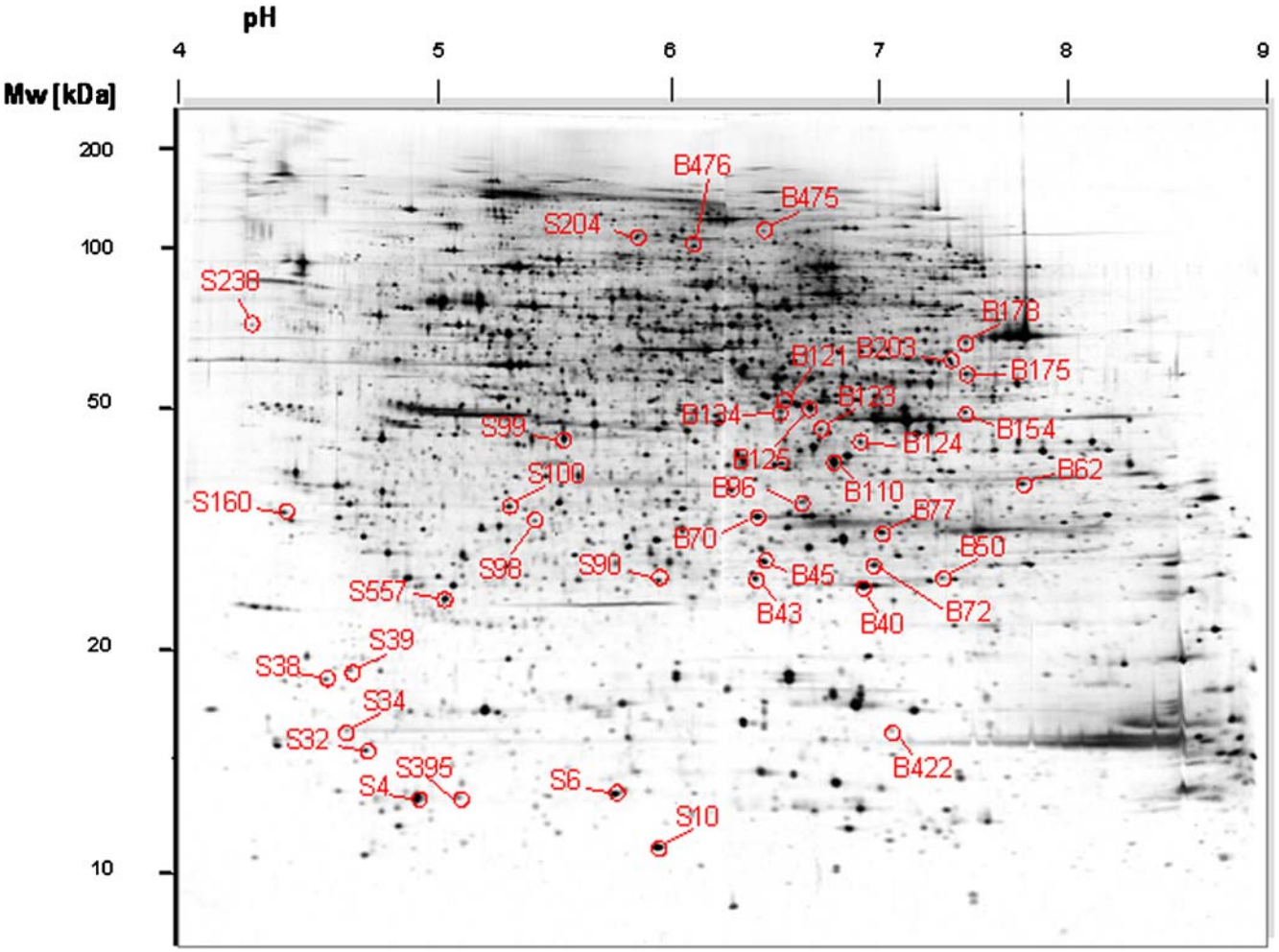

Figure 1. Representative protein expression pattern of mouse embryonic cell lines as revealed by large-gel 2D-electrophoresis. Over 5500 proteins (including protein isoforms) were resolved on a single gel. Highlighted spots correspond to spot ID of candidate balancer proteins detailed in Table 2.
doi:10.1371/journal.pone.0001218.g001

Table 1. Number of quantitatively variant proteins in six transgenic mouse embryonic stem cell lines.

Quantitative changes	Number of variant proteins in different transgenic cell lines					
	mES_14_Mono*	mES_14_Tris*	mES_Dopey2_Tris	mES_Dyrk1a_Tris	mES_hAPP	mES_Snca
Up-regulated	44	44	37	41	46	52
Down-regulated	62	26	45	37	47	57
Total	106	70	82	78	93	109

*The segment from mouse chromosome 17 includes 14 genes.
doi:10.1371/journal.pone.0001218.t001

line (Table 1). In total, 255 distinct variant proteins were observed in the six cell lines (Table S1). The data-adjusted modified t-test SAM (Significance Analysis of Microarrays) was used to calculate that the false discovery rate for obtaining a comparable result was less than 1 %.

In the four cell lines that overexpressed a single gene, 40 to 50 proteins were up-regulated. This was always accompanied by a similar number of down-regulated proteins. A quite different situation was found for the two cell lines with the dosage alteration in 14 genes: If duplicated, 60% of proteins were up-regulated and 40% were down-regulated (40%). In case of deletion, a similar imbalance was found, but in the opposite direction, i.e. about 60% of the variant proteins showed decreased expression, while only about 40% were over-expressed (Figure 2A). The observations described above were based on the number of proteins showing altered expression profiles in the transgenic cell lines. In the next step, we investigated the total protein amount showing altered expression within each cell line by determining relative protein concentrations (protein spot volumes) across all altered proteins. This resulted in a balanced picture, i.e. no significant difference could be detected in the protein amount undergoing up and down-regulation (Figure 2B). Most importantly, this was even true for the two cell lines with 14 genes altered, which showed a drastic imbalance in the number of proteins that underwent up or down-regulation (see above).

When we compared proteins that showed quantitative changes among the six cell lines, we found that many of these proteins were altered in several cell lines. Specifically, 38 proteins showed changes in more than three cell lines. Among them, the expression of three proteins changed in all six cell lines, eight proteins changed in five, while 27 proteins changed in four of six different transgenic ES cell lines. In contrast, 114 proteins were altered only in one cell line. In order to test to which extent changes of expression in the same proteins may occur by chance in multiple cell lines independently, the numbers of observed co-changed proteins in different numbers of cell lines were compared to theoretical numbers of co-changed proteins, assuming that a total of 800 protein spots were investigated, among which 10% were differentially expressed in transgenic and control cell lines (Figure 3). Our calculation showed that the occurrence of the same protein alteration in more than three cell lines was unlikely to be coincidental ($p<0.001$).

An interesting observation was made when we considered proteins that were only altered in both *mES_14_Mono* and *mES_14_Tris*: Two thirds of them showed the same change tendency, i.e., either up-regulated in both cell lines, or down-regulated in both cell lines, despite opposite gene dose alteration (trisomy versus monosomy). This suggested that many changes could be unrelated with respect to the gene(s) that caused the dosage imbalance. Hence, we hypothesize that the proteins showing changes in several cell lines (38 proteins, see above) represent a particular class of proteins, which we propose to call "balancer" proteins (Table 2). Different from that, proteins that were altered only in a single cell line are called here "cell line-specific proteins" to denote protein alterations specific to a cell line characterized by a distinct genetic alteration (114 proteins, see above).

Among the candidate balancer proteins, seven of them were always increased in their expression in our experiment (Table 2). They are: *Atp6v1c1*, *Ccdc25*, *Eno1*, *Nudt16l1*, *Psmb7*, *Ranbp5* and *S100a11*. On the other hand, three balancer proteins (*Bat2d*, *Psmb6* and *Tceb2*) were consistently down-regulated in their expression. One protein (*Psme1*) was down-regulated in three cell lines with transgene overexpression (*mES_14_Tris*, *mES_Dyrk1a_Tris* and *mES_Snca*), while it was up-regulated in *mES_14_Mono*. To determine whether putative balancer or cell line-specific proteins might be direct interaction partners of genes mutated in the six cell lines, we queried all mutated genes, balancer proteins and cell line-specific proteins in the KEGG pathway database. No overlapping KEGG pathway entries were detected between balancers and mutated genes. On the contrary, four KEGG pathway terms of cell line-specific protein overlapped with that of mutated genes in our six ES cell lines. These included methionine metabolism, selenoamino acid metabolism, ABC transporters and purine metabolism. Similar conclusions could be drawn from Biocarta pathway database queries.

In order to investigate whether balancers and cell line-specific proteins might represent two different classes of proteins with certain biochemical and biophysical properties, we compared these two sets according to different parameters. The spectrum of biochemical and biophysical criteria selected for characterization included molecular weight, isoelectric point, predicted protein instability, aliphatic index, hydrophobicity, cellular abundance, polymorphisms (i.e. allelic diversity) and number of direct protein interaction partners. As summarized in Table 3, balancers and cell line-specific proteins showed no perceivable difference in their molecular weights and isoelectric points, neither in their instability, nor regarding aliphatic index or hydrophobicity. However, balancer proteins were significantly more abundant in the cell ($p = 0.008$). Furthermore, cell line-specific proteins were found to have twice as many interaction partners as balancer proteins ($p = 0.004$) (Figure 4B). We then queried the Mouse Genome Informatics Database (www.informatics.jax.org) for the occurrence of single nucleotide polymorphisms (SNPs) in balancer and cell line-specific proteins as a measure of their allelic diversity. Interestingly, the potential balancers had significantly more non-synonymous SNPs in coding regions than potential cell line-specific proteins (Table 3), while no significant difference could be established for other SNP evaluations (total number of SNPs, proportion of synonymous SNPs in the coding regions and the frequency of SNPs in the 5′-UTR, 3′-UTR, introns and sequences flanking upstream and downstream of a locus).

To assign functional categories, a Gene Ontology (GO) term enrichment analysis was performed. Tables 4 and 5 give

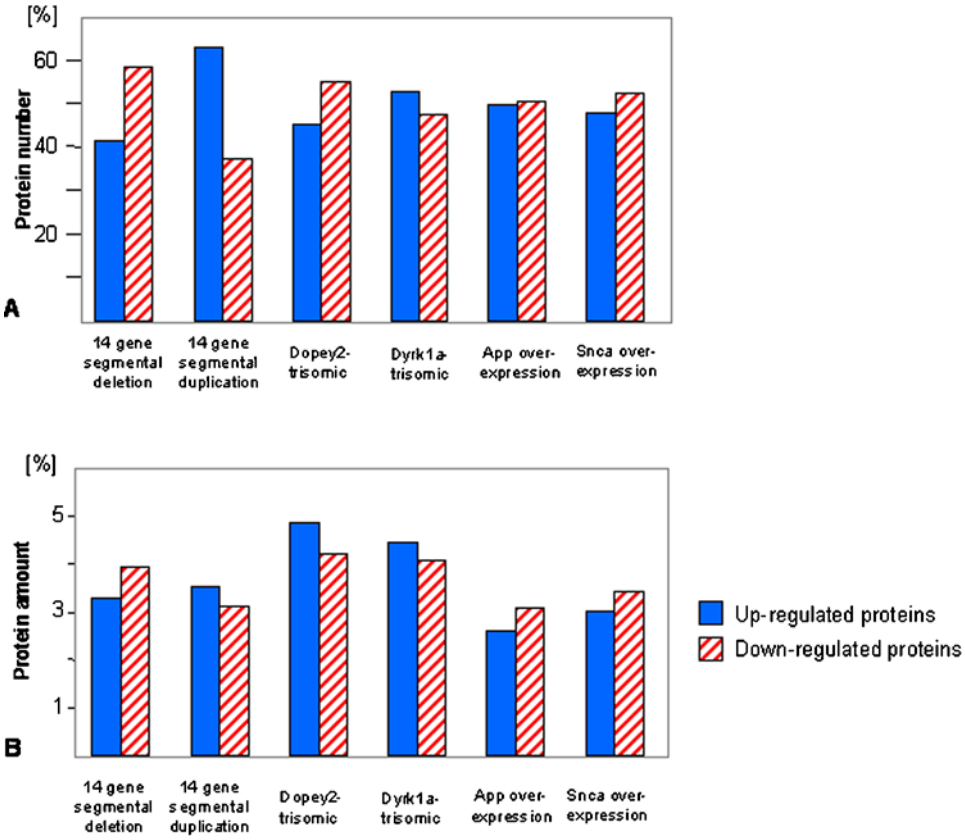

Figure 2. Proteins that showed altered expression in transgenic ES cell lines. (A) Number of altered proteins in each transgenic cell line, expressed as percentile of total number of altered proteins. (B) Amount of proteins that underwent altered expression in each cell line, represented as percent of total spot volume that was up or down-regulated in transgenic cell lines. Dose alteration of 14 genes could no longer be balanced by an equivalent number of variant proteins. However, a balance remained at the level of protein concentration.
doi:10.1371/journal.pone.0001218.g002

a summary of GO-terms that occurred more frequently in balancers or cell line-specific proteins, respectively, based on human GOA database searches (see Methods for details). Eight GO-terms were specifically over-represented in balancer candidates. They comprise protein degradation, disulfide modification and electron carrier processes. In contrast, over 33 GO-terms were enriched in cell line-specific proteins. Notably, a large part of them were involved in mRNA processing and related functions. These two GO-term sets overlap by participating in protein chaperoning of catabolism processes.

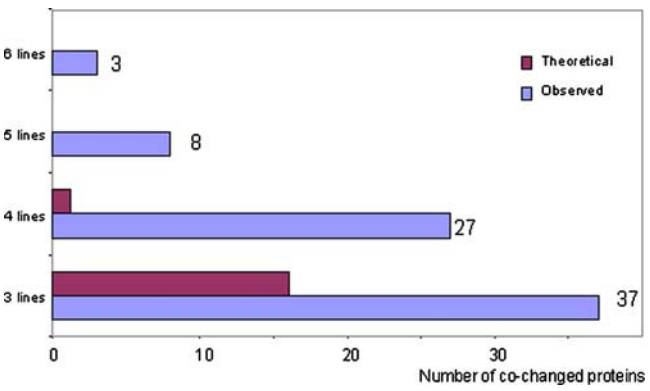

Figure 3. Comparison of observed number of co-changed proteins against a theoretical calculation of co-changed proteins across six different transgenic cell lines. It was assumed that a total of 800 protein spots were investigated, among which 10% of the proteins change in their expression profile. This comparison shows that the occurrence of the same protein alteration in more than three cell lines is unlikely to be coincidental.
doi:10.1371/journal.pone.0001218.g003

Next, we undertook an analysis of protein-protein interactions that balancer and cell line-specific proteins participate in, chiefly based on the Human Reference Protein Database (see methods for details). The protein-protein interaction graph constructed from our ES cell data comprised 2677 nodes (distinct proteins, indicated by gene symbol). This interaction graph shared the common feature of scale-free geometry with other protein interaction networks, such as that of *E. coli* or *Saccharomyces cerevisiae* [16,17]. Among all protein nodes, 2565 (96%) of them could be linked to a giant network component with heterogeneous degree distribution. The remaining 112 proteins formed 41 isolated components, with the number of nodes varying from one to twelve. Figure 5 shows a subset of the protein-protein interaction network centered around the proteasome subunits. In the entropy analysis of the network, we focused on the giant network component, since the network entropy is only defined for the strongly connected components of the network. All 38 balancer proteins belonged to the giant network component, as well as 79 out of 114 cell line-specific proteins.

As network entropy is a measure of system homeostasis, we may expect high-ranking proteins to be affected more frequently as the cell responds to various stimuli. Through a direct comparison of balancers to cell line-specific proteins using their entropic

Table 2. Proteins changed in more than three transgenic ES cell lines (proposed balancer proteins).

Spot ID	Protein Name	Gene Symbol	Behavior
B125	aminolevulinate, delta-, dehydratase	*Alad*	3 ↑, 2 ↓
S37	albumin	*Alb*	1 ↑, 3 ↓
B40	ATPase, H+ transporting, lysosomal V1 subunit C1	*Atp6v1c1*	always up
S34	BAT2 domain containing 1	*Bat2d*	always down
B96	carbonic anhydrase 2	*Car2*	1 ↑, 3 ↓
B476	calcium response factor	*Carf*	2 ↑,2 ↓
B72	coiled-coil domain containing 25	*Ccdc25*	always up
B178	eukaryotic translation elongation factor 1 alpha 1	*Eef1a1*	1 ↑, 3 ↓
B70	enolase 1, alpha non-neuron	*Eno1*	always up
S10	fatty acid binding protein 3, muscle and heart	*Fabp3*	2 ↑, 4 ↓
B110	guanine nucleotide binding protein (G protein), beta polypeptide 2 like 1	*Gnb2l1*	1 ↑, 3 ↓
S98	golgi autoantigen, golgin subfamily b, macrogolgin 1	*Golgb1*	1 ↑, 4 ↓
B175	glutamate oxaloacetate transaminase 2, mitochondrial	*Got2*	3 ↑, 1 ↓
B121	glyoxylate reductase/hydroxypyruvate reductase	*Grhpr*	3 ↑, 2 ↓
S160	histone cell cycle regulation defective interacting protein 5	*Nfu1*	2 ↑, 2 ↓
B154	heterogeneous nuclear ribonucleoprotein A2/B1	*Hnrpa2b1*	4 ↑, 1 ↓
B134	LIM and SH3 protein 1	*Lasp1*	2 ↑, 4 ↓
B123	mitochondrial ribosomal protein L39	*Mrpl39*	3 ↑, 2 ↓
S38	nucleophosmin 1	*Npm1*	1 ↑, 3 ↓
B62	nudix (nucleoside diphosphate linked moiety X)-type motif 16-like 1	*Nudt16l1*	always up
B475	polyribonucleotide nucleotidyltransferase 1	*Pnpt1*	1 ↑, 3 ↓
S238	pyrophosphatase (inorganic) 1	*Ppa1*	2 ↑, 2 ↓
B45	PPAR-alpha interacting complex protein 285	*Pric285*	4 ↑, 1 ↓
S557	proteasome (prosome, macropain) subunit, beta type 6	*Psmb6*	always down
B77	proteasome (prosome, macropain) subunit, beta type 7	*Psmb7*	always up
S90	proteasome (prosome, macropain) 28 subunit, alpha	*Psme1*	1 ↑, 3 ↓
B43	RAN binding protein 5	*Ranbp5*	always up
S6	S100 calcium binding protein A11 (calgizzarin)	*S100a11*	always up
B203	serine (or cysteine) peptidase inhibitor, clade H, member 1	*Serpinh1*	1 ↑, 3 ↓
B422	single-stranded DNA binding protein 1	*Ssbp1*	2 ↑, 2 ↓
B50	transgelin	*Tagln*	1 ↑, 3 ↓
B124	transaldolase 1	*Taldo1*	3 ↑, 2 ↓
S32	transcription elongation factor B (SIII), polypeptide 2	*Tceb2*	always down
S204	thimet oligopeptidase 1	*Thop1*	1 ↑, 3 ↓
S100	tropomyosin 1, alpha	*Tpm1*	1 ↑, 4 ↓
S395	Thioredoxin-like 2	*Txn1*	2 ↑, 2 ↓
S4	Thioredoxin 1	*Txn1*	2 ↑, 2 ↓
S99	Thioredoxin-related protein	*Txnl1*	2 ↑, 2 ↓

doi:10.1371/journal.pone.0001218.t002

contribution, we found that balancers, on average, possess significantly higher values of entropic contribution than cell line-specific proteins ($p = 0.02$, Wilcoxon rank test, Figure 4). Alternatively, we ask to what extent the entropic measurement can distinguish between cell line-specific proteins and balancers within the background of all proteins in the giant component. To this end, we took the same number of top-ranking proteins based on their entropic contribution and studied their overlap with our 38 balancers or 79 cell line-specific proteins, respectively. Assuming a hypergeometric distribution over a total of 2526 proteins, this corresponds to $p = 0.018$ and $p = 0.094$ for balancers and cell line-specific proteins, respectively. This illustrates that the entropic ranking of proteins selects balancers preferentially, thus it validates our previous observation that proteins with high contribution to network entropy are enriched in the set of balancer proteins.

DISCUSSION

We investigated the effect of gene dosage alterations on the proteome of mouse embryonic stem (ES) cells. Using our large-gel 2-DE, extraordinary in its high resolution and reproducibility [7], total protein extracts from six different ES cell lines were analyzed. In four of them, one single gene was overexpressed either by gene duplication (*Dyrk1a*, *Dopey2*) or by conventional stable gene

Table 3. Comparison of protein properties of balancer and cell line-specific proteins.

Protein properties	Balancers	Cell line-specific proteins	p-value
Molecular weight (kD)	47.2±42.5	48.3±47.3	0.906
Isoelectric point	6.52±1.68	6.98±1.71	0.14
Instability	41.3±12.8	41.8±11.2	0.81
Aliphatic index	79.7±14.2	77.7±16.8	0.51
Gravy score	−0.449±0.337	−0.444±0.357	0.94
Cellular abundance (% volume of protein spot)	**0.158±0.169**	**0.118±0.116**	**0.0082**
No. of interaction partners[3]	**4.9**	**7.8**	**0.0048**
Total No. of SNPs per locus	29.5±40.1	30.6±58.7	0.46
No. of upstream SNPs [1]	2.7±4.7	1.9±4.9	0.53
No. of SNPs in 5′-UTR	1.0±2.3	1.9±4.9	0.76
No. of SNPs in introns	18.8±31.3	20.5±48.1	0.43
No. of synonymous SNPs in ORF	1.3±3.1	1.4±0.5	0.12
No. of nonsynonymous SNPs in ORF	**2.8±1.83**	**0.7±1.8**	**0.026**
No. of SNPs in 3′-UTR	2.1±4.6	1.1±3.2	0.0855
No. of SNPs downstream [2]	2.6±5.4	3.2±5.3	0.89
Entropic contribution[3]	**1.51**	**0.97**	**0.02**

Values in bold indicate significant difference between balancer and cell line-specific proteins
[1]Interval up to a position 2000 bp upstream of the transcription start site
[2]Interval from polyadenylation site to a position 2000 bp downstream
[3]Standard errors not shown since the distributions are tend to be screwed.
doi:10.1371/journal.pone.0001218.t003

transfection (*App*, *Snca*). In two other cell lines, the dosage of a whole set of 14 genes was altered so that the segment was either duplicated (trisomic) or deleted (monosomic). According to our observations, dose alteration of a single gene led to quantitative changes in a large number of proteins. Surprisingly however, altering the dosage of 14 genes instead of one gene did not increase the number of altered proteins accordingly. In effect, the frequency of protein variations induced by one or 14 altered gene dosages was in a similar range. Hence, we propose that the protein changes observed might not completely reflect reactions of proteins functionally linked with the genes whose dosage was altered. Rather, these changes may at least be partially explained as a global response of the cellular proteome to the gene dosage defect.

Considering the protein changes observed in our ES cell lines in more detail, we found that in all cases where a single gene was overexpressed, the number of proteins which were up-regulated was always in equilibrium with the number of down-regulated proteins (Figure 2A). Moreover, when we measured up and down-regulation of proteins in terms of protein amount instead of number of proteins, a balance in up and down-regulation was also observed. The situation was different in the two cell lines carrying alterations in 14 genes. Here, the number of proteins up or down-regulated was no longer in equilibrium: In *mES_14_Tris*, about 60% of the altered proteins were up-regulated, whereas about 40% of the proteins were down-regulated. The changes in the *mES_14_Mono* showed the same ratio, but in reversed direction (ca. 60% down, 40% up). However, regarding the protein variations at the level of protein amount, a balance reoccurred even in cell lines with 14 genes altered (Figure 2B).

We therefore hypothesize the existence of a proteome-wide acting regulatory mechanism that leads to a compensation of an imbalance in the quantitative arrangement of the cellular proteome. Within the proteome of a cell, the relative concentration of each particular protein should be precisely arranged and well balanced. In consequence, aberrant quantitative changes, even in a single protein, may alter the relative concentration of many other proteins, thereby disturbing the overall proteomic balance. In this situation, the first response of the cell could be towards restoring the balance in the cellular proteome in order to maintain normal cellular operations. As a result, below certain thresholds, a rebuild of system homeostasis by quantitative rearrangement of the proteome may be achieved.

Several considerations that originate from theoretical biology and experimental model systems are in line with our hypothesis outlined above: The theory of protein minimization [18] states that all protein levels within a cell are maintained at the minimum level compatible with function, while metabolic pathway fluxes are maintained at the maximum. This is explained as a consequence of an increasing number of proteins occurring in the course of evolution, e.g. by gene duplication, that needed to be accommodated in the cells. Since the resources of a cell (such as space, energy, metabolites e.g. amino acids and unbound water to allow diffusion) did not increase accordingly, the occurrence of new proteins in evolution was always accompanied by a concentration reduction of proteins that already present. In order to keep cellular functions intact in spite of protein concentration reduction, the functional efficiency of the already established proteins (e.g. the specific activity of enzymes) had to increase. Another theory, the excluded volume theory established by A.P. Minton [19,20] deals with the high degree of macromolecular crowding in cells. If a protein is overexpressed in a cell, movement of this and surrounding proteins becomes restricted due to excluded volume. Thus the distance between protein molecules becomes smaller than the diameter of moving protein molecules. Proteins react to this situation with conformational changes and tend to aggregate and to lose their function. Apparently, active or passive regulatory mechanisms exist that keep the cellular protein concentrations within a physiologically buffered range.

When the relative cellular proteome composition is disturbed, probably not all proteins are changed in their quantitative

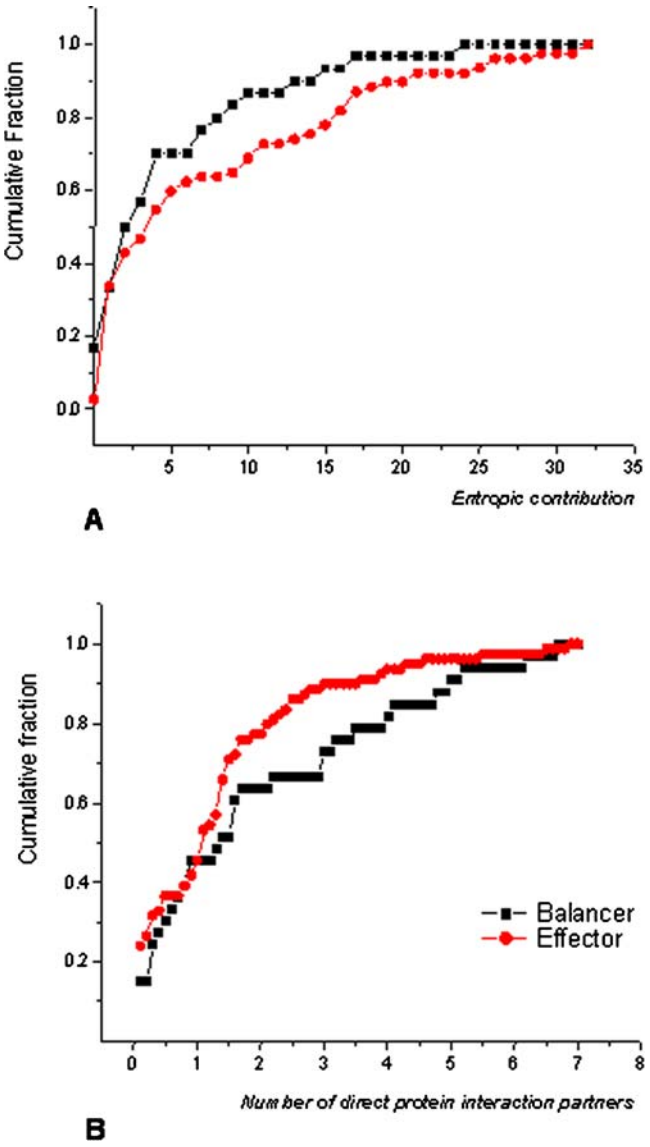

Figure 4. Cumulative fraction plots of ''balancer''-''cell line-specific protein'' comparison. (A) Entropic contribution.; (B) Number of direct protein interaction partners. Compared to cell line-specific proteins, balancers possess significantly higher values of entropic contribution and a low number of direct interaction partners.
doi:10.1371/journal.pone.0001218.g004

occurrence to the same extent. Regarding our hypothesis, we suggest the existence of a special class of proteins that are particularly effective in such rebalancing approaches. This led us to propose discrimination between balancer and cell line-specific proteins. We hypothesize that balancers are proteins that buffer or cushion a cellular system by common properties, i.e., properties not necessarily related to their specific functions. Accordingly, the same proteins may change when different system disturbances have caused protein imbalance. In line with these definitions, we found no considerable overlapping functions between balancer proteins and the transgenes. In contrast, the expression alterations of cell line-specific proteins could more likely have been directly induced by gene dosage modifications. This finding further supports the notion that the changes of balancer proteins represent more peripheral cellular affairs.

To find out whether balancer proteins might have further distinct properties, we analyzed them using multiple categories outlined in tables 3, 4 and 5. We found that potential balancers seem to be of high cellular abundance. This is plausible as very low abundance proteins (e.g. regulatory proteins, transcription factors and receptors) are possibly present only in a few copies per cell and thus have no real buffer capacity to compensate imbalance at the proteomic scale. In retrospect, it is known that all proteins visible on 2-DE patterns are relatively abundant [21]. Still, even under these preconditions, balancer proteins seem to be more abundant than cell line-specific proteins. Moreover, potential balancers turned out to be more polymorphic in their coding regions than cell line-specific proteins. Protein polymorphisms indicate proteins which became less constrained in the course of evolution [22]. As a consequence, proteins bearing a higher degree of polymorphisms (including balancers) may tend to be more flexible in quantitative changes, whereas cell line-specific proteins may require a stronger connection between expression level and function.

Another trait of our candidates for balancer proteins was found by screening a protein-protein interaction database available online (HPRD). Here, balancers possessed less direct interaction partners than cell line-specific proteins. Interestingly, in the protein interaction network published by Stelzl et al. for human proteins [23], disease-related proteins annotated in the *Online Mendelian Inheritance in Man* database (OMIM) were located almost exclusively in the area of low connective level. This correlation may indicate a particular role of balancer proteins in diseases conditions, but at the same time raises our suspicion that balancer proteins are more likely to be identified as disease-associated proteins partially due to their frequent and reproducible alterations.

Towards understanding how balancer proteins in their functional properties may impart elasticity to the proteomic

Table 4. GO-terms enriched among balancer proteins detected in the proteome of mouse ES cells.

GO-ID	Count[§]	Total[#]	p-Value	GO-term	Category*
GO:0009056	7	877	0.002	catabolism	BP
GO:0006091	7	1028	0.003	generation of precursor metabolites and energy	BP
GO:0030508	2	5	0.001	thiol-disulfide exchange intermediate activity	MF
GO:0015035	3	73	0.003	protein disulfide oxidoreductase activity	MF
GO:0016836	3	81	0.003	hydro-lyase activity	MF
GO:0016835	3	92	0.004	carbon-oxygen lyase activity	MF
GO:0015036	3	96	0.004	disulfide oxidoreductase activity	MF
GO:0009055	4	289	0.007	electron carrier activity	MF

[§]Number of balancer proteins bearing this GO-term.
[#]Total number of proteins in the human GOA database annotated with this GO-term.
*BP: biological process; MF: Molecular function.
doi:10.1371/journal.pone.0001218.t004

Table 5. Enriched GO-terms among cell line-specific proteins detected in the proteome of mouse embryonic stem cells.

GO-ID	Count[§]	Total[#]	p-Value	GO-term	Category*
GO:0043170	41	7475	7.85E-07	macromolecule metabolism	BP
GO:0006396	11	503	3.49E-06	RNA processing	BP
GO:0044238	53	11859	3.83E-06	primary metabolism	BP
GO:0016070	12	662	4.71E-06	RNA metabolism	BP
GO:0008152	57	13425	4.76E-06	metabolism	BP
GO:0008614	2	2	1.72E-04	pyridoxine metabolism	BP
GO:0008615	2	2	1.72E-04	pyridoxine biosynthesis	BP
GO:0042816	2	2	1.72E-04	vitamin B6 metabolism	BP
GO:0042819	2	2	1.72E-04	vitamin B6 biosynthesis	BP
GO:0043283	24	4377	0.001	biopolymer metabolism	BP
GO:0006139	27	5422	0.002	nucleobase, nucleoside, nucleotide and nucleic acid metabolism	BP
GO:0016071	6	292	0.002	mRNA metabolism	BP
GO:0006397	5	243	0.006	mRNA processing	BP
GO:0006511	5	248	0.006	ubiquitin-dependent protein catabolism	BP
GO:0019941	5	248	0.006	modification-dependent protein catabolism	BP
GO:0043632	5	248	0.006	modification-dependent macromolecule catabolism	BP
GO:0044260	25	5232	0.007	cellular macromolecule metabolism	BP
GO:0019538	26	5543	0.007	protein metabolism	BP
GO:0000375	4	148	0.007	RNA splicing, via transesterification reactions	BP
GO:0000377	4	148	0.007	RNA splicing, via transesterification	BP
GO:0000398	4	148	0.007	nuclear mRNA splicing, via spliceosome	BP
GO:0006564	2	16	0.009	L-serine biosynthesis	BP
GO:0030530	2	16	0.009	heterogeneous nuclear ribonucleoprotein	BP
GO:0044257	5	288	0.009	cellular protein catabolism	BP
GO:0051603	5	287	0.009	proteolysis during cellular protein catabolism	BP
GO:0003723	14	930	3.83E-06	RNA binding	MF
GO:0008266	2	2	1.72E-04	poly(U) binding	MF
GO:0016018	2	6	0.002	cyclosporin A binding	MF
GO:0050662	5	193	0.002	coenzyme binding	MF
GO:0000166	21	3851	0.003	nucleotide binding	MF
GO:0048037	5	220	0.004	cofactor binding	MF
GO:0003727	2	12	0.006	single-stranded RNA binding	MF
GO:0008144	2	17	0.010	drug binding	MF

[§]Number of cell line-specific proteins bearing this GO-term.
[#]Total number of proteins in the human GOA database annotated with this GO-term.
*BP: biological process; MF: Molecular function.
doi:10.1371/journal.pone.0001218.t005

system, we queried what kind of shared functional categories these proteins may possess (biological process and molecular function GO terms). Compared to the candidate balancers, cell line-specific proteins were associated with a much broader spectrum of GO-categories (Table 4 and 5). In addition, cell line-specific proteins but not balancers were highly involved in mRNA-related processes. This is in line with the fact that these processes are tightly regulated. Proteins involved therein are thus prone to concentration alteration, a property incompatible with a role as balancers. Moreover, our set of putative balancer proteins was enriched in stress and metabolic proteins compared to the remaining proteins altered. The physiological activity of a significant subset of cellular proteins is modified by the redox state of regulatory thiol groups. The cellular redox homeostasis depends on the balance between oxidation of thiols through oxygen and reactive oxygen species and reduction by thiol-disulfide transfer reactions. In this respect, it would make sense that potential balancer proteins are enriched in GO categories implicated in disulfide oxidoreductase and thiol disulfide exchange.

One particularly important feature of a living system is its resilience against external and internal changes, which, at the molecular level, amounts to perturbations in network parameters. In an attempt to analyze this robustness of the cellular system, we applied a network analysis, which is motivated by concepts from statistical mechanics and dynamical systems theory. Our approach is based on the assumption that biological processes often operate at steady state, which corresponds to the observed phenotype [24]. It has been shown that changes in network entropy, a fundamental statistical property, are positively correlated with system robustness. In turn, the entropic contribution of a protein describes its impact on network integrity. Removal of nodes with high entropic contribution more often result in lethal phenotypes from yeast and

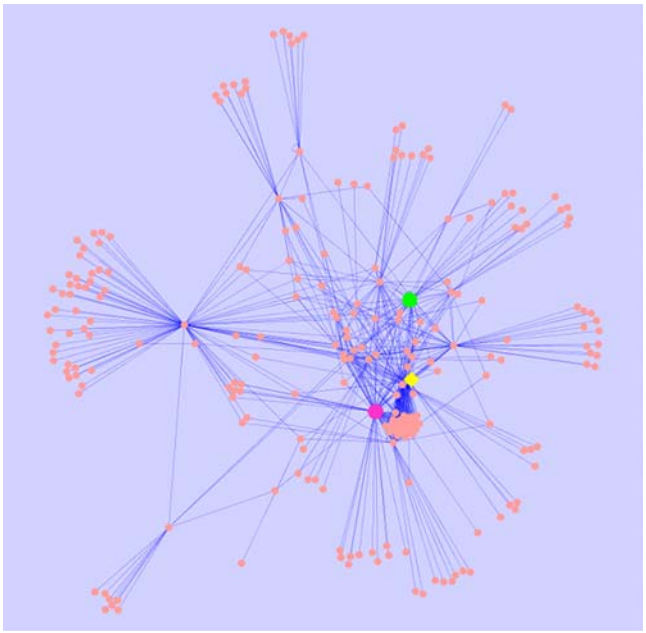

Figure 5. A protein-protein interaction subgraph showing the proteasome subunits, where nodes denote proteins and the edges describe protein-protein interaction. Two local hub proteins of this subgraph (Psma2 and Psma3) belong to cell line-specific proteins, while a candidate balancer protein (Psmb6) represents a connection between these two modules (see discussion for details). This supports our assumption that balancer proteins could be connective hubs between different modules. Protein marked in green: Psma2; yellow: Psmb6; magenta: Psma3.
doi:10.1371/journal.pone.0001218.g005

C. elegans [25]. Our ranking analysis shows that there is a difference between balancers and cell line-specific proteins: Compared to cell line-specific proteins, balancers possessed a higher entropic contribution. This structural property suggests that balancers might be able to attenuate system disturbance more efficiently. The existence of balancer proteins could therefore be responsible for the elasticity of a cellular system.

For example, a number of proteins representing proteasome subunits showed altered expression in our transgenic cell lines. Five of them belong to balancer candidates, while three other proteasome subunits belong to cell line-specific proteins. Considering the proteasome sub-interaction network in detail (Figure 5), we noticed that *Psma2* and *Psma3*, which are local hubs in the subgraph, both belong to candidate cell line-specific proteins. On the other hand, *Psmb6* is a candidate balancer protein connecting between two different nodes of a higher order. This example supports our assumption that balancer proteins could be connective hubs between different modules. Such "bridges" are probably heavily utilized during balancing processes. It is worth noting that the concept of "bridges" discussed here resembles that of "high betweenness" of previous studies on protein interaction networks using graph theory [26,27]. If two clusters of interacting proteins are joined together only through a mutual interacting protein, this protein would have a "high betweeness" measure. "High betweeness" thus indicates the importance of a node within the wider context of the holistic network [27]. Here, the entropic contribution captures this property not in terms of shortest pats (as betweenness), but in terms of random walks inside the network. In this sense, network entropy and entropic contribution provide a conceptual framework to understand the role of the heuristic centrality indices, such as node degree and betweenness.

We are aware that our conclusion provides only one qualitative interpretation of the experimental observations. Under the assumption that gene dosage modifications in the ES cell lines represent small perturbations to the cellular system, more detailed theoretical interpretations can also be sought. For example, previous studies have described that cellular fates such as differentiation, growth, quiescence, or apoptosis may represent the convergence of stochastic cellular program onto a small set of common self-stabilizing "attractors" states [28–30]. These attractor states, which are robust to small perturbations, may also explain our observation that the transgenic ES cells remained in their original steady state as undifferentiated ES cells. However, we are cautious with respect to such a general conclusion, considering that our sample set is very limited, both in terms of sample dimension and its representative nature. Importantly, most of the current network data is of purely structural character, and does not allow for a more detailed understanding of the underlying dynamics, or even its logical abstraction. Moreover, the protein property information was obtained from current protein database entries that are incomplete and may be biased towards intensively studied proteins. Furthermore, due to our small sample sizes, the p-value estimations are not very robust, and may affect our assignment of significance for observed differences. Possible future experiments to test our hypothesis could be, for example, to analyze transgenic cell lines overexpressing one of the candidate balancer proteins in the same *in vitro* system.

In summary, based on our results we hypothesize that the large number of variant proteins detected in mutant ES cells does not necessarily reflect disease-related dysfunctions of these proteins, but rather a quantitative rearrangement of the proteome in response to a disturbance induced by gene dosage alterations. We postulated a regulatory mechanism established in a cell that protects it from deleterious effects of mutations by keeping the macromolecular composition of a cell quantitatively in balance.

MATERIALS AND METHODS

Transgenic ES cell line construction

Pluripotent mouse ES cells were genetically manipulated on single or a set of genes involved in neurodegenerative diseases. A plasmid-mediated gene insertion protocol was used to generate *App* and *Snca*-overexpressing cell lines (*mES_hAPP* and *mES_Snca*, respectively), with CGR8 as parental line [31,32]. For this purpose, a transfer vector based on pMSCV (BD BioSciences Clontech Heidelberg, Germany), which contained a puromycin resistance gene, was modified by inserting a 1.3 kb fragment of the rat promoter for translation elongation factor 1 alpha 1 (*Eef1a1*). This promoter has been shown to be suitable for protein overexpression in ES cells [33]. cDNA of a target gene (human *App* or mouse *Snca*) was inserted in frame with the initiating methionine specified by the rat *Eef1a1* promoter. The vector was electroporated into the ES cells at standard conditions (250V, 500 μF). 24h after electroporation, seven days of puromycin selection followed to select stably transformed ES cell lines. Western blotting was carried out to confirm protein overexpression (monoclonal mouse IgG against human amyloid β peptide, amino acids 1–17, clone 6E10; monoclonal mouse IgG against α-synuclein, clone 5D6, Signet Laboratories, Berkeley, USA). The MICER strategy was used to generate ES cell lines bearing segmental deletion or duplication of *Abcg1-U2af1* on mouse chromosome 17 (30333543 to 31387432 bp), using ES cell line HM-1 as parental line [13,15,34,35] (*mES_14_Mono* and *mES_14_Tris*, respectively). This chromosome segment contains the following genes: *Abcg1*, *Tff3*, *Tff2*, *Tff1*, *Tmprss3*, *Ubash3a*,

Tsga2, *LOC667056*, *Slc37a1*, *Pde9a*, *Wdr4*, *1500032D14Rik*, *Pknox1*, *Cbs* and *LOC623242*. The bordering gene *Abcg1* was deleted in the monosomy, but unaffected in the trisomy cell line. ES cell lines trisomic for murine *Dyrk1a* (*mES_Dyrk1a_Tris*) or murine *Dopey2* (*mES_Dopey2_Tris*) were generated using a BAC gene transfer protocol [36], with D3 as parental cell line (for *Dyrk1a:* BAC 189N10 from the CT7 library, pBeloBac11 vector, 94672437 to 94823558 bp on MMU16; for *Dopey2:* PAC 186P4 from the RP21 library, pPAC4 vector, 93576842 to 93751423 bp on MMU16) [37]. All ES cell lines were able to give germ-line transmission [14,15], except for the CGR8 subclone used, which is primarily intended for work *in vitro* (Savatier, personal communication).

Maintenance of ES cells

ES cell lines were grown in Dulbecco's Modified Eagle Medium (DMEM; Invitrogen, Karlsruhe, Germany) supplemented with 15% fetal calf serum (Biochrom, Berlin Germany), 2mM L-glutamine (Invitrogen), 0.1mM non-essential amino acids (Invitrogen), 1mM sodium pyruvate (Invitrogen), 0.1 mM 2-mercaptoethanol (Invitrogen) and 100U/ml leukemia inhibitory factor (LIF, Chemicon, Hampshire UK) under standard cell culture conditions (37°C, 5% CO2, 95% humidity). Modified and control cell lines were always cultured in parallel. CGR8-derived ES cell lines were maintained on gelatine-coated (0.1% v/v) cell culture plates. ES cells with E3 or HM-1 as parental line were maintained on mitotically inactivated murine embryonic fibroblasts. Prior to cell harvest, these cells were grown for three further passages on gelatine-coated plates to eliminate feeder cells. Cells were grown to 70–90% confluence and met morphological criteria for undifferentiated ES cells at the time of harvest (tightly packed cells forming round colonies). ES cells of three independent 10cm culture dishes were gently dissociated in ice cold PBS containing 5mM EDTA. This resulted in three biological replicates for each cell line. Trypsinization was avoided to preclude protein alteration artifacts.

2D-Electrophoresis

ES cell total protein extraction was carried out using our standard protocol [8]. 70 μg of protein was separated in each 2-DE-run as described previously [7]. Transgenic and their parental cell lines were always run in parallel. Two technical repeats were conducted for each cellular protein extract. Silver staining protocol was employed to visualize protein spots [38]. Computer-assisted manual gel evaluation was performed after scanning of the gel images (600 dpi, UMAX, Willich Germany) (Delta2D version 3.4, Decodon, Greifswald Germany) [39]. Briefly, corresponding gel images were first warped using "exact mode" (manual vector setting combined with automatic warping). A fusion gel image was subsequently generated using union mode, which is a weighted arithmetic mean across the entire gel series. Spot detection was carried out on this fusion image automatically, followed by manual spot editing. Subsequently, spots were transferred from fusion image to all gels. The signal intensities of each spot was computed as a weighted sum of all pixel intensities (volume of protein spot). Percent volume of spot intensities calculated as a fraction of the total spot volume of the parent gel was used for quantitative analysis of protein expression level. Ninety-five percent of the protein spots on the 2D gels that did not vary in their concentration and spot intensity served as reference. Thus, the balancing phenomenon is not due to a normalization artifact that could have arisen from global normalization to a mean or median. Normalized values after local background subtraction were subsequently exported from Delta2D in spreadsheet format for statistical analysis.

Mass spectrometric protein identification

For protein identification by mass spectrometry, 2-DE gels were stained with a mass spectrometry compatible silver staining protocol [40]. Protein spots of interest were excised from 2-DE gels and subjected to in-gel trypsin digestion without reduction and alkylation. Tryptic fragments were analyzed on a LCQ Deca XP nano HPLC/ESI ion trap mass spectrometer (Thermo Fisher Scientific, Waltham, MA, USA) as described previously [11]. For database-assisted protein mass finger printing, monoisotopic mass values of peptides were searched against NCBI-nr (version 20061206, taxonomy: *Mus musculus*), allowing one missed cleavage. Peptide mass tolerance and fragment mass tolerance were set at 0.8 Dalton. Oxidation of methionine and arylamide adducts on cysteine (propionaide) were considered as variable peptide modifications. Criteria for positive identification of proteins were set according to the scoring algorithm delineated in Mascot (Matrix Science, London, UK) [41], with individual ion score cut-off threshold corresponding to $p<0.05$.

Annotation of biochemical properties and functional categories to proteins

Public database queries were performed for the characterization of proteins with altered expression profiles in transgenic ES cells. For this purpose, *GOstat* (http://gostat.wehi.edu.au) was employed to annotate and search against the human GOA database (www.ebi.ac.uk/GOA) in order to determine highly represented functional categories for our proteins of interests [42]. This tool integrates a Fisher's exact test that decides whether the observed GO-term over-representation is significant. $p<0.01$ was set as statistical significance threshold. ProtParam was used to predict the protein instability, aliphatic index and Gravy scores (www.expasy.org/tools/protparam). The Human Reference Protein Database (www.hprd.org) was used to access the number of direct protein interaction partners. Batch searches of overall protein-protein interaction network information were performed via the meta-database UniHi (http://theoderich.fb3.mdc-berlin.de:8080/unihi). Subsequently, information originating from HPRD, BIND, DIP and Reactome, which are curated manually, was extracted. The visualization of the protein interaction network was performed using Cytoscape (www.cytoscape.org) [43]. The Mouse Genome informatics database (MGI 3.5) was used to access the number of SNPs across 86 inbred mouse strains (www.informatics.jax.org). Biological pathway analyses were performed using KEGG (www.genome.ad.jp/kegg) and Biocarta pathway databases (www.biocarta.com). Protein abundance information was extracted from 2-DE data.

Statistics

To assess statistical significance of expression differences between transgenic and control cell lines, Student's T-test was carried out for control vs. transgenic groups (pair-wise, two sided, $n=6$). $p<0.05$ was used as statistical significance threshold. Only protein expression changes over 30% compared to control were retained for further analysis. As a post hoc control analysis, protein expression data generated from 2DE were scrutinized using the Significance Analysis of Microarrays tool (SAM, www-stat.stanford.edu) to identify the false detective rate required to gain the comparable set of altered proteins (100 permutations) [44]. Protein expression alteration (fold change against wild-type controls) was reported with standard error of means (SEM). Due to their non-parametric distribution nature, protein property data (protein cellular abundance, biochemical properties and entropic contribution) were visualized as cumulative fraction plots. Differences of

datasets between balancer and cell line-specific proteins were assessed with the Wilcoxon sum rank test ($p<0.05$).

Network-based approach for system robustness analysis

Many aspects of cellular behavior are mainly determined by the structural properties of the underlying molecular network. In order to characterize the macroscopic resilience properties of the proteomic system, we adopted a network approach which is based on molecular protein interactions. This approach utilizes a fluctuation theorem [24], which states that the resilience of macroscoptic network observables is positively correlated with the pathway diversity, a property which can be measured by network entropy. In this context, network entropy appears as the dynamical entropy of a stochastic process defined on the network, i.e the weighted-average Shannon entropy, $H=\sum_i \pi_i H_i$, where π_i is the stationary distribution of the stochastic process (P_{ij}) and H_i is the standard Shannon entropy defined by:

$$H_i = -\sum_j P_{ij} Log P_{ij}$$

i.e., the uncertainty about the next step of a random walk operating on the network. The stochastic process, P_{ij}, is defined through a variational principle for the leading eigenvalue, which, for unweighted networks, maximizes the overall network entropy [24]. Thus, "H" denotes the network entropy of the whole protein-protein interaction network, whereas "H_i" denotes the entropic contribution of each individual protein (see Methods S1 for details). This entropic characterization leads to a natural importance ranking of proteins within the context of resilience of the global protein interaction network [25]. For this purpose, a protein-protein interaction network was generated from all proteins identified from the 2-DE protein pattern of ES cells. This generates an undirected, un-weighted information transfer graph where nodes denote proteins and the edges describe protein-protein interaction. The topological structure of the graph can be described by an NxN adjacency matrix $A=(a_{ij})$. The entropic contribution of each protein to the global network entropy was calculated as in [25].

SUPPORTING INFORMATION

Table S1 Protein expression profile changes in transgenic ES cell lines.
Found at: doi:10.1371/journal.pone.0001218.s001 (0.11 MB XLS)

Methods S1 Supplementary method of network entropy calculation
Found at: doi:10.1371/journal.pone.0001218.s002 (0.05 MB PDF)

ACKNOWLEDGMENTS

We thank Mrs. Silke Becker for her excellent technical assistance with the mass spectrometric analysis, Pierre Savatier for CGR8 cells, Hans-Jörg Warnatz for the kind gift of cDNA for amyloid beta precursor protein, and Axel Kowald for the fruitful discussions. We would like to thank Mrs. Deirdre West for editorial assistance.

Author Contributions

Conceived and designed the experiments: LM CZ JK. Performed the experiments: LM MH TN FM. Analyzed the data: TM LM DH. Contributed reagents/materials/analysis tools: JD LM CC YH. Wrote the paper: TM LM HH JK.

REFERENCES

1. Goldberg MS, Fleming SM, Palacino JJ, Cepeda C, Lam HA, et al. (2003) Parkin-deficient mice exhibit nigrostriatal deficits but not loss of dopaminergic neurons. J Biol Chem 278: 43628–43635. Epub 42003 Aug 43620.
2. Mangiarini L, Sathasivam K, Seller M, Cozens B, Harper A, et al. (1996) Exon 1 of the HD gene with an expanded CAG repeat is sufficient to cause a progressive neurological phenotype in transgenic mice. Cell 87: 493–506.
3. Palacino JJ, Sagi D, Goldberg MS, Krauss S, Motz C, et al. (2004) Mitochondrial dysfunction and oxidative damage in parkin-deficient mice. J Biol Chem 279: 18614–18622.
4. Zabel C, Klose J (2004) Influence of Huntington's Disease on the Human and Mouse Proteome. Int Rev Neurobiol 61: 241–283.
5. Periquet M, Corti O, Jacquier S, Brice A (2005) Proteomic analysis of parkin knockout mice: alterations in energy metabolism, protein handling and synaptic function. J Neurochem 95: 1259–1276. Epub 2005 Sep 1257.
6. Sturchler-Pierrat C, Abramowski D, Duke M, Wiederhold KH, Mistl C, et al. (1997) Two amyloid precursor protein transgenic mouse models with Alzheimer disease-like pathology. Proc Natl Acad Sci U S A 94: 13287–13292.
7. Klose J, Kobalz U (1995) Two-dimensional electrophoresis of proteins: an updated protocol and implications for a functional analysis of the genome. Electrophoresis 16: 1034–1059.
8. Klose J (1999) Large-gel 2-D electrophoresis. Fractionated extraction of total tissue proteins from mouse and human for 2-D electrophoresis. Methods Mol Biol 112: 147–172.
9. Miller RM, Kiser GL, Kaysser-Kranich T, Casaceli C, Colla E, et al. (2007) Wild-type and mutant alpha-synuclein induce a multi-component gene expression profile consistent with shared pathophysiology in different transgenic mouse models of PD. Exp Neurol 23: 23.
10. Zhang HL, Luo TH, Feng L, Zhao Y, Li WY, et al. (2007) Microarray analysis of gene expression in Men1 knockout embryoid body reveals genetic events involved in early mouse embryonic development. Biochem Biophys Res Commun 352: 456–462. Epub 2006 Nov 2016.
11. Zabel C, Sagi D, Kaindl AM, Steireif N, Klare Y, et al. (2006) Comparative proteomics in neurodegenerative and non-neurodegenerative diseases suggest nodal point proteins in regulatory networking. J Proteome Res 5: 1948–1958.
12. Fowler DM, Koulov AV, Alory-Jost C, Marks MS, Balch WE, et al. (2006) Functional amyloid formation within mammalian tissue. PLoS Biol 4: e6.
13. Lopes C, Chettouh Z, Delabar JM, Rachidi M (2003) The differentially expressed C21orf5 gene in the medial temporal-lobe system could play a role in mental retardation in Down syndrome and transgenic mice. Biochem Biophys Res Commun 305: 915–924.
14. Branchi I, Bichler Z, Minghetti L, Delabar JM, Malchiodi-Albedi F, et al. (2004) Transgenic mouse in vivo library of human Down syndrome critical region 1: association between DYRK1A overexpression, brain development abnormalities, and cell cycle protein alteration. J Neuropathol Exp Neurol 63: 429–440.
15. Brault V, Pereira P, Duchon A, Herault Y (2006) Modeling chromosomes in mouse to explore the function of genes, genomic disorders, and chromosomal organization. PLoS Genet 2: e86.
16. Wuchty S, Oltvai ZN, Barabasi AL (2003) Evolutionary conservation of motif constituents in the yeast protein interaction network. Nat Genet 35: 176–179. Epub 2003 Sep 2014.
17. Balazsi G, Barabasi AL, Oltvai ZN (2005) Topological units of environmental signal processing in the transcriptional regulatory network of Escherichia coli. Proc Natl Acad Sci U S A 102: 7841–7846. Epub 2005 May 7820.
18. Brown GC (1991) Total cell protein concentration as an evolutionary constraint on the metabolic control distribution in cells. J Theor Biol 153: 195–203.
19. Minton AP (2000) Implications of macromolecular crowding for protein assembly. Curr Opin Struct Biol 10: 34–39.
20. Minton AP (2001) The influence of macromolecular crowding and macromolecular confinement on biochemical reactions in physiological media. J Biol Chem 276: 10577–10580. Epub 12001 Feb 10515.
21. Santoni V, Molloy M, Rabilloud T (2000) Membrane proteins and proteomics: un amour impossible? Electrophoresis 21: 1054–1070.
22. Khaitovich P, Hellmann I, Enard W, Nowick K, Leinweber M, et al. (2005) Parallel patterns of evolution in the genomes and transcriptomes of humans and chimpanzees. Science 309: 1850–1854. Epub 2005 Sep 1851.
23. Stelzl U, Worm U, Lalowski M, Haenig C, Brembeck FH, et al. (2005) A human protein-protein interaction network: a resource for annotating the proteome. Cell 122: 957–968.
24. Demetrius L, Gundlach VM, Ochs G (2004) Complexity and demographic stability in population models. Theor Popul Biol 65: 211–225.

25. Manke T, Demetrius L, Vingron M (2006) An entropic characterization of protein interaction networks and cellular robustness. J R Soc Interface 3: 843–850.
26. Chan SK, Hsing M, Hormozdiari F, Cherkasov A (2007) Relationship between insertion/deletion (indel) frequency of proteins and essentiality. BMC Bioinformatics 8: 227.
27. Joy MP, Brock A, Ingber DE, Huang S (2005) High-betweenness proteins in the yeast protein interaction network. J Biomed Biotechnol 2005: 96–103.
28. Kauffman S (1969) Homeostasis and differentiation in random genetic control networks. Nature 224: 177–178.
29. Huang S, Ingber DE (2000) Shape-dependent control of cell growth, differentiation, and apoptosis: switching between attractors in cell regulatory networks. Exp Cell Res 261: 91–103.
30. Huang S, Ingber DE (2006) A non-genetic basis for cancer progression and metastasis: self-organizing attractors in cell regulatory networks. Breast Dis 26: 27–54.
31. Chambers I, Smith A (2004) Self-renewal of teratocarcinoma and embryonic stem cells. Oncogene 23: 7150–7160.
32. Wiles MV, Vauti F, Otte J, Fuchtbauer EM, Ruiz P, et al. (2000) Establishment of a gene-trap sequence tag library to generate mutant mice from embryonic stem cells. Nat Genet 24: 13–14.
33. Chung S, Andersson T, Sonntag KC, Bjorklund L, Isacson O, et al. (2002) Analysis of different promoter systems for efficient transgene expression in mouse embryonic stem cell lines. Stem Cells 20: 139–145.
34. Adams DJ, Biggs PJ, Cox T, Davies R, van der Weyden L, et al. (2004) Mutagenic insertion and chromosome engineering resource (MICER). Nat Genet 36: 867–871. Epub 2004 Jul 2004.
35. Magin TM, McWhir J, Melton DW (1992) A new mouse embryonic stem cell line with good germ line contribution and gene targeting frequency. Nucleic Acids Res 20: 3795–3796.
36. Testa G, Vintersten K, Zhang Y, Benes V, Muyrers JP, et al. (2004) BAC engineering for the generation of ES cell-targeting constructs and mouse transgenes. Methods Mol Biol 256: 123–139.
37. Doetschman TC, Eistetter H, Katz M, Schmidt W, Kemler R (1985) The in vitro development of blastocyst-derived embryonic stem cell lines: formation of visceral yolk sac, blood islands and myocardium. J Embryol Exp Morphol 87: 27–45.
38. Heukeshoven J, Dernick R (1988) Improved silver staining procedure for fast staining in PhastSystem Development Unit. I. Staining of sodium dodecyl sulfate gels. Electrophoresis 9: 28–32.
39. Mao L, Zabel C, Wacker MA, Nebrich G, Sagi D, et al. (2006) Estimation of the mtDNA mutation rate in aging mice by proteome analysis and mathematical modeling. Exp Gerontol 41: 11–24. Epub 2005 Nov 2022.
40. Nebrich G, Herrmann M, Sagi D, Klose J, Giavalisco P (2007) High MS-compatibility of silver nitrate-stained protein spots from 2-DE gels using ZipPlates and AnchorChips for successful protein identification. Electrophoresis 19: 19.
41. Pappin DJC, Hojrup P, Bleasby AJ (1993) Rapid identification of proteins by peptide-mass fingerprinting. Curr Biol 3: 327–332.
42. Ashburner M, Ball CA, Blake JA, Botstein D, Butler H, et al. (2000) Gene ontology: tool for the unification of biology. The Gene Ontology Consortium. Nat Genet 25: 25–29.
43. Shannon P, Markiel A, Ozier O, Baliga NS, Wang JT, et al. (2003) Cytoscape: a software environment for integrated models of biomolecular interaction networks. Genome Res 13: 2498–2504.
44. Tusher VG, Tibshirani R, Chu G (2001) Significance analysis of microarrays applied to the ionizing radiation response. Proc Natl Acad Sci U S A 98: 5116–5121. Epub 2001 Apr 5117.

Available online at www.sciencedirect.com
SCIENCE DIRECT
Experimental Gerontology 41 (2006) 11–24
Experimental Gerontology
www.elsevier.com/locate/expgero

Estimation of the mtDNA mutation rate in aging mice by proteome analysis and mathematical modeling

Lei Mao [a], Claus Zabel [a], Maik A. Wacker [a], Grit Nebrich [a], Dijana Sagi [a], Petra Schrade [b], Sebastian Bachmann [b], Axel Kowald [c], Joachim Klose [a,*]

[a] *Institute for Human Genetics, Charité, University Medicine Berlin, Berlin, Germany*
[b] *Institute for Anatomy, Charité, University Medicine Berlin, Berlin, Germany*
[c] *Max Planck Institute for Molecular Genetics, Kinetic Modelling Group, 14195 Berlin, Germany*

Received 11 April 2005; received in revised form 24 August 2005; accepted 27 September 2005
Available online 22 November 2005

Abstract

The accumulation of mitochondria containing mutated genomes was proposed to be an important factor involved in aging. Although the level of mutated mtDNA has shown to increase over time, it is currently not possible to directly measure the mtDNA mutation rate within living cells. The combination of mathematical modeling and controlled experiments is an alternative approach to obtain an estimate for the mutation rate in a well-defined system. In order to judge the relevance of mitochondrial mutations for the aging process, we used a mouse model to study age-related alterations of the mitochondrial proteins. Based on these experimental data we constructed a mathematical model of the mitochondrial population dynamics to estimate mtDNA mutation rates. Mitochondria were isolated from mouse brain and liver at six different ages (newborn to 24-months). A large-gel 2D-electrophoresis-based proteomics approach was used to analyze the mitochondrial proteins. The expression of two respiratory chain complex I subunits and one complex IV subunit decreased significantly with age. One subunit of complex III and one subunit of complex V increased in expression during aging. Together, these data indicate that complex I and IV deficiency in aged tissues might be accompanied by feedback regulation of other protein complexes in the respiratory chain. When we fitted our experimental data to the mathematical model, mtDNA mutation rate was estimated to be 2.7×10^{-8} per mtDNA per day for brain and 3.2×10^{-9} per mtDNA per day for liver. According to our model and in agreement with the mitochondrial theory of aging, mtDNA mutations could cause the detrimental changes seen in mitochondrial populations during the normal lifespan of mice, while at the same time ensure that the mitochondrial population remains functional during the developmental and reproductive period of mice.

Keywords: Mitochondria; Aging; Proteome; Large-gel 2D electrophoresis; Mouse model; Mathematical modeling.

1. Introduction

Aging is associated with a gradual decline of the organism's capacity to respond to environmental stress (Toescu et al., 2000). An increasing body of literature suggests a pivotal role of mitochondria in aging and age-related diseases (Harman, 1972; Richter, 1988; Linnane et al., 1989; Wallace, 1997; Kowald and Kirkwood, 1999). The mitochondrial theory of aging proposes that the accumulation of impaired mitochondria caused by free-radical-induced mutations is one of the driving forces of aging (Richter, 1988; Linnane et al., 1989; Kowald and Kirkwood, 1999). Over the past years, this theory gained further appreciation. Several lines of evidence support the view that the bio-energetic function of mitochondria deteriorates with age, accompanied by the accumulation of mtDNA mutations (Boffoli et al., 1994; Brierley et al., 1998; Kopsidas et al., 1998). The theoretical contributions of deGrey and Kowald showed that this theory can explain diverse age-related phenomena, including mitochondrial dysfunction in aging, the clonal expansion of a single deletion mutation and the differences observed between dividing and post-mitotic cells (de Grey, 1997; Kowald and Kirkwood, 2000). In two recent important experiments

* Corresponding author. Address: Institut für Humangenetik, Charité, Humboldt Universität, Augustenburger Platz 1, 13353 Berlin, Germany. Tel.: +49 30 450 566133; fax: +49 30 450 566904.
E-mail address: joachim.klose@charite.de (J. Klose).

0531-5565/$ - see front matter © 2005 Elsevier Inc. All rights reserved.
doi:10.1016/j.exger.2005.09.012

the groups of Trifunovic and Kujoth observed a strong increase of mtDNA mutations and several phenotypic changes of premature aging in knock-in mice bearing a proofreading deficient version of the mtDNA polymerase (Trifunovic et al., 2004; Kujoth et al., 2005).

Although these observations hint at a causative link between mtDNA mutations and aging, no hard evidence is available that link mtDNA mutations per se to aging. Since most cells contain hundreds to thousands of mtDNA molecules, it is unclear whether a small number of mutated mitochondria could influence the physiology of the entire cell and play a role in aging (Coller et al., 2002). Previous investigation provided information on mitochondrial mutations at the genetic level (Brierley et al., 1998; Kopsidas et al., 1998), but it is doubtful whether genomic information alone is sufficient to clarify the mechanisms of aging.

There is a range of factors that can potentially influence the impact of mitochondria bearing mutated mtDNA. These include tissue metabolic state, efficiency of mtDNA repair, propagation capability of mutant relative to that of normal mtDNA, effect of mtDNA mutation on mitochondrial proliferation and function, as well as the rate of mitochondrial degradation. These and further factors build a system of complex interactions that cannot be understood by verbal argumentation alone. The real influence of mtDNA mutations on the aging process cannot be assessed without quantitative discussion.

Although the mitochondrial mutation rate is estimated to be 10 times higher than that of nuclear DNA (Osiewacz and Hamann, 1997; Zeviani et al., 1998; DiMauro et al., 2000), currently only few solid data regarding the mitochondrial mutation rate exist. One problem contributes to this lack of data is the heteroplasmic state of the mitochondrial genome in the cells, which makes the mtDNA mutation rate practically inaccessible.

Previous observations indicate that via the stoichiometry of the assembly process of complex I and IV a reduction of mitochondrial encoded protein subunits leads to a reduction of nuclear encoded protein subunits in the mitochondrial membrane (Bentlage et al., 1996; Bruno et al., 1999; Rahman et al., 1999; Remacle et al., 2004). Based on this observation we try to access the mtDNA mutation rate indirectly through changes of nuclear encoded respiratory chain subunits.

A combination of computational methods and experimental investigations can be useful for probing into the details of complex systems (Swat et al., 2004). In this study, a mouse model was used to gain quantitative data on age-related mitochondrial respiratory protein alterations that are encoded by nuclear DNA. In parallel, we converted the hypothetical mechanisms involved in the mitochondrial theory of aging (Kowald and Kirkwood, 2000) into a simplified mathematical model. By fitting our experimental data to this model, the mtDNA mutation rates of mouse brain and liver tissue were estimated. Our results show that mitochondrial mutations could, in principle, be of considerable importance for aging.

2. Material and methods

If not indicated otherwise, all chemicals and reagents were purchased from Merck (Darmstadt, Germany).

2.1. Animals and tissues

The experimental protocol of this study was approved by the Institutional Review Committee of Charité, University Medicine of Berlin, according to German Animal Protection Law (TSchG). Specific-pathogen-free C57BL/6 mice were purchased from Charles River Germany (Sulzfeld, Germany). Healthy mice of mixed sex with equal number of male and female animals at various ages were used: newborn (0–2 weeks), 5-, 10-, 15-, 20- and 24-months. Eight mice were used in each age group, except for newborns, where thirteen mice were used (mixed sexes). Animals were sacrificed by swift decapitation. The use of anesthetics was avoided to eliminate possible influence on mitochondrial protein level. Mouse liver was perfused through the portal vein with 5 ml 0.9% (w/v) NaCl before removal. Mouse brain tissue was obtained according to an already published protocol (Klose, 1999).

2.2. Mitochondria isolation

Mitochondria were isolated as described in detail previously (Jungblut and Klose, 1985). Except for newborn tissue, which was pooled due to the small sample quantity, mitochondria of each organ (either brain or liver) were isolated separately. Electron microscopic analysis was carried out as previously described to assess purity and structure integrity of isolated mitochondria. For this purpose, mitochondria were fixed in 2.5% glutaraldehyde/PBS and embedded in Epon (Bachmann et al., 2004).

2.3. Two-dimensional gel electrophoresis

Mitochondrial proteins were extracted as previously described (Klose, 1999). Protein extracts were separated by large-gel two-dimensional electrophoresis (30×40 cm) (Klose, 1999; Klose and Kobalz, 1995), which involves the isoelectric focusing at the first dimension and SDS-PAGE at the second dimension. Multiple gels ($n = 3$–6 for each time stage) were run for each sample to ensure reproducibility of the 2D-gels. Analytical silver staining was performed as described elsewhere (Klose, 1999). Preparative silver staining was carried out using the protocol of Giavalisco (Giavalisco et al., 2005). Gel images were digitalized using a densitometer (Umax Mirage-II DIN A3 scanner, Willich, Germany). Protein expression differences were determined by comparisons of 2D-gels from mitochondrial protein extracts at different ages. Due to the overall similarity of gel patterns, the majority of spots were assigned to their respective counterparts on each gel manually according to relative identity of position and spot form. Spot differences were determined by evaluating alterations in spot intensity and appearance.

Protein spots found to be reproducibly altered among different age groups were further evaluated with Proteinweaver imaging software (version 2.1, Definiens, Munich, Germany). Manual corrections were applied after automatic spot recognition. In order to reduce in-group gel-to-gel variation, one average gel was generated for each age group using Proteinweaver. Average gels from six different ages were matched to each other, and the gel-matching pattern was controlled and edited manually (Challapalli et al., 2004). For spot quantification, spot volumes were calculated by a build-in feature of the software. Subsequently, spot information was extracted from Proteinweaver. Spot intensities were normalized by calculating the 'relative intensity', which was defined as percentage to the total spot volume on its parent gel. Ultimately, spot differences detected by visual gel evaluation were quantified and subjected to statistical analysis to determine significance. Kruskal–Wallis test was employed to access multiple-groups variation. If a significant difference was detected ($p<0.05$), a non-parametric Mann–Whitney U test was conducted to gain group-to-group difference information. Standard error of mean (mean $\pm$ SEM) of relative spot intensities were presented in this study.

2.4. Mass spectrometric protein identification

Protein identification was carried out using to MALDI-Tof mass spectrometry. Identification of each protein spot was carried out at least twice. Briefly, protein spots of interests were manually excised from 2D-gels and in-gel digested with trypsin (Seq. Grade modified Porcine trypsin, Promega WI, USA) with ZipPlate (Millipore, Schwalbach Germany), according to the manufacture's instruction. Subsequently, peptides were recovered in 15 μl 50% (v/v) acetonitril with 0.1% (v/v) trifluoracetic acid (TFA). 1.5 μl of peptide extract was mixed with 1.5 μl matrix solution (3.3 g/l solution of 2, 5-dihydroxybenzoic acid in one part of acetonitril and two parts of 0.1% TFA) directly on the MALDI target (Anchor Chip, Bruker, Bremen, Germany). Mass spectra from peptide mixtures were generated using MALDI-TOF mass spectrometer (Bruker Reflex IV, Bruker, Bremen, Germany), operated in reflector mode. Signals corresponding to mass-to-charge (m/z) ranging from 0 to 3500 were monitored. The XMASS/NT software package (version 5.1.16, Bruker, Bremen, Germany) was used for data processing. Internal calibration against the mass peaks derived from autolytic trypsin fragments was employed. A mass list of the first of each set of monoisotopic peaks was searched against the NCBInr protein databases (National Center for Biotechnology Information, Bethesda, USA, mouse database) using Mascot (http://www.matrixscience.com). Search parameters allowed for one miscleavage, peptide mass tolerance was set to 100 ppm. Methionine oxidation and cysteinyl-S-propionamide were considered as possible modifications. Criteria for positive identification of protein with peptide mass fingerprinting were set according to the scoring algorithm delineated in Mascot ($p<0.05$) (Pappin et al., 1993). Additionally, the molecular weight and isoelectric point of each protein determined through the Database search were compared to the observed range during electrophoresis. Identified spots on one gel of the matched group were considered to be the same on the other gel and therefore considered to be indirectly identified.

2.5. Model description

Our mathematical model was constructed based on the following assumptions and Fig. 4a gives an overview of the current model.

- Free radicals induce mtDNA deletions and mitochondrial membrane damage.
- Mitochondria with an intact genome have a growth advantage over mitochondria bearing deletions.
- Mutated mitochondria produce less free radicals than wild type mitochondria. For a detailed justification of this assumption see (de Grey, 1997; Kowald and Kirkwood, 2000).
- Accumulation of membrane damage is proportional to the free radical level.
- The degradation rate of mitochondria is positively correlated to their membrane damage level.

The mitochondrial replication process is relaxed in that it is independent of the cell cycle (Chinnery and Samuels, 1999; Garesse and Vallejo, 2001). However, on average the number of mitochondria has to double for each cell division. This influences also the mitochondrial turnover rate, which is therefore different for post-mitotic and mitotic tissues (Neubert et al., 1966; Dallman, 1967). Accordingly, we set the turnover rate for mouse brain and liver to 21 and 8.4 days, respectively (Korr et al., 1998).

Mitochondria are not fully autonomous entities, but depend on the cytosolic protein synthesis machinery (most mitochondrial proteins are imported from the cytosol). Consequently, mitochondria do not show exponential growth, but the production of mitochondria has an upper limit depending on cellular housekeeping (Brown, 1991; Kowald and Kirkwood, 2000). The mathematical construct used to simulate this behavior is given by the following expression:

$$\text{Current proliferation rate} = \text{maximum proliferation rate} \times (A - M_w - M_m), \quad (1)$$

where 'A' is the maximum number of mitochondria in a cell, M_w are wildtype mitochondria and M_m are mutant organelles. The maximum proliferation rate is different for intact and damaged mitochondria and is represented by α and β, in Eqs. (2)–(4). This construct reflects the dependency of the mitochondrial proliferation rate on the synthetic capacity of the cell and leads to a declining proliferation rate the closer the total number of mitochondria comes to this limit.

The rate of mitochondrial degradation is assumed to be proportional to the level of mitochondrial membrane damage (Kowald and Kirkwood, 2000). Since mitochondria with mtDNA deletions have a defective respiratory chain and

a reduced proton gradient, it is assumed that they generate less of the reactive perhydroxyl radical, $HO_2^{\cdot}$, (de Grey, 1997; Kowald and Kirkwood, 2000). This leads to a reduced accumulation rate of membrane damage and hence causes a slower degradation rate of defective mitochondria compared to wildtype ($\varphi_1 > \varphi_2$ Eqs. (2) and (3), where φ_1 and φ_2 are the degradation rates of wild type and mutated mitochondria, respectively). This is deGrey's idea of the 'Survival of the Slowest' or the SOS hypothesis (de Grey, 1997).

Through the continuous exposure to free radicals, mitochondrial genomes are continuously accumulating damage during the aging process. This process is described by mutation terms in the reaction system. Free radicals can damage mtDNA with a rate 'k', converting intact mitochondria into defective ones. The mutation rate is proportional to the free radical level and the amount of intact mitochondria.

As a side-product of respiratory chain enzyme activities, free radicals are produced by all mitochondria during the oxidative phosphorylation process. It is assumed that wild type mitochondria generate more radicals than mutated mitochondria due to their higher respiratory activity ($f_1 > f_2$ in Eq. (4), where f_1 and f_2 are the free radical production rates of wild type and mutated mitochondria, respectively). In our simplified mathematical model it is assumed that the cell has a constant antioxidant capacity to remove radicals. The detoxification rate is therefore proportional to the amount of existing radicals (Eq. (4)).

Within the framework of compartmental analysis (Jaequez, 1985), our model represents a non-linear single compartment model. Using the above assumptions a set of ordinary differential equations can now be developed that govern the behavior of the system. In these equations, 'M_w', 'M_m' and 'Rad' are the number of wildtype mitochondria, mutated mitochondria and free radicals in the cell, respectively.

$$\frac{dM_w}{dt} = \alpha M_w(A - M_w - M_m) - k\,\mathrm{Rad}\,M_w - \varphi_1 M_w \quad (2)$$

$$\frac{dM_m}{dt} = \beta M_m(A - M_w - M_m) + k\,\mathrm{Rad}\,M_w - \varphi_2 M_m \quad (3)$$

$$\frac{d\,\mathrm{Rad}}{dt} = f_1 M_w + f_2 M_m - \varphi_3 \mathrm{Rad} \quad (4)$$

The first and third term in Eq. (2) and (3) represent the synthesis and degradation rates of the healthy and defective mitochondrial sub-populations, respectively. The second term in Eq. (2) and (3) describes the mutation reaction that transfers wild type mitochondria into the pool of mutated mitochondria. Table 2 lists the actual values used for the different parameters. Where possible, known values from the literature have been used.

2.6. Simulation and model fitting

The set of differential equations was solved numerically using the software package Mathematica (NDSolve, which employs fourth order Runge-Kutta method. Default parameter setting). The initial values for wild type mitochondria, mutated mitochondria and free radicals were set to 1000, 0 and 0, respectively. This assumes that there were 1000 intact mitochondria in the cell at time point zero, whereas no mutated mitochondria or free radicals exist in the system.

To determine the mtDNA mutation rate that optimally fits the experimental data, a parameter scan regarding the value of

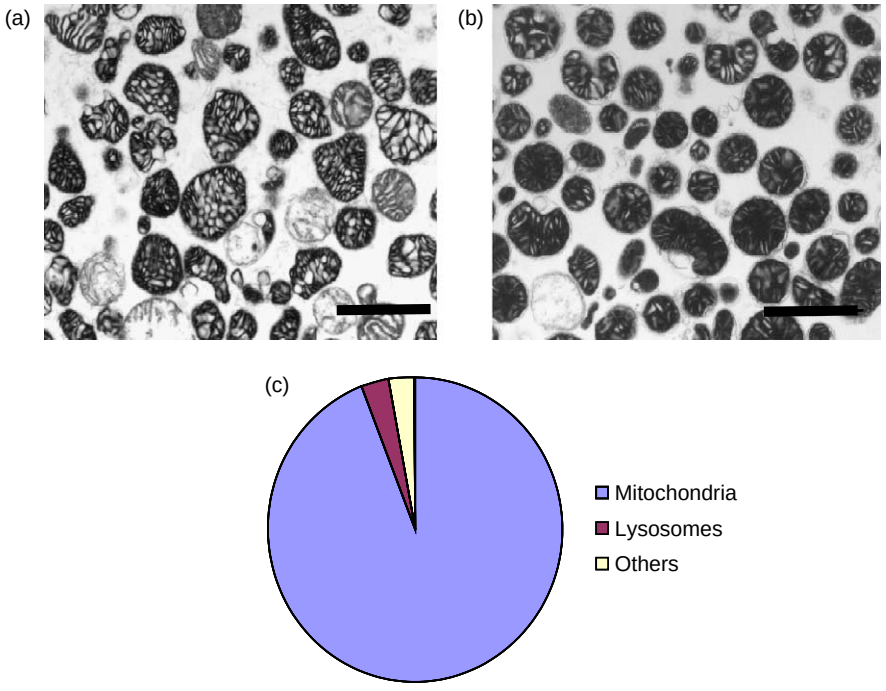

Fig. 1. Electronic micrographs of isolated mitochondria using continuous gradient centrifugation. (a) Brain mitochondria, (b) Liver mitochondria (10,000× original magnification). Scale bar: 100 nm. (c) Percentage of mitochondria, lysosomes and debris in the mitochondria fraction accounted 94%, 3% and 3%, respectively.

'k' was performed. For this purpose, the equation system was solved for 'k' values ranging from 10^{-3} to 10^{-12} per day and the values of $M_{w(t=\text{newborn})}$, $M_{w(t=5\text{-months})}$, $M_{w(t=10\text{-months})}$, $M_{w(t=15\text{-months})}$, $M_{w(t=20\text{-months})}$ and $M_{w(t=24\text{-months})}$ were recorded from the simulation. These data points were then compared to the set of experimentally obtained data by calculating the sum of square deviations.

The 'k' resulting in the minimal sum of squares was treated as the estimated mtDNA mutation rate of our mouse model. Statistical significance of the fits was analyzed using ANOVA test (using StatView, Abacus, NC, USA). Pearson's correlation coefficient was recorded to report the proportion of variation in the experimental data that could be explained by our simulation model. The corresponding experimental data set consisted of the alterations of respiratory chain complex I and IV subunits at those six time points, which were found to change significantly during aging using 2D-electrophoresis.

3. Results

3.1. Mitochondrial protein separation

Mitochondria were isolated from mouse brain and liver tissues using a combination of gravity and gradient centrifugation. Using electron microscopy, representative sections of isolated mitochondria showed a highly homogeneous population ($94.2 \pm 0.7\%$, $n=6$) with inner and outer membranes intact (Fig. 1). Fig. 2 shows a typical 2D-gel pattern generated from brain (Fig. 2a) and liver (Fig. 2b) mitochondrial total protein extract, respectively. Typically, around 800 protein spots were found on the 2D-gel map of mitochondrial total protein extract.

3.2. 2D-gel evaluation and protein identification

In order to obtain age-related changes in mitochondrial proteins, we evaluated two-dimensional mitochondrial protein

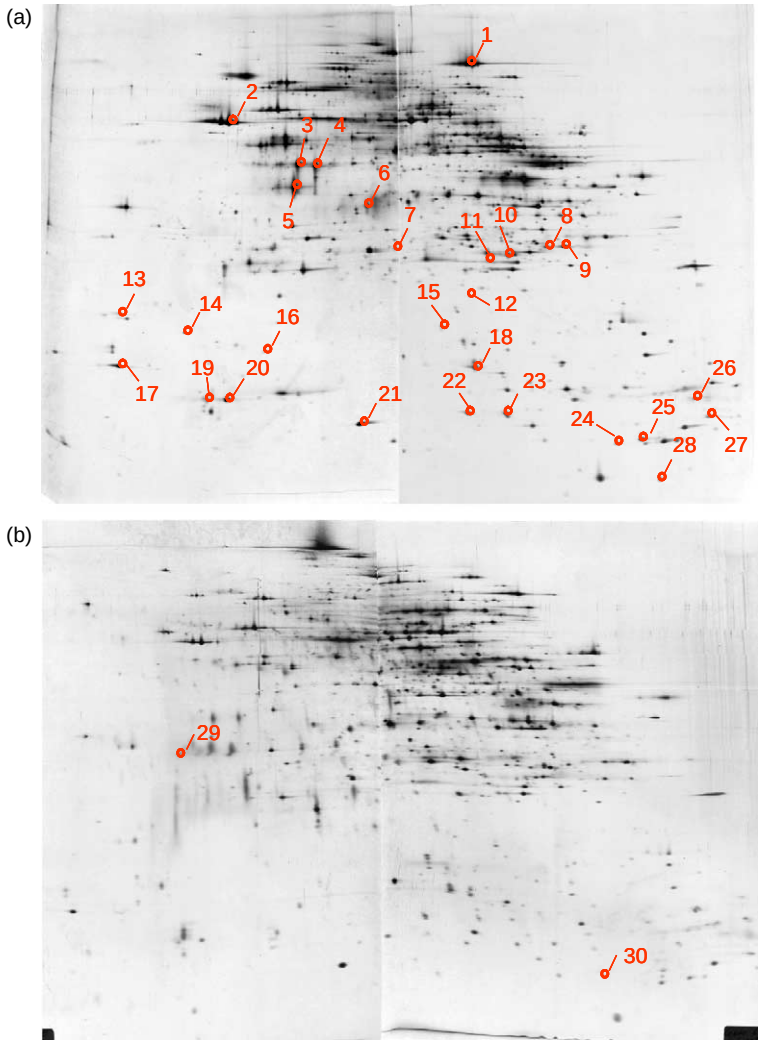

Fig. 2. 2D-gel images of mouse mitochondrial proteins. Mouse brain (a) and liver (b) mitochondrial protein total extracts (5-months old mouse) were separated by large-gel 2D-electrophoresis. Representative analytical silver stained 2D-gels with a protein load of 100 μg are shown. By convention, the resulting high-resolution spot patterns of a 2D-electrophoresis are shown with the low, acidic isoelectric points to the left and the lower molecular weight proteins at the bottom. The numbers indicate positions of protein spots that have been identified with peptide mass fingerprinting. Two spots (spot 29 and 30) were visible only on 2D-gels of liver mitochondria.

patterns of six different age groups. 2D-gels generated from the same samples during independent gel runs were first compared. They were found to be highly reproducible, yielding similar 2D-gel spot pattern. Through visual comparison of the mitochondrial protein spot patterns of different age groups bearing the same organ type, numerous differences among the different age groups were detected in both brain and liver mitochondria. Intensities of 22 spots were observed to decrease or increase with age, indicating the concentration change of the corresponding proteins in mitochondria during aging, while 16 proteins showed irregular profiles. All these 38 spots underwent mass spectrometric identification. From these 36 spots were successfully identified. They represent 30 different proteins (indicated in Fig. 2). Two protein spots showing irregular change profile were determined to be cytoplasmic proteins, while all other protein spots represented mitochondrial proteins. Detailed information of protein identification is given in Table 3.

All identified spots with regular quantitative changes were subjected to computer-aided spot volume quantification (20 spots). Interestingly, inconsistencies between visual gel evaluation and computer-aided gel evaluation were observed. According to protein quantification using the ProteomWeaver software, four protein spots showed a fluctuating behavior inside certain age groups that were evaluated visually to either decrease or increase with age. This further reduces the number of spots showing a consistent decrease or increase to 16.

The concentration changes of these remaining 16 protein spots were subjected to statistical analysis. Among them, ten proteins showed statistically significant changes with $p < 0.05$. Table 1 shows the ratio of the amount of these proteins in 24 months old mice compared to newborns. Since our main interest was the estimation of the mtDNA mutation rate we describe in the following only the changes of mitochondrial respiratory chain proteins.

Table 1
Mitochondrial proteins showing altered expression during aging

Protein name	NCBI Acc**	Change ratio*	
		Brain	Liver
NADH-ubiquinone oxidoreductase 13 kDa—a subunit	38075371	0.713	0.861
NADH-ubiquinone oxidoreductase 1 alpha subcomplex 5	13386100	0.188	ND
Cytochrome *c* oxidase, subunit Vb	6753500	0.913	0.817
Ubiquinol–cytochrome *c* reductase binding protein	133885726	ND	4.6
ATP synthase, H+ transporting, mitochondrial F0 complex, subunit F	7949005	3.1	ND
Mitochondrial ribosomal protein L12	22164792	ND	1.5
10 kDa Mitochondrial heat shock protein	6680309	0.58	0.20
Regucalcin	6677739	ND	0.62
Alpha-synuclein	6678047	1.7	ND
Peroxiredoxin 1	6754976	ND	0.66

*Ratios of 24-month stage protein concentration to that of newborn stage are presented. **CBI Accession number (gi number).

3.3. Down-regulation of complex I and IV components in old mice

Expression of four protein subunits of complex I (NADH-ubiquinone oxidoreductase) decreased with age. Among these, changes of two proteins were of statistical significance. The reduced expression of NADH-ubiquinone oxidoreductase 13 kDa—a subunit (gi: 38075371) was observed in brain and liver mitochondria (Fig. 3a), whereas a diminished expression of NADH-ubiquinone oxidoreductase 1 alpha subcomplex 5 (gi: 13386100) was detected only in the brain mitochondria (Fig. 3b).

In brain mitochondria, the expression level of NADH-ubiquinone oxidoreductase 13 kDa—a subunit initially increased from newborns to 10-months of age, and then dropped to significantly lower levels than newborns, at 15-months of age. This reduced level remained until 24 months of age. Unlike in brain, liver expression of this protein initially decreased from newborns to 5-months of age. The level remained low compared to newborns and showed an additional mild decrease from 10-months to 24-months. In brain mitochondria, the expression level of NADH-ubiquinone oxidoreductase 1 alpha subcomplex 5 decreased significantly from newborns to 5-months. Expression recovered partially at 10-months of age and remained nearly constant from 10- to 20-months. Another drastic decrease in expression was detected at 24-months, when only trace amount of the protein were detectable.

Likewise, three proteins of complex IV (cytochrome *c* oxidase, or COX) showed decreasing spot intensity with age. Among them, the expression level of COX subunit Vb (gi: 6753500) in brain mitochondria was not changed significantly from newborns until the age of 10-months (Fig. 3c). However, a pronounced decrease was observed at 15-months of age, which persisted until 24-months of age. In liver mitochondria, COX Vb level showed at first a higher level in the 5-months group. A similar decrease tendency to that of brain mitochondria sustained until 24-months of age.

The data of these three proteins (NADH-ubiquinone oxidoreductase 13 kDa—a subunit, NADH-ubiquinone oxidoreductase 1 alpha subcomplex 5 and COX Vb) were used for the model fitting procedure.

3.4. Up-regulation of complex III and V subunits

In 2D-gels of liver mitochondria, one subunit of the cytochrome *c* reductase (respiratory chain complex III), the ubiquinol–cytochrome *c* reductase binding protein (gi: 133885726) showed a significant increase in expression at 20-months of age (data not shown). This level remained high until at least 24-months of age. In brain mitochondrial 2D-gels, one complex V (ATP synthase) subunit, the subunit F of ATP synthase F0 complex (gi: 7949005) showed a fluctuating

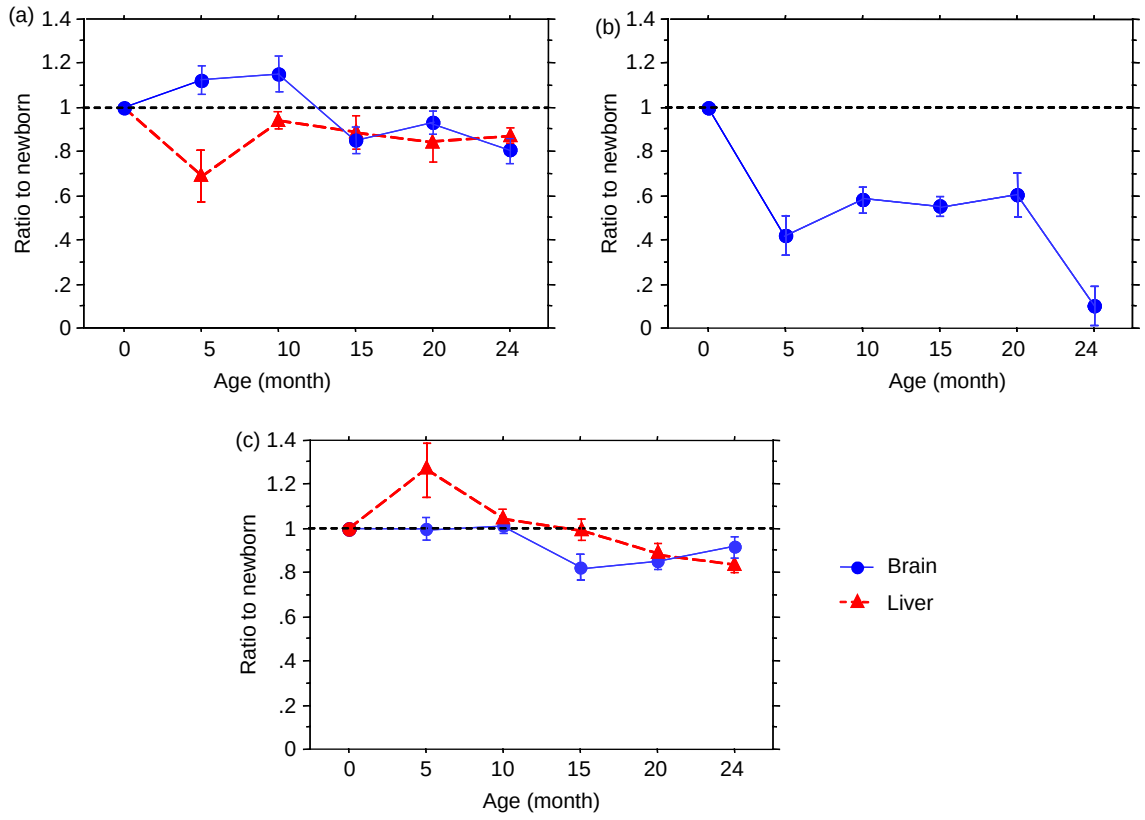

Fig. 3. Decreasing expression profiles of respiratory chain complex I and IV subunits in mouse mitochondria during aging. (a) NADH-ubiquinone oxidoreductase 13 kDa—a subunit in brain and liver mitochondria; (b) NADH-ubiquinone oxidoreductase 1 alpha subcomplex 5 in brain mitochondria; (c) Cytochrome *c* oxidase subunit Vb only in brain and liver mitochondria.

pattern, with increased expression at both 5- and 20-months of age (data not shown).

3.5. Model behavior

We created a mathematical model describing the temporal development of a cellular population of mitochondria subject to radical induced mutations. This model is a simplified version of an earlier, more complex, model (Kowald and Kirkwood, 2000). Using the standard parameters, the equations were solved numerically and plotted against time. Fig. 4b is an example of such a numerical calculation. For this simulation the parameter values shown in Table 2 and a mtDNA mutation rate, k, of 10^{-8} per day was used.

This diagram shows the time course of wild type mitochondria (M_w), mutated mitochondria (M_m) and free radicals (Rad). Initial values were 1000 for M_w, 0 for M_m and 0 for Rad. The amount of intact mitochondria showed initially a stable period from 0 to ca. 400 days. Then, a progressive decrease appeared. This drastic decrease of intact mitochondria continued until ca. day 1000, after which no substantial amount of intact mitochondria remains.

The time-dependent curve of mutated mitochondria behaves the opposite way. While no mutated mitochondria were available at the starting time, trace amounts of mutated mitochondria began to accumulate with time, but at a very slow pace. This gives a quasi-stable period of low numbers of mutated mitochondria from 0 to ca. 400 days of life. The number of mutated mitochondria started to increase drastically at about 500 days of life. This tendency continued until the whole mitochondrial population is transformed from intact (M_w) to mutated organelles (M_m) around day 1000.

Unlike the mitochondrial subpopulations, the level of free radicals (Rad) changed not that drastically. Although the simulation started with no radicals, this variable reached almost instantaneously a quasi steady state where the radical level remained stable for the first 600 days. The level of free radicals decreased slightly around day 650, when the majority of the mitochondrial population consisted of mutated mitochondria (Fig. 4b).

Since there exists an accelerating decrease of intact mitochondria with time, the position of the inflection point is of special interest to us. As the mutation rate is the driving force of the decrease of intact mitochondria in our system, we investigated the effect of varying the mutation rate, k, on the behavior of the system. Variation of the mutation rate, k, from 10^{-3} to 10^{-12} per day, changed the time course of intact and defective mitochondria dramatically. If 'k' is 10^{-4} per day, the number of intact mitochondria (M_w) decreases to almost zero within 300 days. For much smaller values of k, such as 10^{-11} per day, the fraction of wild-type mitochondria is hardly affected before day 1200 (data not shown).

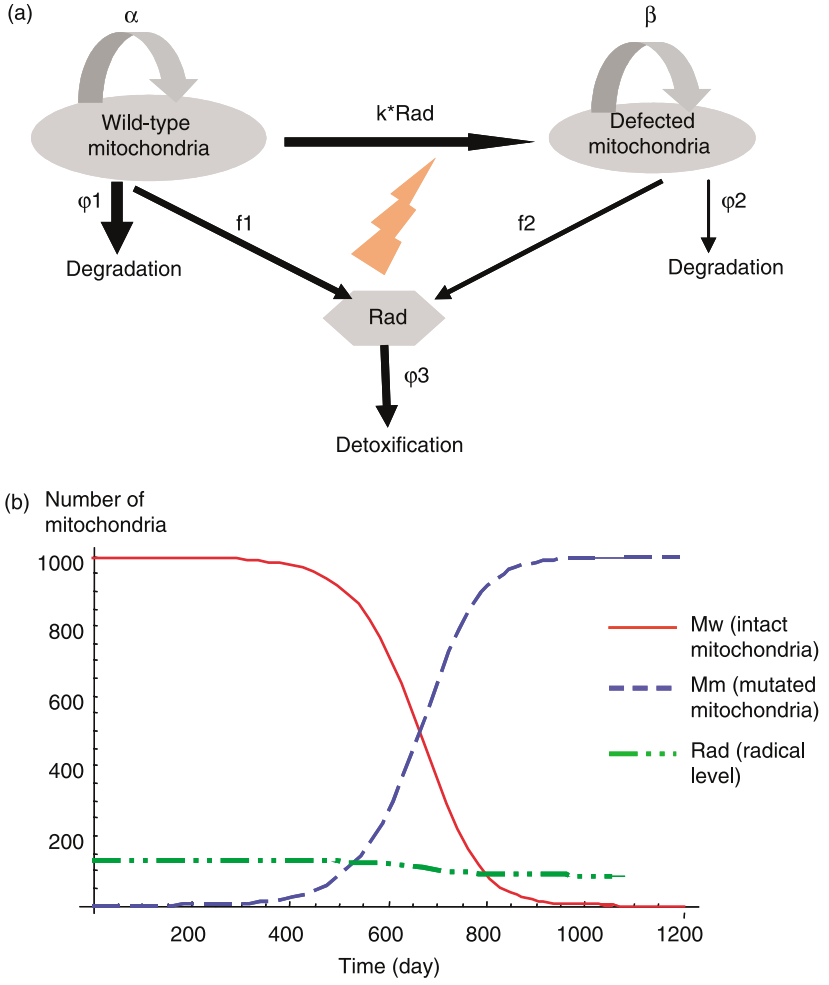

Fig. 4. Modeling concept and representative simulation result. (a) Biochemical reactions described by the current model. Two different classes of mitochondria were considered, those with intact genomes (M_w) and those with mutated genomes (M_m). The different classes produce different amounts of free radicals (f_1, f_2), which cause the transition of mitochondria from wild type to mutated type. Mitochondria reproduce with rate constants α, respectively, β and also undergo degradation with rate constants $\varphi 1$ and $\varphi 2$. Following the ideas of the SOS hypothesis (de Grey, 1997; Kowald and Kirkwood, 2000), we assume that wild type mitochondria are degraded faster than defective ones. (b) Diagram showing a time course of the components of the model. The population of wild type mitochondria decreased, while the number of mutated mitochondria in a cell increased with age. For this simulation the standard parameters described in Table 2 (parameters of brain mitochondria) and a mutation rate $k = 10^{-8}$ per mtDNA per day was used. $M_{w,}$ number of intact mitochondria; $M_{m,}$ number of mutated mitochondria; Rad, number of free radicals.

Table 2
Standard parameters used for the mathematical simulation

Parameter name	Value (d^{-1})	Description
α	0.1	Maximum growth rate of healthy mitochondria, according to Kowald (Kowald and Kirkwood, 1993)
β	0.07	Maximum growth rate of defective mitochondria was set as 70% of that of healthy mitochondria
A	1000	Maximum number of total mitochondria in a cell (Satoh and Kuroiwa, 1991)
φ_1	Brain: 0.033 Liver: 0.0825	Degradation rate of wild type mitochondria was set at 21 days for brain cells, 8.4 days for liver cells according to Korr (Korr et al., 1998)
φ_2	Brain: 0.011 Liver: 0.0275	Degradation rate of defective mitochondria, set to one third of that of wild type mitochondria.
φ_3	7×10^9	Rate of free radical removal by antioxidants, according to Rotilio (Rotilio et al., 1972)
f_1	9×10^8	Free radical production rate of intact mitochondria, according to Joenje (Joenje et al., 1985)
f_2	3×10^8	Free radical production rate of mutated mitochondria was set to one third that of intact mitochondria (Kowald and Kirkwood, 2000)
k	To be calculated	Mutation rate of mouse mitochondrial DNA

Table 3
Protein spots on the large-gel 2D-gels that have been identified in our study

Spot*	ID**	NCBI Acc***	Probability based Mowse score	Matched Peptide†	Sequence coverage† (%)	M_w (kDa)	pI	Protein name
1	2	18079339	202	26	36	85	8.08	Aconitase 2, mitochondrial
2	2	31980648	186	26	52	56	5.19	ATP synthase, H+ transporting mitochondrial F1 complex, alpha subunit
3 & 4	4	18250284	141	19	40	40	6.27	Isocitrate dehydrogenase 3 (NAD+) alpha
5	2	18152793	197	23	60	39	6.41	Pyruvate dehydrogenase (lipoamide) beta
6	2	37589957	92	11	36	36	6.16	Malate dehydrogenase, soluble
7	2	38082750	67	9	37	27	7.63	NADH dehydrogenase (ubiquinone) flavoprotein 2
8	2	31981724	161	27	64	25	8.76	Glutathione S-transferase, alpha 3
9	2	21313138	154	19	65	26	8.97	Glutathione S-transferase class kappa
10	2	21759114	131	16	61	27	8.57	Electron transfer flavoprotein beta-subunit (Beta-ETF)
11	2	20899100	170	19	82	21	8.19	NADH dehydrogenase (ubiquinone) 1 beta subcomplex, 10
12	3	6754976	197	19	60	22	8.26	Peroxiredoxin 1
13	2	20806153	66	5	30	18	5.16	ATP synthase, H+ transporting, mitochondrial F1 complex, delta subunit
14	3	6678047	186	7	60	14	4.74	Synuclein, alpha; alpha SYN; alpha-synuclein
15	2	226471	127	12	64	16	6.03	Cu/Zn superoxide dismutase
15	2	20896095	126	12	63	16	6.02	Superoxide dismutase 1, soluble
16	2	22164792	109	9	35	22	9.34	Mitochondrial ribosomal protein L12
17	4	13385268	154	11	58	15	4.96	Cytochrome $b-5$
18	3	6753500	64	8	36	14	8.69	Cytochrome *c* oxidase, subunit Vb
19 & 20	4	6680986	103	14	62	16	6.08	Cytochrome *c* oxidase, subunit Va
21	2	6680309	173	14	91	11	7.93	Heat shock protein 1 (chaperonin 10); heat shock 10 kDa protein 1 (chaperonin 10); mitochondrial chaperonin 10
22	2	6753498	93	5	46	19	9.25	Cytochrome *c* oxidase, subunit IVa
23	3	13386100	130	12	78	13	7.82	NADH dehydrogenase (ubiquinone) 1 alpha subcomplex, 5
24	2	7949005	92	9	55	12	9.36	ATP synthase, H+ transporting, mitochondrial F0 complex, subunit F; mitochondrial ATP synthase coup
25	4	38075371	103	11	61	18	10.32	NADH-ubiquinone oxidoreductase 13 kDa—a subunit, mitochondrial precursor
26	2	13385726	126	12	72	14	9.1	Ubiquinol–cytochrome *c* reductase binding protein
27	2	13385260	81	9	71	15	8.95	Thioesterase superfamily member 2
28	3	5834958	65	2	57	8	9.88	ATP synthase F0 subunit 8
29	3	6677739	278	24	74	33	5.15	Regucalcin
30	3	8393343	148	22	91	14	8.59	Fatty acid binding protein 1, liver; fatty acid binding protein liver

*Spot numbers correspond to the numbers annotated on Fig. 2. **Number of identification using mass spectrometry. ***NCBI Accession number (gi number). †The highest Mouse score among multiple measurements and its corresponding sequence coverage value are shown.

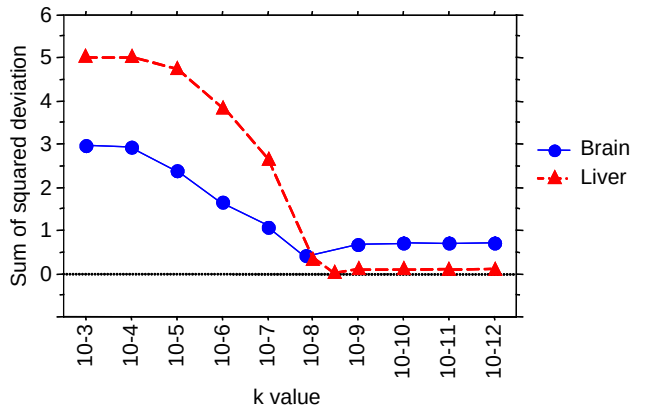

Fig. 5. Fitting the model against the proteomics data. The fit of the model to the available data was calculated for different values of the mutation rate constant, k, ranging from 10^{-3} to 10^{-12} per mtDNA per day. As a measure of fit, the sum of squares deviations is used.

3.6. Model fitting

To optimize the fit between experimental data and modeling data we used regression analysis. For this purpose, all parameters were kept constant except for the mutation rate, 'k', that was varied logarithmically from 10^{-3} to 10^{-12} per day. For the six time points for which experimental data exist, the corresponding simulation data were obtained and the sum of squared deviations was calculated. Fig. 5 shows that for brain and liver there exists a mutation rate for which the sum of squared deviations is minimized. For brain tissue a mutation rate of 2.7×10^{-8} per mtDNA per day was obtained, while for liver a lower value of 3.2×10^{-9} was found. Both fits were shown to be significant ($p<0.05$ for brain and $p<0.01$ for liver). The corresponding correlation coefficient (r^2) was 0.66 and 0.92 for brain and liver, respectively. Accordingly, we estimate the mitochondrial DNA mutation rate in mice to be 10^{-8} per mtDNA per day for brain and 10^{-9} for liver.

For model parameters without experimentally verified values (α, β, φ_2 and f_2), we performed sensitivity tests to determine their possible influence on the mtDNA mutation rate estimation. For this purpose, the value of each uncertain parameter was varied over a wide range of possible values and the optimal value for 'k' was calculated in each case. Specifically, α was varied from 0.01 to 0.5, β from 0.007 to 0.098, φ_2 from 1/4 to 2/3 of φ_1 and f_2 from 1/4 to 2/3 of f_1. Fig. 6 shows the simulation results for all four examined parameters. As can be seen the optimal value of 'k', is not very sensitive to the chosen parameter values.

4. Discussion

Among the most popular hypotheses of aging are those involved in the progressive accumulation of error-bearing or altered macromolecules with advancing age. The model of Kowald and Kirkwood is a purely theoretical description of the mitochondrial theory of aging and successfully simulated the accumulation of mutated mitochondria in the aging process (Kowald and Kirkwood, 2000). However, validation of such models is not trivial because of a general lack of experimentally confirmed parameter values.

To challenge the mitochondrial theory of aging (Harman, 1972; Linnane et al., 1989), we employed large-gel 2D-electrophoresis combined with a mathematical model in

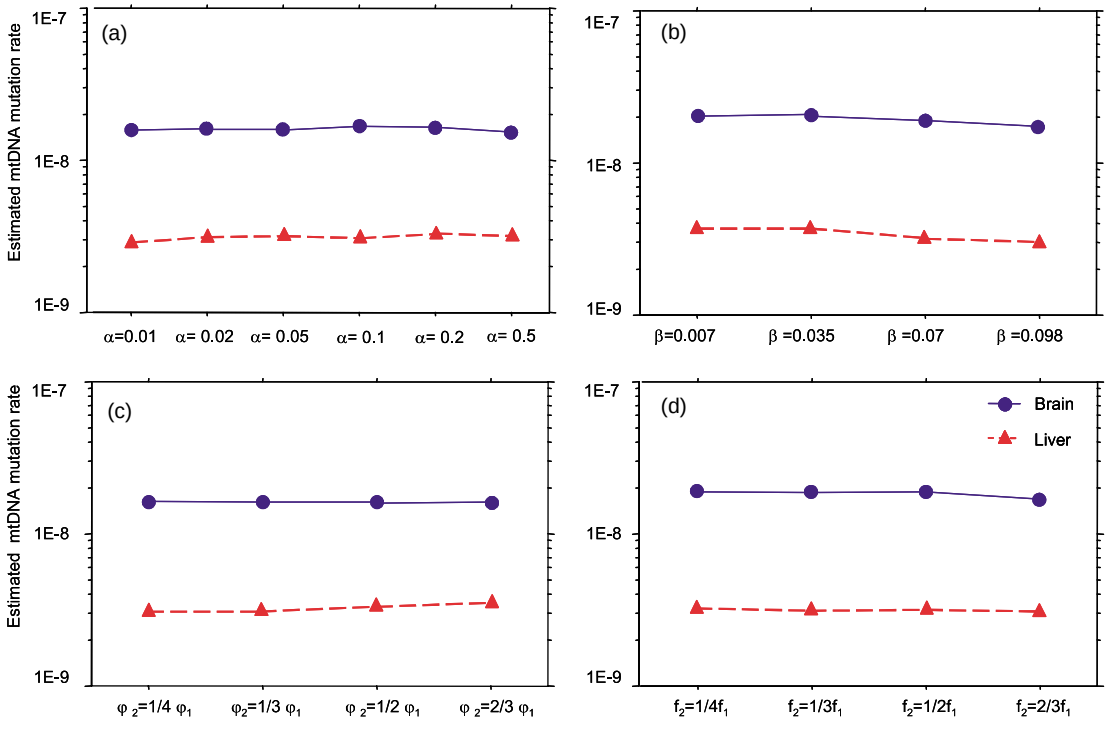

Fig. 6. Sensitivity tests for uncertain parameters of the model. The values of α, β, φ_2 and f_2 were varied over a wide range of possible values and the optimal value for 'k' was calculated in each case. (a) α was varied from 0.01 to 0.5, (b) β from 0.007 to 0.098, (c) φ_2 from 1/4 to 2/3 of φ_1 and (d) f_2 from 1/4 to 2/3 of f_1.

order to obtain a more integrated view of the biology of aging. Phenotypes of senescent cells appear through expressed and modified protein networks, rather than by genes themselves (Pirt, 1991). Differential protein expression that went undetected on the gene-level will be accessible by a proteomics study. In this sense, a quantitative proteomic analysis is a means of determining the magnitude of influence of mitochondrial mutations on aging.

For the experiment, at least eight animals of an inbred mouse strain were employed per time stage. This minimized the inter-animal variance. Multiple gel runs for each sample further reduced the gel-induced artifacts. Consequently, we are confident that genuine differences of biological relevance were accessed in our study, which represent age-related changes of mitochondrial proteins.

Four and three protein spots with decreasing spot intensities were observed in complex I and IV, respectively. Among them, two subunits of complex I and one subunit of complex IV were significantly down-regulated during aging. This could indicate a deficiency in respiratory chain complex subunits induced by abnormalities of mitochondrial DNA (Bruno et al., 1999; Rahman et al., 1999). Previous work showed that most mtDNA deletions occur in the region between the genes of ATP synthase subunit 8 and cytochrome *b*, which encodes predominantly for subunits of complex I and IV (Cortopassi and Wong, 1999; Vu et al., 2000). Similarly, mitochondrial tRNA mutations affect most severely complex I and IV subunits (Arenas et al., 1999; Triepels et al., 2001). An age-associated progressive impairment of complex I and IV activity in humans has been documented previously (Yen et al., 1991; Cooper et al., 1992; Bowling et al., 1993). Our results add evidence that complex I and IV may be the most vulnerable mitochondrial protein complexes in aging mice.

In a chain of biochemical reactions it is possible that a change in the activity of an up-stream enzyme (complex I or IV) also leads to a change of the down-stream metabolite pools and enzyme activities (Stryer, 1995). A reduced complex I and IV functionality triggers a cell response to maintain the required level of functionality of the respiratory chain. Although ultimately not effective, this could lead to an increased synthesis of proteins located downstream of complex I or IV (Manczak et al., 2005). The observed up-regulation of several complex III subunits, especially ubiquinol–cytochrome-*c* binding protein (complex III subunit in liver mitochondria) and subunit F of ATP synthase F0 complex (complex V subunit in brain mitochondria) might indicate such a feedback mechanism.

It has been noticed that changes in expression of only part of the protein complex subunits were observed in this study. A similar phenomenon was also reported by other authors (Marusich et al., 1997; Rana et al., 2000). Since predominantly hydrophilic proteins are visualized on 2D-gels, it is possible that certain hydrophobic polypeptides of complex I are missing (Santoni et al., 2000). Alternatively, this observation could suggest the essential role of these subunits in the complex assembly, and their close relation to mtDNA-encoded subunits either sterophysically or biochemically (Rana et al., 2000; Manczak et al., 2005). In this vein, the 13 kDa subunit of complex I is involved in the ion–sulfur cluster fragment, and thus would be the more likely candidate for a primary alteration due to mtDNA mutation (Moreadith et al., 1984). Vijayasarathy suggested that the association of COX Vb in complex IV, whose corresponding gene possess a unique promoter characteristics (it contains an upstream negative enhancer region) (Basu et al., 1997), is essential for the maintenance of basal COX activity (Vijayasarathy et al., 1999). This could explain the high vulnerability of these proteins to age-related changes.

To validate the idea that the gradual accumulation of defective mitochondria could be the cause of the aging process, the quantitative value of parameters can play an important role. The specific value of the mitochondrial mutation rate is obviously an important factor, directly influencing the long-term fate of a mitochondrial population. If the mutation rate is too small the effects of mitochondrial mutations on the aging process are negligible, since there is not enough time in the lifespan of an individual to accrue mitochondrial mutants to a significant degree. Unfortunately, it is currently difficult to assess the level of mutant mtDNA within living cells (Linnane et al., 1989; Chinnery and Samuels, 1999). The major goal of our current study was therefore to combine mathematical simulations and experimental data obtained from a proteomics study to estimate the mitochondrial mutation rate in mice.

Based on previous knowledge (Kowald and Kirkwood, 2000), we have constructed a strongly simplified mathematical model in order to reduce the number of required parameters. For example the dependency of mitochondria on the biosynthetic machinery of the host cell was reduced to a single parameter, an upper limit of mitochondria that can be sustained by the cell. The advantage of this simpler version is that it contains less free parameters so that the estimation of the mutation rate is more robust. This strong simplification largely facilitated the integration of experimental data, and in turn hypothesis validation. In this model, the accumulation of mutated mitochondria with time was a possible consequence of the interplay of the components of the system. This includes the reactions of free radicals with mitochondria as well as the competition of intact and mutated mitochondrial sub-populations.

Fig. 4b shows that our model could still reproduce the proposed accumulation of mutated mitochondria over time despite its simple structure. Notice that there exists a 'quasi-stable phase' at the beginning of the simulation period for both the intact and defective mitochondrial sub-population. Thereafter, defective mitochondria accumulated dramatically, accompanied by a rapid decrease of intact mitochondria.

For modeling purposes we used proteomics data that were obtained through the examination of the age related decline of nuclear encoded complex I and IV subunits. The main reason for choosing nuclear encoded subunits and not mitochondrial encoded ones, is the generally agreed difficulty to separate mitochondria-encoded proteins on 2D gels.

A profound study by Nijtmans investigated intrinsic alterations of COX subunits in an experiment using cultured

human cells depleted of mitochondrial gene products by continuous inhibition of mitochondrial protein synthesis. In their in vitro system, there was a drastic increase of nuclear DNA encoded proteins turnover rate, as well as a severe reduction of steady-state level of these nuclear DNA encoded proteins. Using Blue native electrophoresis, they showed that no assembly of nuclear DNA encoded proteins occurred. Thus, they concluded that "the increased turnover of nuclear DNA encoded proteins was due to increased susceptibility of unassembled nuclear DNA encoded proteins" (Nijtmans et al., 1995). Based on this and other (Bentlage et al., 1996; Bruno et al., 1999; Rahman et al., 1999; Remacle et al., 2004) studies, we think that mitochondrial damage should also be observable through the nuclear encoded subunits chosen by us. We did not employ data from complex III and V subunits. This is due to the suspected feedback regulation and the unknown strength of feedback.

For efficient parameter scanning, we assumed that the change of wild type mitochondria was directly correlated with the change of the respiratory chain complex I and IV subunits. This was based on the assumption that only wild type mitochondria contained intact respiratory chain complexes I and IV subunits, while mutated mitochondria were totally depleted of these subunits. Assembly of the functional respiratory chain complexes requires the coordinated contribution of subunits synthesized in both the cytoplasm and the mitochondria (Hood et al., 1989; Bentlage et al., 1996; Vijayasarathy et al., 2003). In case there is a lack of mtDNA-encoded subunits, there should be correlated lack of nuclear DNA encoded subunits in the same protein complex (di Rago et al., 1997).

Under the assumptions of our theoretical and experimental setting we could estimate the mtDNA mutation rate of the mouse strain C57BL/6 to be 2.7×10^{-8} per mtDNA per day in brain tissue and 3.2×10^{-9} in liver tissue. This corresponds to 3.8×10^{-7}, respectively, 4.4×10^{-8} per mtDNA replication (assuming a mtDNA half-life of 14 days). This result is consistent with data of Shenkar et al., who estimated the mutation rate of the 4977 bp deletion to be 5.95×10^{-8} per mitochondrial genome replication (Shenkar et al., 1996). Our estimation of mtDNA mutation rate was not significantly influenced by the free parameters (α, β, φ_2 and f_2).

With this mutation rate, a substantial accumulation of mutated mitochondria will not appear until approximately 600 days of age in our mouse model. This ensures that the vast majority of mitochondria remain intact throughout the developmental and reproduction phase of the mouse. According to our simulation results, at day 800, which is the average lifespan of the C57BL/6 mouse (Rowlatt et al., 1976), the mitochondrial population should consist of about 30% intact and 70% defective mitochondria. This correlates well with the observation of mitochondrial dysfunction in old age (Sugiyama et al., 1993). Taken together, our results indicate that the somatic mitochondrial mutations could be one of the pivotal factors controlling aging.

Interestingly, the estimated mutation rate for brain is higher than for liver. The two tissues differ in various ways and thus more than one explanation is possible. Brain has a high demand for oxygen, thus it is possible that this leads to increased oxidative stress and consequently to the observed increased mutation rate. However, also a more complicated explanation is possible, which rests on the fact that brain tissue is post-mitotic while liver is a mitotic organ. According to the SOS hypothesis defective mitochondria can accumulate faster in post-mitotic organs because the synthesis rate of mitochondria is lower than in mitotic tissues where the complete mitochondrial population has to double once every cell division. But because no experimental data are available on this issue, we used the same values for α and β for brain and liver. Had we used lower values for brain, as proposed by the SOS hypothesis, defective mitochondria would have had a stronger selection advantage in the simulations for brain tissue. Under those circumstances a lower estimated mutation rate would have been sufficient to fit the experimental data. So the high mutation rate in brain could be an overestimation since we used identical mitochondrial growth rates for brain and liver. Future work (Experimental & Modeling), including more tissue types could help to clarify this point.

The purpose of this study was to use mathematical modeling and experimental data to test the mitochondrial theory of aging. This hypothesis indicates that the initial event leading to mitochondrial dysfunction could be damage to the mtDNA, which might cause a continuous, age-related rise of oxidative damage to mitochondrial components. With the help of a simplified model, our experimental data give a guess on the mouse mitochondrial mutation rate, one of the key parameters of this system. When studying such a complex phenomenon as the aging process, systems biology approaches (close integration of modeling and experiment) seem to be very promising to investigate the behavior of the system. Future studies of this kind might hopefully provide a deeper understanding of this fascinating biological process.

Acknowledgements

We would like to thank Bettina Esch and Marion Herrmann for their excellent technical support. We are indebted to Patrick Giavalisco for his valuable suggestions. This work was supported by the German Ministry for Education and Research (BMBF), the German National Research Network (NGFN) and by grant number HA3260/1-2 from German Research Society (DFG).

References

Arenas, J., Campos, Y., Bornstein, B., Ribacoba, R., Martin, M.A., Rubio, J.C., Santorelli, F.M., Zeviani, M., DiMauro, S., Garesse, R., 1999. A double mutation (A8296G and G8363A) in the mitochondrial DNA tRNA (Lys) gene associated with myoclonus epilepsy with ragged-red fibers. Neurology 52, 377–382.

Bachmann, S., Schlichting, U., Geist, B., Mutig, K., Petsch, T., Bacic, D., Wagner, C.A., Kaissling, B., Biber, J., Murer, H., Willnow, T.E., 2004. Kidney-specific inactivation of the megalin gene impairs trafficking of renal inorganic sodium phosphate cotransporter (NaPi-IIa). J. Am. Soc. Nephrol. 15, 892–900.

Basu, A., Lenka, N., Mullick, J., Avadhani, N.G., 1997. Regulation of murine cytochrome oxidase Vb gene expression in different tissues and during myogenesis. Role of a YY-1 factor-binding negative enhancer. J. Biol. Chem. 272, 5899–5908.

Bentlage, H.A., Wendel, U., Schagger, H., ter Laak, H.J., Janssen, A.J., Trijbels, J.M., 1996. Lethal infantile mitochondrial disease with isolated complex I deficiency in fibroblasts but with combined complex I and IV deficiencies in muscle. Neurology 47, 243–248.

Boffoli, D., Scacco, S.C., Vergari, R., Solarino, G., Santacroce, G., Papa, S., 1994. Decline with age of the respiratory chain activity in human skeletal muscle. Biochim. Biophys. Acta 1226, 73–82.

Bowling, A.C., Mutisya, E.M., Walker, L.C., Price, D.L., Cork, L.C., Beal, M.F., 1993. Age-dependent impairment of mitochondrial function in primate brain. J. Neurochem. 60, 1964–1967.

Brierley, E.J., Johnson, M.A., Lightowlers, R.N., James, O.F., Turnbull, D.M., 1998. Role of mitochondrial DNA mutations in human aging: implications for the central nervous system and muscle. Ann. Neurol. 43, 217–223.

Brown, G.C., 1991. Total cell protein concentration as an evolutionary constraint on the metabolic control distribution in cells. J. Theor. Biol. 153, 195–203.

Bruno, C., Martinuzzi, A., Tang, Y., Andreu, A.L., Pallotti, F., Bonilla, E., Shanske, S., Fu, J., Sue, C.M., Angelini, C., DiMauro, S., Manfredi, G., 1999. A stop-codon mutation in the human mtDNA cytochrome *c* oxidase I gene disrupts the functional structure of complex IV. Am. J. Hum. Genet. 65, 611–620.

Challapalli, K.K., Zabel, C., Schuchhardt, J., Kaindl, A.M., Klose, J., Herzel, H., 2004. High reproducibility of large-gel two-dimensional electrophoresis. Electrophoresis 25, 3040–3047.

Chinnery, P.F., Samuels, D.C., 1999. Relaxed replication of mtDNA: a model with implications for the expression of disease. Am. J. Hum. Genet. 64, 1158–1165.

Coller, H.A., Bodyak, N.D., Khrapko, K., 2002. Frequent intracellular clonal expansions of somatic mtDNA mutations: significance and mechanisms. Ann. N.Y. Acad. Sci. 959, 434–447.

Cooper, J.M., Mann, V.M., Schapira, A.H., 1992. Analyses of mitochondrial respiratory chain function and mitochondrial DNA deletion in human skeletal muscle: effect of ageing. J. Neurol. Sci. 113, 91–98.

Cortopassi, G.A., Wong, A., 1999. Mitochondria in organismal aging and degeneration. Biochim. Biophys. Acta 1410, 183–193.

Dallman, P.R., 1967. Cytochrome oxidase repair during treatment of copper deficiency: relation to mitochondrial turnover. J. Clin. Invest. 46, 1819–1827.

de Grey, A.D., 1997. A proposed refinement of the mitochondrial free radical theory of aging. Bioessays 19, 161–166.

di Rago, J.P., Sohm, F., Boccia, C., Dujardin, G., Trumpower, B.L., Slonimski, P.P., 1997. A point mutation in the mitochondrial cytochrome *b* gene obviates the requirement for the nuclear encoded core protein 2 subunit in the cytochrome *bc*1 complex in Saccharomyces cerevisiae. J. Biol. Chem. 272, 4699–4704.

DiMauro, S., Hirano, M., Schon, E.A., Andreu, A.L., 2000. Mitochondrial encephalomyopathies: therapeutic approaches. Neurol. Sci. 21, S901–S908.

Garesse, R., Vallejo, C.G., 2001. Animal mitochondrial biogenesis and function: a regulatory cross-talk between two genomes. Gene 263, 1–16.

Giavalisco, P., Nordhoff, E., Kreitler, T., Kloppel, K.D., Lehrach, H., Klose, J., Gobom, J., 2005. Proteome analysis of Arabidopsis thaliana by two-dimensional gel electrophoresis and matrix-assisted laser desorption/ionisation-time of flight mass spectrometry. Proteomics 5, 1902–1913.

Harman, D., 1972. The biologic clock: the mitochondria? J. Am. Geriatr. Soc. 20, 145–147.

Hood, D.A., Zak, R., Pette, D., 1989. Chronic stimulation of rat skeletal muscle induces coordinate increases in mitochondrial and nuclear mRNAs of cytochrome-*c*-oxidase subunits. Eur. J. Biochem. 179, 275–280.

Jaequez, J.A., 1985. Compartmental Analysis in Biology and Medicine, second ed. University of Michigan Press, Ann Arbor.

Joenje, H., Gille, J.J., Oostra, A.B., Van der Valk, P., 1985. Some characteristics of hyperoxia-adapted HeLa cells. A tissue culture model for cellular oxygen tolerance. Lab. Invest. 52, 420–428.

Jungblut, P., Klose, J., 1985. Genetic variability of proteins from mitochondria and mitochondrial fractions of mouse organs. Biochem. Genet. 23, 227–245.

Klose, J., 1999. Large-gel 2-D electrophoresis. Fractionated extraction of total tissue proteins from mouse and human for 2-D electrophoresis. Methods Mol. Biol. 112, 147–172.

Klose, J., Kobalz, U., 1995. Two-dimensional electrophoresis of proteins: an updated protocol and implications for a functional analysis of the genome. Electrophoresis 16, 1034–1059.

Kopsidas, G., Kovalenko, S.A., Kelso, J.M., Linnane, A.W., 1998. An age-associated correlation between cellular bioenergy decline and mtDNA rearrangements in human skeletal muscle. Mutat. Res. 421, 27–36.

Korr, H., Kurz, C., Seidler, T.O., Sommer, D., Schmitz, C., 1998. Mitochondrial DNA synthesis studied autoradiographically in various cell types in vivo. Braz. J. Med. Biol. Res. 31, 289–298.

Kowald, A., Kirkwood, T.B., 1993. Mitochondrial mutations, cellular instability and ageing: modelling the population dynamics of mitochondria. Mutat. Res. 295, 93–103.

Kowald, A., Kirkwood, T.B., 1999. The mitochondrial theory of aging: do damaged mitochondria accumulate by delayed degradation? Exp. Gerontol. 34, 605–612.

Kowald, A., Kirkwood, T.B., 2000. Accumulation of defective mitochondria through delayed degradation of damaged organelles and its possible role in the ageing of post-mitotic and dividing cells. J. Theor. Biol. 202, 145–160.

Kujoth, G.C., Hiona, A., Pugh, T.D., Someya, S., Panzer, K., Wohlgemuth, S.E., Hofer, T., Seo, A.Y., Sullivan, R., Jobling, W.A., Morrow, J.D., Van Remmen, H., Sedivy, J.M., Yamasoba, T., Tanokura, M., Weindruch, R., Leeuwenburgh, C., Prolla, T.A., 2005. Mitochondrial DNA mutations, oxidative stress, and apoptosis in mammalian aging. Science 309, 481–484.

Linnane, A.W., Marzuki, S., Ozawa, T., Tanaka, M., 1989. Mitochondrial DNA mutations as an important contributor to ageing and degenerative diseases. Lancet 1, 642–645.

Manczak, M., Jung, Y., Park, B.S., Partovi, D., Reddy, P.H., 2005. Time-course of mitochondrial gene expressions in mice brains: implications for mitochondrial dysfunction, oxidative damage, and cytochrome *c* in aging. J. Neurochem. 92, 494–504.

Marusich, M.F., Robinson, B.H., Taanman, J.W., Kim, S.J., Schillace, R., Smith, J.L., Capaldi, R.A., 1997. Expression of mtDNA and nDNA encoded respiratory chain proteins in chemically and genetically-derived Rho0 human fibroblasts: a comparison of subunit proteins in normal fibroblasts treated with ethidium bromide and fibroblasts from a patient with mtDNA depletion syndrome. Biochim. Biophys. Acta 1362, 145–159.

Moreadith, R.W., Batshaw, M.L., Ohnishi, T., Kerr, D., Knox, B., Jackson, D., Hruban, R., Olson, J., Reynafarje, B., Lehninger, A.L., 1984. Deficiency of the iron-sulfur clusters of mitochondrial reduced nicotinamide-adenine dinucleotide-ubiquinone oxidoreductase (complex I) in an infant with congenital lactic acidosis. J. Clin. Invest. 74, 685–697.

Neubert, D., Bass, R., Helge, H., 1966. Conversion rate of DNA in the mitochondria of warm-blooded animals. Naturwissenschaften 53, 23–24.

Nijtmans, L.G., Spelbrink, J.N., Van Galen, M.J., Zwaan, M., Klement, P., Van den Bogert, C., 1995. Expression and fate of the nuclearly encoded subunits of cytochrome-*c* oxidase in cultured human cells depleted of mitochondrial gene products. Biochim. Biophys. Acta 1265, 117–126.

Osiewacz, H.D., Hamann, A., 1997. DNA reorganization and biological aging. A review. Biochemistry (Mosc) 62, 1275–1284.

Pappin, D.J.C., Hojrup, P., Bleasby, A.J., 1993. Rapid identification of proteins by peptide-mass fingerprinting. Curr. Biol. 3, 327–332.

Pirt, S.J., 1991. Genome project. Nature 350, 104.

Rahman, S., Taanman, J.W., Cooper, J.M., Nelson, I., Hargreaves, I., Meunier, B., Hanna, M.G., Garcia, J.J., Capaldi, R.A., Lake, B.D., Leonard, J.V., Schapira, A.H., 1999. A missense mutation of cytochrome oxidase subunit II causes defective assembly and myopathy. Am. J. Hum. Genet. 65, 1030–1039.

Rana, M., de Coo, I., Diaz, F., Smeets, H., Moraes, C.T., 2000. An out-of-frame cytochrome *b* gene deletion from a patient with parkinsonism is associated with impaired complex III assembly and an increase in free radical production. Ann. Neurol. 48, 774–781.

Remacle, C., Gloire, G., Cardol, P., Matagne, R.F., 2004. Impact of a mutation in the mitochondrial LSU rRNA gene from Chlamydomonas reinhardtii on the activity and the assembly of respiratory-chain complexes. Curr. Genet. 45, 323–330.

Richter, C., 1988. Do mitochondrial DNA fragments promote cancer and aging? FEBS Lett. 241, 1–5.

Rotilio, G., Bray, R.C., Fielden, E.M., 1972. A pulse radiolysis study of superoxide dismutase. Biochim. Biophys. Acta 268, 605–609.

Rowlatt, C., Chesterman, F.C., Sheriff, M.U., 1976. Lifespan, age changes and tumour incidence in an ageing C57BL mouse colony. Lab. Anim. 10, 419–442.

Santoni, V., Molloy, M., Rabilloud, T., 2000. Membrane proteins and proteomics: un amour impossible? Electrophoresis 21, 1054–1070.

Satoh, M., Kuroiwa, T., 1991. Organization of multiple nucleoids and DNA molecules in mitochondria of a human cell. Exp. Cell Res. 196, 137–140.

Shenkar, R., Navidi, W., Tavare, S., Dang, M.H., Chomyn, A., Attardi, G., Cortopassi, G., Arnheim, N., 1996. The mutation rate of the human mtDNA deletion mtDNA4977. Am. J. Hum. Genet. 59, 772–780.

Stryer, L., 1995. Biochemistry, fourth ed. W.H. Freeman New York.

Sugiyama, S., Takasawa, M., Hayakawa, M., Ozawa, T., 1993. Changes in skeletal muscle, heart and liver mitochondrial electron transport activities in rats and dogs of various ages. Biochem. Mol. Biol. Int. 30, 937–944.

Swat, M., Kel, A., Herzel, H., 2004. Bifurcation analysis of the regulatory modules of the mammalian G1/S transition. Bioinformatics 1, 1–5.

Toescu, E.C., Myronova, N., Verkhratsky, A., 2000. Age-related structural and functional changes of brain mitochondria. Cell Calcium 28, 329–338.

Triepels, R.H., Van Den Heuvel, L.P., Trijbels, J.M., Smeitink, J.A., 2001. Respiratory chain complex I deficiency. Am. J. Med. Genet. 106, 37–45.

Trifunovic, A., Wredenberg, A., Falkenberg, M., Spelbrink, J.N., Rovio, A.T., Bruder, C.E., Bohlooly, Y.M., Gidlof, S., Oldfors, A., Wibom, R., Tornell, J., Jacobs, H.T., Larsson, N.G., 2004. Premature ageing in mice expressing defective mitochondrial DNA polymerase. Nature 429, 417–423.

Vijayasarathy, C., Damle, S., Lenka, N., Avadhani, N.G., 1999. Tissue variant effects of heme inhibitors on the mouse cytochrome *c* oxidase gene expression and catalytic activity of the enzyme complex. Eur. J. Biochem. 266, 191–200.

Vijayasarathy, C., Damle, S., Prabu, S.K., Otto, C.M., Avadhani, N.G., 2003. Adaptive changes in the expression of nuclear and mitochondrial encoded subunits of cytochrome *c* oxidase and the catalytic activity during hypoxia. Eur. J. Biochem. 270, 871–879.

Vu, T.H., Tanji, K., Pallotti, F., Golzi, V., Hirano, M., DiMauro, S., Bonilla, E., 2000. Analysis of mtDNA deletions in muscle by in situ hybridization. Muscle Nerve 23, 80–85.

Wallace, D.C., 1997. Mitochondrial DNA in aging and disease. Sci. Am. 277, 40–47.

Yen, T.C., Su, J.H., King, K.L., Wei, Y.H., 1991. Ageing-associated 5 kb deletion in human liver mitochondrial DNA. Biochem. Biophys. Res. Commun. 178, 124–131.

Zeviani, M., Moraes, C.T., DiMauro, S., Nakase, H., Bonilla, E., Schon, E.A., Rowland, L.P., Tiranti, V., Piantadosi, C., 1998. Deletions of mitochondrial DNA in Kearns-Sayre syndrome. Neurology 51, 1525–1533.

research articles Journal of proteome research

Comparative Proteomics in Neurodegenerative and Non-neurodegenerative Diseases Suggest Nodal Point Proteins in Regulatory Networking

Claus Zabel,[†,⊥] Dijana Sagi,[†,⊥] Angela M. Kaindl,[†,‡,⊥] Nicole Steireif,[†] Yvonne Kläre,[†] Lei Mao,[†] Hartmut Peters,[§] Maik A. Wacker,[†] Ralf Kleene,[∥] and Joachim Klose*[,†]

Institute of Human Genetics, Charité, University Medicine Berlin, Augustenbuger Platz 1, 13353 Berlin, Germany, Department of Pediatric Neurology, Charité, University Medicine Berlin, Augustenbuger Platz 1, 13353 Berlin, Germany, Institute of Medical Genetics, Charité, University Medicine Berlin, Augustenbuger Platz 1, 13353 Berlin, Germany, and Center for Molecular Neurobiology, University of Hamburg, Martinistrasse 52, 20246 Hamburg, Germany

Received March 21, 2006

Neurodegenerative disorders (ND) encompass clinically and genetically heterogeneous diseases with considerable overlap of their clinical, neuropathological and molecular phenotype. Various causes of neurodegeneration in disease may affect eventually the same proteins within protein networks. To identify common changes in ND, we compared brain protein changes detected by 2-D electrophoresis in four mouse models for ND: (i) Parkinson's disease, (ii) Huntington's disease, (iii) prion disease Scrapie, and (iv) a model for impaired synaptic transmission. To determine specificity of these changes for ND, we extended the scope of our investigation to three neurological conditions that do not result in neurodegeneration (non-ND). We detected 12 to 216 consistent qualitative or quantitative protein changes in individual ND and non-ND models when compared to controls. Up to 36% of these proteins were found to be altered in multiple disease states (at least three) and were therefore termed nodal point proteins. Alterations in alpha B-Crystallin and splicing factor 3b (subunit 4) occurred in at least three ND but not in non-ND. In contrast, alterations in peroxiredoxin 1 and 3, astrocytic phosphoprotein PEA15, complexin 2 and aminoacylase 1 were common to both ND and non-ND. Finally, we investigated the expression pattern of the nodal point proteins in three inbred mouse strains and found different protein abundance (expression polymorphisms) in all cases. Nodal point proteins showing expression polymorphisms may be candidate proteins for disease associated modifiers.

Keywords: neurodegeneration • brain • proteome • mouse model • nodal points • protein network

Introduction

Neurodegenerative disorders (ND) encompass clinically and genetically heterogeneous diseases of the central and peripheral nervous system with considerable overlap of their clinical, neuropathological and molecular phenotype. ND are marked by selective and progressive neuronal cell death.[1] While our understanding of ND has progressed, the fundamental mechanisms that underlie neurodegeneration in these disorders are unknown.[1] In recent years, the study of protein complexes, protein−protein interactions, signal transduction, and metabolic pathways has disclosed an increasing number of proteins that interact in networks rather than in singular reactions within a specific metabolic pathway.[2−4] Such molecular networks support the existence of nodal point proteins which may integrate different pathways into one pathway, i.e., the occurrence of neuronal degeneration at late stage of genetically heterogeneous ND where distinct pathological pathways result in the same endpoint. Altered expression in several disorders does not necessarily imply physical interaction with other proteins. According to this model, ND are based on pathological modulation of different but finally converging pathways mediated by nodal point proteins. On the other hand, the existence of nodal points may also offer an explanation for the clinical heterogeneity of a genetically distinct disorder through a divergence of one into several pathways at nodal points. Moreover, changes in proteins at central network positions may generate unspecific dysregulation of disease unrelated proteins. This may explain the difficulties which arise in the attempt to elucidate the fundamental mechanism that underlie a specific ND when investigating late stage disease.

We will now consider how a protein network can be perturbed by disease. Theoretical considerations supported by experimental results[5] suggest that the relative concentration

* To whom correspondence should be addressed. Phone/Fax: +49-30-450-566133/566904. E-mail: joachim.klose@charite.de.
† Institute of Human Genetics, Charité, University Medicine Berlin.
‡ Department of Pediatric Neurology, Charité, University Medicine Berlin.
§ Institute of Medical Genetics, Charité, University Medicine Berlin.
∥ Center for Molecular Neurobiology, University of Hamburg.
⊥ These authors contributed equally to this work.

10.1021/pr0601077 CCC: $33.50
Published on Web 06/24/2006

of each protein within a cell is subject to constraints determined by cellular resources such as space (cell size), energy, free water, and amount of precursor molecules, e.g., amino acids. Consequently, if a protein is overexpressed in a cell due to a genetic defect, and this overexpression cannot be balanced by a down regulation of other proteins in the cell due to limitations of resources, the cell may enter a disease state due to disruption of homeostasis. It has been described for Huntington's, Parkinson's and other ND that mere overexpression of a disease related protein causes disease.[6] Protein overexpression may cause molecular crowding resulting in changes in protein conformation.[7] This may lead to protein aggregation, inhibition of protein degradation and generation of protein formations such as inclusion bodies, plaques and fibrillary structures, i.e., perturbations which promote pathological processes.[7] The significance of these network perturbations for disease development may, however, differ widely. Changes of protein expression observed in ND may be (i) detrimental but specific for one ND (e.g., disease causing gene *IT15* for HD[8]), (ii) may be detrimental but occur in several ND or/and non-ND as common nodal point proteins, or may be (iii) disease unspecific and irrelevant for disease pathology.

Using large gel two-dimensional electrophoresis (2-DE), we analyzed brain proteome changes in four mouse models for ND, Parkinson's disease (PD),[9] Huntington's disease (HD),[10] prion disease Scrapie and a model for impaired synaptic transmission (IST; involved in the pathogenesis of Alzheimer's disease (AD) and HD[11−15]). In addition, three neurological conditions without neurodegeneration, fragile X syndrome (FRAXA),[16] mice exposed to oxidative stress (OXSTR) and old aged mice, were studied. This approach allowed for the identification of both, nodal point proteins specific for ND (as a group of disorders) and ND-unspecific. We also observed that nodal point proteins differentially expressed in disease conditions (ND and non-ND) frequently vary in expression between mouse strains. We hypothesize that protein expression polymorphisms occurring in nodal point proteins may be candidates for disease associated modifiers.

Materials and Methods

Experimental Animals. Animal experiments were performed according to institutional guidelines. We investigated the brain proteome of various mouse models of ND and non-ND. In all cases except PD total brain extracts were used. As a mouse model for HD,[10,17,18] we analyzed twelve-week-old R6/2 transgenic mice with CBAxC57BL-6 background ($n = 5$). Ventral midbrains from a mouse model for PD,[9,19] with 129 genetic background, containing a disruption of exon 3 of the parkin gene, were investigated at eight months of age ($n = 10$). Furthermore, we analyzed neuronal cell adhesion molecule (N-CAM) knock-out mice (IST,[13−15]) of C57BL/6 background, a well-established mouse model for impaired synaptic transmission at 15 weeks of age ($n = 5$). A mouse model for FRAXA[16] of C57BL/6 background, where mice carry a dysfunctional fragile X mental retardation 1 protein FMR1 was studied at 27 weeks ($n = 3$). In all cases, disease models were compared with an equal number of age, sex and genetic background matched controls. To create a Scrapie mouse model, six-week old C57BL/6 ($n = 6$, Charles River, Sulzfeld, Germany) mice were infected through an intraventricular injection of 20 μL brain homogenate obtained from terminally ill scrapie mouse strain 139A. The injected brain homogenate was prepared by dissolving 500 mg sonicated brain tissue in 4.5 mL phosphate-buffered saline. Scrapie mice were sacrificed 21 weeks post-infection, close to terminal disease. Age and sex matched C57BL/6 control mice were injected with 20 μL phosphate-buffered saline alone ($n = 6$). A model for OXSTR[20] was created, when C57BL/6 mice ($n = 6$) were exposed four times to an inspiratory oxygen concentration of 80% in an oxygen chamber for 24 h every other day at three weeks of age and sacrificed immediately after the fourth treatment at an age of four weeks. Controls were kept at room air. This is a modification of a rodent model for oxidative stress described previously.[20] Protein alterations related to aging were determined by comparing 75 and 100 weeks old to 14 and 22 weeks old C57BL/6 mice ($n = 6$). To study protein polymorphisms, six 14 to 22 weeks old mice of the inbred strain *Mus spretus* (SPR) ($n = 6$; MRC, Oxfordshire, UK) or 129/Sv ($n = 6$; Charles River, Sulzfeld, Germany) were compared to C57BL/6 mice. All brains were removed, snap-frozen in liquid nitrogen and stored at −80 °C for protein extraction. Lens tissue was obtained from 100 weeks old C57BL/6 mice ($n = 6$) as described elsewhere.[21]

Protein Extraction Procedure. Total protein extracts were prepared from brain tissue. Frozen tissue, 1.6 parts v/w of buffer P (50 mM TRIZMA Base (Sigma-Aldrich, Steinheim, Germany), 50 mM KCl and 20% w/v glycerol at pH 7.5), supplemented with a final CHAPS concentration of 4% w/v in the sample, 0.08 parts of protease inhibitor solution I (1 Complete tablet (Roche Applied Science, Mannheim, Germany) dissolved in 2 mL of buffer 1) and 0.02 parts of protease inhibitor solution II (1.4 μM pepstatin A and 1 mM phenylmethylsulfonyl fluoride in ethanol) were ground to fine powder in a mortar pre-cooled in liquid nitrogen. The tissue powder was transferred into a 2 mL tube (Eppendorf, Hamburg, Germany), quickly thawed and supplied with glass beads (0.034 units of glass beads per combined weight of tissue, buffers and inhibitors in mg; glass beads, 2.5 mm ± 0.05 mm diameter, Worf Glaskugeln GmbH, Mainz, Germany). Each sample was sonicated 6 times in an ice-cold water bath for 10 s each, with cooling intervals of 1 min 50 s in between. The homogenate was stirred for 30 min in buffer P without CHAPS at 4 °C in the presence of 0.025 parts v/w of benzonase (Merck, Darmstadt, Germany) and a final concentration of 5 mM magnesium chloride in the sample. Subsequently, 6.5 M urea and 2 M thiourea were added, and stirring was continued for 30 min at room temperature until urea and thiourea were completely dissovled. The protein extract was supplied with 70 mM dithiothreitol (Biorad, Munich, Germany), 2% v/w of ampholyte mixture Servalyte pH 2−4 (Serva, Heidelberg, Germany), corrected by the amount of urea added (correction factor = sample weight prior to addition of urea/sample weight after addition of urea), and stored at −80 °C. Protein concentrations were determined in sample aliquots without urea using Biorad DC Protein Assay according to the protocol supplied by the manufacturer. Lens proteins were extracted as described previously.[21]

Two-Dimensional Gel Electrophoresis (2-DE). Protein samples were separated by the large-gel 2-DE technique developed in our laboratory as described previously.[21−23] The gel format was 40 cm (isoelectric focusing) × 30 cm (SDS-PAGE) × 0.75 mm (gel width). For isoelectric focusing (IEF) using the carrier ampholyte technique, we applied 6 μL (~20 μg/μL) protein extract of each sample to the anodic end of an IEF-gel and used a carrier ampholyte mixture to establish a pH-gradient from 3 to 10. Proteins were visualized in SDS-PAGE polyacrylamide gels by high sensitivity silver staining.[22]

2-DE gels were evaluated visually by a trained observer on a light box (Biotec-Fischer, Reiskirchen, Germany). Spot changes were considered with respect to presence/absence, quantitative variation and altered mobility. Mobility variants are spots that "move" to a different position in the 2-DE gel indicating a shift of isoelectric point (p*I*) and/or molecular weight (Mw). Protein spots which were reproducibly altered in the protein patterns of a mouse disease model when compared to control animals were further evaluated by DELTA2D imaging software version 3.3 (Decodon, Greifswald, Germany). Densitometric measurements of relative spot intensities were statistically analyzed for matched spots by Student's t-test to reveal significant differences between groups.

Protein Identification. For protein identification by mass spectrometry (MS), 40 μL (~20 μg/μL) protein extract was separated on 1.5 mm diameter IEF and 1.0 mm (width) SDS-PAGE gels, and resulting 2-DE gels were stained with a MS-compatible silver staining protocol.[24]

Protein spots of interest were excised from 2-DE gels and subjected to in-gel trypsin digestion. Tryptic fragments were analyzed by liquid chromatography (LC)/electrospray ionization (ESI) -mass spectrometry (MS) and -MS/MS on a LCQ Deca XP ion trap instrument (Thermo Finnigan, Waltham, MA). LC was directly coupled to ESI−MS analysis. Proteinspot eluates of 15 μL were loaded onto a PepMap C18 Nano-Precolumn (5 μm, 100 Å, 300 μm I.D. × 1 mm; LC Packings, Amsterdam, Netherlands) using 0.1% v/v tri-fluoroacetic acid at a flow rate of 20 μL/min. Peptides were separated onto a PepMap C18 100 column (length 15 cm, I.D. 75 μm; LC Packings, Amsterdam, Netherlands). The elution gradient was created by mixing 0.1% v/v formic acid in water (solvent A) and 0.1% v/v formic acid in acetonitrile (solvent B) and run at a flow rate of 200 nL/min. The gradient was started at 5% v/v solvent B and increased linearly up to 50% v/v solvent B after 40 min. ESI−MS data acquisition was performed throughout the LC run. Three scan events, (i) full scan, (ii) zoom scan of most intense ion in full scan, and (iii) MS/MS scan of the most intense ion in full scan were applied sequentially. No MS/MS scan on single charged ions was performed. The isolation width of precursor ions was set to 4.50 m/z, normalized collision energy at 35%, minimum signal required at 10 × 104, zoom scan mass width low/high at 5.00 m/z. Dynamic exclusion was enabled, exclusion mass width low/high was set at 3.00 m/z.

Raw data were extracted by the TurboSEQUEST algorithm, and trypsin auto-lytic fragments and known keratin peptides were subsequently filtered. All DTA files generated by TurboSEQUEST were merged and converted to MASCOT generic format files (MGF). Mass spectra were analyzed using our MASCOT in-house license with automatic searches in NCBI databases. MS/MS ion search was performed with the following set of parameters: (i) taxonomy: mammalia, (ii) proteolytic enzyme: trypsin, (iii) maximum of accepted missed cleavages: 1, (iv) mass value: monoisotopic, (v) peptide mass tolerance ±1 Da, (vi) fragment mass tolerance: ±1 Da, and (vii) variable modifications: oxidation of methionine and acrylamide adducts (propionamide) on cysteine. Only proteins with scores of $p < 0.01$, with at least three peptides identified and two independent identifications were considered.

Western Blots. For Western blotting, protein samples were prepared and concentrations determined as described above. For blots of one-dimensional SDS-PAGE, protein extracts at equal amounts (~100 μg) and a Mw marker (Rainbow marker, Amersham Biosciences, Freiburg, Germany) were dissolved in Laemmli sample loading buffer (pH 6.8, 50% glycerol, 2% SDS, 5% β-mercaptoethanol, 62.5 mM Tris, 0.1 mg/mL bromophenol blue), separated by 10% SDS-PAGE at equal protein amounts and electro-transferred to a polyvinylidene fluoride membrane (PVDF) (Millipore, Billerica, MA) using a discontinuous semi-dry blot system (current 0.8 mA/cm^2 of gel area). For blots of large 2-DE gels, gel sections of interest were used. Blotted SDS-PAGE gels were silver stained to ensure that equal amounts of protein were transferred to the PVDF membrane.

Subsequently, blotting membranes were rinsed with Tween-containing Tris-buffered saline (TBST; 10 mM Tris, 133 mM NaCl, 0,1% Tween 20, pH 7,4) and treated with blocking solution (10% nonfat milk in TBST) overnight at 4 °C to prevent nonspecific antibody binding. Membranes were incubated with alpha B-Crystallin (CRYAB) rabbit polyclonal antibody (SPA-223, Stressgen, Victoria, Canada) at a dilution of 1:2,500 in blocking solution for 2 h. For nitro blue tetrazolium (NBT)/5-bromo-4-chloro-3-indolyl phosphate disodium salt (BCIP) staining, a polyclonal goat anti-rabbit antibody (SAB-301, Stressgen) conjugated to alkaline phosphatase at a dilution of 1:2000 in blocking solution was used as secondary antibody. 400 μL BCIP (0.4 mM) in dimethyl sulfoxide (DMSO) and 0.4 mM NBT were added to 100 mM TrisBase, 100 mM NaCl and 5 mM $MgCl_2$. For luminescence staining, a horseradish peroxidase conjugated donkey anti-rabbit antibody in 10% w/v nonfat milk in TBST was utilized that was provided with the luminescence detection kit (ECL detection reagents, Amersham Biosciences). Both secondary antibodies were incubated for 1.5 h. Antibody incubations were preceded and followed by three washes in washing buffer (20 mM TrisBase, 0.9% w/v NaCl, 0.1% w/v Tween 20) of 5 min each. Four brief washes with TBST prepared for both staining reactions. Luminescence staining was carried out according to the manufacturer's protocol and serial exposures were made on autoradiographic film (X-OMAT UV Plus Film, EKC, Rochester, NY).

Protein Phosphorylation Assay. Proteins in 2-DE gels were assayed for phosphorylation using a phospho-staining kit (ProQ Diamond Phosphoprotein Gel Stain, Molecular Probes, Leiden, Netherlands) according to the manufacturer's instructions with some modifications. Briefly, each 2-DE gel section (30 cm × 20 cm) was stained in 500 mL phospho-staining solution for 3 h, de-stained in bi-distilled water three times for 1 h, overnight and for 30 min. Gels were scanned with a green laser (532 nm) at an intensity of 580 V with a Typhoon 9400 laser scanner (Amersham Biosciences).

Results

Brain Protein Changes in Neurodegenerative and Non-neurodegenerative Diseases. To identify protein changes common to neurodegenerative diseases (ND), we separated total protein extracts of brain tissue by 2-DE and compared expression patterns from disease models of Huntington's disease (HD), Parkinson's disease (PD), Scrapie, and impaired synaptic transmission (IST) with controls. To determine ND-specificity of protein changes three mouse models representing neurological conditions which had no neurodegenerative pathology were investigated: a mouse model for FRAXA, mice subjected to oxidative stress (OXSTR) and old aged mice. Protein patterns analyzed revealed approximately 7000 protein spots for each sample (Figure 1). We were interested in the overall reproducibility of our data. The HD data were selected in order to investigate reproducibility. We created a box and whisker blot for each individual sample (Figure 2). Most spots in all

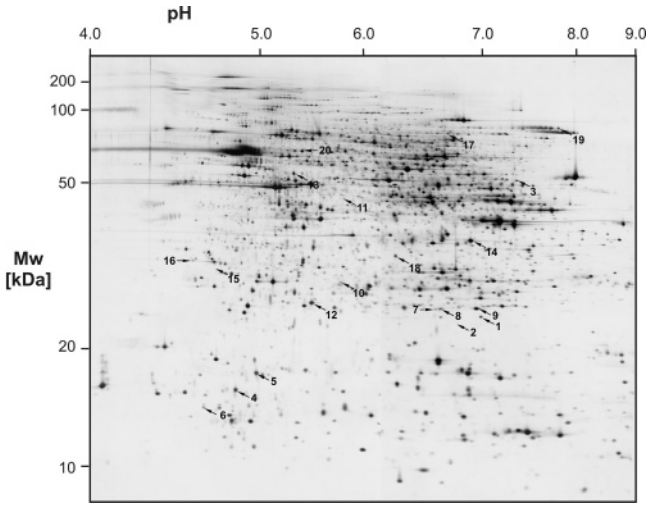

Figure 1. Nodal point protein location on a large 2-DE gel. Total brain protein extracts were separated according to their isoelectric point (p*I*) in the first and their molecular weight (Mw) in the second dimension. Protein spots were revealed by silver staining. Protein spots altered in several neurodegenerative disorders (ND) or/and non-ND in mouse disease models were indicated by numbers and black arrows. For an explanation of the protein spots 1 to 11 refer to Table 2 and for spots 12 to 14 refer to Table 3. Protein spots 15 to 20 belong to six randomly selected proteins unaltered in all disorders and between the three mouse strains studied: Tyrosine 3-monooxygenase/tryptophan 5-monooxygenase activation protein, beta polypeptide (14-3-3b) (Q59EQ2), 14-3-3 epsilon polypeptide (14-3-3e) (Q5SS40), EF-hand domain-containing protein 2 (Q9D9Y0), Proteasome subunit alpha type 1 (PSMA1) (Q9R1P4), Synapsin 1 (O88935) and Alpha−Internexin (P46660). Swiss-Prot. accession number is indicated in brackets after each protein.

individual samples were within the same intensity range (0.002−0.04 relative spot intensity). The mean for all samples was about 0.01 of relative spot intensity. The distribution of the spot intensities was of a similar range. In all mouse models investigated, we found mostly differences in protein expression abundance and only to a lower degree presence/absence changes as compared to controls. Only in very few cases, spot changes due to altered electrophoretic mobility were found (Table 1[9,17,18]). In the following section, we will consider only those proteins which were altered in several NDs but not in non-NDs. Subsequently, proteins which were altered in both NDs and non-NDs are considered. To determine the age for investigation of our mouse models the first and foremost criterion was to analyze the most severe disease state possible.

Brain Protein Changes Associated With models of ND Conditions Only. We identified alterations of the two proteins, alpha B-Crystallin (CRYAB; Swiss-Prot *P*23927) and splicing factor 3B, subunit 4 (SF3B4; synonym spliceosome-associated protein, 49 kD; Swiss-Prot Q8QZY9) in models of ND but not non-ND (spot nos. 1−3; Table 2), a finding that indicates their specificity for ND. SF3B4, detected as a single spot, was down-regulated in mouse models for HD, Scrapie and IST. In PD and all non-ND its expression was unaltered (Table 2). CRYAB was the only protein altered in all four models of ND investigated. Two isospots of this protein were found in the brain. Both spots were up-regulated in Scrapie but down-regulated in HD, PD, and IST and remained unchanged in FRAXA, OXSTR, and aging. With exception of Scrapie, isospot 2 was only detected by Western blot (Figure 3A and B). Differences in protein spot intensity on 2-DE gels are difficult to interpret, if several isospots ("spot family") for one distinct protein are altered in response to disease. The quantitative changes may result from a change in total protein concentration (spot family) or from a change of only one or several isospots within a spot family. We therefore analyzed the total amount of CRYAB in ND and controls by Western blots of one-dimensional SDS-PAGE gels and confirmed a decrease of total CRYAB abundance in HD, PD, and IST and a slight increase in Scrapie brains (Figure 3C). One protein, ATP synthase H+ transporting mitochondrial F0 complex subunit d (ATM, GI:16741459) was altered ND-specific in two out of four ND studied but not in non-ND (Table 3).

To characterize modification(s) responsible for the occurrence of two CRYAB isospots, we determined the phosphorylation status of both brain isoproteins. Phosphorylation is known to modulate CRYAB function. We suspected a difference in phosphorylation between the two isospots since this modification adds negative charges to a protein without changing its apparent molecular weight on a 2DE gel and we found differences in the isoelectric point of CRYAB isoproteins (spot no. 2 has a more negative p*I* as compared to spot no. 1) without apparent changes in molecular weight. Large 2-DE gels from brain total extracts were phospho-stained in order to determine the phosphorylation status of both CRYAB isoforms. A large number of stained spots on the 2-DE gels were detected and the identity of the two CRYAB isospots on the large 2-DE gel remained ambiguous. Therefore, a means to determine the phosphorylation status of CRYAB isospots unambiguously had to be found. Brain tissue contains only a relatively low amount of CRYAB. However, in lens CRYAB is highly abundant and therefore its phosphorylation status should be easily detectable. In addition, lens has only a limited number of other high abundant proteins and a low protein turnover.[25]

Total lens extracts of old aged mice (100 weeks) were separated by large gel 2-DE, gels blotted to identify CRYAB or stained to determine phosphorylation status. We identified CRYAB isoproteins (spot nos. 1 and 2) in lens 2-DE gels corresponding to the two isospots in brain 2-DE gels based on their pI and Mw as well as similarities in geometry, location and color of CRYAB spot patterns. Isospot 2 but not isospot 1 was phosphorylated (Figure 4). Interestingly, Western blotting for CRAYB revealed a total of seventeen isospots in the lens, six isospots showing phosphorylation. Therefore, lens tissue showed fifteen isospots more than brain. The identity of all isospots identified in the lens by Western blot was confirmed by MS (data not shown). In conclusion, brain tissue possessed only two CRYAB isoforms (15 less than lens), only one of them phosphorylated. Since both spots are down-regulated in disease, altered phosphorylation is not responsible for CRYAB loss in ND.

Brain Protein Changes Common to ND and Non-ND. We identified changes in five proteins that were altered in both models of neurological diseases with and without neurodegenerative pathology: complexin 2 (CPLX2 [2 isospots]), astrocytic phosphoprotein PEA15, peroxiredoxin 1 and 3 (PRDX1 [3isospots] and PRDX3) and aminoacylase 1 (ACY1) (Figure 1, Table 2). In an effort to investigate protein alterations common to both groups of disorders, we specifically looked only at proteins that were differentially expressed in at least three of the seven disease conditions. On the basis of the number of identified altered proteins in each of the seven conditions, 6 to 36% of the total differentially expressed proteins of a condition were found in at least three disorders (Tables 1 and

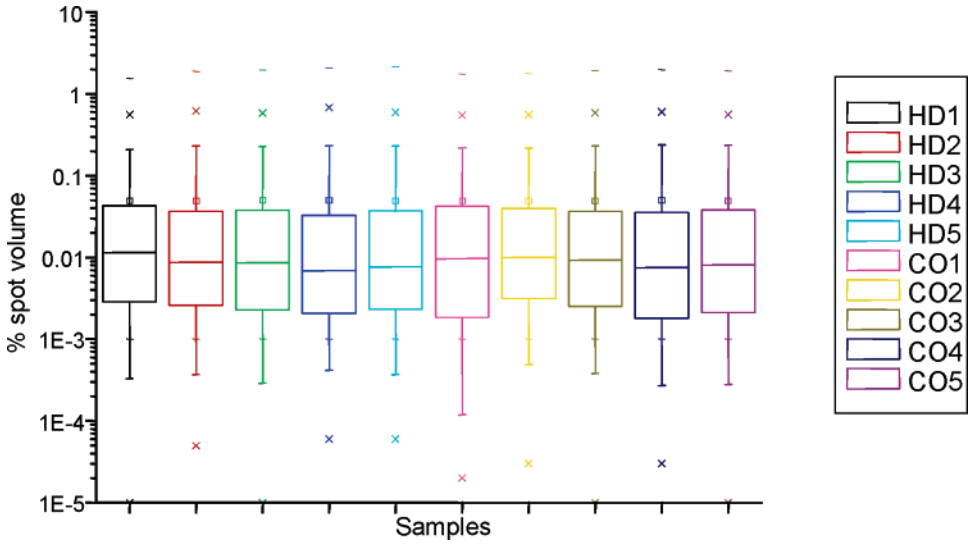

Figure 2. Similar quality of disease and conrol HD data set. A box-and-whisker plot of all 2006 spots detectable on the high pH side of the master gel for the HD data set was created. Five HD (HD1−HD5, left) and five control (CO) (CO1−CO5, right) samples are shown.

Table 1. Number of Brain Protein Alterations Detected in Mouse Models for Neurodegenerative Disorders (ND) and Non-ND

disorder	no. of proteins				
	expression		total	identified	unspecific alterations
	increased	decreased			
Huntington's disease[a]	8	32	40	34	7 (21%)
Parkinson's disease[a]	2	14	16	16	3 (18%)
Scrapie	75	18	93	44	4 (9%)
Impaired synaptic transmission	6	6	12	11	4 (36%)
Fragile X-syndrome	11	4	15	15	3 (20%)
Oxidative stress	5	7	12	12	3 (25%)
Aging	141	75	216	64	4 (6%)

[a] Part of data obtained from refs 9, 17.

2). The abundance of dysregulated spots was predominantly decreased in ND while it was equally decreased and increased in non-ND. We detected a reduced abundance of a CPLX2 isospot (spot no. 5) in HD and IST, while that of a further CPLX2 isospot (spot no. 4) was increased in PD and decreased in IST. Similarly, the abundance of PRDX1 isospots differed between various neurological disorders investigated. The abundance of one PRDX1 isospot (spot no. 7) was increased in Scrapie and aging but decreased in OXSTR. On the other hand, the abundance of PRDX1 spot 8 was only altered (reduced) in PD and that of spot 9 was increased in HD and FRAXA. Three proteins were altered in two out of seven disorders investigated (Table 3). Such a differential regulation of protein isoforms may contribute to fine-tuning and adjustment of a pathway. Since the spots so far were evaluated by a trained observer a bias in terms of protein selection might have been introduced. To test if a bias in spot selection actually occurred, we evaluated the HD data set with our spot evaluation software. All six nodal point proteins were found significantly dysregulated ($p < 0.05$) using the standard protocol supplied with the software except: CRYAB (−1.98), SF3B4 (−1.43), CPLX2 (−1.68), PEA15 (−1.20), PDX1 (1.21), and ACY1 (−1.36) showed the same direction and magnitude in dysregulation as with manual spot selection and editing (Table 2).

Polymorphisms of Proteins Altered in Disease. To determine whether proteins which were altered in ND and non-ND show similar or even the same changes between normal mouse strains due to protein polymorphisms, we compared brain protein patterns between inbred mouse strains, i.e., C57BL/6 compared to either Mus spretus (SPR) or 129/Sv. We investigated expression levels and positions of the seven proteins which were altered in ND and/or non-ND and found that all proteins also displayed differences in their abundance between normal mouse strains. Spots of CRYAB, SF3B4, CPLX2, PRDX1, and ACY1 were altered between all strains compared, whereas PEA15 was altered only between SPR and C57BL/6 and PRDX3 only between 129/Sv and C57BL/6 (Table 2). When considering a distinct ND or non-ND disorder, several of their nodal point protein alterations were found to be polymorph simultaneously between mouse strains. In most cases, the polymorphism of a protein showed even the same trend in expression variation as in disease. For example, CRYAB, SF3B, CPLX2, PEA15, and PDX3 were down-regulated in HD as well as 129/Sv (Table 2). Interestingly, three proteins changed only in two out of seven disorders were altered only in one out of two strains studied as compared to two when three out of seven proteins were altered (Tables 2 and 3). To obtain an estimate how common expression changes between mouse strains were we investigated the overall magnitude of change between two strains. Expression changes were determined by DELTA2D. A maximum expression change of 34% for Mus spretus and 33% for strain 129 was determined when spots were included which

Table 2. Nodal Point Proteins in ND and Non-ND

protein name	spot no.	accession no.[d]	quantitative and qualitative changes of proteins[a]								
			neurodegenerative disorders[b]				nonneurodegenerative disorders[b]			protein polymorphism[c]	
			HD	PD	Scrapie	IST	FRAXA	OXSTR	Aging	SPR	129/Sv
Alpha B−Crystallin (CRYAB)	1	*P*23927	▼*2.3*[#]	▼*1.4*	△1.2	▼*16.7*[#]				▼*3.6*[#]	▼*10.2*[#]
	2	*P*23927			△1.6	▼*5.9*[#]					
Splicing factor subunit 4 (SF3B4)	3	Q8QZY9	▼*1.8*[#]		▼*1.2*[#]	▼*1.1*[#]				▼*1.4*	▼*1.4*
Complexin 2 (CPLX2)	4	P84086		△1.2		▼*1.6*					▼*2.0*[#]
	5	P84086	▼*1.8*[#]			▼*1.6*			▼*1.4*	△1.7[#]	▼*1.8*[#]
Astrocytic Phosphoprotein (PEA15)	6	Q62048	▼*1.3*		△1.3[#]	▼*1.8*		▼1.5		mV	
Peroxiredoxin 1 (PDX1)	7	P35700			△1.3			▼1.5	△1.4	▼*1.9*[#]	
	8	P35700		▼*1.4*							
	9	P35700	△1.2[#]				△1.2				▼*1.3*
Peroxiredocxin 3 (PDX3)	10	6680690	▼*1.2*	*absent*			△1.6	▼*1.9*[#]	▼*1.5*		*absent*
Aminoacylase 1 (ACY1)	11	Q99JW2	▼*1.5*				▼*1.3*[#]		△1.5	▼*3.0*[#]	△1.7*

[a] Quantitative changes: Ratios were calculated by (Higher spot intensity)/(lower spot intensity) and shown as fold change compared to control ($p < 0.05$, $p < 0.01$ indicated by #). ▼: down regulation, △: up regulation. Qualitative changes: mV, variation in electrophoretic mobility. [b] Abrreviations: HD: Huntington's disease, PD: Parkinson's disease, IST: Impaired synaptic transmission, FRAXA: Fragile X-syndrome, OXSTR: Oxidative stress. [c] Mouse strain C57BL/6 compared with strain SPR and strain 129/Sv. [d] Accession number from Swiss-Prot. database or NCBI (for PDX3).

were down-regulated <0.9 or up-regulated >1.1 and $p < 0.05$ was used as criterion for significance. The maximum of expression change was 19% in both cases when using <0.5 or >2.0 ($p < 0.05$) as selection criterion. These results do not represent the number of polymorphisms found by Klose et al. 2002.[23] There, the number of polymorphisms needs to be lower since the changes in protein expression have to follow an inheritance pattern. Our results indicate that the probability of three proteins changing concomitantly between disease and control by chance is ($0.34 \times 0.34 \times 0.34 = 0.039$) 3.9% which is <5%, our selection criteria for differentially expressed spots. After determining the extent of overall changes, it was of interest how uniform protein changes occurred within a species. Individual spot intensities for all seven nodal point proteins for each M. spretus vs C57BL/6 sample pair were compared manually. Only in case of SF3B4 one spot intensity value showed inverse behavior as compared to the overall trend. All other spot intensities for individual proteins followed the overall trend of expression for a specific protein. When comparing 129 and C57BL/6 the proteins PDX1 and ACY1 showed deviant behavior in only one case each. Therefore, the intra-strain variation can be considered small since out of 84 sample pairs only 3 (3.6%) deviated from the overall trend. Since all mouse models were of different age, age specific effects on protein polymorphisms common to certain disease groups were excluded.

To determine the specificity of expression polymorphisms between strains we randomly selected six proteins (Figure 1 spots 15−20) which were not altered in the disorders investigated. None of these proteins showed differential expression between the strains tested. The proteins investigated were Tyrosine 3-monooxygenase/tryptophan 5-monooxygenase activation protein, beta polypeptide (14-3-3b), 14-3-3, epsilon polypeptide (14-3-3e), EF-hand domain-containing protein 2, Proteasome subunit alpha type 1 (PSMA1), Synapsin 1 and Alpha−Internexin, spot nos. 15 to 20 in Figure 1, respectively.

Discussion

In our study, we investigated the brain proteome in mouse models of four neurodegenerative disorders (HD, PD, and Scrapie and IST, a condition that is associated with neurodegeneration) and three neurological conditions without neurodegeneration (FRAXA, oxidative stress and aging) and compared the protein changes found in each disease between different disorders. We identified proteins which were altered in several neurodegenerative diseases (ND) but restricted in their alterations to ND and proteins which were altered in both ND and non-ND. In addition, we investigated whether proteins altered in disease show changes in normal mice due to protein polymorphisms.[23]

In all diseases investigated, including old aged mice, numerous changes in protein abundance were found (Table 1). Interestingly however, up to 36% of abnormal protein changes occurred in multiple disease states. Seven proteins (11 protein isospots) were differentially regulated in at least three of seven investigated neurological conditions (Figure 1, Table 2). Differentially regulated proteins in ND displayed a trend to reduced abundance whereas changes in abundance occurred with similar frequency in non-ND. Unexpectedly, when investigating the seven proteins differentially expressed in several disorders, we observed that all proteins were altered in expression between different mouse strains as well. These differences were in some cases very similar to those observed under disease conditions. Our comparative approach to study neurological diseases revealed proteins that are altered simultaneously under quite different diseases and different but normal genotypes. These proteins may occupy nodal points in the network of protein−protein interaction and regulation and be responsible for overlapping metabolic pathways and clinical symptoms of different genetic disorders. Thus these proteins may have an important role in disease pathology.

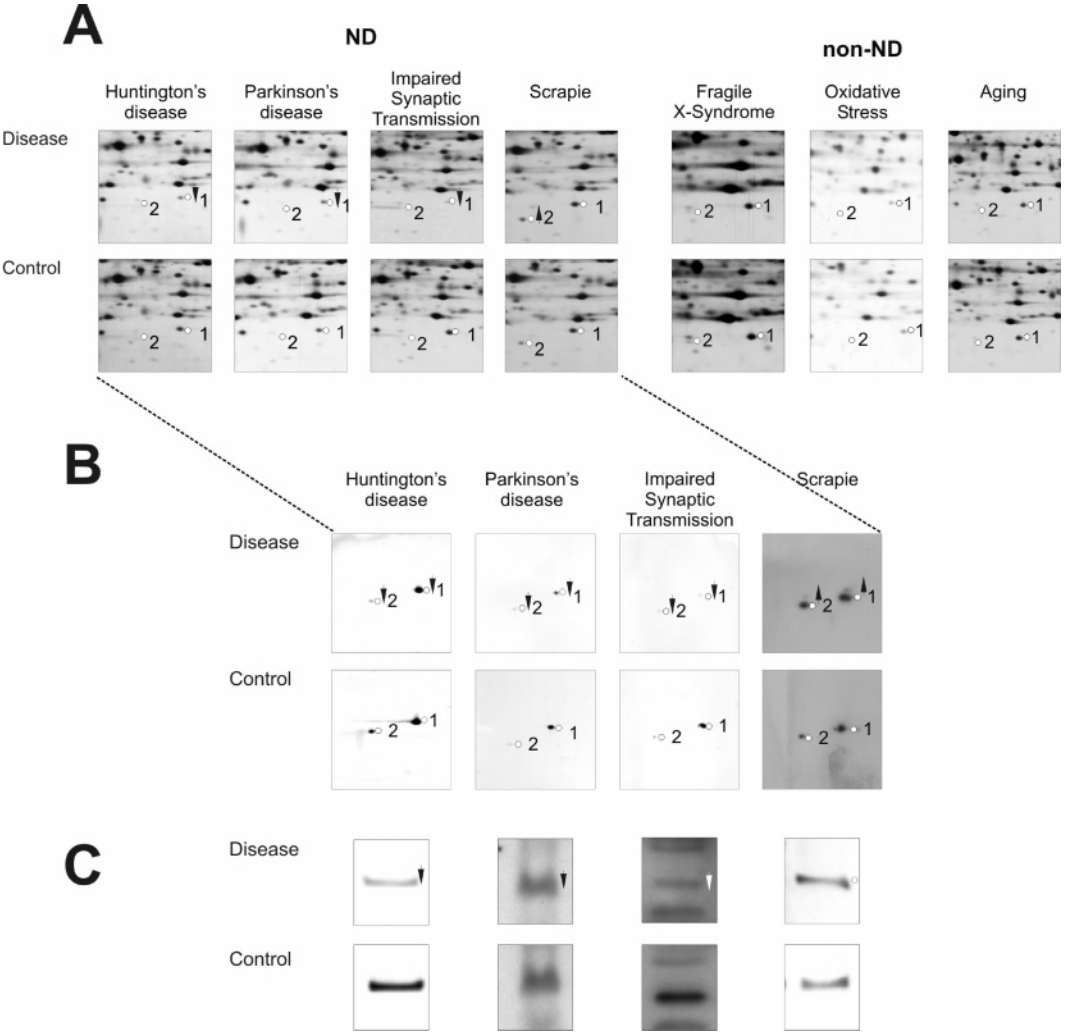

Figure 3. CRYAB alteration in four neurodegenerative disorders (ND). (A) Comparisons of mouse models of ND and non- non-ND revealed reproducible changes in the relative abundance of CRYAB in the four ND, HD, PD, Scrapie and IST. CRYAB was unaltered in three models for non-ND conditions: FRAXA, mice treated with OXSTR and old aged mice (100 weeks). CRYAB is represented by two isospots (protein isoforms) on brain 2-DE gels. CRYAB isospots are marked by dots on their right side and numbers; the upward and downward arrows mark an increase or decrease, respectively, of spot intensity in disease mice as compared to controls. Western blot analysis for CRYAB following 2-DE (B) and one-dimensional SDS-PAGE (C) confirmed the decrease of CRYAB isoforms in HD, PD, and IST and an increase in Scrapie found in (A).

Table 3. Proteins Altered Twice in ND and Non-ND

protein name			quantitative and qualitative changes of proteins[a]								
	spot no.	accession no.[d]	neurodegenerative disorders[b]				nonneurodegenerative disorders[b]			protein polymorphism[c]	
			HD	PD	Scrapie	IST	FRAXA	OXSTR	Aging	SPR	129/Sv
ATP synthase H+ transporting mitochondrial F0 complex subunit d (ATM)	12	GI:16741459			▼ *1.16*	▼ *1.18*				△*1.36*#	
guanine deaminase (GUAD)	13	Q9R111	▼ *1.59*				△*1.10*			▼ *3.85*#	
voltage-dependent anion channel 1 (VDAC1)	14	Q60932				▼ *1.16*		△*1.17*			▼ *1.52*

[a] Quantitative changes: Ratios were calculated by (Higher spot intensity)/(lower spot intensity) and shown as fold change compared to control ($p < 0.05$, $p < 0.01$ indicated by #). ▼: down regulation, △: up regulation. Qualitative changes: mV, variation in electrophoretic mobility. [b] Abrreviations: HD: Huntington's disease, PD: Parkinson's disease, IST: Impaired synaptic transmission, FRAXA: Fragile X-syndrome, OXSTR: Oxidative stress. [c] Mouse strain C57BL/6 compared with strain SPR and strain 129/Sv. [d] Accession number from Swiss-Prot. database or NCBI (for PDX3).

Brain Protein Changes Associated only with Models of Neurodegenerative Disorders. ND such as PD, HD, and Scrapie are associated with degeneration and death of specific neuronal cell populations due to mechanisms that include modulation of molecular chaperones,[26] aberration in splicing events,[27] misfolding and accumulation of prion proteins,[28] disturbed

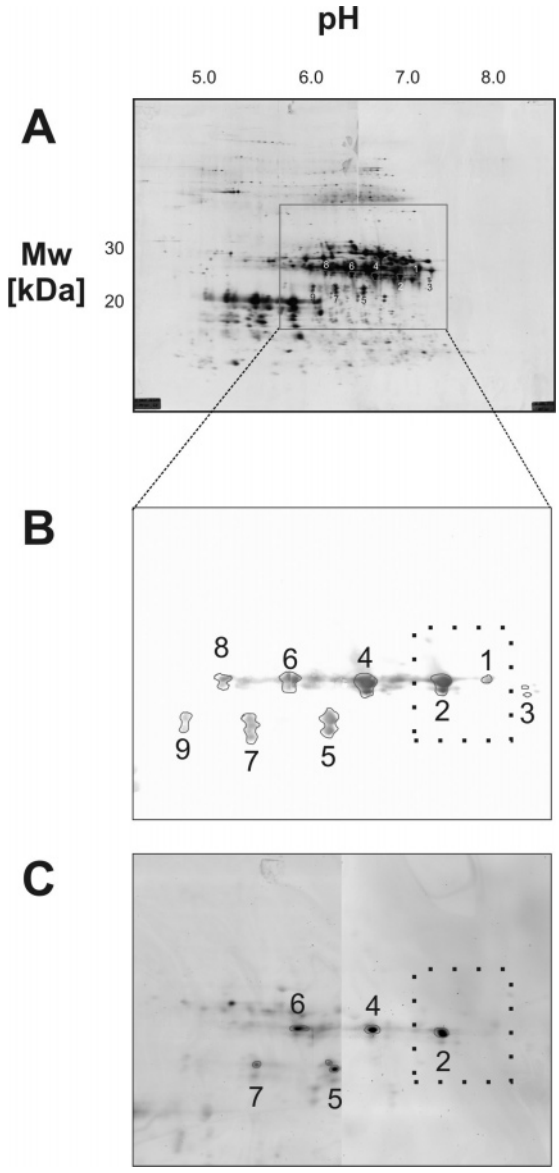

Figure 4. Phosphorylation of CRYAB isospots in the lens. (A) The location of CRYAB isospots on a representative silver stained 2-DE gel of lens extracts from 100-week-old C57BL/6 mice are indicated by a black, solid square. (B) Black circles and numbers 1−9 indicate seventeen single CRYAB spots as revealed by Western blotting. The identification of these spots was confirmed by MS. (C) Phosphostaining of the 2-DE gel section shown in (A) revealed 5 phosphorylated CRYAB isoforms. The numbers in A, B, and C indicate the same CRYAB isospots. The black, dotted square indicates the location of the two CRYAB isospots found in the brain. A comparison of brain (Figures 1 and 2) and lens 2-D pattern shows that brain CRYAB isospot 2 but not 1 is phosphorylated.

axonal transport[29] and impaired synaptic transmission.[12] While ND have different causes, many of them show strikingly similar cellular and molecular mechanisms, which promises that insights found for one ND may be applicable to others as well. Accordingly, we found alterations of alpha B-Crystallin (CRYAB) in all four ND investigated and splicing factor 3B, subunit 4 (SF3B4) associated with at least three models of ND tested.

Considering SF3B4, differential splicing is essential in the central nervous system (CNS) for physiological processes such as tissue differentiation and development, learning, memory, neuronal cell recognition, neurotransmission, ion channel function, and receptor specificity.[30] In mouse models of HD, Scrapie and IST, we observed a down-regulation of SF3B4, a protein essential for 'pre-spliceosome' assembly and recognition of intron branch points in pre-mRNA splicing.[31] Down-regulation of this protein may be associated with altered splicing, a pathomechanism implicated previously with ND of the central and peripheral nervous system: (i) Huntingtin interacts with spliceosome proteins,[32,33] (ii) aberrant tau mRNA splicing leads to protein aggregation and neurodegeneration similar to that seen in Alzheimer's disease,[34] and (iii) mutant spinal muscular atrophy gene, encoding a protein required for pre-mRNA splicing, causes severe degenerative motor neuron disease spinal muscular atrophy.[35]

Many ND have been associated with neuronal death due to accumulation of abnormal polypeptides indicating an involvement of chaperones and subsequently proteolytic systems in the pathology of these disorders. The chaperone CRYAB, a member of the small heat shock protein family, facilitates protein folding, refolding and degradation of misfolded polypeptides, prevents protein aggregation, plays a role in formation of the aggresome and promotes cell survival.[36] Therefore, chaperone function may have become altered in our ND models by the dysregulation of CRYAB found in all four models. Consistent with our finding, CRYAB dysregulation has been associated previously with several ND such as AD,[37] PD,[38] amyotrophic lateral sclerosis,[39] Alexander's disease,[40] Creutzfeldt-Jakob disease,[41] tauopathies,[42] and multiple sclerosis.[43,44] Accumulation of aggregation prone proteins activates signal transduction pathways that control cell death.[45] CRYAB, on the other hand, has been suggested to interfere with these pathways and thereby promote cell survival. The CRYAB reduction in HD, PD and IST seen in our study may cause cell death and promote aggregation. The increase in CRYAB in Scrapie may have been caused by gliosis as indicated by an increase in glial fibrillary acidic protein (GFAP) in Scrapie brain samples. No gliosis was detected in HD, PD, and IST (data not shown). Gliosis, a drastic increase in astrocytes, in diseased Scrapie brain tissue, may mask a down-regulation of CRYAB per cell as compared to normal brain tissue. Since even normal astrocytes contain considerably more CRYAB than neurons, gliosis increases the glia/neuron ratio and thereby CRYAB significantly.

The ability to promote cell survival and reduce aggregation is decreased by phosphorylation: CRYAB oligomerization is decreased by phosphorylation and leads to impaired chaperone function.[45−47] We therefore analyzed the phosphorylation status of our CRYAB isoforms altered in ND models. Our results suggest that only one CRYAB isoform found in the brain is phosphorylated in ND models and in controls. The higher abundant isoform is not phosphorylated (Figure 4). Therefore, a decrease of CRYAB in brain tissue per se and not of phosphorylated CRYAB seems to be detrimental in ND. Supported by previous reports, our findings indicate that pre-mRNA splicing and chaperone function may be involved in the development of ND and highlight SF3B4 and CRYAB as possible nodal points common to this group of diseases.

Brain Protein Changes Common to ND and Non-ND. In our study, the differential regulation of the five brain proteins PRDX1 (3 isoforms), PRDX3, CPLX2 (2 isoforms), PEA15, and ACY1 occurred in both ND and non-ND. These proteins may be nodal points in pathways affected in diseases of the CNS both with and without neurodegeneration. Oxidative stress has

been observed in acute and chronic disorders of the CNS such as ischemia, trauma, inflammation, aging, and various ND.[48−50] Since peroxiredoxins protect against oxidative stress through redox regulation,[48] the alteration of PDX1 abundance observed in all neurological conditions (except for IST), and of PDX3 in HD and all non-ND may be associated with oxidative stress. A common disturbance in vesicle trafficking in disorders of the CNS may cause the dysregulation of CPLX2 in models of HD, PD, and IST and aging. This protein is highly abundant in the CNS and is crucial for exocytosis.[51] In accordance with our data, an impairment of exocytosis was implicated in the pathology of ND,[11,12] and CPLX2 was decreased in the brains of HD transgenic mice and of humans with HD.[52] Moreover, mRNA expression of other genes involved in vesicle trafficking was decreased in human PD post-mortem brains.[53] Cell death by apoptosis is common in ND such as HD[54] and PD.[55] Both, PEA15 and ACY1 protect from apoptosis: (i) PEA15 inhibits tumor necrosis factor alpha (TNF-α) activity and modulates extra-cellular signal-regulated kinase mitogen activated protein kinase (ERK-MAPK) cascade;[56] (ii) ACY1 interacts with TRAF2, up-regulates NF-κB signaling and thereby prevents apoptosis during TNF-α stimulation.[57] The deregulation of PEA-15 in HD, Scrapie, IST, and OXSTR, and of ACY1 in HD, FRAXA and aging (and trend to down-regulation in Scrapie and IST; data not shown) indicate a common pattern of dysregulation of nodal point proteins involved in cell death.

Protein Networks. Protein expression changes that are not specific for a single disease may be explained by integration of proteins within networks. Widespread interaction between proteins in highly complex protein networks has already been demonstrated for several organisms such as yeast,[58] drosophila[3] and humans.[4,59] An alteration of one protein in a protein network may therefore cause changes in many other proteins within the network by direct or indirect protein−protein interactions. Thus, while genetic defects, nongenetic disorders and naturally occurring variations such as polymorphisms may primarily modulate only one or a few proteins specifically, many other proteins may become involved due to network effects. Proteins most frequently targeted may be those which occupy nodal points in the proteome network. Therefore, alterations in a tissue or cell induced by conditions that differ as much as ND, non-ND and normal populations (polymorphisms) may, nevertheless, affect to some extent the same nodal point proteins, which will become obvious by quantitative changes in these proteins. An interesting observation of our study was that all seven nodal point proteins detected were also polymorphic between mouse strains. Expression polymorphisms of a nodal point protein may be caused by alterations of proteins interacting with it. Nodal point protein encoding genes are unlikely to carry mutations themselves since adaptive evolution suggests that this is least likely for proteins that hold a high number of interactions.[60,61] Between mouse strains C57BL/6 and SPR, a frequency of 15% protein polymorphisms was observed, representing a high level of variation between mouse strains.[23] Therefore, many proteins altered by polymorphisms may act on nodal point proteins and alter their expression which is seen as protein expression polymorphisms. In this way, protein polymorphisms may serve as disease associated modifiers, e.g., changing the onset of disease.

In conclusion, our investigation has shown that quantitative changes of proteins in various neurological diseases can be quite unspecific to a disease under consideration and may even reflect frequently normal variability of proteins due to polymorphisms. Moreover, our investigation demonstrates that studies of various diseases and other abnormal physiological conditions within the same biological system, such as the mouse, may offer a strategy to detect regulatory nodal points in proteomic networks of the cell.

Acknowledgment. The authors acknowledge the excellent technical assistance by Mario Wolters and Marion Herrmann. This work was supported by the German ministry for education and research (BMBF) within the German National Genome Research Network (NGFN) program, and by a grant from Sanitätsrat-Dr.-Emil-Alexander-Huebner-und-Gemahlin-Stiftung.

References

(1) Martin, J. B. Molecular basis of the neurodegenerative disorders. *N. Engl. J. Med.* **1999**, *340* (25), 1970−1980.
(2) Peifer, M., Signal transduction. Neither straight nor narrow. *Nature* **1999**, *400* (6741), 213−215.
(3) Giot, L.; Bader, J. S.; Brouwer, C.; Chaudhuri, A.; Kuang, B.; Li, Y.; Hao, Y. L.; Ooi, C. E.; Godwin, B.; Vitols, E.; Vijayadamodar, G.; Pochart, P.; Machineni, H.; Welsh, M.; Kong, Y.; Zerhusen, B.; Malcolm, R.; Varrone, Z.; Collis, A.; Minto, M.; Burgess, S.; McDaniel, L.; Stimpson, E.; Spriggs, F.; Williams, J.; Neurath, K.; Ioime, N.; Agee, M.; Voss, E.; Furtak, K.; Renzulli, R.; Aanensen, N.; Carrolla, S.; Bickelhaupt, E.; Lazovatsky, Y.; DaSilva, A.; Zhong, J.; Stanyon, C. A.; Finley, R. L., Jr.; White, K. P.; Braverman, M.; Jarvie, T.; Gold, S.; Leach, M.; Knight, J.; Shimkets, R. A.; McKenna, M. P.; Chant, J.; Rothberg, J. M., A protein interaction map of Drosophila melanogaster. *Science* **2003**, *302* (5651), 1727−1736.
(4) Stelzl, U.; Worm, U.; Lalowski, M.; Haenig, C.; Brembeck, F. H.; Goehler, H.; Stroedicke, M.; Zenkner, M.; Schoenherr, A.; Koeppen, S.; Timm, J.; Mintzlaff, S.; Abraham, C.; Bock, N.; Kietzmann, S.; Goedde, A.; Toksoz, E.; Droege, A.; Krobitsch, S.; Korn, B.; Birchmeier, W.; Lehrach, H.; Wanker, E. E., A human protein−protein interaction network: a resource for annotating the proteome. *Cell* **2005**, *122* (6), 957−968.
(5) Brown, G. C., Total cell protein concentration as an evolutionary constraint on the metabolic control distribution in cells. *J. theor. Biol.* **1991**, *153*, 195−203.
(6) Zoghbi, H. Y.; Botas, J., Mouse and fly models of neurodegeneration. *Trends Genet* **2002**, *18* (9), 463−471.
(7) Minton, A. P., Implications of macromolecular crowding for protein assembly. *Curr. Opin. Struct. Biol.* **2000**, *10* (1), 34−39.
(8) HDCRG, A novel gene containing a trinucleotide repeat that is expanded and unstable on Huntington's disease chromosomes. The Huntington's Disease Collaborative Research Group. *Cell* **1993**, *72* (6), 971−983.
(9) Palacino, J. J.; Sagi, D.; Goldberg, M. S.; Krauss, S.; Motz, C.; Klose, J.; Shen, J., Mitochondrial dysfunction and oxidative damage in Parkin-deficient mice. *J. Biol. Chem.* **2004**, *279* (18), 18614−18622.
(10) Mangiarini, L.; Sathasivam, K.; Seller, M.; Cozens, B.; Harper, A.; Hetherington, C.; Lawton, M.; Trottier, Y.; Lehrach, H.; Davies, S. W.; Bates, G. P., Exon 1 of the HD gene with an expanded CAG repeat is sufficient to cause a progressive neurological phenotype in transgenic mice. *Cell* **1996**, *87* (3), 493−506.
(11) Li, J. Y.; Plomann, M.; Brundin, P., Huntington's disease: a synaptopathy? *Trends. Mol. Med.* **2003**, *9* (10), 414−420.
(12) Yao, P. J., Synaptic frailty and clathrin-mediated synaptic vesicle trafficking in Alzheimer's disease. *Trends. Neurosci.* **2004**, *27* (1), 24−29.
(13) Cremer, H.; Lange, R.; Christoph, A.; Plomann, M.; Vopper, G.; Roes, J.; Brown, R.; Baldwin, S.; Kraemer, P.; Scheff, S.; et al. Inactivation of the N−CAM gene in mice results in size reduction of the olfactory bulb and deficits in spatial learning. *Nature* **1994**, *367* (6462), 455−459.
(14) Polo-Parada, L.; Bose, C. M.; Landmesser, L. T. Alterations in transmission, vesicle dynamics, and transmitter release machinery at NCAM-deficient neuromuscular junctions. *Neuron* **2001**, *32* (5), 815−828.
(15) Polo-Parada, L.; Bose, C. M.; Plattner, F.; Landmesser, L. T. Distinct roles of different neural cell adhesion molecule (NCAM) isoforms in synaptic maturation revealed by analysis of NCAM 180 kDa isoform-deficient mice. *J. Neurosci.* **2004**, *24* (8), 1852−1864.
(16) Fragile_X_Consortium, Fmr1 knockout mice: a model to study fragile X mental retardation. The Dutch-Belgian Fragile X Consortium. *Cell* **1994**, *78* (1), 23−33.

(17) Zabel, C.; Chamrad, D. C.; Priller, J.; Woodman, B.; Meyer, H. E.; Bates, G. P.; Klose, J. Alterations in the mouse and human proteome caused by Huntington's disease. *Mol. Cell. Proteomics* **2002**, *1* (5), 366−375.
(18) Zabel, C.; Klose, J. Influence of Huntington's disease on the human and mouse proteome. *Int. Rev. Neurobiol.* **2004**, *61*, 241−283.
(19) Goldberg, M. S.; Fleming, S. M.; Palacino, J. J.; Cepeda, C.; Lam, H. A.; Bhatnagar, A.; Meloni, E. G.; Wu, N.; Ackerson, L. C.; Klapstein, G. J.; Gajendiran, M.; Roth, B. L.; Chesselet, M. F.; Maidment, N. T.; Levine, M. S.; Shen, J. Parkin-deficient mice exhibit nigrostriatal deficits but not loss of dopaminergic neurons. *J. Biol. Chem.* **2003**, *278* (44), 43628−43635.
(20) Kaindl, A. M.; Sifringer, M.; Zabel, C.; Nebrich, G.; Wacker, M. A.; Felderhoff-Mueser, U.; Endesfelder, S.; von der Hagen, M.; Stefovska, V.; Klose, J.; Ikonomidou, C. Acute and long-term proteome changes induced by oxidative stress in the developing brain. *Cell Death Differ.* **2005**.
(21) Jungblut, P. R.; Otto, A.; Favor, J.; Lowe, M.; Muller, E. C.; Kastner, M.; Sperling, K.; Klose, J. Identification of mouse crystallins in 2D protein patterns by sequencing and mass spectrometry. Application to cataract mutants. *FEBS Lett.* **1998**, *435* (2−3), 131−137.
(22) Klose, J. Large-gel 2-D electrophoresis. *Methods Mol. Biol.* **1999**, *112*, 147−172.
(23) Klose, J.; Nock, C.; Herrmann, M.; Stuhler, K.; Marcus, K.; Bluggel, M.; Krause, E.; Schalkwyk, L. C.; Rastan, S.; Brown, S. D.; Bussow, K.; Himmelbauer, H.; Lehrach, H. Genetic analysis of the mouse brain proteome. *Nat. Genet.* **2002**, *30* (4), 385−393.
(24) Shevchenko, A.; Wilm, M.; Vorm, O.; Mann, M. Mass spectrometric sequencing of proteins silver-stained polyacrylamide gels. *Anal.Chem* **1996**, *68* (5), 850−858.
(25) Wistow, G. J.; Piatigorsky, J. Lens crystallins: the evolution and expression of proteins for a highly specialized tissue. *Annu. Rev. Biochem.* **1988**, *57*, 479−504.
(26) Muchowski, P. J.; Wacker, J. L. Modulation of neurodegeneration by molecular chaperones. *Nat. Rev. Neurosci.* **2005**, *6* (1), 11−22.
(27) Dredge, B. K.; Polydorides, A. D.; Darnell, R. B. The splice of life: alternative splicing and neurological disease. *Nat. Rev. Neurosci.* **2001**, *2* (1), 43−50.
(28) Mallucci, G.; Collinge, J. Update on Creutzfeldt-Jakob disease. *Curr. Opin. Neurol.* **2004**, *17* (6), 641−647.
(29) Sheetz, M. P.; Pfister, K. K.; Bulinski, J. C.; Cotman, C. W. Mechanisms of trafficking in axons and dendrites: implications for development and neurodegeneration. *Prog. Neurobiol.* **1998**, *55* (6), 577−594.
(30) Grabowski, P. J.; Black, D. L. Alternative RNA splicing in the nervous system. *Prog. Neurobiol.* **2001**, *65* (3), 289−308.
(31) Golas, M. M.; Sander, B.; Will, C. L.; Luhrmann, R.; Stark, H. Major conformational change in the complex SF3b upon integration into the spliceosomal U11/U12 di-snRNP as revealed by electron cryomicroscopy. *Mol. Cell* **2005**, *17* (6), 869−883.
(32) Ross, C. A. Huntington's disease: new paths to pathogenesis. *Cell* **2004**, 118 (1), 4−7.
(33) Passani, L. A.; Bedford, M. T.; Faber, P. W.; McGinnis, K. M.; Sharp, A. H.; Gusella, J. F.; Vonsattel, J. P.; MacDonald, M. E. Huntingtin's WW domain partners in Huntington's disease post-mortem brain fulfill genetic criteria for direct involvement in Huntington's disease pathogenesis. *Hum. Mol. Genet.* **2000**, *9* (14), 2175−2182.
(34) D'Souza, I.; Schellenberg, G. D. Regulation of tau isoform expression and dementia. *Biochim. Biophys. Acta* **2005**, *1739* (2−3), 104−115.
(35) Winkler, C.; Eggert, C.; Gradl, D.; Meister, G.; Giegerich, M.; Wedlich, D.; Laggerbauer, B.; Fischer, U. Reduced U snRNP assembly causes motor axon degeneration in an animal model for spinal muscular atrophy. *Genes. Dev.* **2005**, *19* (19), 2320−2330.
(36) Meriin, A. B.; Sherman, M. Y. Role of molecular chaperones in neurodegenerative disorders. *Int. J. Hyperthermia.* **2005**, *21* (5), 403−419.
(37) Mao, J. J.; Katayama, S.; Watanabe, C.; Harada, Y.; Noda, K.; Yamamura, Y.; Nakamura, S. The relationship between alphaB-Crystallin and neurofibrillary tangles in Alzheimer's disease. *Neuropathol Appl. Neurobiol.* **2001**, *27* (3), 180−188.
(38) Renkawek, K.; Stege, G. J.; Bosman, G. J. Dementia, gliosis and expression of the small heat shock proteins hsp27 and alpha B-Crystallin in Parkinson's disease. *Neuroreport* **1999**, *10* (11), 2273−2276.
(39) Shinder, G. A.; Lacourse, M. C.; Minotti, S.; Durham, H. D. Mutant Cu/Zn-superoxide dismutase proteins have altered solubility and interact with heat shock/stress proteins in models of amyotrophic lateral sclerosis. *J. Biol. Chem.* **2001**, *276* (16), 12791−12796.
(40) Iwaki, T.; Kume-Iwaki, A.; Liem, R. K.; Goldman, J. E. Alpha B-Crystallin is expressed in nonlenticular tissues and accumulates in Alexander's disease brain. *Cell* **1989**, *57* (1), 71−78.
(41) van Rijk, A. F.; Bloemendal, H Alpha-B-Crystallin in neuropathology. *Ophthalmologica* **2000**, *214* (1), 7−12.
(42) Dabir, D. V.; Trojanowski, J. Q.; Richter-Landsberg, C.; Lee, V. M.; Forman, M. S. Expression of the small heat-shock protein alphaB-Crystallin in tauopathies with glial pathology. *Am. J. Pathol.* **2004**, *164* (1), 155−166.
(43) Tajouri, L.; Mellick, A. S.; Ashton, K. J.; Tannenberg, A. E.; Nagra, R. M.; Tourtellotte, W. W.; Griffiths, L. R.; van Veen, T.; van Winsen, L.; Crusius, J. B.; Kalkers, N. F.; Barkhof, F.; Pena, A. S.; Polman, C. H.; Uitdehaag, B. M. Quantitative and qualitative changes in gene expression patterns characterize the activity of plaques in multiple sclerosis. *Brain Res. Mol. Brain Res.* **2003**, *119* (2), 170−183.
(44) van Veen, T.; van Winsen, L.; Crusius, J. B.; Kalkers, N. F.; Barkhof, F.; Pena, A. S.; Polman, C. H.; Uitdehaag, B. M. AlphaB-Crystallin genotype has impact on the multiple sclerosis phenotype. *Neurology* **2003**, *61* (9), 1245−1249.
(45) Gutekunst, C. A.; Li, S. H.; Yi, H.; Mulroy, J. S.; Kuemmerle, S.; Jones, R.; Rye, D.; Ferrante, R. J.; Hersch, S. M.; Li, X. J. Nuclear and neuropil aggregates in Huntington's disease: relationship to neuropathology. *J. Neurosci.* **1999**, *19* (7), 2522−2534.
(46) Kamradt, M. C.; Chen, F.; Sam, S.; Cryns, V. L. The small heat shock protein alpha B-Crystallin negatively regulates apoptosis during myogenic differentiation by inhibiting caspase-3 activation. *J. Biol. Chem.* **2002**, *277* (41), 38731−38736.
(47) Ito, H.; Kamei, K.; Iwamoto, I.; Inaguma, Y.; Nohara, D.; Kato, K. Phosphorylation-induced change of the oligomerization state of alpha B-Crystallin. *J. Biol. Chem.* **2001**, *276* (7), 5346−5352.
(48) Barnham, K. J.; Masters, C. L.; Bush, A. I. Neurodegenerative diseases and oxidative stress. *Nat. Rev. Drug Discov.* **2004**, *3* (3), 205−214.
(49) Chong, Z. Z.; Li, F.; Maiese, K. Oxidative stress in the brain: novel cellular targets that govern survival during neurodegenerative disease. *Prog. Neurobiol.* **2005**, *75* (3), 207−246.
(50) Harper, M. E.; Bevilacqua, L.; Hagopian, K.; Weindruch, R.; Ramsey, J. J. Aging, oxidative stress, and mitochondrial uncoupling. *Acta Physiol. Scand.* **2004**, *182* (4), 321−331.
(51) Marz, K. E.; Hanson, P. I. Sealed with a twist: complexin and the synaptic SNARE complex. *Trends. Neurosci.* **2002**, *25* (8), 381−383.
(52) Morton, A. J.; Edwardson, J. M. Progressive depletion of complexin II in a transgenic mouse model of Huntington's disease. *J. Neurochem.* **2001**, *76* (1), 166−172.
(53) Hauser, M. A.; Li, Y. J.; Xu, H.; Noureddine, M. A.; Shao, Y. S.; Gullans, S. R.; Scherzer, C. R.; Jensen, R. V.; McLaurin, A. C.; Gibson, J. R.; Scott, B. L.; Jewett, R. M.; Stenger, J. E.; Schmechel, D. E.; Hulette, C. M.; Vance, J. M. Expression profiling of substantia nigra in Parkinson disease, progressive supranuclear palsy, and frontotemporal dementia with parkinsonism. *Arch. Neurol.* **2005**, *62* (6), 917−921.
(54) Hickey, M. A.; Chesselet, M. F. Apoptosis in Huntington's disease. *Prog. Neuropsychopharmacol Biol. Psychiatry* **2003**, *27* (2), 255−265.
(55) Tatton, W. G.; Chalmers-Redman, R.; Brown, D.; Tatton, N. Apoptosis in Parkinson's disease: signals for neuronal degradation. *Ann. Neurol.* **2003**, 53 Suppl 3, S61−70; discussion S70−72.
(56) Kitsberg, D.; Formstecher, E.; Fauquet, M.; Kubes, M.; Cordier, J.; Canton, B.; Pan, G.; Rolli, M.; Glowinski, J.; Chneiweiss, H. Knock-out of the neural death effector domain protein PEA-15 demonstrates that its expression protects astrocytes from TN-Falpha-induced apoptosis. *J. Neurosci.* **1999**, *19* (19), 8244−8251.
(57) Xia, P.; Wang, L.; Moretti, P. A.; Albanese, N.; Chai, F.; Pitson, S. M.; D'Andrea, R. J.; Gamble, J. R.; Vadas, M. A. Sphingosine kinase interacts with TRAF2 and dissects tumor necrosis factor-alpha signaling. *J. Biol. Chem.* **2002**, *277* (10), 7996−8003.
(58) Schwikowski, B.; Uetz, P.; Fields, S. A network of protein−protein interactions in yeast. *Nat. Biotechnol.* **2000**, *18* (12), 1257−1261.

(59) Goehler, H.; Lalowski, M.; Stelzl, U.; Waelter, S.; Stroedicke, M.; Worm, U.; Droege, A.; Lindenberg, K. S.; Knoblich, M.; Haenig, C.; Herbst, M.; Suopanki, J.; Scherzinger, E.; Abraham, C.; Bauer, B.; Hasenbank, R.; Fritzsche, A.; Ludewig, A. H.; Buessow, K.; Coleman, S. H.; Gutekunst, C. A.; Landwehrmeyer, B. G.; Lehrach, H.; Wanker, E. E. A protein interaction network links GIT1, an enhancer of huntingtin aggregation, to Huntington's disease. *Mol. Cell* **2004**, *15* (6), 853−865.

(60) Jain, R.; Rivera, M. C.; Lake, J. A. Horizontal gene transfer among genomes: the complexity hypothesis. *Proc. Natl. Acad. Sci. U.S.A.* **1999**, *96* (7), 3801−3806.

(61) Aris-Brosou, S. Determinants of adaptive evolution at the molecular level: the extended complexity hypothesis. *Mol. Biol. Evol.* **2005**, *22* (2), 200−209.

PR0601077